

2022

Molecular Control of the Migratory Phase During Cutaneous Wound Healing

Bolton, Chloe Elizabeth

<http://hdl.handle.net/10026.1/18644>

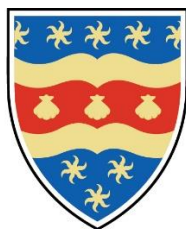
<http://dx.doi.org/10.24382/367>

University of Plymouth

All content in PEARL is protected by copyright law. Author manuscripts are made available in accordance with publisher policies. Please cite only the published version using the details provided on the item record or document. In the absence of an open licence (e.g. Creative Commons), permissions for further reuse of content should be sought from the publisher or author.

Statement of Copyright

This copy of the thesis has been supplied on condition that anyone who consults it is understood to recognise that its copyright rests with its author and that no quotation from the thesis and no information derived from it may be published without the author's prior consent.



**UNIVERSITY OF
PLYMOUTH**

**Molecular Control of the Migratory Phase
During Cutaneous Wound Healing**

By

Chloe Elizabeth Bolton

A thesis submitted to the University of Plymouth in partial fulfilment for the degree of

DOCTOR OF PHILOSOPHY

Peninsula Dental School

January 2022

Acknowledgements

Supervisory Team

Professor Bing Hu

Professor Oliver Hanemann

Professor Shouqing Luo

Research Group

Dr Wai-Ling Kok

Dr Tulay Gulsen

Dr Donald Singer

Dr Jemma Walker

Dr Jonathan Davies

Portia Maddick

Charlotte Illsley

Tracy Edwards

Collaborators

Professor Sabine Werner

Dr Christian Hacker

Paulina Cherek

Authors Declaration

At no time during the registration for the degree of Doctor of Philosophy has the author been registered for any other University award without prior agreement of the Doctoral College Quality Sub-Committee.

Work submitted for this research degree at the University of Plymouth has not formed part of any other degree either at the University of Plymouth or at another establishment.

Word Count of main body of thesis: 57, 591

Signed:

A handwritten signature in dark ink, appearing to read 'Bolton', with a long horizontal stroke extending to the right.

Date: January 2022

Publications accepted since commencing PhD

Transit Amplifying Cells Coordinate Mouse Incisor Mesenchymal Stem Cell Activation

J. V. Walker, H. Zhuang, D. Singer, C. S. Illsley, W. L. Kok, K. K. Sivaraj, Y. Gao, C. Bolton, Y. Liu, M. Zhao, P. R. C. Grayson, S. Wang, J. Karbanová, T. Lee, S. Ardu, Q. Lai, J. Liu, M. Kassem, S. Chen, K. Yang, Y. Bai, C. Tredwin, A. C. Zambon, D. Corbeil, R. Adams, B. M. Abdallah, B. Hu

Nature Communications, 2019

DOI: 10.1038/s41467-019-11611-0

Notch signalling coordinates periodontal ligament maturation through regulating Lamin A

B.J. Denes, C. Bolton, C.S. Illsley, W.L. Kok, J.V. Walker, A. Poetsch, C. Tredwin, S. Kiliaridis, B. Hu

Journal of Dental Research, 2019

DOI: 10.1177/0022034519871448

Conferences attended since commencing PhD

- British Society for Oral and Dental Research, Plymouth, 2017
- International Association for Dental Research, London, 2018
(Poster presentation)

Dedications

Firstly, to my wonderful husband, Adam....

I offer my sincerest gratitude for your unwavering love and support throughout this process, for putting up with the late nights and the tearful outbursts, for your endless encouragement and belief in me when I couldn't find it within myself and for the comfort you gave in times when things just seemed too much to cope with. I'm not sure I would have got through it without you by my side. Thank you for keeping me grounded, for teaching me to keep things in perspective and for showing me that being with those you love will always be more important than any other endeavour in life.

To my loving family....

I would not be where I am today without the unconditional support from my parents; Helen and Diego, my sister; Emily and my wider family. I thank you for never failing to provide the welcome relief of fun, laughter, love and happiness. I will always be grateful to you for shaping me into the person I have become.

To the faithful friends I have made along the way....

I never realised quite how important it would be to have such a fantastic group of work colleagues alongside me. I will forever be indebted to the kindness you have shown, for your willingness to teach me and to answer my questions without hesitation and for the invaluable guidance you have given. Knowing that we were all going through the same tough experiences together worked wonders in retaining some degree of sanity over the years, as did the escape of our daily lunchtime natters. I appreciate you all more than I perhaps ever let on.

*“And once the storm is over, you won’t remember how you made it through,
how you managed to survive.
You won’t even be sure whether the storm is really over.
But one thing is certain.
When you come out of the storm, you won’t be the same person who walked in.

That’s what this storm is all about.”*

Haruki Marakami

Abstract

Molecular Control of the Migratory Phase During Cutaneous Wound Healing

By Chloe Elizabeth Bolton

Superficial cutaneous injuries occur on a huge scale across the globe; while most will resolve without intervention or any lasting damage, many will experience complications that arise through delayed healing or as a consequence of the skins protective barrier being breached.

The migration of cutaneous cells across a wound site is a crucial factor in establishing permanent restoration of the skins integrity. This study provides insight into molecular events that facilitate the migratory ability of cutaneous cells during this phase of the healing process. Through subcellular analysis, molecular manipulation and various imaging techniques of *in vivo* and *in vitro* wound models, this project has discovered that the autophagy pathway is activated in response to injury and also that the resultant autophagosomes form in a polarised manner towards the trailing end of migrating keratinocytes. Results indicate that initiation of autophagy is responsive to Wnt5a signals secreted by several cell types within the wound site and these signals must pass through Frizzled 3 receptors and Rho-associated protein kinase to activate nucleation of phagophore membranes.

This study also develops and tests the use of novel wound healing platforms in the form of *ex vivo* murine models and 3-dimensional full-thickness human skin equivalents to help assess the role of autophagy specifically in the context of wound healing.

Contents

STATEMENT OF COPYRIGHT.....	0
ACKNOWLEDGEMENTS.....	2
AUTHORS DECLARATION	3
PUBLICATIONS ACCEPTED SINCE COMMENCING PHD	4
CONFERENCES ATTENDED SINCE COMMENCING PHD	4
DEDICATIONS.....	5
ABSTRACT	7
1. INTRODUCTION.....	23
1.1 THE STRUCTURE AND IMPORTANCE OF VERTEBRATE SKIN	23
1.1.1 INTRODUCTION TO THE SKIN	23
1.1.2 ANATOMY OF THE EPIDERMIS	26
1.1.3 COMPOSITION AND ARCHITECTURE OF THE BASEMENT MEMBRANE	34
1.1.4 ANATOMY OF THE DERMAL COMPARTMENT	35
1.1.5 ANATOMY OF THE HYPODERMIS	36
1.1.6 SKIN APPENDAGES AND OTHER NOTABLE CELL TYPES.....	37
1.1.7 FUNCTIONS OF THE SKIN AND COMPLICATIONS ASSOCIATED WITH WOUNDING	40
1.2 THE PATHOPHYSIOLOGY OF WOUND HEALING	45
1.2.1 AN INTRODUCTION TO WOUND HEALING	45
1.2.2 THE HAEMOSTASIS PHASE	46
1.2.3 THE INFLAMMATORY PHASE	49
1.2.4 THE PROLIFERATIVE PHASE AND RE-EPITHELIALISATION.....	50
1.2.5 MECHANISMS OF CELL MIGRATION AND CYTOSKELETON REARRANGEMENT.....	52
1.2.6 THE REMODELLING PHASE AND ANGIOGENESIS	54
1.2.7 COMPLICATIONS ASSOCIATED WITH ABERRANT WOUND HEALING	57

1.2.8	THE GLOBAL IMPACT OF CUTANEOUS WOUNDS AND CURRENT DEVELOPMENTS IN WOUND CARE STRATEGIES.....	60
1.3	WNT SIGNALLING PATHWAYS.....	64
1.3.1	THE CANONICAL WNT / B-CATENIN SIGNALLING PATHWAY	65
1.3.2	CANONICAL WNT SIGNALLING IN THE SKIN	67
1.3.3	THE NON-CANONICAL PLANAR CELL POLARITY PATHWAY	68
1.3.4	PLANAR CELL POLARITY IN THE SKIN.....	71
1.4	AUTOPHAGY	73
1.4.1	INTRODUCTION TO AUTOPHAGY	73
1.4.2	MECHANISTIC OVERVIEW OF AUTOPHAGY.....	73
1.4.3	SELECTIVE AUTOPHAGY AND THE ROLE OF CARGO RECEPTORS	78
1.4.4	AUTOPHAGY IN UNDAMAGED SKIN	79
1.4.5	CURRENT UNDERSTANDING OF AUTOPHAGY IN WOUNDED SKIN.....	80
1.5	THE USE OF ANIMAL MODELS TO STUDY WOUND HEALING.....	85
1.5.1	COMMON ANIMAL MODELS USED IN THE SKIN FIELD	85
1.5.2	A COMPARISON OF MOUSE AND HUMAN SKIN – PHYSICAL FEATURES.....	85
1.5.3	A COMPARISON OF MOUSE AND HUMAN SKIN – MOLECULAR COMPONENTS.....	89
<u>2.</u>	<u>AIMS</u>	<u>91</u>
<u>3.</u>	<u>MATERIALS AND METHODS</u>	<u>95</u>
3.1	CELL CULTURE	95
3.1.1	HUMAN DERMAL FIBROBLASTS.....	95
3.1.2	HUMAN EPIDERMAL KERATINOCYTES.....	95
3.1.3	CELL CULTURE DISHES.....	96
3.1.4	PASSAGING CELLS	96
3.1.5	FREEZING CELLS.....	97

3.1.6	THAWING CELLS	97
3.2	CELL STRETCHING.....	97
3.2.1	STRETCH CHAMBER COLLAGEN COATING AND CELL SEEDING	97
3.2.2	CELLS UNDER CONSTANT STRAIN	98
3.3	SCRATCH ASSAYS	98
3.4	SENESCENCE ASSAYS.....	99
3.5	LENTIVIRUS PREPARATION.....	99
3.5.1	PRODUCTION OF Ki67P-FUCCI LENTIVIRAL REPORTERS	99
3.5.2	INFECTION OF KERATINOCYTES WITH FUCCI LENTIVIRUS	100
3.6	cDNA ANALYSIS	101
3.6.1	RNA EXTRACTION FROM CELLS	101
3.6.2	REVERSE TRANSCRIPTION	102
3.6.3	Q-PCR.....	102
3.6.4	Q-PCR STATISTICAL ANALYSIS	103
3.6.5	PRIMER DESIGN.....	104
3.7	PROTEIN ANALYSIS.....	106
3.7.1	TOTAL PROTEIN EXTRACTION FROM CELLS.....	106
3.7.2	BICINCHONINIC ACID ASSAY TO DETERMINE PROTEIN CONCENTRATION	106
3.7.3	WESTERN BLOTTING – PROTEIN SEPARATION AND MEMBRANE TRANSFER	107
3.7.4	WESTERN BLOTTING – DETECTION OF PROTEINS	109
3.8	<i>IN VIVO</i> MOUSE WOUND MODEL	110
3.9	<i>EX VIVO</i> MOUSE WOUND MODEL.....	111
3.9.1	MOUSE STRAINS, ETHICS AND ANIMAL LICENSES	111
3.9.2	PROTOCOL ONE: EMPTY WOUNDS ON SEMI-SOLID.....	111
3.9.3	PROTOCOL TWO: PROTEIN SOAKED AFFI-GEL BEADS.....	112
3.9.4	PROTOCOL THREE: COLLAGEN GELS IMPREGNATED WITH PROTEIN.....	113

3.9.5	PROTOCOL FOUR: CELL STRAINERS AND LIQUID CULTURE MEDIA.....	114
3.9.6	PROTOCOL FIVE: BLADE INCISIONS, CELL STRAINERS AND LIQUID CULTURE MEDIA.....	115
3.10	THREE-DIMENSIONAL BIOENGINEERED HUMAN SKIN MODEL	117
3.10.1	INSERT BASED EPIDERMAL MODEL	117
3.11	TISSUE PROCESSING AND STAINING	117
3.11.1	FROZEN TISSUE SAMPLES	117
3.11.2	PARAFFIN EMBEDDED TISSUE SAMPLES.....	118
3.11.3	TISSUE SECTIONING.....	119
3.11.4	HISTOLOGICAL STAINING – HEMATOXYLIN AND EOSIN	120
3.11.5	IMMUNOFLUORESCENCE STAINING	121
3.12	TRANSMISSION ELECTRON MICROSCOPY	123
4.	<u>RESULTS</u>	<u>125</u>
	<u>RESULTS SECTION I</u>	<u>125</u>
	CHARACTERISATION OF PLANAR CELL POLARITY AND WNT SIGNALLING IN THE WOUND ENVIRONMENT	125
I.I	THE <i>IN VIVO</i> MURINE WOUND MODEL	125
I.II	HISTOLOGICAL ASSESSMENT OF THE <i>IN VIVO</i> MURINE WOUND MODEL	126
I.III	IDENTIFICATION OF DIFFERENT CELL TYPES AT THE WOUND BORDER.....	129
I.IV	PCP MARKERS HAVE A DISTINCT EXPRESSION PATTERN AT THE WOUND BORDER.....	133
I.V	FRIZZLED 3 IS POLARISED TOWARDS THE WOUND <i>IN VIVO</i> BUT FRIZZLED 6 IS NOT	134
I.VI	FRIZZLED 3 IS ALSO POLARISED TOWARDS THE WOUND <i>IN VITRO</i>	136
I.VII	EXPRESSION OF OTHER PCP RECEPTORS AT THE WOUND SITE.....	140
I.VIII	A SUMMARY OF IMMUNOFLUORESCENT PCP MARKERS AT THE WOUND SITE	141
I.IX	MRNA ANALYSIS CONFIRMS UPREGULATION OF PCP FAMILY MEMBERS IN RESPONSE TO INJURY	141
I.X	WNT5A SIGNALS IN THE <i>IN VIVO</i> MOUSE MODEL	146
I.XI	DERMAL FIBROBLASTS PRODUCE WNT5A IN RESPONSE TO SCRATCH ASSAYS	148

I.XII	STRETCHING FORCES INDUCE WNT5A EXPRESSION IN DERMAL FIBROBLASTS	149
I.XIII	EPIDERMAL KERATINOCYTES PRODUCE WNT5A IN RESPONSE TO SCRATCH ASSAYS	152
I.XIV	WNT5A TREATMENT UPREGULATES EXPRESSION OF PCP COMPONENTS <i>IN VITRO</i> WITHOUT PRIOR WOUNDING	152
I.XV	SUMMARY OF RESULTS SECTION 1	155

RESULTS SECTION II 157

CHARACTERISATION OF AUTOPHAGY IN THE WOUND ENVIRONMENT. 157

II.I	ATG5 IS POLARISED AWAY FROM THE WOUND <i>IN VIVO</i>	157
II.II	ATG5 IS POLARISED AWAY FROM THE SCRATCH <i>IN VITRO</i>	160
II.III	ASYMMETRICAL LOCALISATION OF ATG16L IS NOT AS PRONOUNCED AS ATG5	163
II.IV	LC3 IS CLUSTERED AROUND THE NUCLEUS AWAY FROM THE WOUND <i>IN VIVO</i>	166
II.V	TOTAL P62 IS POLARISED TOWARDS THE WOUND <i>IN VIVO</i>	170
II.VI	TOTAL P62 IS POLARISED TOWARDS THE SCRATCH <i>IN VITRO</i>	172
II.VII	PHOSPHORYLATED P62 IS POLARISED AWAY FROM THE WOUND <i>IN VIVO</i>	175
II.VIII	PHOSPHORYLATED P62 IS POLARISED AWAY FROM THE SCRATCH <i>IN VITRO</i>	177
II.IX	TRANSMISSION ELECTRON MICROSCOPY CONFIRMS LOCATION OF AUTOPHAGOSOMES TOWARDS THE TRAILING END OF HUMAN KERATINOCYTES	180
II.X	MRNA ANALYSIS CONFIRMS UPREGULATION OF CORE AUTOPHAGY GENES IN RESPONSE TO INJURY ... 186	185
II.XI	SUMMARY OF RESULTS SECTION II	187

RESULTS SECTION III 190

INVESTIGATING THE MOLECULAR MECHANISMS THAT CONTROL ACTIVATION OF AUTOPHAGY IN A WOUND

ENVIRONMENT 190

III.I	WNT5A TREATMENT UPREGULATES EXPRESSION OF AUTOPHAGY GENES <i>IN VITRO</i> WITHOUT PRIOR WOUNDING	190
-------	---	-----

192	
III.II	WNT3A DOES NOT ACTIVATE PCP OR AUTOPHAGY PATHWAYS IN HUMAN KERATINOCYTES 193
194	
III.III	WNT5A ACTS VIA FRIZZLED 3 TO ACTIVATE AUTOPHAGY..... 195
III.IV	INVESTIGATING ROCK AS A POTENTIAL MEDIATOR OF AUTOPHAGY IN THE WOUND ENVIRONMENT ... 198
III.V	SUMMARY OF RESULTS SECTION III 206
 <u>DISCUSSION OF SECTIONS I-III 207</u>	
 <u>RESULTS SECTION IV 217</u>	
IV.I	INVESTIGATING THE CELL CYCLE STATUS OF CELLS AT THE WOUND BORDER USING THE FLUORESCENCE- ACQUIRED UBIQUITINATION CELL CYCLE INDICATOR REPORTER SYSTEM. 217
IV.II	ANALYSIS OF CDKS AND CYCLINS SUGGEST THAT COLOURLESS CELLS AT THE SCRATCH BORDER ENTER A TRANSIENT G ₀ -LIKE STATE 222
IV.III	COLOURLESS CELLS AT THE WOUND BORDER ARE NOT SENESCENT 225
	SUMMARY AND DISCUSSION OF RESULTS SECTION IV 230
 <u>RESULTS SECTION V 232</u>	
 <u>OPTIMISATION AND USE OF AN <i>EX VIVO</i> MURINE WOUND MODEL 232</u>	
V.I	PROTOCOL ONE – EMPTY PUNCH BIOPSY WOUNDS 233
V.II	PROTOCOL TWO – INCORPORATION OF PROTEIN SOAKED AFFI-GEL BLUE AGAROSE BEADS 237
V.III	PROTOCOL THREE – COLLAGEN GELS IMPREGNATED WITH PROTEINS..... 240
V.IV	PROTOCOL FOUR – CELL STRAINERS AND LIQUID MEDIA..... 247
V.V	PROTOCOL FIVE: BLADE INCISIONS WITH COLLAGEN EMBEDDED FIBROBLASTS..... 255
 <u>RESULTS SECTION VI 263</u>	
 <u>OPTIMISATION AND USE OF A THREE-DIMENSIONAL BIOENGINEERED HUMAN SKIN MODEL 263</u>	

VI.I	THE CONCEPT OF AN ARTIFICIALLY CREATED HUMAN SKIN MODEL	263
VI.II	DEVELOPMENT OF AN INSERT BASED EPIDERMIS MODEL.....	264
VI.III	DEVELOPMENT OF A DERMAL COMPARTMENT MODEL	266
VI.IV	DEVELOPMENT OF A FULL THICKNESS SKIN MODEL.....	269
VI.V	ASSESSMENT OF THE BIOENGINEERED, FULL THICKNESS SKIN MODEL AND ITS SUITABILITY FOR USE IN THE WOUND HEALING FIELD.....	271
<u>5. IMPACT OF THE STUDY AND FUTURE WORK.....</u>		<u>273</u>
<u>6. SUPPLEMENTARY MATERIAL</u>		<u>275</u>
<u>7. REFERENCES.....</u>		<u>281</u>

Table 1 Abbreviations	20
Table 2 Thermo Cyclor program used for reverse transcription	102
Table 3 LightCycler program used for qPCR	103
Table 4 Human Primers.....	105
Table 5 Program used for processing paraffin embedded tissue samples.....	119
Table 6 Experimental details of primary antibodies.....	123
Table 7 Composition of Dulbecco's Modified Eagle's medium.....	275
Table 8 Composition of Epilife media	276
Table 9 Composition of Human Keratinocyte Growth Supplement.....	277

Figure 1 Overview of the skins structure	25
Figure 2 Arrangement of keratin filaments across keratinocytes in the epidermis	27
Figure 3 Mitotic spindle orientation during cell divisions	28
Figure 4 Arrangement of the stratified epidermal layers	30
Figure 5 Assembly of the cornified envelope	32
Figure 6 The haemostasis phase of wound healing	48
Figure 7 Cytoskeleton rearrangements in a migrating cell.....	53
Figure 8 Sequential diagram showing molecular interactions during wound healing ...	56
Figure 9 The transcutaneous electrical potential of damaged and undamaged skin ...	63
Figure 10 The molecular pathway of canonical Wnt/ β -catenin signalling	66
Figure 11 Arrangement of PCP components in polarised epithelial cells	69
Figure 12 The molecular pathway of non-canonical Wnt signalling: The Planar Cell Polarity pathway	70
Figure 13 Overview of the autophagy mechanism	74
Figure 14 Complexes involved in the formation of autophagosomes.....	77
Figure 15 A comparison between the physical features of mouse and human skin.....	88
Figure 16 Western blot transfer assembly	108
Figure 17 Schematic diagram of the method used in 'Protocol One' of the ex vivo mouse model.....	112
Figure 18 Schematic diagram of the method used in 'Protocol Four' of the ex vivo mouse model.....	115
Figure 19 Histological staining of an <i>in vivo</i> mouse wound model 4 days post injury .	127
Figure 20 Histological staining of an <i>in vivo</i> mouse model 7 days post injury	128
Figure 21 Expression pattern of the proliferation marker P63 in an <i>in vivo</i> murine wound model 4 days post injury	130

Figure 22 Expression of proliferation markers KI67 and P63 in the proliferative region of an <i>in vivo</i> wound model 4 days post injury	132
Figure 23 Expression pattern of Frizzled 3 and Frizzled 6 in <i>in vivo</i> mouse wound models.....	135
Figure 24 Using scratch assays as an <i>in vitro</i> tool to monitor wound closure	137
Figure 25 Expression pattern of Frizzled 3 receptors in <i>in vitro</i> scratch assays	138
Figure 26 Quantification of polarised Frizzled 3 expression.....	139
Figure 27 mRNA analysis of PCP components in different populations of keratinocytes following <i>in vitro</i> scratch assays.....	145
Figure 28 Wnt5a expression in the <i>in vivo</i> mouse model.....	147
Figure 29 HDF cells secrete Wnt5a in response to <i>in vitro</i> injury and tensile forces ...	150
Figure 30 Epidermal keratinocytes secrete Wnt5a in response to <i>in vitro</i> injury	151
Figure 31 Wnt5a treatment induces upregulation of PCP markers, independent of injury	154
Figure 32 Expression pattern of ATG5 <i>in vivo</i>	159
Figure 33 Expression pattern of ATG5 in <i>in vitro</i> scratch assays	161
Figure 34 Quantification of polarised ATG5 expression	162
Figure 35 Expression pattern of ATG16L <i>in vivo</i>	164
Figure 36 Quantification of unpolarised ATG16 expression.....	165
Figure 37 Expression pattern of LC3 <i>in vivo</i>	167
Figure 38 Expression pattern of LC3 <i>in vivo</i>	168
Figure 39 Quantification of polarised LC3 expression	169
Figure 40 Expression pattern of total p62 <i>in vivo</i>	171
Figure 41 Expression pattern of total p62 <i>in vitro</i>	173
Figure 42 Quantification of polarised p62 expression.....	174

Figure 43 Expression pattern of phosphorylated p62 <i>in vivo</i>	176
Figure 44 Expression pattern of phosphorylated p62 <i>in vitro</i>	178
Figure 45 Quantification of polarised phosphorylated p62 expression	179
Figure 46 Transmission electron microscopy of autophagosomes in human keratinocytes 2 hours post scratch	181
Figure 47 Transmission electron microscopy of autophagosomes in human keratinocytes 6 hours post scratch	182
Figure 48 Transmission electron microscopy of autophagosomes in human keratinocytes 12 hours post scratch	183
Figure 49 Transmission electron microscopy of autophagosomes in human keratinocytes 24 hours post scratch	184
Figure 50 mRNA analysis of core autophagy genes in different populations of keratinocytes following <i>in vitro</i> scratch assays.....	186
Figure 51 Schematic diagram summarising expression patterns and localisation of autophagy and PCP markers <i>in vivo</i> and <i>in vitro</i>	189
Figure 52 Wnt5a treatment induces upregulation of autophagy markers, independent of injury	192
Figure 53 Wnt3a does not activate PCP or autophagy	194
Figure 54 Wnt5a acts via Frizzled 3 to regulate autophagy in keratinocytes.....	197
Figure 55 Mechanisms of Y27632, Bafilomycin and Rapamycin	200
Figure 56 Y27632 prevents Wnt5a induced autophagy in keratinocytes.....	202
Figure 57 Y27632 treatment has no effect on activation of PCP in response to injury but does prevent activation of autophagy <i>in vitro</i>	205
Figure 58 Proposed mechanism for the joint activation of Wnt5a mediated PCP and autophagy in migrating epidermal cells at the periphery of a wound	213

Figure 59 Using the Fucci reporter system to analyse cell cycle status in scratch assays	220
Figure 60 Cyclin and CDK mRNA expression in leader vs follower cells	224
Figure 61 Senescence at the scratch border.....	226
Figure 62 Migratory direction and displaced distance travelled by wounded keratinocytes.....	228
Figure 63 <i>Ex vivo</i> wound model at 24 hours post injury- protocol one.....	235
Figure 64 <i>Ex vivo</i> wound model - protocol two with Affi-Gel beads	239
Figure 65 <i>Ex vivo</i> wound model - collagen gels impregnated with protein	242
Figure 66 <i>Ex vivo</i> wound model - collagen gel measurements.....	245
Figure 67 <i>Ex vivo</i> wound model - cell strainer male mouse	249
Figure 68 <i>Ex vivo</i> wound model - cell strainer female mouse	250
Figure 69 <i>Ex vivo</i> wound model - cell strainer box and whisker plots of raw data	252
Figure 70 <i>Ex vivo</i> wound model - cell strainer relative closure rates	254
Figure 71 <i>Ex vivo</i> wound model – blade incisions with embedded fibroblasts.....	257
Figure 72 <i>Ex vivo</i> wound model – dermal fibroblasts embedded into collagen gel packing material significantly improves healing rates.....	259
Figure 73 <i>Ex vivo</i> wound model - histology of superficial incisions filled with fibroblast embedded collagen gel	260
Figure 74 <i>Ex vivo</i> wound model – KI67 and P63 expression in superficial incisions filled with fibroblast embedded collagen gel	262
Figure 75 Insert based human epidermis model	265
Figure 76 Development of the dermal compartment	268
Figure 77 Full thickness human skin model	270

Table 1 Abbreviations

AGEs	Advanced glycation end-products
Ambra1	Activating Molecule in Beclin 1-Regulated Autophagy Protein 1
Ankrd6	Ankyrin Repeat Domain Containing Protein 6
ATG	Autophagy-related protein
BCA	Bicinchoninic acid
BLIMP	B-Lymphocyte-Induced Maturation Protein 1
BMP	Bone Morphogenic Protein
CCL2	C motif chemokine ligand 2
CD26	Cluster Differentiation 26
CD34	Cluster Differentiation 34
CDK	Cyclin Dependent Kinase
Celsr	Cadherin EGF LAG seven-pass G-type receptor
DETC	Dendritic Epidermal T-Cell
DLK1	Delta-Like homologue 1
DMEM	Dulbecco Modified Eagle's Medium
Dvl	Dishevelled-like
EDC	Epidermal Differentiation Complex
FBS	Fetal Bovine Serum
FGF	Fibroblast Growth Factor
FGF-2	Fibroblast Growth Factor -2
FIP200	Focal Adhesion Kinase Family Interacting Protein of 200kDa
FUCCI	Fluorescence-acquired Ubiquitination Cell Cycle Indicator
Fzd	Frizzled
GapDH	Glyceraldehyde-3-phosphate dehydrogenase
HBSS	Hanks Balanced Salt Solution
JNK	c-Jun N-terminal Kinase
K1	Keratin 1
K10	Keratin 10
K14	Keratin 14
K5	Keratin 5

KLK	Kallikrein
LC3	Microtubule Associated Protein Light Chain 3
LIR	LC3-Interacting Region
MMP	Matrix Metalloproteinase
mRNA	Messenger Ribonucleic Acid
mTOR	Mechanistic Target of Rapamycin
NRF2	NF-E2-Related Factor 2
OPTN	Optineurin
PAMP	Pathogen Associated Molecular Pattern
PBS	Phosphate-buffered Saline
PCP	Planar Cell Polarity
PDGFRα	Platelet-Derived Growth Factor Receptor alpha
PI3KC3	Phosphatidylinositol 3-Kinase complex
PI3P	Phosphatidylinositol-3 phosphate
Pk	Prickle
PKC	Protein Kinase C
RLUC	Renilla Luciferase
ROCK	Rho-associated protein kinase
SPR	Small Proline-Rich proteins
TG	Transglutaminase
TGF-β	Transforming Growth Factor- β
TIMP	Tissue Inhibitor of Metalloproteinase
TNF-α	Tumour Necrosis Factor – α
ULK1	Unc-51-like Kinase 1
UV	Ultraviolet
UVRAG	Ultraviolet Radiation Resistance-Associated Gene
Vangl	Van Gogh-like
VEGF	Vascular Endothelial Growth Factor
Vsp	Vacuolar Protein Sorting
Wnt	Wingless-Type
α-SMA	α -Smooth Muscle Actin

1. Introduction

1.1 The structure and importance of vertebrate skin

1.1.1 Introduction to the skin

Vertebrate skin is a fascinatingly complex organ comprised of highly heterogeneous sub-tissues and structures which allow it to provide biological, chemical and aesthetic functions throughout an individual's lifetime. It plays a fundamental role in our survival by creating a tough physical barrier that protects the more fragile internal organs from harsh conditions in the surrounding environment as well as warding off potential infection from opportunistic pathogens. It also helps sustain an optimal body temperature through a variety of thermoregulatory processes. It is therefore critical that it remains healthy and functional for the entirety of our existence.

However, it is inevitable that we will experience injury at some point during our lives and that this will lead to disruption of the skins protective properties, leaving us temporarily vulnerable to a number of environmental threats. These injuries can be the result of everyday life where activities may cause minor cuts or grazes to the skins surface but these tend to be superficial in their nature with limited damage sustained to surrounding tissues. Other types of injury can arise from planned surgical procedures where incisions are made to access internal cavities of the body or they may be much more extensive in their nature such as gun shot and stab wounds or catastrophic injuries such as those sustained in military battlefields. These larger

wounds will typically involve more wide spread damage not only to the skin but also to blood vessels, nerves, muscle and deeper tissues.

Owing to the prevalence of cutaneous injury across the global population, cutaneous wound healing as a research field has sustained a high degree of interest amongst scientists and healthcare professionals for several decades.

In order to study the mechanisms of cutaneous wound healing, one must first understand the basic architecture of normal skin.

It is considered to have three main sections that begin with the epidermis at the outermost surface of the skin. This is the layer that has direct contact with the outside world and is made of tough, keratinised tissue that can withstand strong abrasive forces. Beneath this is the dermis; the collagen rich layer which makes up the largest portion of the skin, followed finally by the hypodermis. The hypodermis is a layer of subcutaneous fat made of adipocytes that are used as an energy store. They also create an insulating layer beneath the skin that helps regulate the body's temperature and cushions heavy impacts to protect internal organs from damage (Figure 1).

Numerous blood vessels pass through the dermal compartment as do sensory, autonomic and sympathetic nerve fibres to facilitate crosstalk between the brain and the skin tissue. Several skin appendages are also embedded in the skin such as hair follicles and sweat glands (Figure 1).

Each of these cutaneous features and their contribution to normal functioning of the skin are discussed in more detail in the following sections.

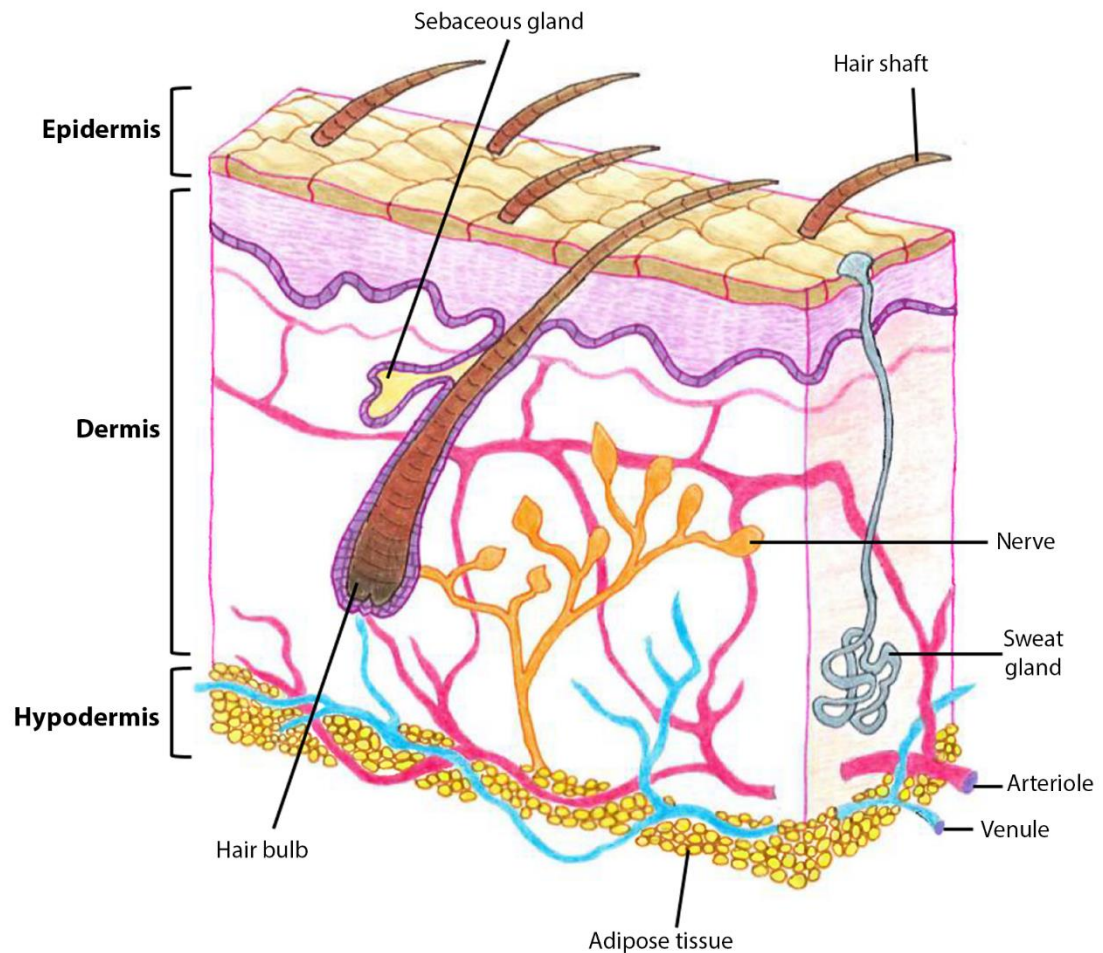


Figure 1 Overview of the skins structure

There are three main compartments to human skin. The outermost layer is the epidermis which forms a protective barrier against the external environment. It is comprised mainly of keratinocyte cells arranged in stratified sheets. Below this lies the dermal compartment which makes up the majority of the skins mass. Dermal fibroblasts are the predominant cell type in the dermis and are responsible for secreting a specialised extracellular matrix that forms connective tissue made mostly of collagen. The hypodermis is the final compartment and creates a subcutaneous fat layer that cushions the skin, provides an insulating layer used in thermoregulation and acts as an energy reserve. Other structures such as sweat glands, nerves, hair follicles and blood vessels are embedded throughout the skins structure.

1.1.2 Anatomy of the epidermis

Adult epidermis is a highly adaptable and dynamic component of the skin that acts as the first line of defence against external threats and injury. It is made predominantly of cells called keratinocytes. These cells undergo an elaborate differentiation process which sees them transition from stem-like cells to fully differentiated, mature keratinocytes. As the cells progress through the differentiation process, they create epidermal layers whereby the least differentiated keratinocytes reside in the inner layers and the most differentiated keratinocytes are at the outermost layer. Each of these layers possess unique characteristics and properties that collectively form a tough, water-impermeable barrier to protect the individual ². There is constant renewal of cells within the epidermis with those reaching the outermost layers being sloughed to make way for newly differentiated cells that replenish the skin from below ³.

The differentiation process begins with a layer of proliferating keratinocytes that are anchored to the basement membrane via integrin-mediated attachment. These cells, like all keratinocytes, express major structural components called keratins ⁴. Within each cell, heterodimer filaments form between pairs of acidic (type I) and basic (type II) versions of these proteins ⁵. The elastic filaments created by keratins extend across the whole width of the cell from desmosomes junctions at the cell membrane to the nuclear lamina. Together with microtubules and actin microfilaments, they create an extensive mechanical network within the epidermis which infers a strong tensile strength across the tissue (Figure 2) ^{6, 7}.

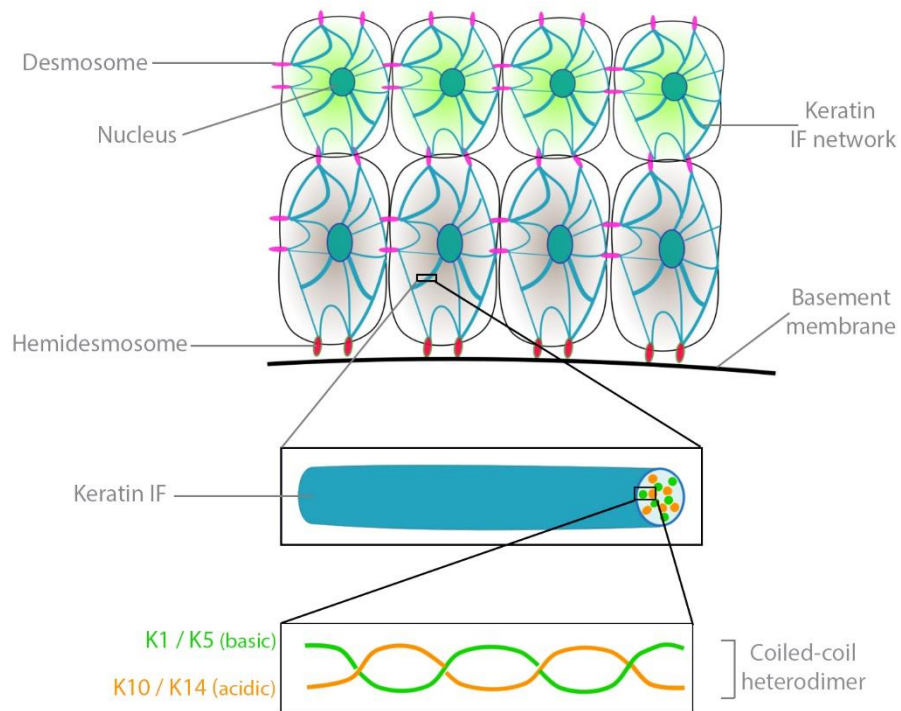


Figure 2 Arrangement of keratin filaments across keratinocytes in the epidermis

Basic and acidic pairs of keratin proteins assemble themselves into a coiled-coil heterodimer configuration which associate closely with one another to form bundles of filaments that are approximately 10nm in diameter. These keratin filaments create a network across the cell that extends from the nucleus and attaches to hemidesmosome cell-ECM and desmosome cell-cell contact points to infer strength and support to the cell.

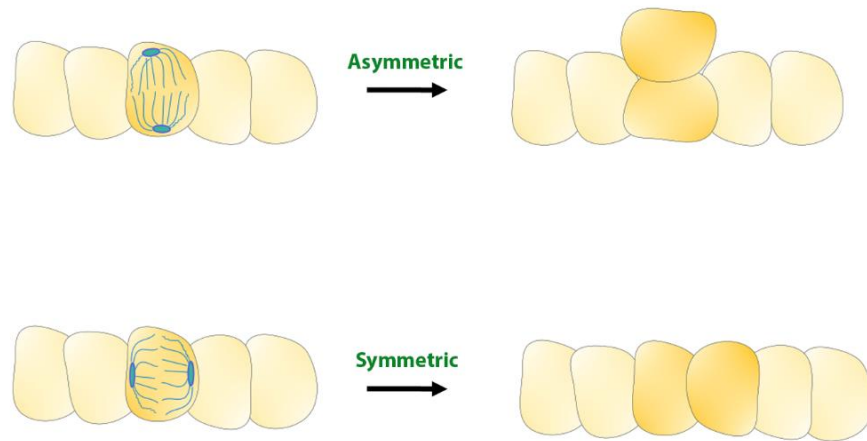


Figure 3 Mitotic spindle orientation during cell divisions

During mitosis, the position of the two resulting daughter cells in relation to the surrounding tissue relies on the positioning of the centrosomes and the mitotic spindle that nucleates from them. In the epidermis, symmetric division occurs when the mitotic spindle orientates itself parallel to the basement membrane and yields two equal daughter cells that reside in the same basal layer of tissue. Asymmetric division occurs when the spindle is orientated perpendicular to the basement membrane and creates distinct daughter cells that differ in their spatial positions.

Keratinocytes attached to the basement membrane highly express a specific subset of smaller keratins, K5 (basic, type II) and K14 (acidic, type I), which can often be used as markers to identify the basal layer ⁸.

Determined by specific orientations of the mitotic spindle, these basal cells can either divide symmetrically to yield two identical daughter cells to maintain the proliferative pool or they can divide asymmetrically to yield daughter cells with distinct cell fates. In this case, one cell remains in the basal layer and continues to maintain the

proliferative pool while the other detaches from the basement membrane and begins its journey to terminal differentiation (Figure 3) ⁹.

At this stage, the cell permanently withdraws from the cell cycle and migrates into the spinous layer where it undergoes a change in its gene expression profile. A typical indicator used to identify this phase is a shift in keratin expression where K1 (basic, type II) and K10 (acidic, type I) are upregulated ¹⁰.

As the cell continues to migrate upwards, it transitions from the spinous layer to the granular layer which is accompanied by an upregulation of protein kinase C (PKC) activity. PKC initially contributes to the downregulation of K1 and K10 in the granular layer which is subsequently followed by activation of a gene cluster known as the epidermal differentiation complex (EDC) ¹¹. An important member of this complex is profilaggrin - a major component of keratohyalin granules to which the granular layer owes its name. The profilaggrin precursor is modified through dephosphorylation and proteolysis to convert it to filaggrin which is dispersed throughout the cell to cause aggregation of keratin filaments into tight bundles ¹². This facilitates some of the morphological changes that are associated with the later stages of keratinocyte differentiation including the collapse of the cell into a flattened shape and a reduction in its cell volume ¹³ (Figure 4).

The EDC also generates proteins such as loricrin, involucrin and trichohyalin, all of which are cross-linked by the transglutaminase (TG) family of enzymes ¹⁴. The most prevalent of these TGs, TG1, is localised to the cell membrane thus leading to an accumulation of cross-linked involucrin, loricrin and trichohyalin that begin to form an insoluble structure known as the cornified envelope near the cells surface ¹³.

Small proline-rich proteins (SPRs) are another important family of molecules that function as TG substrates during keratinocyte differentiation. SPRs preferentially bind to TG3 enzymes to facilitate their cross-bridging function between loricrin proteins ¹⁵. These bonds are weaker and more disorganised and are therefore used to infer elasticity within the cornified envelope as opposed to the stronger TG1 mediated crosslinks that are responsible for mechanical resistance ¹⁶.

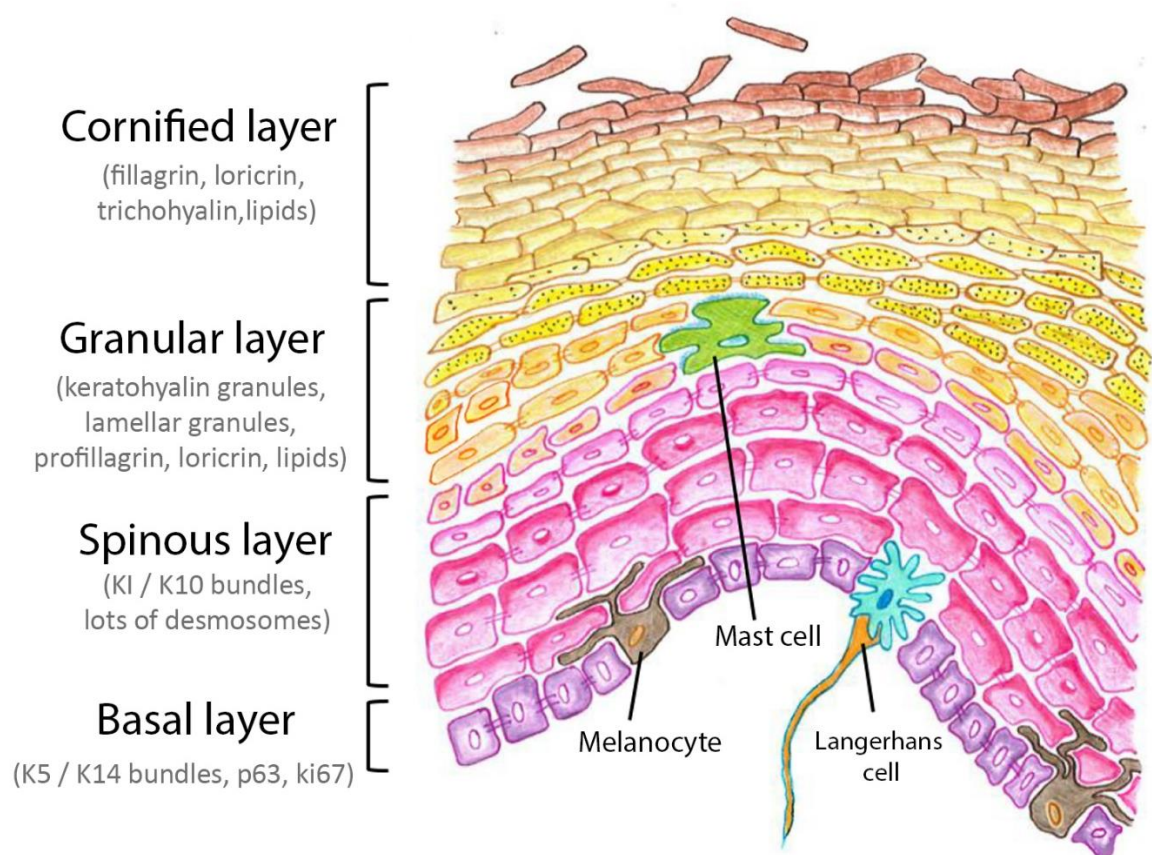


Figure 4 Arrangement of the stratified epidermal layers

Mammalian epidermis is composed primarily of keratinocytes. Structurally, they arrange themselves into stratified layers whereby undifferentiated, stem-like cells reside in the basal layer. As these cells progress through the differentiation process, they migrate upwards into the spinous layer then into the granular layer and finally into the cornified layer. An assortment of other cells such as melanocytes, mast cells and Langerhans cells can be found amongst the keratinocytes that contribute to the overall functioning of the skin.

The ratio of SPRs to loricrin has been correlated to the flexibility and rigidity of the epidermis where thinner regions have much lower ratios compared to tougher regions such as the palms and soles of the feet ¹⁷ (Figure 5).

Aside from the proteomic changes that occur in the granular layer, the keratinocytes begin to accumulate lamellar bodies which are membranous structures that develop from and bud off the Golgi apparatus ¹⁴. They contain a variety of barrier forming lipids as well as enzymes that modify secreted lipids outside the cell in the extracellular milieu. These enzymes aid in the conversion of sphingomyelin and glucosylceramides to ceramides while phospholipids are converted to free fatty acids and glycerol ¹⁸. As the keratinocytes transition into the final cornified layer of the epidermis, membranes of the lamellar bodies fuse with the apical plasma membrane causing them to release their contents into extracellular space. One such component contained within these is omega-hydroxyceramide. This is a specialised lipid that has a particularly long fatty acid chain that can span the entire width of the plasma membrane lipid bilayer, leaving one end projecting into the cell while the other is exposed to the extracellular environment. The intracellular tails are covalently bonded to glutamine residues on the scaffold proteins of the cornified envelope which eventually leads to cells that are completely surrounded by lipids to seal the intercellular spaces and protect against water loss ^{19,20}.

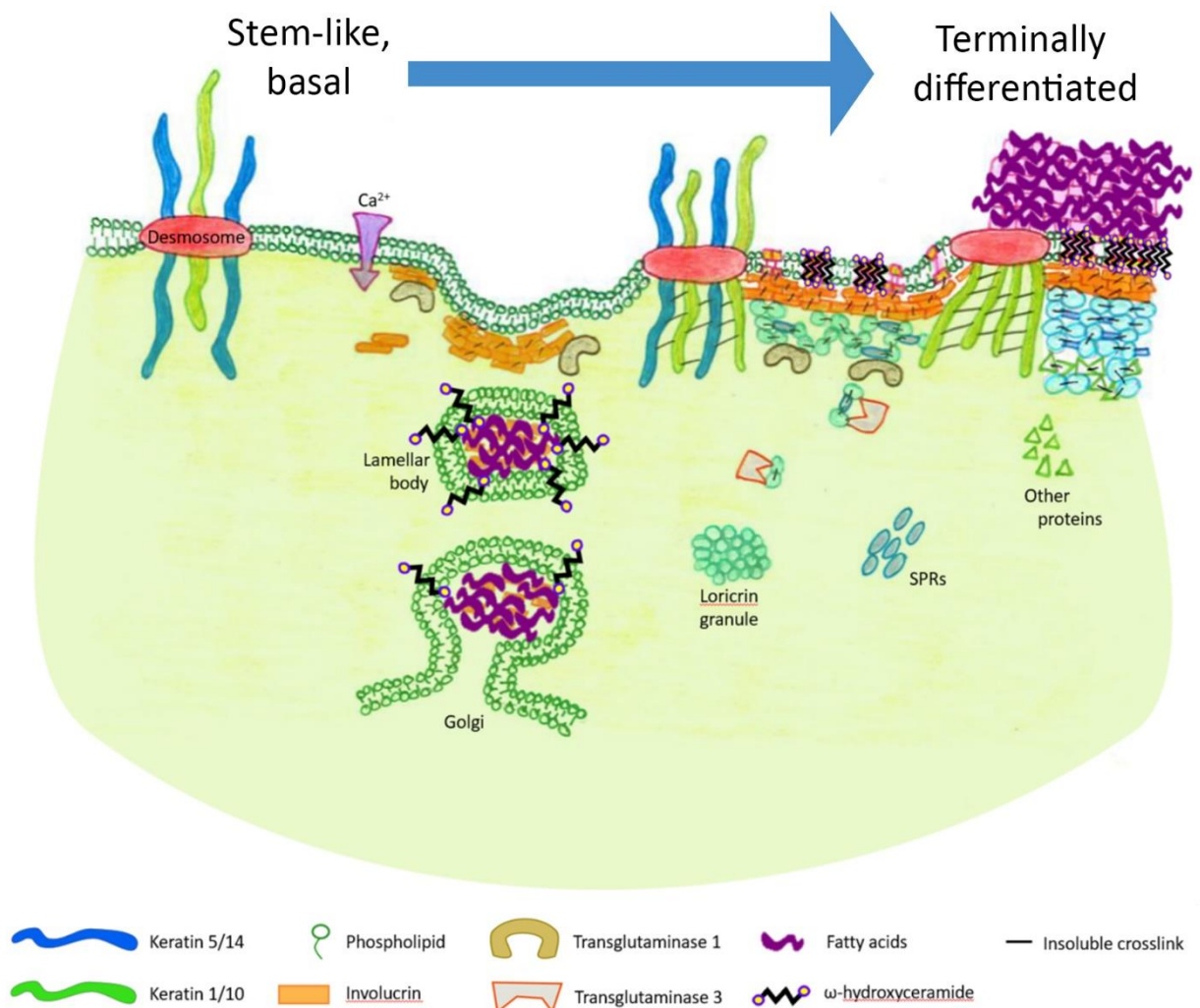


Figure 5 Assembly of the cornified envelope

Immature keratinocytes must develop into terminally differentiated cornified cells to establish the protective surface layer of the skin. This requires assembly of the cornified envelope scaffold at the inner surface of the cell membrane, achieved through the build-up of involucrin, loricrin and SPR molecules. The outer surface of the cell membrane and the extracellular spaces between keratinocytes are filled with fatty acids to create a barrier against water loss.

The final significant event that occurs during the differentiation process is the complete loss of cytoplasmic organelles, including the nucleus. It is assumed that this is to allow for higher proportions of cornified envelope proteins in each cell so that the skin barrier can be established effectively across the rigid cell layer although the mechanism by which this is achieved remains largely unknown. However, some studies

have reported an increase in lysosome-like bodies concomitant with the degradation of mitochondria, Golgi apparatus, ribosomes and endoplasmic reticulum suggesting that targeted autophagy may play a role ^{21,22}.

Once these processes are complete and the cells have acquired all the features of a terminally differentiated keratinocyte, they are considered to be dead cells termed corneocytes that populate the final, outermost, cornified layer of epidermis.

Desmosome junctions that connect adjacent cells via their keratin networks, are, at this stage, reinforced by a group of proteins that form closely packed sheets of cells that retain the integrity of the skin barrier.

However, in the interest of homeostasis, the epidermal thickness must be regulated by shedding corneocytes at the outer surface through a process called desquamation.

This requires extensive proteolytic cleavage activity to break apart the desmosome junctions which is carried out by kallikreins (KLKs), a family of serine proteases ²³. Two particular members, KLK5 and KLK7, also known as stratum corneum tryptic enzyme and stratum corneum chymotryptic enzyme respectively, are stored in lamellar bodies and released into the intercellular space where they mature and target the components of desmosomes ²⁴.

In healthy epidermis, there is a delicate balance reached between the rate of desquamation, the rate at which basal cells proliferate and the proportion of these that enter terminal differentiation. These processes must be tightly regulated to ensure that the pool of stem-like cells is not exhausted in the basal layer or that over-proliferation does not cause extensive thickening of the skin. Not surprisingly, there are many skin disorders associated with dysregulated stages of epidermal differentiation including Netherton syndrome, atopic dermatitis and psoriasis ²⁵.

1.1.3 Composition and Architecture of the basement membrane

Despite contributing only a small portion of the skins overall structure, the basement membrane provides a highly specialised interface between the epidermis and the dermis. Created by input from both the epidermal keratinocytes and dermal fibroblasts, it consists of a lamina lucida, a lamina densa and a sublamina densa fibrous zone ²⁶. Due to the abrasive, mechanical insults experienced by the skin, the basement membrane serves an important role in firmly anchoring the overlying epidermis to the underlying dermis whilst also regulating cross-talk between the two compartments. As with all basement membranes in the body, several laminins are abundant and form honeycomb-like structures that are essential for maintaining structural integrity as well as supporting keratinocyte adhesion ²⁷.

Below this laminin network lies a network of collagen IV ²⁸. Although it's not entirely clear how, these two networks must be connected together to stabilise the basement membrane. Collagen VII also plays an important part in attachment of the epidermal basement membrane to the papillary matrix of the dermis.

There are several inherited disorders caused by genetic mutations to genes encoding basement membrane proteins such as epidermolysis bullosa which causes easy blistering of the skin due to breaches in the integrity of the membrane and separation of the skins layers ²⁹. Dystrophic epidermolysis bullosa is a subtype of this disease caused by mutations to the *COL7A1* gene. Suffers usually present with complete absence or substantial reduction in collagen VII expression preventing the basement membrane from anchoring to the underlying dermis. In severe cases, mucous membranes are affected alongside the skin leading to multiple health complications including blistering of the oral cavity and tongue making feeding difficult, chronic

inflammation and infection and manifestations in the gastrointestinal tract, kidneys and heart. Patients are also prone to aggressive squamous cell carcinoma which is often the cause of premature death ¹⁷⁷.

1.1.4 Anatomy of the dermal compartment

The dermis makes up a significant portion of the skin and is composed predominantly of dermal fibroblasts alongside the extracellular matrix proteins that they deposit and remodel. Unlike the densely populated epidermis, fibroblasts in the dermis have a much sparser arrangement with most of the dermal mass coming from non-cellular connective tissue such as collagen fibres, elastic fibres, glycoproteins and proteoglycans ³⁰. The organisation of these components can be divided into two histologically distinct layers called the papillary and reticular dermis ³¹.

The papillary dermis lies directly beneath the basement membrane and is approximately 300-400um thick – this is largely dependent on factors such as age and anatomical location ³². It has a loosely arranged fine meshwork of connective tissue fibres that are spatially arranged into undulating, ridge-like structures called dermal papillae. These create a much larger interface between the epidermis and dermis to increase the opportunity for epithelial-mesenchymal interactions and maximises the surface area over which soluble molecules can be delivered to the epidermis. In contrast, the reticular dermis is much thicker with coarser, more compacted connective tissue and even fewer fibroblasts that appear to be less active.

The histological variation seen between the two layers can be attributed to differences in the composition and organisation of their extracellular matrices. While the papillary dermis has thin, poorly organised collagen fibre bundles, the reticular dermis has

stronger, better organised ones. Although both consist of type I and type III collagen, there is a higher proportion of type III in the papillary dermis ³³. The distribution of certain proteoglycans and glycoproteins can also be used to distinguish the two dermal layers. For example, decorin and tenascin-C are intensely expressed in the papillary dermis but only weakly so in the reticular dermis whereas versican shows the opposite pattern ³⁴.

Another important feature of the dermis is its vasculature system. The two dermal layers are conveniently intercepted by the subpapillary plexus which supplies blood to the upper regions of the dermis as well as the basal layers of the epidermis and can be used to demarcate the boundary between the papillary and reticular layers. Beneath this is the deeper cutaneous plexus which feeds capillaries leading to hair follicles, sebaceous glands and sweat glands. It separates the dermis from the final layer of the skin, the hypodermis.

1.1.5 Anatomy of the hypodermis

The hypodermis is a layer of subcutaneous fat made largely of adipocytes. It plays roles in thermoregulation by providing a layer of expanding insulation and in mechanical protection by cushioning the body but its primary function is to serve as an energy reserve, storing fat in a semi-liquid state composed primarily of triglycerides. In fact, it is considered by many to be two separate layers of fat that are separated by a membranous tissue layer ¹⁷⁸. The upper layer is often referred to as the superficial adipose or areolar tissue. It is formed from a stable structure of fatty lobules that are interspersed with fibrous septa made of collagen and elastic fibres that connect it to

the reticular dermis above. In contrast, the lower layer, referred to as the deep adipose or lamellar tissue, has larger, flattened and less defined fat lobules with minimal fibrous septa ^{35,36}. As more evidence emerges from this field, it is becoming apparent that the adipose tissue of the hypodermis is responsible for far more functions than previously thought. For instance, hormones and cytokines released from adipocytes have been implicated in metabolic and pathological process such as hair follicle cycling ³⁷, skin aging ³⁸ and wound healing ³⁹.

1.1.6 Skin appendages and other notable cell types

Although the previous sections have described the overall structure and key components of the skin, there are various other features and cells types that are imperative to the correct functioning of the skin.

Melanocytes are specialised cells derived from the neural crest that synthesise melanin, a ubiquitous pigment that is used to colour the skin, hair, fur, feathers and scales of many vertebrates. In the epidermis, they embed themselves predominantly within the basal layer where they use dendritic cell protrusions to contact the surrounding keratinocytes (Figure 4). Melanocytes use a modified lysosomal membrane bound compartment known as a melanosome to synthesise and store melanin granules which are then transported along microtubules to the tips of the dendrites where they are transferred to the keratinocytes and consequently pigment the skin ^{40,41}.

Langerhans cells are antigen-presenting dendritic cells that are derived from bone marrow and function as mediators between the innate and adaptive immune responses when the skin is under attack from invading pathogens ⁴². They most often reside in the squamous and granular layers of the epidermis and possess unique organelles called Birbeck granules ⁴³. The main molecular component of these granules is the C-type lectin receptor, langerin which has a suspected role in antigen uptake and internalisation ⁴⁴. Once activated, Langerhans cells migrate towards secondary lymphoid tissues where they interact with naïve T-cells to prime the adaptive immune response ⁴⁵.

Another type of cell found in the skin that is also linked to immunity as well as allergic responses, anaphylaxis and inflammation is the mast cell. These become activated by a number of different antigens, allergens, neuropeptides and lipoproteins that the skin comes into contact with from the surrounding environment. Once activated, mast cells can release a wide range of cytokines and chemokines depending on their activating cue which in turn, triggers the recruitment of immune related cells or inflammation at the site. One of these well-studied mediators is histamine which is involved in the dilation of post-capillary venules ⁴⁶, activation of the endothelium and increased blood vessel permeability – responses that lead to redness, swelling and warming of the skin typically seen after exposure to an allergen or following injury.

The body's ability to perceive pain, heat and other external stimuli brings us to another group of important cells, the cutaneous mechanoreceptive neurons that innervate the skin and the specialised cells that lie at their unmyelinated endings. There are four types of mechanosensitive cells found in the skin; Merkel cells, Meissner corpuscles,

Pacinian corpuscles and Ruffini corpuscles and these respond to acute changes at the skin's surface, allowing the body to sense stimuli such as compression, strain and stretching ⁴⁷. Through the opening of ion channels and the generation of action potentials along the mechanoreceptive neurons, the information is relayed back to the brain and appropriate action is carried out by the body.

Skin appendages are more complex structures that include things such as sweat glands and hair follicles. There are two types of sweat gland in the skin – the eccrine and apocrine- which vary slightly in their distribution and function. Eccrine sweat glands are simple, coiled tubular structures that are found extensively throughout the body, with a high density on the soles of the feet. Their primary role is in thermoregulation through evaporative heat loss but they also participate in ion and nitrogenous waste excretion ¹⁸¹.

Apocrine sweat glands, on the other hand, do not start to become active until puberty and are under the influence of sex hormones. They consist of a glomerulus of secretory tubules and an excretory duct that opens into a hair follicle. They are more restricted in their location with most being concentrated in the armpits, groin and around the nipples. They produce an oily fluid containing proteins, lipids and steroids that mixes with sebum from sebaceous glands and interacts with microbes in the skin's microflora. This results in pungent compounds that act as pheromones which many animals, including humans, use to signal to each other. They may be used as territory markers, warning signals, defence mechanisms or to attract a mate ⁴⁸. The apocrine sweat glands are sensitive to adrenaline therefore associating them with emotional sweating induced by anxiety, stress, fear, sexual stimulation and pain ¹⁷⁹.

Hair follicles are dynamic structures that begin with a hair bulb embedded deep within the dermis, extending to and merging with the epidermis. They cover the body except for the soles of the feet and palms of the hands and produce hair shafts on a cyclic basis. Hair follicles are found in conjunction with arrector pili muscles which are able to contract and cause the hairs to stand on end in response to certain stimuli.

1.1.7 Functions of the skin and complications associated with wounding

By covering the complexity of the skin in the sections above, it is clear that as the organ situated at the interface between ourselves and the outside world, the skin is essential to our overall health and wellbeing. It is the first line of defence against invading pathogens by providing a physical barrier that cannot be penetrated by microbes and plays host to a variety of resident immune cells that fend off potential infections. The extracellular matrix of the cornified layer is also enriched with antimicrobial peptides that disrupt pathogens before they can invade. Having said this, the skin does have a symbiotic relationship with a special group of commensal micro-organisms known as the normal flora of the skin and these microbes arguably form part of the skin's defence system as well. Secretions of lipids and fatty acids maintain a pH of 3-5 on the cutaneous surface which makes it inhospitable to most species but the commensal organisms have adapted to be able to survive under these conditions and make use of the shedding dead keratinocytes as a food source. They primarily protect the body by outcompeting harmful pathogenic species through their niche occupancy and competition for nutrients. They also secrete inhibitory metabolic products such as acetic and propionic acid to maintain the low pH, antibiotic

substances like penicillin and surfactants to dissolve lipid membranes or envelopes of competing pathogenic species ^{49,50}.

Ultraviolet (UV) radiation from the sun is another significant threat from the outside world that the skin protects us from. Historically, UV exposure was only considered an occupational threat for those working outside for prolonged periods of time but more recently, a rise in recreational sun exposure for cosmetic and aesthetic reasons has led to a large increase in sun related diseases ⁵¹.

UV radiation is a component of the electromagnetic spectrum and falls between the wavelengths of visible light and gamma radiation. It can be subdivided into UV-C with the shortest wavelengths (100-280nm) but highest energy, UV-B in the middle fraction (280-315nm) and UV-A with the longest wavelengths (315-400nm) but least energetic particles. Each fraction of the spectrum penetrates the skin differently, with UV-A reaching the furthest depths, affecting both the epidermis and dermis but UV-B affecting only the epidermis. The majority of UV-C is absorbed by the atmosphere before it reaches the Earth's surface so has minimal effects on the skin ¹⁸⁰.

The consequences of excessive UV exposure can be separated into acute and delayed responses. The most obvious and immediate of these is erythema (sunburn) where a large scale inflammatory response is triggered through a cascade of cytokines, vasoactive and neuroactive mediators and infiltration of inflammatory cells.

Another dangerous event that happens soon after UV exposure is the generation of free radicals in the skin. Nucleotides are highly susceptible to free radical injury because it promotes mispairing of the bases, making mutations much more likely to occur ^{52,53}. In response to this, damage signals are activated such as the induction of

p53 activity which mediates cell cycle arrest and activates DNA repair machinery to prevent the accumulation of damaged DNA and proteins in affected cells. If damage to the cells is deemed too great to repair, cell death via apoptotic pathways will remove it from the skin.

Long term effects of UV on the skin can include increased production of suppressor T-cells, induction of antigen-specific immunosuppression and a lowering of cell-mediated immunity. Collectively, this reduces the immune system's capacity to reject highly antigenic skin cancers, the most common of which are basal cell carcinoma, squamous cell carcinoma and malignant melanoma ⁵⁴.

To better protect the body from future UV exposures, the damage response signals and inflammation abate to allow for a rapid increase in keratinocyte proliferation. This leads to UV-induced hyperplasia to increase the thickness of the epidermis and reduce the level of penetration in the future ^{55,56}.

Adaptive melanisation is another protection mechanism that the skin uses following UV exposure that enables it to soak up more of the harmful UV radiation in the future. Initial skin darkening, or tanning, is due to redistribution and molecular changes to existing melanin pigment in keratinocytes which is then followed by an upregulation in the production and subsequent transfer of new melanin ⁵⁷. Interestingly, it is well documented that sunlight does have positive as well as negative effects on the skin which leads on nicely to its next function, as a synthesiser.

The majority of the world's population rely solely on sun exposure to satisfy their requirements for vitamin D despite many foods in developed countries being fortified for it and some people choosing to take dietary supplements. This is particularly true for hotter countries in the Middle East where people rely on air conditioned buildings to avoid the heat and the modest hijab dress of women in these areas meaning they do not acquire enough vitamin D from their environment.

To naturally synthesise vitamin D, the body uses 7-dehydrocholesterol molecules embedded in the skin to absorb UV-B radiation, transforming it to vitamin D₃ which is then metabolised in the liver to 25-hydroxyvitamin D₃. In its final step, it passes through the kidneys, converting it to 1,25-dihydroxyvitamin D₃ to become biologically active ⁵⁸.

Another protective role of the skin is in regulating transcutaneous water loss which is crucial in a desiccating, terrestrial environment. This function comes from the permeability barrier that is created by the cornified cell layer and various components of its extracellular matrix such as the lipids and lamellar bodies discussed previously. A delicate balance must be reached between the amount of water that is lost at the surface of the skin through evaporation and the volume of water that is retained. Due to the lack of vasculature system in the epidermis, cells at the outer surface rely on water gradients to retain enough moisture to ensure that they don't become too brittle and can maintain their mechanical flexibility ⁵⁹.

This section highlights just a few of the skin's key roles in keeping us alive so when it becomes compromised through events such as burns, lacerations or blistering, our barrier to the outside world is undermined and can cause a plethora of problems.

When the skin is wounded, the body tries to mitigate the damage as quickly as possible by re-establishing its integrity and sealing the skin barrier once more. This is, however, a complicated process, calling upon many different signalling pathways to orchestrate effective, timely wound healing.

1.2 The pathophysiology of wound healing

1.2.1 An introduction to wound healing

A wound can be defined as damage that causes disruption to the normal anatomy of the skin and impairs its function in some way. They can vary from superficial wounds that affect only the surface of the skin, such as everyday grazes and scratches or more severe injuries that extend into the subcutaneous tissue and are associated with damage to other structures such as tendons, blood vessels, muscle and nerves ⁶⁰. The healing process brings together a variety of cell types, originating from within the skin as well as surrounding tissues and even distant sites. There is considered to be four main phases during wound healing but these merge seamlessly into each other to create an elegant repair system. It begins with coagulation and haemostasis, initiated immediately after injury to stem blood loss and plug the wound bed. The inflammation phase follows shortly after this, recruiting necessary immune related cells to the wound site to prevent infection which then leads on to the proliferative stage. Here, cells depart from a highly proliferative zone at the wound border by directionally dividing towards the wound bed while collectively migrating to replace the damaged epidermis. The final stage of wound healing is the remodelling phase which encompasses extensive structural rearrangements, predominantly in the dermal compartment, to fully restore the skins functions ⁶¹. Each of these phases are discussed in more detail in the following sections.

1.2.2 The haemostasis phase

Almost all cutaneous wounds will involve damage to blood vessels in the skin so the body's immediate response is to protect the vascular system and prevent exsanguination. This halts excessive blood loss and ensures that the blood supply to other vital organs is not interrupted. The neuronal reflex mechanism plays a key part in this. Upon recognising injury, rapid constriction of the smooth muscle layer surrounding blood vessels is triggered to restrict blood flow at the wound site. This is a temporary response that lasts only few minutes and is soon overridden by increasing hypoxic and acidic conditions that cause the passive relaxation of the muscle and blood flow to resume ⁶² (Figure 6, part 2).

The body therefore requires a more long term solution to plug the wound site while the healing process progresses and this comes in the form of a clot. The majority of components in the clot are proteins that are delivered to the site through the blood. This includes platelets which assemble onto a network of cross-linked fibrin fibres together with fibronectin, vitronectin and thrombospondin to fill the wound ⁶³. As well as temporarily restoring the skin barrier by creating a shield against pathogens, the clot also provides a matrix over and through which cells can migrate during subsequent stages of the healing process ⁶⁴ (Figure 6).

Platelets are a specialised type of cell that have no nucleus and are instead, fragments of cytoplasm that bud off from megakaryocytes in bone marrow ⁶⁵. They are an important source of cytokines, chemokines and growth factors that are released as

activated platelets degranulate and are amongst the first signalling cues to recruit necessary cells to the site and promote the next steps of wound healing.

Of the granules released by platelets, α -granules are the most common. They contain platelet derived growth factor (PDGF) which is chemotactic for macrophages and promotes fibroblast proliferation ⁶⁶ as well as epidermal growth factor (EGF) which promotes keratinocyte proliferation ⁶³. Other α -granule components include CXC chemokine ligands (CXCL's), platelet factor 4 (PF4) and transforming growth factor- β (TGF- β) that are involved in recruiting inflammatory cells, promoting keratinocyte migration and synthesis of fibroblast matrix ⁶⁷.

Dense granules are smaller and less abundant than α -granules and contain adenosine diphosphate, serotonin and polyphosphate which stimulate further recruitment of platelets and promote their aggregation ⁶⁸. Serotonin also causes vasodilation and increased vascular permeability, enhancing fluid extravasation to aid in the next stage of wound healing ⁶⁹ – the inflammatory phase.

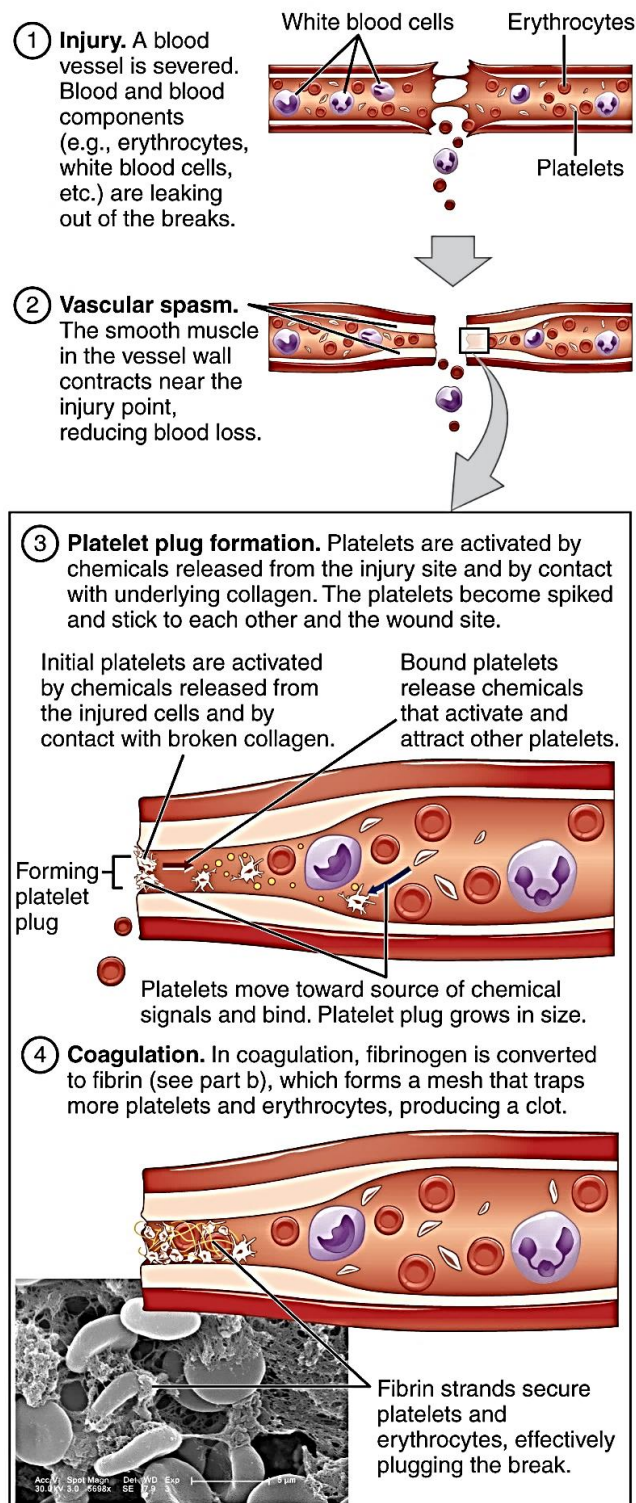


Figure 6 The haemostasis phase of wound healing

The immediate response to injury is to reduce blood loss. Smooth muscle fibres in severed blood vessels at the wound site briefly constrict to stem blood flow followed by the formation of a fibrin clot to plug the wound until properly repaired.

Diagram adapted from Anatomy and Physiology, Chapter 18. The Cardiovascular System: Blood, Section 18.5 Hemostasis.

<https://opentextbc.ca/anatomyandphysiology/chapter/18-5-hemostasis/>

1.2.3 The inflammatory phase

The primary aim of the inflammatory phase is to prevent infection in the wound bed and can be divided into two separate stages. The early stage occurs almost concurrently with the final steps of coagulation and is characterised by the infiltration of neutrophils. These are white blood cells that follow various chemotactic gradients released at the wound site and arrive within 24 hours of injury. Due to changes that occur in the surface adhesion molecules of endothelial cells that line capillaries at the wound site, these neutrophils begin to be extracted from the circulating blood ⁷⁰. The first of these to be expressed are members of the selectin family which mediate rapid but relatively weak adhesion to neutrophils to draw them out of circulation ⁷¹. The weak attachments cause the neutrophils to roll along the surface of the endothelium, being pushed forward by the flow of blood. A stronger adhesion system is soon activated, mediated by the $\beta 2$ class of integrins, which arrests the movement of neutrophils, instead causing them to migrate between the endothelial cells and out of the blood vessels into the extravascular space in a process known as diapedesis ⁷². They now form part of the wound environment and begin the important task of phagocytosis to rid the site of bacteria, foreign particles and damaged tissue by releasing proteolytic enzymes and oxygen-derived free radical species ⁷³. Neutrophils are, however, relatively short lived and their demise marks the end of early inflammation. To make way for the late inflammatory stage, the expended neutrophils must be eliminated from the wound. They are extruded to the surface where they undergo apoptosis, with the resultant apoptotic bodies being phagocytosed by macrophages ⁷⁴.

Macrophages are phagocytic cells that begin life as blood-borne monocytes. Upon arrival at the wound site, they undergo phenotypic changes and differentiate into tissue macrophages to take over from neutrophils in clearing the wound of pathogens and cell/matrix debris. Their appearance indicates the start of the late inflammatory stage. Once activated, macrophages also release a barrage of growth factors and cytokines including TGF- β , FGF and TGF- α to amplify earlier signals that activate proliferation and migration of keratinocytes, fibroblasts and endothelial cells ⁷⁵. In situations where macrophage activity is impaired, wounds often fail to heal effectively due to poor wound debridement, delays in fibroblast proliferation and inadequate fibrosis.

1.2.4 The proliferative phase and re-epithelialisation

Once the immediate threats of blood loss and infection have been dealt with accordingly, the healing process shifts towards tissue repair, replacing the damaged skin with newly synthesised extracellular matrix in the dermis and restoring the epithelial layer of keratinocytes across the surface. This phase is initiated approximately three days after injury and can last around two weeks depending on the extent of damage ⁶¹.

The array of stimulating factors that have been secreted into the wound site up to this point cause a surge in proliferation of fibroblasts at the periphery which then migrate into the wound across the scaffolding provided by the fibrin clot. Here, they begin rapid production of extracellular matrix components that include hyaluronic acid, fibronectin, vitronectin, proteoglycans, collagens I-IV, laminin and thrombospondin, gradually forming granulation tissue to replace the lost dermis ⁷⁶. At the same time,

the fibroblasts produce various matrix metalloproteinases (MMPs) to degrade the clot as the new tissue replaces it.

The presence of TGF- β , released by macrophages in the wound, stimulates the differentiation of fibroblasts into myofibroblasts. These are specialised contractile cells that begin to express stress fibres and α -smooth muscle actin (α -SMA) ⁷⁷. They use these to create lamellipodia that project out into the extracellular matrix and attach to fibronectin and collagen via cell-matrix adherins ⁷⁸. As these cell extensions retract back, they cause the wound to contract, drawing the edges in towards one another to promote closure ⁹⁴.

Restoration of the epidermal layer requires proliferation and migration events as well as a series of molecular changes within the keratinocytes. Under normal conditions, keratinocytes are linked to one another through hemidesmosomes and anchored to the basement membrane through $\alpha 6\beta 4$ integrin attachment to laminin. To allow keratinocytes at the leading edge of the wound to migrate, the hemidesmosome attachments have to first be dissolved to free them from the surrounding healthy tissue. They also alter their integrin expression by upregulating $\alpha 5\beta 1$, $\alpha \nu \beta 6$ and $\alpha \nu \beta 5$ to enhance their ability to grasp hold of and crawl across fibronectin, tenascin and vitronectin in the newly synthesised granulation tissue respectively ^{80,81}.

In a similar fashion to the migrating fibroblasts, the collection of keratinocytes at the leading edge of the wound produce proteases to cut a path through the wound bed, dissolving the fibrin clot as they migrate. The chief fibrinolytic enzyme at play here is plasmin.

Initial migration of cells at the leading edge alone is not sufficient to achieve complete re-epithelialisation so must be coupled with a burst of proliferation that occurs in the

region of keratinocytes just behind the leading edge to replace damaged cells lost during injury. Further reinforcements of epidermal cells also come from hair follicle stumps that are left intact at the wound border, highlighting how the skin calls upon cells from a multitude of sources to speed up the rate of healing ⁶³.

Once a monolayer of keratinocytes has been established, contact inhibition sends signals to cease proliferation and migration whilst differentiation and stratification is activated. The underlying basal lamina is gradually re-established from the periphery inwards with hemidesmosomal junctions being reformed ⁸². The re-epithelialisation process culminates in a fully stratified epidermis being restored across the wound.

1.2.5 Mechanisms of cell migration and cytoskeleton rearrangement

As discussed above, migration into the wound bed is predominantly governed by chemotactic agents that instruct cells to move in an orchestrated, directional manner that relies heavily on rearrangements in the actin-rich cytoskeleton. The complex process can be split into three distinct steps. The first requires protrusion at the front of the cell, towards the wound bed, which is coupled with the second step, adhesion, where the actin cytoskeleton attaches to the underlying wound bed matrix via focal adhesion points. The final step is traction where the trailing cytoplasm is propelled forward ⁸³.

Protrusion occurs in response to chemotactic gradients sensed by cell surface receptors that trigger polymerisation of actin filaments at the leading edge, where the gradient is felt most strongly. This pushes the plasma membrane outwards into a lamellipodia that is filled with filamentous actin ⁸⁴. This event is perpetuated through

cyclic assembly and disassembly of actin filaments in front of and well behind the leading edge respectively, to continue the unidirectional movement.

During the traction phase, contractile forces that are transmitted through the integrin-cytoskeletal connections allow the cell to pull the cytoplasm forward by generating traction to the substratum. The force needed for this is provided by myosin motor proteins that interact with the actin bundles (Figure 7).

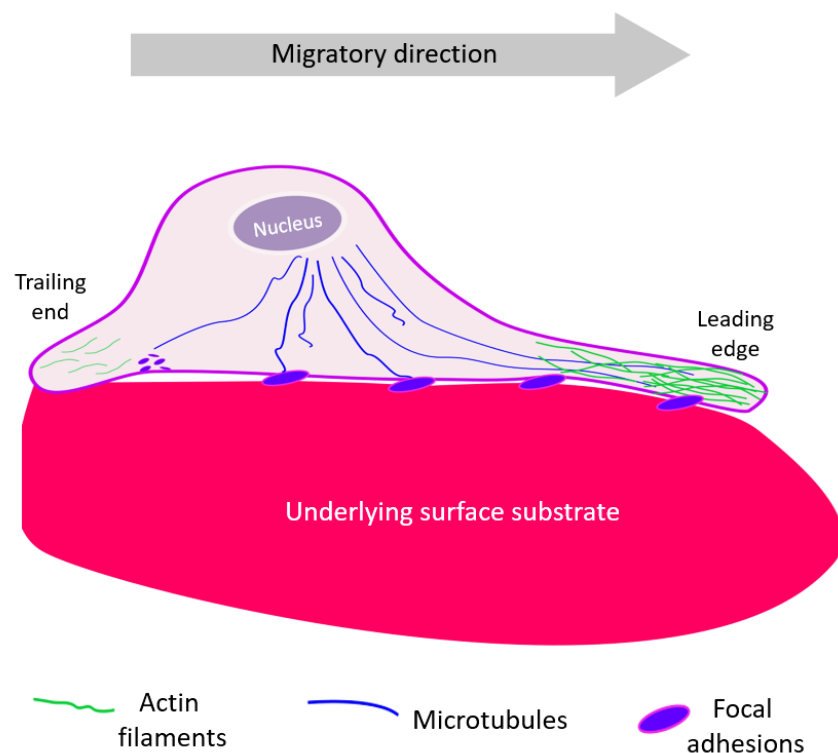


Figure 7 Cytoskeleton rearrangements in a migrating cell

Cell migration begins with polymerisation of an actin network that forms at the cells leading edge in response to chemotactic signals. A lamellipodia is created as the cells membrane is pushed outwards across the underlying matrix. This is accompanied by the turnover of focal adhesions which generate newly formed contact points as the cell continues to move forward. Contractile forces behind the leading edge create traction against the surface of the substrate beneath to drive a forward motion. Focal adhesions and actin filaments at the trailing edge disassemble to maintain the migratory direction.

1.2.6 The remodelling phase and angiogenesis

As new granulation tissue is laid down in the wound bed, the skin's vasculature system needs to be reconstructed to re-establish its blood and nutrient supply. Delays in this occurring lead to prolonged hypoxic conditions in the tissue and poor healing outcomes as a result ⁸⁵. The process of angiogenesis requires three key players; fibroblast growth factor -2 (FGF-2), vascular endothelial growth factor (VEGF) and tumour necrosis factor - α (TNF- α). These, together with the initial hypoxic environment of the wound bed, promote increased plasmin levels which, in turn, facilitates proliferation and migration of endothelial cells at the raw ends of severed capillaries ⁸⁶. As VEGF is crucial to angiogenesis, it is released from a variety of cells during wound healing, including keratinocytes, platelets, neutrophils, macrophages and fibroblasts ⁸⁷⁻⁸⁹. The activated endothelial cells assemble themselves into tube like structures that sprout off from the parent blood vessel and infiltrate the new granulation tissue to support its survival.

The early stages of wound healing are very good at providing a rapid response to protect the body from further damage but in its haste to plug the injury, the resultant granulation tissue is disorganised and has a relatively weak tensile strength compared to healthy skin. In order to restore some finesse to the situation, the final stage of wound healing is a much longer, dynamic phase that remodels the wound matrix for up to a year or more after injury.

Most of the responses initially activated upon wounding begin to wind down and cease with many endothelial cells, macrophages and fibroblasts exiting the site or being removed through apoptosis, returning the cell number to a normal level ⁹⁰.

This leaves behind a tissue mass consisting mainly of collagen and other extracellular matrix components mentioned previously that gradually get rearranged and altered in strength and form until it becomes scar tissue. A delicate balance is struck between the rate of collagen synthesis and collagen removal which facilitates a gradual change from a collagen III rich tissue, which is quick to produce and deposit in early healing, to predominantly collagen I which has a much higher tensile strength but is more costly to produce^{91,92}. The dynamic equilibrium between degradation and synthesis is controlled by the action of MMPs and tissue inhibitors of metalloproteinases (TIMPs) respectively. Eventually, over a few months, the balance tips in favour of TIMPs, inhibiting the degradative action of MMPs and promoting higher rates of collagen deposition⁹³. Bundles of collagen I fibres become thicker, much more organised, oriented and cross-linked over time, restoring the skin to approximately 80% of its unwounded strength.

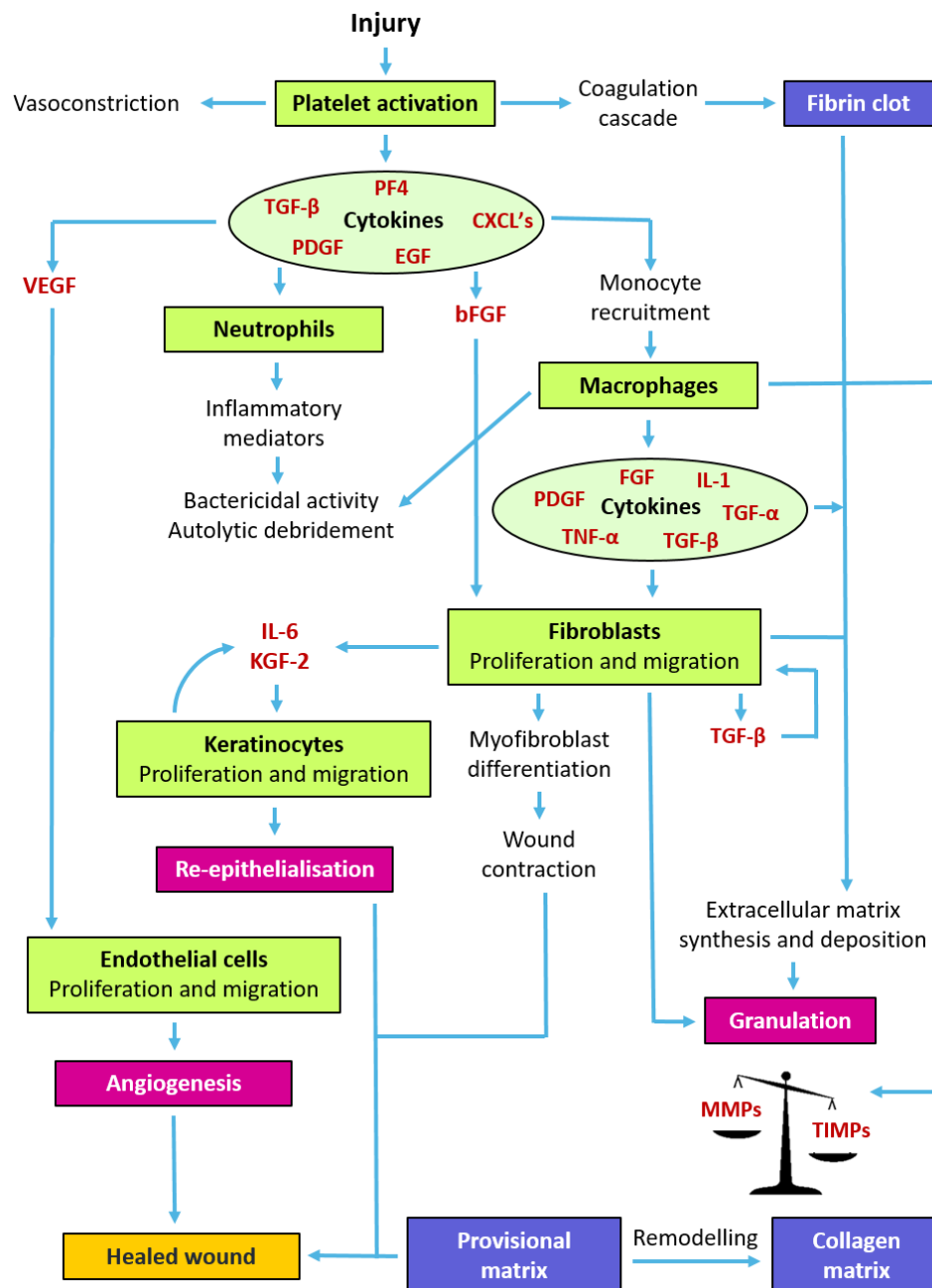


Figure 8 Sequential diagram showing molecular interactions during wound healing

The wound healing process encapsulates responses from a range of cells in the surrounding environment. For repair to be achieved effectively, several different signalling cascades are needed, many of which involve cytokines released by cells that are recruited to the site during the early stages of repair.

Diagram adapted from Mendes & Neves, 2012⁹⁴.

1.2.7 Complications associated with aberrant wound healing

Although the skin has remarkable healing abilities and the vast majority of wounds will resolve without excessive intervention, there are unfortunately cases where complications in the healing process can arise.

One such example is when a wound becomes chronic in nature. This can be caused by a range of complex factors that usually impede the rate of healing, with many chronic wounds being stalled in a prolonged inflammatory state ²⁰³. These types of wound are often associated with patients already suffering from underlying health conditions such as diabetes mellitus where a seemingly minor injury can quickly become a non-healing ulcer that is predisposed to infection and may even become gangrenous and require amputation ²⁰³. It is estimated that at least 25% of diabetes patients will experience complications from ulcers in their lower extremities ²⁰⁴. One of the main factors responsible for their prevalence is a reduced sensitivity in the lower leg and foot due to neuropathy and ischemic conditions caused by microvascular disease. This reduced sensitivity allows repeated trauma or mechanical stress to be applied to the limb without the patient experiencing the associated pain thus resulting in more frequent wounds ²⁰⁵. Hyperglycaemia; the hallmark symptom of diabetes mellitus, has been postulated to then hinder the healing of these wounds by indirectly inducing inflammatory molecules, interfering with collagen synthesis, decreasing cell proliferation and causing abnormal differentiation of keratinocytes ^{206, 207}.

Pressure ulcers or bed sores are another prevalent group of chronic wound characterised by progressive and deepening damage to skin and the soft tissue beneath. They are most likely to affect immobilised patients that are chair or bed

ridden through age related frailty or those suffering paralysis as a result of spinal-cord injury. Pressure ulcers develop over a prolonged period of continuous pressure concentrated in specific regions of the body, most often occurring at bony prominences which become accentuated by gradual atrophy of soft tissue when patients spend extended time in an immobile state. When this pressure exceeds the pressure within blood vessels, it leads to cessation of blood flow to the skin and surrounding tissue, causing localised ischaemic conditions to develop ²⁰⁸. Occlusion of lymphatic vessels can also arise which causes anaerobic waste products to accumulate in the affected area and contributes to tissue necrosis at the ulcer site ²⁰⁹.

Pressure is frequently accompanied by a shearing force or friction caused by the patient's inability to control gravitational shifts in their body weight. For instance, a patient may be placed in an upright, seated position in the morning but find themselves slumped against their pillows by the afternoon. The friction generated between the body's surface and the bed sheets beneath cause abrasion to the layers of epidermis in an already weakened region of skin ²¹⁰.

The pathophysiological changes related to skin aging also contribute to increased susceptibility to pressure ulcers in the elderly. Rete ridges at the dermal-epidermal junction begin to flatten and become thinner with age causing a reduction in the surface over which the epidermis can anchor to the dermal compartment. This weakens this skin making it less able to withstand shearing forces ²¹¹.

An increased presence of senescent cells in the dermis causes the structure and composition of its extracellular matrix to be poorly maintained ²¹². The volume of

dermal space occupied by collagen declines rapidly with age, as does its density, fragmentation and the proportions of different collagen types ²¹³. Additionally, the overall elasticity of the skin reduces, its tensile strength weakens and the tissue becomes stiffened ²¹⁴.

The combined effect of these factors hinder the migratory ability of healthy keratinocytes and fibroblasts in elderly patients. The altered extracellular matrix provides fewer focal adhesion sites which restricts the frequency of interactions between cells and dermal substrate ²¹⁵. The rate of migration is therefore slower compared to younger skin and the area of damaged tissue around the pressure ulcer is not repaired as efficiently. Adding to this, age-related changes to dermal architecture causes a reduced capacity to generate the tensile forces needed to promote contractile closure of an open wound.

Other forms of aberrant wound healing can arise during the more advanced stages of the repair process where the remodelling phase is dysregulated. This is particularly important in cases of pathological scarring such as hypertrophic or keloid scars that result in an excessive build-up of fibrous tissue. In the worst cases, tissue can build up beyond the initial wound margins and begin to resemble a benign tumour that will require further treatment. Such scarring can cause other health complications including reduced mobility when located near joints and reduced peripheral sensory perception in hands and feet ¹⁷⁶.

These conditions are understood to develop through a pathological persistence of wound healing signals where fibroblasts at the wound site remain in an active state and continue to deposit vast amounts of ECM components without initiating the

counteracting degradation process that would normally occur as part of the natural remodelling phase.

1.2.8 The global impact of cutaneous wounds and current developments in wound care strategies

The combined burden of acute and chronic wounds is estimated to cost the NHS billions of pounds a year ¹. Vast amounts of resources and time are pumped into the system to ensure healthcare workers can provide adequate wound care to their injured patients. If this is extrapolated onto a global scale, it reveals the huge financial impacts that wound healing can have worldwide.

With both an ever growing and rapidly aging population across much of the developed world, this situation is inevitably going to get worse ²¹⁶. These factors bring with them increasing incidences of obesity, diabetes and age-related diseases which will serve only to exacerbate an already struggling healthcare system.

Another worrying consideration in the field of wound care is the increased emergence of resistance to routinely used antibiotics ²¹⁷. An injury that currently presents itself as a very minor graze may potentially have catastrophic consequences in the future if infection is free to ravish the wound.

It is therefore not surprising that the wound healing field attracts a broad range of research topics in a bid to address growing pressures placed upon healthcare settings. A large proportion of these focus on clinical aspects of wound healing like reducing

pain and inflammation or limiting the risk of infection while other areas try to improve wound care strategies by developing novel tools such as wound dressings. The overarching aim of each research topic is to enhance recovery times meaning that injuries heal sooner with a lower chance of complication, time spent in hospitals is reduced and ultimately, the burden on the healthcare system is lifted.

The last few decades have seen huge technological advances in the type of treatments available in wound care, particularly for extensive injuries that would once have been life threatening.

The immediate risk following injury is blood loss and infection but there is now a wide variety of haemostats available to promote the haemostasis phase at the wound site. Some of these have been developed as active agents containing fibrinogen and thrombin that play an active role in promoting coagulation and formation of the clot^{218, 219}. They are particularly valuable in treating patients with spontaneous or drug-induced coagulation disorders²²⁰.

Mechanical hemostats are another group of treatments developed to stem bleeding. Whilst not biologically active themselves, they facilitate platelet activation and aggregation by forming a matrix at the wound site which also promotes the patient's own clotting processes through production of endogenous fibrin²²⁰. They often contain materials such as porcine gelatin, oxidised cellulose, bovine collagen or plant derived polysaccharides to create a suitable matrix material that can be administered to the wound^{221, 222}.

Jin Zhou and colleagues have devised an incredibly elegant solution to tackle wound infections and overuse of antimicrobial agents. They have created a theranostic, bacterial-responsive, intelligent dressing that can respond to the microbiological environment of the wound by detecting changes in pH, bacterial toxins or the presence of particular enzymes. It is capable of distinguishing pathogenic species from skin commensals and will then release appropriate antimicrobials into the wound only when required. This strategy will greatly reduce the use of broad-spectrum antibiotics when not necessary, playing an important role in preventing widespread resistance ²²³.

Another development in wound care strategy is based upon the recent discovery that healthy skin tissue has a natural electrical potential of approximately 10-60mV between its epidermal and dermal layers ²²⁴. The movement of sodium ions through epidermal ion transport channels causes frequent depolarisation and then repolarisation of the skin cells. When injury disrupts a portion of the epithelium, the system breaks down and the electrical potential is lost locally whilst the surrounding healthy skin continues to transport ions as normal. The diminished presence of sodium ions in the wound bed causes the electrical field to shift into the lateral plane where the surrounding healthy tissue has a much higher positive charge compared the more negative injury site (Figure 9). Clinical studies have shown that the voltage difference between damaged and undamaged skin can be as large as 150mV/mm ^{226, 227}. These endogenous currents act as electrostatic cues to help guide migrating cells towards the wound bed. In studies where the endogenous electrical field could not be established, wound healing occurred at a rate 25% slower than average ²²⁸.

As a result of these discoveries, numerous electrical stimulation devices have been incorporated into wafer thin wound dressings. They heighten the effect of the electrical field across the injury site to accelerate migration and wound closure.

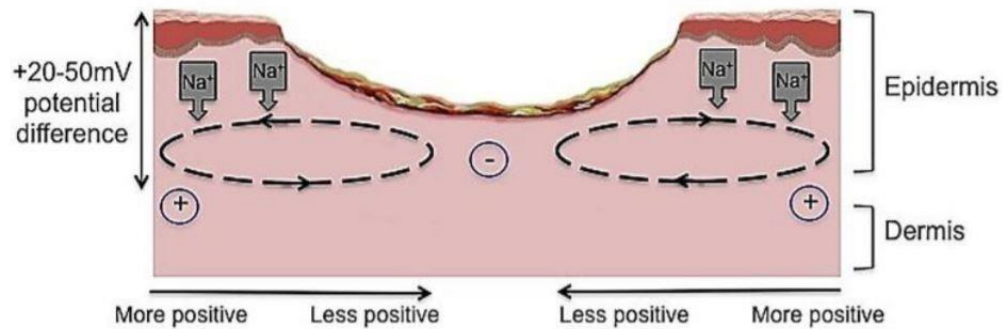


Figure 9 The transcutaneous electrical potential of damaged and undamaged skin

Uninjured human skin has an endogenous electrical potential created by the movement of sodium ions through Na^+ / K^+ ATPase pumps in the epidermis. Cutaneous injury, and therefore localised disruption to the electrical field, causes the current to redirect itself across the lateral plane where the wound edges have a higher positive charge compared to the more negative wound bed. This acts as an electrostatic cue to help initiate cell migration towards the wound bed.

(Image taken from ²²⁵)

The principle events of wound healing have been known about for decades but we owe many of the newer wound healing strategies to recent discoveries made on the finer molecular details of the healing process. In order to continue advancing the treatment options available to the healthcare system, we need to delve deeper into understanding the molecular pathways and interactions that occur during each stage of wound repair and how they are orchestrated within the system. By continuing to dissect the processes involved, we may be able to highlight novel targets to be investigated for drug based therapies that will go some way in improving wound care strategies.

1.3 Wnt signalling pathways

A huge number of signalling pathways are activated in response to injury. One of particular interest to this study is initiated by a group of molecules called Wnt proteins; a large family of cysteine-rich secreted glycoproteins of which there are 19 encoded by the mammalian genome. These Wnt ligands bind to and activate a specific family of transmembrane receptors called Frizzled (Fzd)⁹⁵. There has currently been 10 distinct Frizzled receptors identified in humans which means that, together with the 19 known Wnt ligands, there is a vast number of different interactions that can occur between the two families. Although there is some functional redundancy amongst the pairings, literature suggests that distinct ligand-receptor compositions can activate different intracellular signalling pathways in a tissue and context dependent manner.

When Wnt1, 3a or 8 is present and binds to Fzd via specific co-receptors, the canonical pathway is activated which causes cytoplasmic β -catenin to be translocated into the nucleus where it triggers transcription of target genes⁹⁶.

Alternatively, when Wnt5a or 11 is present, the non-canonical Planar Cell Polarity (PCP) pathway is initiated which activates c-Jun N-terminal kinase (JNK) and leads to small GTPase activation, cell polarity, cytoskeletal remodelling and cell migration.

The third signalling cascade that is activated through interactions between Wnt and Fzd is the non-canonical Wnt- Ca^{2+} pathway which is responsible for releasing Ca^{2+} from intracellular stores thus activating effectors that regulate transcription of genes controlling cell fate and migration⁹⁷.

Both the canonical and non-canonical branches of Wnt signalling play roles in normal embryonic development and homeostasis of adult skin. These roles and the mechanisms by which the pathways act are discussed in the following sections.

1.3.1 The canonical Wnt / β -catenin signalling pathway

Of the three branches, Wnt/ β -catenin signalling is by far the best characterised pathway. In the absence of Wnt ligands, a destruction complex residing in the cytoplasm targets free β -catenin molecules, phosphorylates them and subsequently triggers their demise through ubiquitin-mediated proteasomal degradation. This tertiary destruction complex consists of axin, adenomatous polyposis coli (APC), casein kinase 1 (CK1) and glycogen synthase kinase 3 beta (GSK3 β).

When Wnt signals are available in the environment, the Wnt ligands bind to Frizzled receptors via LRP co-receptors to suppress the kinase activity of GSK3 β . This inhibits the phosphorylation of β -catenin and prevents its destruction allowing it to accumulate in the cytoplasm before translocating to the nucleus. Here, it associates with the transcription complex of LEF/TCF to drive expression of target genes (Figure 10) ¹⁶⁷.

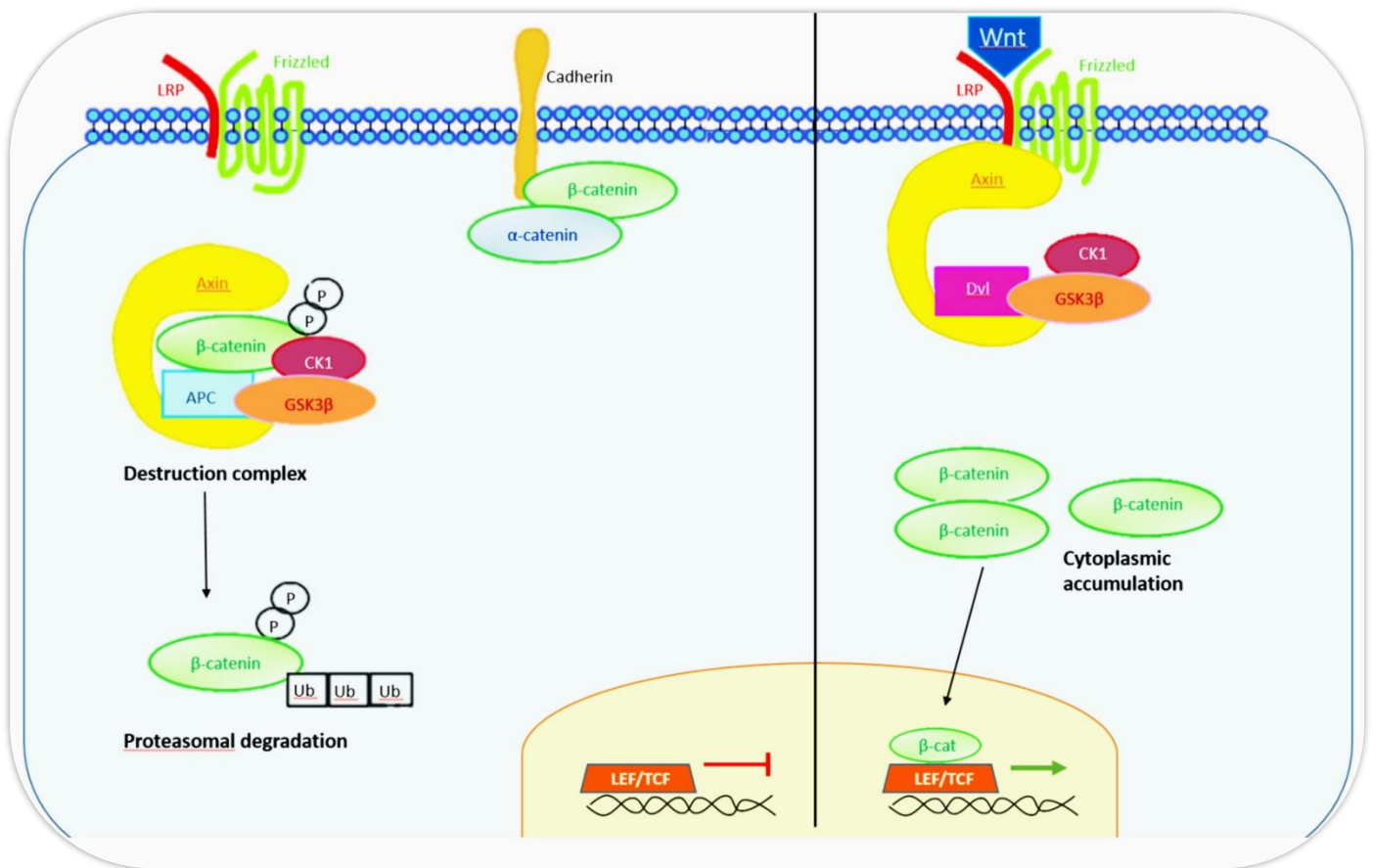


Figure 10 The molecular pathway of canonical Wnt/β-catenin signalling

In the absence of Wnt ligands (i.e. the 'Wnt Off') state, the destruction complex, a tertiary complex formed by axin, APC, CK1 and GSK3β, phosphorylates free β-catenin molecules in the cytoplasm which subsequently causes its ubiquitin-mediated proteasomal degradation. When Wnt signals are present in the extracellular environment (i.e. the 'Wnt On' state) ligands bind to Frizzled receptors along with the LRP-co-receptor to suppress the kinase activity of GSK3β. This prevents phosphorylation of β-catenin allowing it to accumulate in the cytoplasm and then translocate into the nucleus where it associates with the transcription complex LEF/TCF to mediate Wnt-triggered gene activation. β-catenin can also be stabilised at adherens junctions through association with E-cadherin and α-cadherin.

1.3.2 Canonical Wnt signalling in the skin

Wnt/ β -catenin signalling plays an essential role in determining various features of the skin, even before we are born. During embryogenesis, the fate of ectoderm tissue is governed by Wnt signalling where it determines which regions develop into the epidermis and which become part of the nervous system ^{111 112}.

Once ectodermal cells commit to an epidermal fate, it is understood that Wnt ligands then act as an autocrine stimulus to promote extracellular calcium-induced keratinocyte differentiation by coupling with the Wnt/ β -catenin pathway to create stratified layers of epidermis later in development ¹⁶⁸.

As the embryo continues to grow, Wnt signalling plays a pivotal role in hair follicle formation and maturation to such an extent that it is considered to be the master regulator. In what has become the newly formed dermal compartment, fibroblasts receive a widespread epidermis-derived Wnt signal which gets converted to a dermal-derived Wnt signal and mirrored back to the overlying epidermis. This induces aggregation in epidermal basal cells at regularly spaced intervals leading to the formation of hair placodes. In turn, the developing placode sends out further Wnt signals to induce underlying fibroblasts to form a dermal condensate that will subsequently mature into the dermal papilla. The hair placode continues to grow and invaginate down into the dermis until it meets the dermal papilla, joining to form a complete hair follicle from which a hair shaft protrudes ^{169, 170}.

Wnt signalling continues to be important into adulthood where it plays crucial roles in controlling the hair follicle cycle. Similar morphogenic Wnt signals are believed to support the onset of anagen; the active growth phase that regenerates a new hair shaft.

1.3.3 The non-canonical Planar Cell Polarity pathway

The PCP branch of Wnt signalling is not as widely studied but also has significant roles in the skin. The establishment and maintenance of its molecular pathway fundamentally relies upon the tissues ability to sense directional cues, often in the form of morphogen gradients, which cause the molecular components of its signalling pathway to position themselves asymmetrically and for this arrangement to be radiated into neighbouring cells and throughout the tissue. These cues come in the form of Wnt ligands and are detected by a group of transmembrane receptors that include Cadherin EGF LAG seven-pass G-type receptor (Celsr), Van Gogh –like (Vangl) and the previously mention Frizzled. These, in turn, are associated with intracellular components of the pathway; Dishevelled-like (Dvl), Ankyrin Repeat Domain-Containing Protein 6 (Ankrd6) and Prickle (Pk). Together, these six highly conserved molecules are considered to be the core PCP components and are activated predominantly by Wnt ligands secreted into the environment ¹⁰².

The receptors typically form complementary domains at opposing apical junctions within a cell. At the proximal side of the plasma membrane, the seven-pass Fzd receptors create a complex with the intracellular scaffolds Dvl and Ankrd6 while the opposing side of the membrane is marked by the tetraspanin Vangl receptor and the intracellular scaffold Pk. Correct localisation of the two complexes is maintained by intracellular antagonism between them as well as intercellular interactions between the opposing complexes on adjacent cells ¹⁰³. Both sides of the membrane are enriched for Celsr which form homodimers between themselves on neighbouring cells (Figure 11).

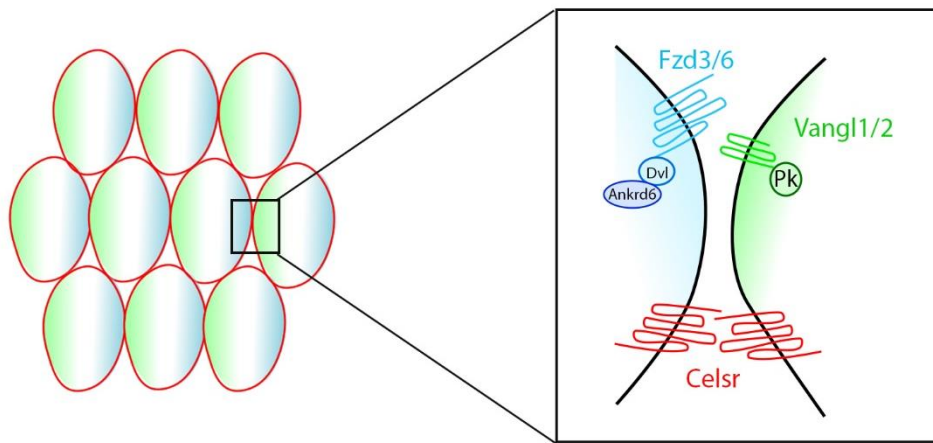


Figure 11 Arrangement of PCP components in polarised epithelial cells

Receptors of the PCP pathway and their associated intracellular components become localised to distinct positions at either side of a polarised cell. Intercellular interactions that occur between opposing receptor complexes on neighbouring cells allow the polarised distribution of PCP components to be perpetuated through a tissue.

The widely accepted model of PCP states that upon extracellular binding of Wnt5a or Wnt11 to Fzd, a signal is transduced to Dvl, leading to its activation. Dvl can then initiate two parallel pathways that activate the small GTPases Rho and Rac^{105,106}. To activate the Rho pathway, Dvl forms a complex with Dishevelled associated activator of morphogenesis 1 (Daam1) which then creates a cascade of activation from Daam1, through Rho via at least one Rho guanine exchange factor. This leads to activation of Rho-associated protein kinase (ROCK), which phosphorylates myosin phosphatase and the regulatory light chain on myosin II to increase actin-myosin contractility^{107,108}. The resultant effect on the cell causes disassembly of focal adhesions and retraction of the cells trailing end whilst promoting cytoskeletal rearrangements and protrusion at the leading edge¹⁰⁹. These events are critically important in facilitating directional

migration in motile cells. To activate the Rac pathway, Dvl stimulates JNK activity and leads to similar mechanisms of cytoskeletal rearrangement.

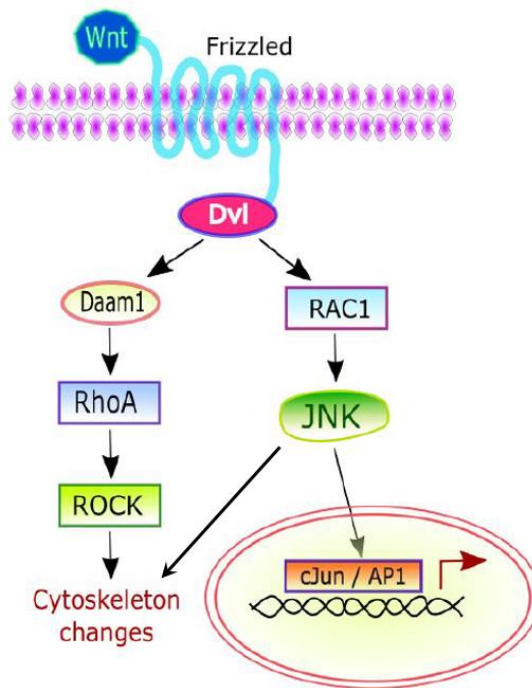


Figure 12 The molecular pathway of non-canonical Wnt signalling: The Planar Cell Polarity pathway

The PCP pathway is regulated through the interaction of specific Wnt ligands with Frizzled receptors. This activates the intracellular Dishevelled protein which subsequently initiates two signalling cascades to cause a variety of cytoskeletal rearrangements and upregulated expression of downstream target genes.

It has recently emerged that ROR2, a member of the Ror-family of receptor tyrosine kinases, is also capable of acting as a receptor or co-receptor for Wnt5a and can activate the PCP pathway in a similar manner to Frizzled associated induction. Much of this recent research has looked at the role ROR2 plays in regulating PCP, directing cell migration and mediating epithelial-mesenchymal interaction during developmental morphogenesis but its importance in postnatal tissue is also beginning to gain interest.

The contribution of Vangl2 to PCP is less understood but some evidence has suggested that the extracellular region, particularly the cysteine rich domain, interacts at a molecular level with Frizzled receptors. This interaction allows cells to sense Frizzled expression levels and activity in neighbouring cells, thus perpetuating local polarisation¹¹⁰.

1.3.4 Planar Cell Polarity in the skin

Polarisation is a fundamental characteristic of the skin that applies both at the single cell level as well as globally across the whole tissue. In both instances, it arises from differential distribution of cellular components such as proteins, lipids, RNA and organelles that infer asymmetry in form and function⁹⁸.

Perhaps the most obvious role for polarisation at the single cell level is to establish apical-basal positioning in the epidermis, where the basal surface of keratinocytes is towards the basement membrane while the apical surface faces the external environment. This type of polarity can influence the orientation of the mitotic spindle in basal cells to decide whether divisions occur symmetrically or asymmetrically. When the spindle forms parallel to the basement membrane, two symmetrical daughter cells are formed that remain in the basal layer to maintain the proliferative pool. However, when the spindle aligns perpendicular to the basement membrane, the cytoplasmic differences inferred through apical-basal polarity cause asymmetrical division where one cell remains in the basal layer while the other is pushed upwards into the subbasal layer. This phenomenon causes the suprabasal daughter cell to possess a distinct set of markers compared to its basal sister and seals its fate along the path to terminal differentiation^{9,99}.

Global polarisation is traditionally regarded as planar cell polarity (PCP) and refers to the coordinated alignment of cells and their structures across a tissue plane, orthogonal to the apical-basal axis. It is governed by the complex integration of global directional cues with locally produced polarised cell arrangements¹⁰⁰. It is responsible for many events during development including vertebrate gastrulation and neural tube closure and directs collective cell behaviours such as unidirectional cilia beating and meticulous patterning of scales, feathers and hairs across the skin¹⁰¹. In recent years, a role for PCP during wound healing has been postulated to help the coordinated migration of cells into the wound bed.

To summarise this section, examples of Wnt signalling can be seen in several layers of the epidermis, in hair follicles and in their underlying dermal cells. The multitude of different ligand/receptor compositions that are possible under this umbrella of signalling creates complex branches within the pathway that can be divided into canonical and non-canonical responses. These play crucial roles throughout skin development but also continue to be vital in maintaining correct functioning of adult tissues. In addition to its homeostatic roles, Wnt signalling can be activated in response to certain stimuli such as injury where its polarising ability helps guide migrating cells into the wound bed.

1.4 Autophagy

1.4.1 Introduction to autophagy

Autophagy has been a particularly hot topic discussed amongst the scientific community in recent years. It is a highly conserved catabolic process that is often triggered during various conditions of cellular stress such as energy or nutrient shortages and is used as a mechanism to recycle non-essential cell components such as proteins and organelles in order to utilise them elsewhere ¹¹³. Owing to early work carried out by Christian de Duve and Yoshinori Ohsumi, the basic mechanism of autophagy has been elucidated and is understood to involve 15 core autophagy-related proteins (ATGs). These are responsible for targeting cell components, engulfing them into a double-membraned vesicle and delivering them to lysosomes containing a barrage of hydrolytic enzymes that digest the encapsulated cargo. It was originally considered to be a non-selective process but new evidence has suggested that it can be directed towards specific organelles such as mitochondria (mitophagy), peroxisomes (pexophagy) and intracellular bacteria (xenophagy).

1.4.2 Mechanistic overview of autophagy

When autophagy is activated, the process begins with recruitment of ATGs to a specific location in the cell called the phagophore assembly site. The phagophore is an isolation membrane that nucleates from this site and begins to create a cup shaped structure. As the isolation membrane elongates, it surrounds and engulfs its cytosolic target, with each arm eventually joining up to form a completely sealed, double-membraned vesicle called an autophagosome. This autophagosome travels along microtubules until

it is delivered to a lysosome. The outer membrane of the autophagosome then fuses with the lysosome membrane, releasing its contents for destruction ¹¹⁴. The cargo is broken down into its constituent parts such as amino acids and macromolecules which are expelled back into the cytosol for reuse (Figure 13).

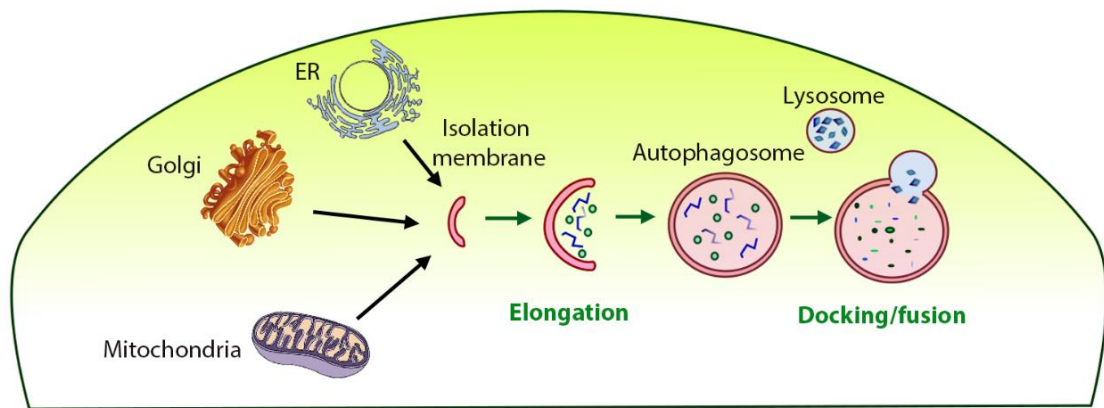


Figure 13 Overview of the autophagy mechanism

Autophagy begins with the nucleation of an isolation membrane. Fragments used to construct this membrane are believed to originate from the ER, Golgi apparatus and mitochondria. The structure elongates to engulf its target, eventually forming a sealed, double-membraned vesicle which then fuses with a lysosome containing hydrolytic enzymes to degrade the internalised material.

The ATG proteins involved in initiation and formation of autophagosomes arrange themselves into three distinct complexes that act sequentially throughout the process. The first complex that comes into play is the Unc-51-like kinase 1 (ULK1) complex. This consists of ULK1 itself along with ATG13, focal adhesion kinase family interacting protein of 200kDa (FIP200) and ATG101 ¹¹⁵. Under affluent, unchallenging conditions, this complex is inhibited by mechanistic target of rapamycin (mTOR). mTOR is a

serine/threonine protein kinase that is activated in the presence of amino acids ¹¹⁶. It inhibits autophagy by associating with the ULK1 complex via Raptor adaptor proteins whilst phosphorylating both ULK1 and ATG13 at multiple sites to suppress their catabolic activity ¹¹⁷. During starvation, mTOR is no longer activated by the presence of amino acids causing it to dissociate from the complex and ULK1 and ATG13 to be rapidly dephosphorylated as a consequence. This activates the kinase ability of ULK1 where it autophosphorylates itself at alternative sites as well as ATG13, FIP200 and ATG101 ¹¹⁸. The active complex then translocates to the phagophore assembly site where autophagy is initiated (Figure 14) ¹¹⁵.

From here, the ULK1 complex recruits the next autophagy unit to the nucleation site – the class III phosphatidylinositol 3-kinase (PI3KC3) complex. This provides lipid kinase activity needed to generate phosphatidylinositol-3-phosphate (PI3P) from phosphatidylinositol to start forming the phagophore. There are two distinct forms of the PI3KC3 complex – PI3KC3-CI binds to ATG14 while PI3KC3-CII binds to ultraviolet radiation resistance-associated gene (UVRAG) ¹¹⁹. PI3KC3-CI is more commonly involved in nucleation of the phagophore and consists of the catalytic subunit vacuolar protein sorting 34 (Vsp34), Beclin 1, Vsp15, ATG14 and activating molecule in Beclin 1-regulated autophagy protein 1 (Ambra1). The activated ULK1 complex recruits PI3KC3-CI to the nucleation site by phosphorylating Beclin 1 to trigger its activation (Figure 14) ¹²⁰.

The last complex to be recruited to the site is ATG12-ATG5-ATG16L which is needed for elongation and completion of the double-membraned autophagophore. The three components of the complex are brought together and assembled with the help of

ATG7 and ATG10 which act as E1- and E2-like enzymes respectively. The complex is responsible for orchestrating the lipidation and conjugation of microtubule associated protein light chain 3 (LC3). Molecules of LC3-I are delivered to an E2-like protein, Atg3, which is bound to Atg12 in the complex. This event facilitates conjugation of LC3 to phosphatidylethanolamine, thus converting LC3-I to LC3-II, which decorates the phagophore membrane ¹²¹.

The final stage of autophagy is the fusion of lysosomes with autophagosomes which is mediated by the PI3KC3-CII unit mentioned previously, with particular input from its UVRAG domain ^{122,123}.

There has been much speculation regarding the origin of the initial isolation membrane but the general consensus is that the endoplasmic reticulum appears to be the most likely candidate ¹²⁴. However, other cell entities such as the Golgi, mitochondria, plasma membrane and endosomes are thought to contribute membrane components during elongation of the phagophore in a cell and context dependent manner ^{125,126}.

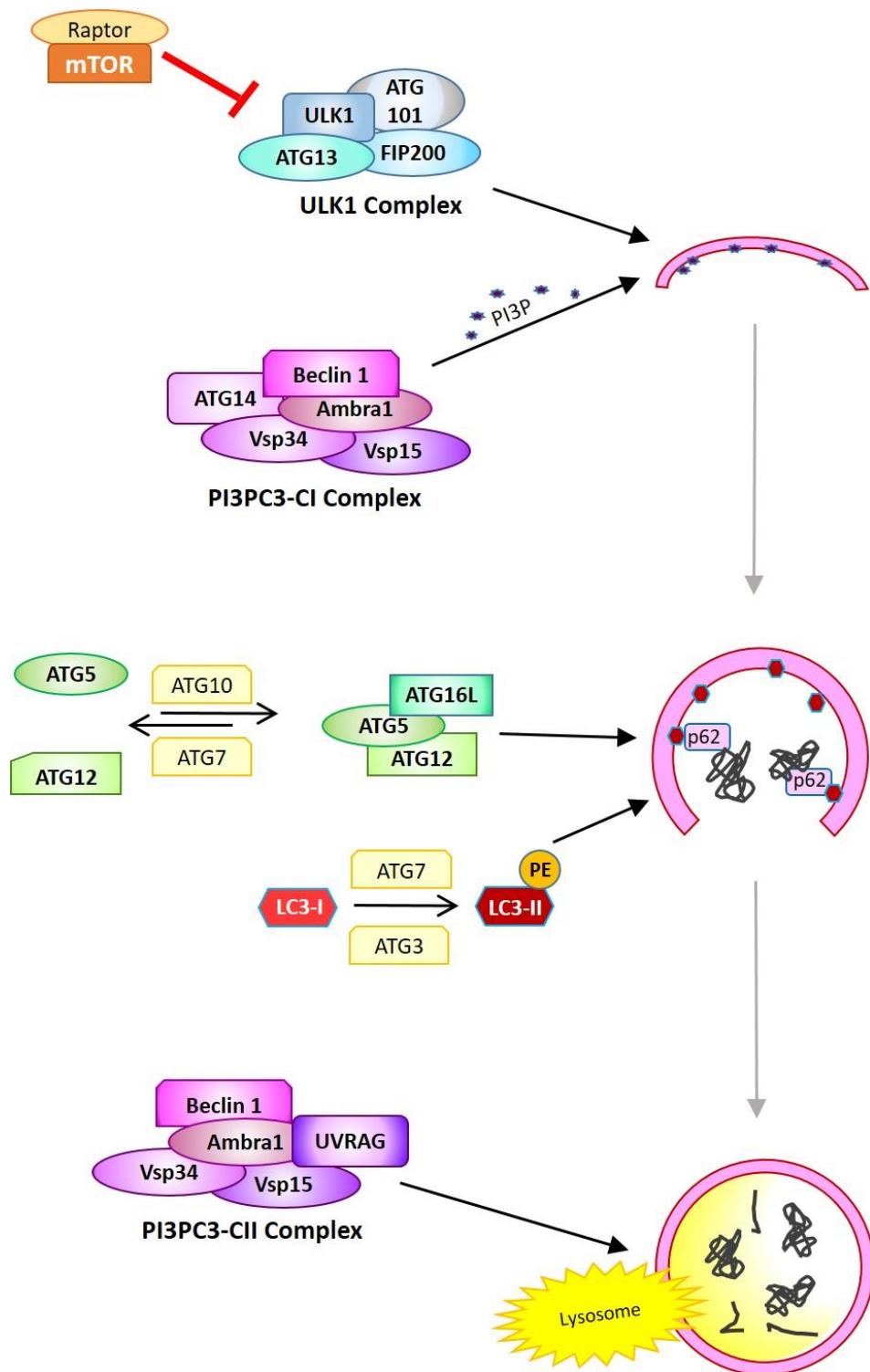


Figure 14 Complexes involved in the formation of autophagosomes

Four key complexes are required to synthesise autophagosomes. ULK1 is the first to be activated and is responsible for initiating nucleation of the phagophore membrane. ULK1 recruits the PI3PC3-CI complex to elongate the membrane and generate PI3P. The ATG5-ATG12-ATG16L complex is needed next to produce LC3-II molecules that decorate the phagophore membrane. The final complex is the PI3PC3-CII that aids fusion between the now sealed autophagosome and destructive lysosomes.

1.4.3 Selective autophagy and the role of cargo receptors

As aforementioned, autophagy was long considered a nonselective process that resulted in the indiscriminate degradation of cytoplasmic material but opinions have since change and it is now believed that specific cargo can be targeted for autophagic destruction, even under nutrient rich conditions ¹²⁷.

This poses questions therefore, of how specific cargo is recognised and how it is exclusively encapsulated within the autophagosome. It has been revealed that this is largely mediated by cargo receptors that recognise their targets following ubiquitination and then tether them to the growing isolation membrane via interaction with membrane bound LC3 molecules ¹²⁸.

One such cargo receptor is p62 which was the first mammalian cargo receptor identified and has been implicated in numerous branches of selective autophagy ¹²⁹. It contains several domains that are pivotal to its function and these include a ZZ type zinc finger domain and a C-terminal ubiquitin-associated domain which both mediate its interaction with ubiquitin as well as a central LC3-interacting region (LIR) ¹³⁰.

Collectively, these domains allow p62 to capture both its target cargo and the phagophore, bringing them together to facilitate selective engulfment.

Many other cargo receptors have since been discovered, each with distinct entities that they seek out depending on metabolic and environmental conditions. These include neighbour of BRCA1 (NBR1), optineurin (OPTN) and nuclear dor protein 52 (NDP52).

1.4.4 Autophagy in undamaged skin

There are many reports of autophagy occurring in the skin. It promotes normal homeostasis across all of its compartments by targeting toxic insults, invading pathogens and dysfunctional cell components, as it does in the majority of other tissues, to keep the cells healthy. This is particularly important for longer lived cells such as melanocytes, Merkel cells, secretory cells of sweat glands and dermal fibroblasts. The constant renewal of keratinocytes makes them shorter-lived and less prone to accumulated damage.

Due to its physical proximity and exposure to the outside environment, the skin experiences more frequent pathogenic insults than other internal organs. Autophagy is believed to hold a disputed role in dendritic cells of the skin such as Langerhans cells where reports have suggested that autophagic machinery aids in the engulfment and subsequent antigen presentation to major histocompatibility complex (MHC) molecules to initiate T cell immunity ¹⁷⁵.

Autophagy also has several skin specific functions, one of which has already been alluded to earlier in the introduction. The loss of intracellular organelles to maximise space for the cornified envelope scaffold is a significant event associated with late stage keratinocyte differentiation in the epidermis. Increases in the size and number of functional lysosomal bodies have been reported to coincide with the onset of organelle elimination and several strains of autophagy deficient mice have been found to display aberrant epidermal stratification with significant reductions in cornified

envelope proteins such as loricrin, fillagrin and involucrin. Together, these reports suggest that autophagy is paramount to fulfil terminal differentiation ^{171, 172}.

Autophagy is also understood to play an important role in determining ethnic diversity in skin colour. Melanin pigment is largely responsible for creating the wide variety of skin tones that exist across the world with higher concentrations leading to darker skin. Keratinocytes derived from Caucasian skin have been found to exhibit higher rates of autophagic activity compared to those derived from African American skin. It is therefore assumed that autophagy plays a role in controlling the level of melanosome accumulation in keratinocytes and consequently determines the amount of melanin delivered to the cell ¹⁷³.

As an individual ages, the replenishing pool of basal stem-like cells in the epidermis slowly diminishes and the skins renewal capability slows down. The rate of autophagy also diminishes and together, this causes slower cycling cells that are at higher risk of accumulated damage. The cells also become less able to cope with environmental stressors which makes them more susceptible to dysfunction, infection and disease ¹⁷⁴.

1.4.5 Current understanding of autophagy in wounded skin

Research into autophagy as a direct response to injury is both limited and contradictory.

Under normal conditions, resting platelets express core autophagy markers such as Beclin-1, LC3 and ATG7 which contribute to a state of constitutively active autophagy used to maintain cellular homeostasis ²²⁹. Upon injury, platelets are activated and rates of autophagy increase. This is indicated by a higher turnover rate of the autophagy

marker LC3-II which suggests that lysosomal degradation of autophagosomes is occurring at an increased rate.

To assess the physiological role of autophagy in platelets, mouse strains were generated containing a platelet-specific deletion of ATG7. While platelet numbers and size distributions were found to be normal in these mice, they exhibited defects in platelet aggregation and granule cargo packaging and were more prone to bleeding diathesis compared to their wildtype counterparts. While the precise mechanisms remain poorly understood, it would appear that autophagy is indispensable during the hemostasis and clot formation stages of wound healing ²²⁹.

During the inflammatory phase that follows, neutrophils are activated to fight off infection. They are derived from hematopoietic stem cells from the bone marrow that go through successive stages of differentiation to become mature neutrophils ²³⁰. The early progenitor cells in this sequence utilise a specific form of autophagy called lipophagy which breaks down fatty acid-enriched lipid droplets. This frees up fatty acids to be used as substrates in oxidative phosphorylation to generate ATP needed for the later stages of neutrophil differentiation ²³¹. When either ATG5 or ATG7 is knocked down in neutrophil precursors, the differentiation process is stalled and fewer cells reach terminal differentiation, likely due to limited substrates for oxidative phosphorylation and a resulting lack of ATP supply ^{231, 232}.

When neutrophils reach maturity, they begin executing their role of eliminating pathogens at the wound site. The predominant method used is phagocytosis where foreign particles become sequestered in highly organised endocytic compartments

known as phagosomes which are then degraded via fusion with lysosomes ²³⁴. This exposes neutrophils to pathogen associated molecular patterns (PAMPs). These are small molecular motifs that are conserved amongst many microbes and allow the host to recognise infection and activate their innate immune response accordingly. When neutrophil PAMP sensing pathways are activated, it initiates a unique form of selective autophagy called LC3-associated phagocytosis ²³⁵. It serves to augment the phagocytosis of pathogens by targeting intracellular bacteria or bacteria that has evaded the normal phagocytic pathway.

When neutrophil specific autophagy is enhanced in wounded tissue, there is an effective increase in the elimination of both drug-sensitive and multi drug-resistant bacterial strains ²³⁶. In contrast, when autophagy is suppressed or inhibited in neutrophils, there is an enhanced survival and growth of bacteria in infected tissue, suggesting that autophagy has a positive effect during the inflammatory phase. ²³⁷.

However, several papers contradict this notion and argue that autophagy has detrimental effects on wound repair when active during the inflammatory phase.

Yuanyuan Guo and colleagues demonstrated that intraperitoneal administration of rapamycin to wildtype C57BL/6 mice caused an increase in autophagic behaviour and consequently delayed normal skin wound healing while subsequent administration of the compound 3-MA inhibited autophagy and restored the rate of healing back to normal levels ²³⁸. They also show that increased levels of autophagy at the wound site regulates macrophage polarisation into the M1 phenotype. Activated M1 macrophages are typically found in the wound environment during the early stages of wound healing and contribute to repair by secreting proinflammatory cytokines such as TNF- α and interleukins. However, as normal healing progresses, M1 macrophages are replaced

with alternatively activated M2 macrophages which exhibit an anti-inflammatory function to prepare the tissue for its transition to the migratory phase ²³⁹.

Diabetic patients are prone to accumulation of advanced glycation end-products (AGEs). These are proteins or lipids that become glycated as a result of exposure to elevated sugar levels. AGEs often activate autophagy pathways and in doing so, they stimulate the production of far more M1 macrophages at a diabetic wound site ²⁴⁰. The sustained presence of AGEs in diabetic tissues therefore sustains the population of M1 macrophages to promote a prolonged inflammatory state and consequently impairs wound healing ²³⁸.

These contradictory findings would suggest that autophagy is necessary during the early inflammatory stage by aiding neutrophil-mediated pathogen clearance and activation of M1 macrophages but must be closely regulated in a temporal and cell specific manner to allow the late stages of inflammation to progress.

There is also evidence of autophagy playing a crucial role in keratinocytes during wound healing. Lei Qiang and colleagues have demonstrated that mice with genetic ablation of either *Atg5* or *Atg7* in keratinocytes can form normal, functional skin barriers but upon injury, they experience aberrant healing responses. Despite having only epidermal-specific autophagy deficiency, the infiltration of immune cells into the wound site was reduced, including macrophages, neutrophils and mast cells.

Keratinocyte proliferation and migration was inhibited which consequently affected rates of re-epithelialisation and the deposition of new granulation tissue in the wound bed was reduced due to suppression of fibroblast activation ²⁴¹. It was later found that wound-induced autophagy in keratinocytes regulates C motif chemokine ligand 2

(CCL2) expression. CCL2 is a major macrophage chemoattractant that recruits monocytes/macrophages to the wound site but also regulates the activity of several other cell types in the wound environment ²⁴². Through ablation of core autophagy machinery in keratinocytes, the expression of CCL2 is not upregulated and as a result, many wound healing events are affected ²⁴³.

1.5 The use of animal models to study wound healing

1.5.1 Common animal models used in the skin field

Although there are many *in vitro* models in existence that incorporate several cell types to try and mimic a wound healing environment, it is very difficult to recreate the complexity of the healing process accurately ¹³⁸. This therefore necessitates the use of *in vivo* animal models to effectively elucidate the physiological and pathological mechanisms of tissue repair ¹³⁹.

Mouse models are frequently used for a number of reasons including their rapid reproduction rate, ease of handling and relatively low husbandry costs compared to larger mammals ¹⁴⁰. They can also be standardised according to sex, age and strain and can be used in higher numbers to allow for statistical validation.

Occasionally, pig models will be used in place of mice as they are physiologically closer to humans with the porcine skin structure and wound healing process sharing more similarities with humans. Although they provide a better model to study wound healing, the higher costs incurred during their maintenance and upkeep and the increased difficulty of surgical and post-surgical procedures on pigs mean they are used less frequently than mice ¹⁴¹. Another consideration is the lack of available antibodies and other reagents that are reactive with pig tissue, making some experiments impossible to conduct in pig models.

1.5.2 A comparison of mouse and human skin – physical features

Although the majority of major skin components can be found in both mouse and human skin, there are some subtle differences in morphology that alter its function

and behaviour under certain conditions. One of the most obvious and important differences is the overall thickness of the skin. In humans, it is typically over 100um with the epidermis being composed of 5-10 cell layers whereas murine skin is less than 25um with only 2-3 layers of cells in its epidermis ¹³⁸. This discrepancy causes reduced barrier function in mice and enhances percutaneous absorption which is a consideration for studies involving cutaneous drug delivery.

With respect to wound healing studies, the thickness of skin in both humans and mice varies greatly depending on site, age, sex and nutritional status. Murine dermis is thicker and can be 40% firmer in males compared to females whereas females often have thicker layers of epidermis and subcutaneous tissue ¹⁴². These factors can influence the biomechanics of the healing process so should be standardised across experiments where possible.

The density of hair across the skin is another striking difference between human and mouse skin. Mice are covered in hair follicles all over their bodies but human skin displays a much sparser, uneven arrangement of hair follicles with much of the skin being classed as interfollicular. This is significant in terms of wound healing because areas with a higher density of follicles heal faster than sparse areas ¹⁴³.

It is well known that hair follicles undergo cycles of anagen (hair growth), catagen (regression phase) and telogen (resting phase). During the anagen phase, there is rapid proliferation of cells in the hair bulb with subsequent hair shaft and inner root sheath differentiation to generate a new hair. However, during catagen and telogen phases, proliferation and differentiation rates fall to virtually nothing as the follicle becomes quiescent and the cycle nears completion ¹⁴⁴. When a wound occurs in proximity to follicles in an active state, the rate of healing is quicker than if they were in a resting phase. This is due in part to quicker re-epithelialisation caused by activated hair follicle

stem cells that contribute to the healing process ¹⁴⁵. In fact, up to 25% of newly formed epidermis is derived from hair follicle stem or progenitor cells ¹⁴⁶. Also, mice are able to regenerate their hair follicles following injury whereas human scar tissue cannot. These differences between human and mouse hair follicles influence the pathophysiology of wound healing in each species and to some extent, limit the translation of results from mouse models to humans.

There are some dermal features that are unique to each species and must also be taken into account. For example, eccrine sweat glands that are usually responsible for body temperature control and innate immune responses, also harbour a stem cell population that contributes to re-epithelialisation in humans ¹⁴⁷. Mice however, lack eccrine sweat glands so cannot utilise the same stem cell pool.

Similarly, the panniculus carnosus is a subcutaneous muscle layer found below the dermal compartment in mice but not in humans. It provides a great contraction potential to murine skin which is used to draw together the wound edges with up to 90% of excisional wounds closing predominantly through contraction ¹⁴². This contraction is much less pronounced in humans who rely much more heavily on the formation of granulation tissue to close the wound instead.

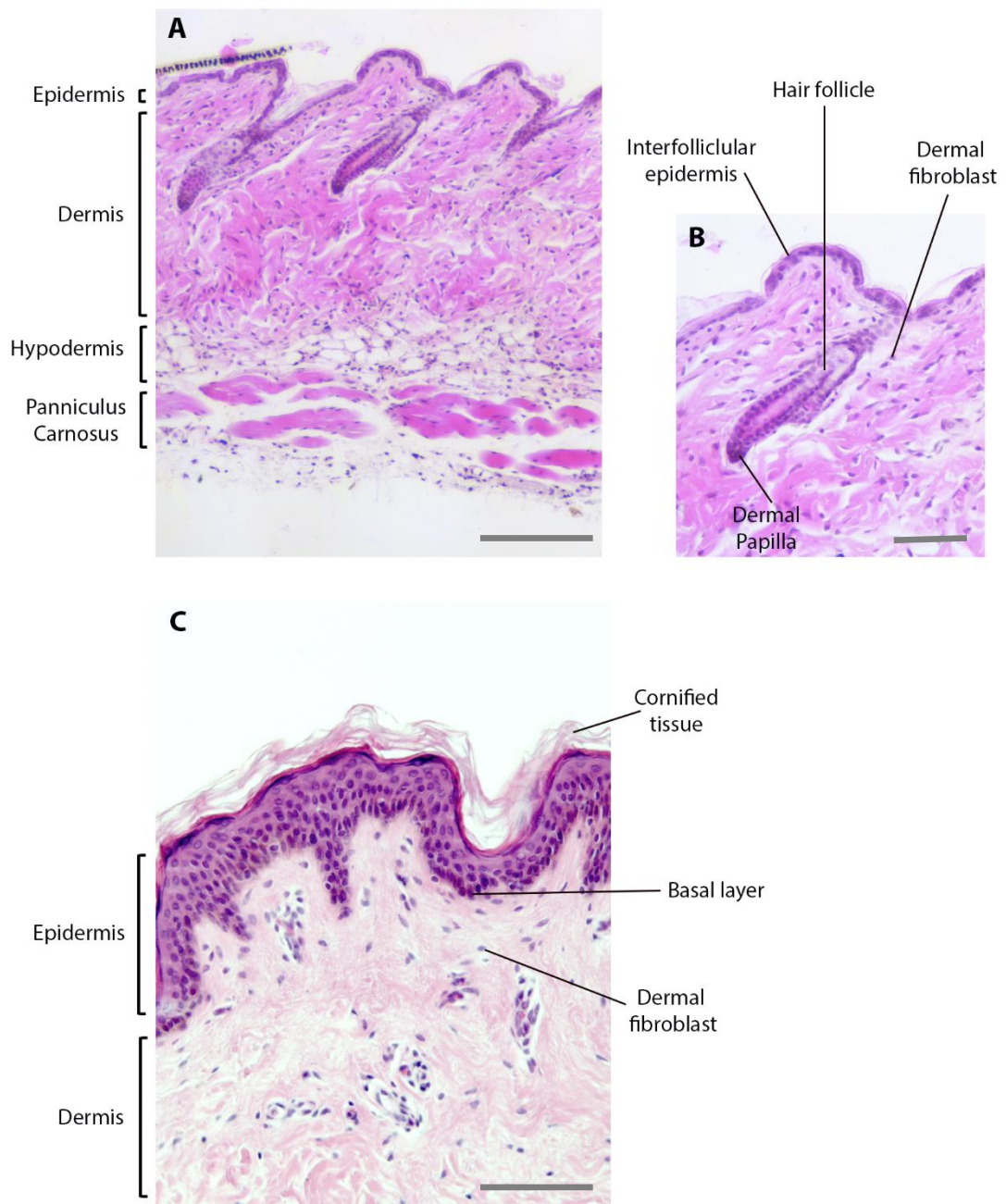


Figure 15 A comparison between the physical features of mouse and human skin

(A) A histological overview of the murine skin structure highlighting the location and thickness of a typical epidermis, dermis, hypodermis and panniculus carnosus. (B) An enlarged image of a murine hair follicle with interfollicular epidermis flanking either side. Tissue was taken from regions of skin in the telogen phase (C) A histological overview of human skin highlighting a much deeper epidermis with substantial cornification at its surface. (Image provided by Prof. Bing Hu)
Scale bars A, C = 200um, B = 50um

1.5.3 A comparison of mouse and human skin – molecular components

It is estimated that mice and humans last shared a common ancestor over 90 million years ago so it is not surprising that although our genomes share 95% identity with one another, the mouse genome is 14% smaller than the human genome and there is only 40% alignment between the two species ^{148,149}. This has naturally caused the molecular components of wound healing to diverge.

To start with, the percentages of peripheral blood leukocytes are different with humans having 50-70% neutrophils and 30-50% lymphocytes whereas mice have 10-25% and 75-90% respectively ¹⁵⁰. However, the effect this has during the inflammatory stage of wound healing is not fully understood.

Likewise, Langerhans and CD8-positive T-cells populate both human and mouse epidermis but in addition to these cell types, mice contain a specific population of $\gamma\delta$ dendritic epidermal T-cells (DETCs) fundamental for skin homeostasis and tissue repair. DETCs secrete FGF-9 upon injury which promotes Wnt activation ²³³. Owing to the role Wnt ligands play in polarisation, this is a difference that should not be overlooked. It should also be noted that Wnt-4 and Wnt-16, associated with epithelial-mesenchymal interactions and keratinocyte differentiation respectively, are present in human but not in mouse skin. Activated cytokines, particularly from the CXC... and CC... chemokine groups, also differ in mice and humans.

Despite the range of physical and molecular discrepancies between the two species, mouse models have contributed greatly to the field of wound healing and tissue repair. Modern techniques can now be used and developed to mitigate some of the drawbacks of using mice such as the use of splints around a wound site to restrict its

contraction and transgenic mice that carry functional human genes or cells to better mimic the human environment.

2. Aims

Wnt signalling has been studied across a broad variety of biological fields including extensive work carried out on its role during cutaneous wound healing. The mechanisms that underpin the three branches of Wnt signalling are well understood with Planar Cell Polarity playing the most prominent role during the healing process. It serves to create a global polarisation in cells at the periphery of a wound to orchestrate co-ordinated, uni-directional migration towards the affected area. Wnt morphogen gradients released from the wound bed are believed to be responsible for activating the pathway.

The primary focus of this study was to investigate these polarisation and migration events in keratinocytes during the re-epithelialisation phase of wound healing. The cells undergo several extensive changes over this period which are both physical and chemical in nature. To achieve polarisation in response to the morphogen gradient, large scale restructuring of cell components is needed to create asymmetrical distribution across the cell. This is accompanied by substantial rearrangement of cytoskeleton networks where actin filaments and microtubules must reorganise themselves to facilitate directed migration into the wound bed. This also involves alterations to cell-cell contacts and cell-substrate attachments to free the migrating cells from the surrounding epithelial sheets and underlying matrix respectively to continue a forward motion.

Owing to the existing diverse functions of autophagy in the skin, we aim to explore whether the degradative nature of autophagosomes could play a role in facilitating the cellular rearrangements associated with the wound healing process. There is currently a distinct lack of knowledge regarding any autophagy in the wound environment but given that it plays major roles in many other biological processes, it is certainly within reason to suspect that it may also contribute to wound healing.

If autophagy is found to be active at a wound site, we have identified several potential rearrangement events that it could target. First, we speculate that it may contribute to depolymerisation of the cytoskeleton at the trailing end of a cell, allowing it to be redistributed to the leading edge where extensive actin network assembly occurs, thus speeding up the rate of migration into the wound. Similarly, it could also be involved in targeting and breaking down cell-cell contacts or integrin attachments to the underlying matrix to facilitate quicker migration.

Secondly, we speculate that autophagy could target cell components such as receptors responding to the morphogen gradient in order to eradicate them from certain locations in the cell. By eliminating them from the trailing end of cells, receptors would become concentrated at the leading edge and maintain migration in a uniform direction.

Thirdly, and perhaps most obviously, it could simply serve to rid cells at the wound border of any components that became damaged as result of injury; an idea that is more in keeping with traditional roles of autophagy. If damaged, malfunctioning

components are not disposed of in a timely fashion, it may hinder the cells ability to effectively respond to injury.

Because so little is known about autophagy in the context of wound healing, we also aim to explore what mechanisms may be involved in its molecular control, what cues it may respond to in the wound environment and how its activity may be regulated.

To address these lines of investigation and to test the proposed hypotheses, the following aims were devised for the study:

1. To characterise when and where the planar cell polarity pathway becomes active in the wound environment

The study will begin by using the existing knowledge of PCP induction in migrating cells to help characterise different populations of cells within and surrounding the wound site. This will allow us to validate *in vivo* and *in vitro* wound models, highlighting when migration begins and in what groups of cells.

2. To investigate whether there is any evidence of active autophagy in the wound environment

Immunofluorescence staining and RT-qPCR will be used to assess whether there is any sign of increased autophagy at the wound site, particularly in populations of polarised, migratory cells.

3. To investigate potential targets of autophagy in the wound environment

If autophagy is found to be upregulated in response to injury, experiments will be conducted to identify the specific cell components targeted by selective autophagy and to understand the role of autophagy with respect to wound healing.

4. To uncover the molecular mechanisms that control autophagy in the wound environment

This line of study will be largely guided by the results obtained in the first half of the project. Once we have investigated the extent of autophagy at a wound site and whether it is limited to specific cell types, we will begin to investigate the known injury response cues that these cells experience in the natural wound environment and whether they may have any influence over the induction of autophagy. We will also attempt to investigate possible signalling pathways that may be involved in targeted autophagy at a wound site – again this section of the project will be guided by the ongoing outcomes of early experiments and will be developed over the course of the project, depending on the results achieved.

Overall, this study was designed to shed more light on the wound healing process and to gain a better understanding of the pathways that are involved. We hoped that by contributing to the growing bank of knowledge surrounding this field, we could contribute to the development of novel strategies employed to treat wounds more effectively.

3. Materials and Methods

3.1 Cell culture

3.1.1 Human Dermal Fibroblasts

Human dermal fibroblasts from a single adult donor were purchased commercially (Invitrogen) and cultured in Dulbecco's Modified Eagle's medium (21969-035, Gibco) supplemented with 10% Foetal Bovine Serum (F7524, Sigma-Aldrich) and 1% Antibiotic-Antimycotic solution (15240062, Gibco). The composition of Dulbecco's Modified Eagle's medium is outlined in Table 7 Composition of Dulbecco's Modified Eagle's medium (Supplementary material). Culture conditions were maintained at 5% CO₂ and 37°C throughout.

3.1.2 Human Epidermal Keratinocytes

Human epidermal keratinocytes from the foreskin of a single male, neonatal donor were also purchased commercially (C0015C, Fisher Scientific) and cultured in Epilife medium (MEPI500CA, Gibco) supplemented with Human Keratinocyte Growth Supplement (S0015, Gibco) and 1% Antibiotic-Antimycotic solution (15240062, Gibco). The components of both Epilife and HKGS are outlined **Error! Reference source not found.** Table 8 and Table 9 (Supplementary material), however the exact concentrations present in the final culture medium are not documented publically. Again, culture conditions were maintained at 5% CO₂ and 37°C.

3.1.3 Cell culture dishes

Stocks of all cells used in this project were maintained and amplified in either 6cm (10111351, Fisher Scientific) or 10cm (15347026, Fisher Scientific) cell culture dishes with Nunclon™ Delta surface treatment.

Where specific experiments required well plates to be used, the same Nunclon™ Delta coating was used for consistency.

3.1.4 Passaging cells

Care was taken not to allow cell stocks to become too confluent in their culture vessels as this often leads to undesirable phenotypic changes in the cell as well as rapid nutrient depletion and excessive cell death. This was particularly important in the keratinocyte populations as overcrowded culture conditions are known to induce differentiation in the cells, greatly reducing the number of stem-cell like cells and potential population doublings.

To avoid this, cells were passaged at approximately 60-70% confluency by removing the media and washing in pre-warmed Hanks Balanced Salt Solution (HBSS) (14175-053, Fisher Scientific) to remove cell debris. This was then aspirated and replaced with TrypLE dissociation reagent (12563-029, Gibco). Cells were returned to the incubator and checked regularly with gentle agitation until cells had detached and could be collected into a 15ml falcon tube containing culture media. To pellet the cells, tubes were spun down in a centrifuge at 1000rcf for three minutes. The supernatant was then discarded and the pellet re-suspended in fresh culture media and plated out.

3.1.5 Freezing cells

To maintain a sufficient, long term stock, cultured cells were often frozen down for future use. Cells were detached, spun down and pelleted as described in the previous section. The cell concentration was then measured using an automated cell counter so that the pellet could be re-suspended at 1×10^6 cells/ml in culture media. This cell suspension was then divided into 1ml aliquots in cryovials with 10% dimethyl sulfoxide (D2660, Sigma-Aldrich) added as a cryoprotectant. Cryovials were then placed at -80°C overnight before being transferred to liquid nitrogen for long term storage.

3.1.6 Thawing cells

To re-establish culture stocks from frozen vials, cells were removed from liquid nitrogen and thawed rapidly. The dimethyl sulfoxide used to preserve cell integrity during the freezing process can be harmful to the cells if they are thawed slowly and exposed to it for long periods at ambient temperatures so to minimise cell damage, pre-warmed media was added to the vials to speed up thawing and to dilute the DMSO. Once thawed the cells were spun down and pelleted at 1000rcf for three minutes, re-suspended in fresh culture media and then plated out as before.

3.2 Cell stretching

3.2.1 Stretch chamber collagen coating and cell seeding

10cm² PDMS (silicone) stretch chambers (STB-CH-10, Strex) were autoclaved to sterilise them prior to use. The silicone material was very hydrophobic with two methyl-bases on its surface so collagen coating was used to promote cell adhesion.

Hydrochloric acid (H1758, Sigma-Aldrich) was prepared at 1mM and combined with rat tail collagen 1 (11519816, Fisher Scientific) at a ratio of 1:1. A thin layer was applied to each stretch chamber and incubated overnight at 37°C. Excess solution was removed and the chamber washed in sterile HBSS three times before adding fresh media and seeding the cells at the desired density.

3.2.2 Cells under constant strain

Cells were grown on the stretch chamber for 1-2 days and then subjected to 12% constant strain by attaching the chamber to the Strex Cell Stretching STB-1400-10 device which is designed to fit inside a standard 37°C incubator so that cells can continue to be cultured under their normal conditions.

3.3 Scratch assays

Cells were grown in appropriate culture dishes until they reached complete confluency, forming a uniform monolayer across the surface of the dish. This was to mimic intact epithelial sheets with tight cell-cell junctions and contact inhibition. A specialised cell scratching tool was used to create vertical 'wounds' across the dish that were uniform in size and shape to allow accurate and comparable analysis of scratch closure rates.

3.4 Senescence assays

Solutions from the Senescence β -Galactosidase Staining Kit (9860, Cell Signalling) were prepared according to manufacturer's instructions. Care was taken to adjust the pH of the final staining solution to the desired level using HCl and NaOH.

Media from the cells was removed, the dish washed with sterile PBS and replaced with the fixative solution provided for 10-15 minutes at room temperature. This was removed and the cells washed a further two times in PBS before addition of the β -galactosidase staining solution. Dishes were sealed with parafilm to prevent evaporation and incubated at 37°C overnight in a dry incubator. CO₂ was omitted from the incubator as this alters the pH and can affect staining results. The following morning, dishes were collected and imaged immediately.

3.5 Lentivirus preparation

3.5.1 Production of Ki67p-FUCCI lentiviral reporters

Plasmids containing the Ki67p-FUCCI lentiviral reporters were kindly donated by Dr. Alexander Zambon of Keck Graduate Institute, Claremont. Generation of the lentiviral reporters was achieved using open reading frames of the mCherryhCdt1 (30-120)-pCSII-EF-MCS and mAG-hGeminin(1-110)-pCSII-EF-MCS plasmids which were kindly supplied by Dr. Astsushi Miyawaki and were subcloned into the pENTR-D-Topo vectors (K240030, Life Technologies). Subcloning using Gateway recombination of the 1.5kb Ki67 proximal promoter upstream of mAG and mCherry FUCCI reporters was performed into 2k7 lentiviral vectors. This allowed for neomycin and blasticidin

antibiotic selection of cells successfully expressing Ki67p-mAG-hGem(1-110) and Ki67p-mCherry-hCdt1(30-120) respectively.

The resulting Ki67p-FUCCI vectors were then transfected into HEK293T cells (R70007, Life Technologies) together with pCMV-VSV-G (envelope plasmid) and pCMV delta R8.2 (packaging plasmid). This generated the lentiviral particles required for subsequent cell infections which were collected as supernatants 48 and 72 hours later.

3.5.2 Infection of keratinocytes with FUCCI lentivirus

Keratinocytes were incubated with the viral supernatants together with 10µg/ml polybrene (TR-1003-G, EMD Millipore) at 37°C and 5% CO₂. The standard protocol for viral infections of this nature is to incubate for 2 hours but alterations had to be made due to the viral particles being produced in DMEM media containing serum rather than the Epilife media usually used to maintain keratinocytes. This type of media has significant detrimental effects on the morphology and differentiation status of keratinocytes so incubation with the virus had to be monitored closely to find the optimum time that allowed sufficient infection whilst maintaining the health of the cells. This was found to be approximately 90 minutes after which the supernatant was removed and replaced with standard culture medium. The cells were left for 24hrs before being placed under indefinite selection with 5µg/ml blasticidin and 125µg/ml neomycin.

3.6 cDNA analysis

3.6.1 RNA extraction from cells

For RNA extraction and purification, the acid guanidium thiocyanate-phenol-chloroform extraction technique, originally devised by Piotr Chomczynski and Nicoletta Sacchi in 1987, was used for this project. Total RNA was collected by adding TRI-Reagent (93289, Sigma-Aldrich) to cells and incubated at room temperature for five minutes before being collected into a 1.5ml Eppendorf tube. Chloroform was added at a ratio of 1:5 with the volume of lysate collected and then centrifuged at 13000rpm for 10 minutes. This results in phase separation where nucleic acids are partitioned into the upper aqueous phase while proteins, dissolved in phenol, and lipids, dissolved in chloroform, can be found in the lower phase. The aqueous phase was collected into a fresh Eppendorf tube and an equal volume of 2-Propanol (I9516, Sigma-Aldrich) added. To help visualise the RNA pellet, 1ul of GlycoBlue (AM9514, Fisher Scientific), a nucleic acid coprecipitant, was added to each sample and they were then incubated overnight at -20°C. The following morning, samples were centrifuged at 13000rpm for 45 minutes at 4°C. The supernatant was discarded, the pellet washed in 70% ethanol and spun down again at 9000rpm. In the final step, the pellet was air-dried and re-suspended in distilled water treated with 0.1% diethylpyrocarbonate (D5758, Sigma-Aldrich). RNA samples were stored at -80°C.

In order to analyse the yield and quality of RNA, a Nanodrop 2000 UV-Vis Spectrophotometer (Thermo Scientific) was used to quantify each sample. This device also gives information on the purity of the sample which was analysed by assessing the 260/230 and 260/280 ratios, indicating levels of phenol and DNA contamination respectively.

3.6.2 Reverse transcription

To convert RNA samples into cDNA, a High-Capacity cDNA Reverse Transcription Kit (4368814, Applied Biosciences) was used according to manufacturer's instructions.

Where yield was high enough, a starting amount of 700-1000ng of RNA was used per sample. These were run on a 96 well Veriti™ Thermal Cycler, using the manufacturer's suggested program outlined in Table 2. Samples were then diluted in 0.1% diethylpyrocarbonate treated water and stored at -20°C.

Table 2 Thermo Cycler program used for reverse transcription

Temperature	Time
25°C	10 Minutes
37°C	120 Minutes
28°C	5 Minutes
4°C	Indefinitely

3.6.3 q-PCR

Once cDNA samples had been obtained, qualitative PCR was used to analyse transcriptional fold changes in genes of interest. LightCycler® 480 SYBR Green I master mix (48873520001, Roche Life Science) was used in accordance with manufacturer's instructions. A total reaction volume of 10µl was used per well which consisted of 1µl cDNA sample, 1µl primer mix (outlined below), 5µl SYBR Green and 3µl DEPC water provided with the kit. This equated to a final primer concentration of 1µM. For each sample, reactions were performed in triplicate as technical repeats.

The q-PCR was carried out using a Roche LightCycler 480 Instrument II 384-well block real-time PCR machine. The program used is outlined in Table 3.

Table 3 LightCycler program used for qPCR

Program step	Temperature	Time (mm:ss)	Repeats
Pre-incubation	95°C	05:00	1
Amplification	95°C	00:10	40-55
	60°C	00:20	
	72°C	00:10	
Melting curves	95°C	00:05	1
	65°C	01:00	
	97°C	Until reached	
Cooling	95°C	00:01	1

3.6.4 q-PCR statistical analysis

Experimental data obtained from q-PCR work was inputted into GraphPad PRISM 5 software and analysed using the $\Delta\Delta C_t$ method. This method compares all experimental C_t values against values from housekeeping genes (GapDH or 36 β 4) to remove background expression as well as comparing them against control samples. Two-way ANOVA and Student's t-Tests were then carried out. Statistical significance values were set at * $p < 0.05$, ** $p < 0.01$, *** $p < 0.001$ and annotated on graphs where appropriate.

3.6.5 Primer design

The coding sequence, or CDS, for each gene was obtained through the NCBI Gene webpage (<https://www.ncbi.nlm.nih.gov/gene>). In cases where several isoforms exist, the shortest was often chosen with the idea that any primer designed against this sequence would also bind to longer variants. The Primer 3 online program (https://primer3plus.com/primer3web/primer3web_input.htm) was used to generate primers against the target sequence. Primer length was set at 20 nucleotide bases with an ideal amplicon product of 200 bases to reduce the risk of dimers and hairpins. Primer pairs were selected if the resulting product spanned at least two exons to reduce the chance of DNA contaminants being amplified. The UCSC In-SilicoPCR webpage (<https://genome-euro.ucsc.edu/cgi-bin/hgPcr>) was used to validate the primers and their target.

Table 4 Human Primers

Gene	Forward sequence	Reverse sequence	Product length (bp)
36β4	GCAATGTTGCCAGTGTCTGT	GCCTTGACCTTTTCAGCAAG	142
ATG12	AATCAGTCCTTTGCTCCTTCC	CACGCCTGAGACTTGACAGTA	104
ATG3	TTTGGCTATGATGAGCAACG	AAGTTCTCCCCCTCCTCCTG	201
ATG5	CAGATGGACAGTTGCACACA	CTGTTGGCTGTGGGATGATA	201
ATG7	CTGGGGACTTGTGTCCAAAC	AGAGGTTGGAGGCTCATTCA	296
Beclin1	AGGTTGAGAAAGGCGAGACA	AATTGTGAGGACACCCAAGC	196
CDK1	ACAGGTCAAGTGGTAGCCATG	CCATGTACTGACCAGGAGGG	225
CDK2	CGGATCTTTGCGACTCTGGG	ACTGGCTTGGTCACATCCTG	239
CDK4	GGATGACTGGCCTCGAGATG	AGCCACTCCATTGCTCACTC	222
Celsr1	GGACTATGGGATGGACCAGA	TGACCTTGAGTGC GTTGTTC	200
Cyclin A	AACTTCAGCTTGTGGGCACT	CAGTTTGCAGGCTGCTGATG	226
Cyclin B1	CCCCTGCAGAAGAAGACCTG	AGTGACTTCCCGACCCAGTA	188
Cyclin D1	GGCGGAGGAGAACAAACAGA	TGTGAGGCGGTAGTAGGACA	181
Cyclin E1	TGGCGTTTAAGTCCCCTGAC	AAGGCCGAAGCAGCAAGTAT	197
Fzd3	TCAACTCAGCTGGCTATGGT	GTTAGTCGTGACATGCTGCC	170
Fzd3	GCTCTCATAGTTGGCATTCCC	GGAGTATTTGGATCCCTCAGG	170
Fzd6	TGCTGTCTTCTGGGTTGGAA	TCAGCTTGTGTGAACTTGGT	188
LC3	CGTCCTGGACAAGACCAAGT	TCCTCGTCTTTCTCCTGCTC	183
Rac1	TTTGAAAATGTCCGTGCAAA	TCGCTTCGTCAAACACTGTC	250
RhoA	CTCCCAAAGTGCTGGGATTA	GCTTTCCATCCACCTCGATA	181
Vangl2	CTCGGAGGAAAACAGCAC	CAGCCGCTTAATGTGAGTGA	192
Wnt5a	GGACCACATGCAGTACATCG	CCTGCCAAAAACAGAGGTGT	118

3.7 Protein analysis

3.7.1 Total protein extraction from cells

Media was removed from the culture vessel and cells washed briefly in pre-warmed HBSS to remove cell debris. This was immediately replaced with 1ml ice-cold HBSS. The cells were detached from the dish using a cell scraper and then collected into an Eppendorf tube on ice. Tubes were centrifuged at 10,000rpm for three minutes at 4°C to pellet the cells. HBSS was removed and replaced with ice-cold radioimmunoprecipitation assay, or RIPA, buffer (89901, ThermoFisher) supplemented with Halt™ Phosphatase Inhibitor Cocktail (78420, ThermoFisher) at 1:100. The pellet was re-suspended and incubated on ice for 30 minutes with frequent agitation for efficient cell lysis and solubilisation of proteins. Tubes were spun down at 10,000rpm for 10 minutes at 4°C so the supernatant containing the protein could be collected and stored at -20°C.

3.7.2 Bicinchoninic acid assay to determine protein concentration

The bicinchoninic acid (BCA) assay was used to calculate the concentration of protein yielded from each sample. Reagents from the Pierce BCA Protein Assay Kit (23225, ThermoFisher) were combined with the samples according to manufacturer's instructions along with a set of nine albumin protein standards with pre-defined concentrations to generate a standard curve (0, 25, 125, 250, 500, 750, 1000, 1500 and 2000µg/ml). The assay utilises the well-known reduction of Cu²⁺ to Cu¹⁺ by protein in an alkaline medium with the highly sensitive and selective colorimetric detection of the cuprous cation (Cu¹⁺) by BCA. This produces a purple colour that increases in

intensity depending on the amount of protein in the sample. Once the BCA reagents had been added to the samples/standards, the plate was incubated at 37°C for 25 minutes. Care was taken not to exceed this as the higher protein standards would be at risk of becoming saturated. Absorbance at 562nm was then measured using a PHERAstar FS plate reader. Readouts from the standards were used to plot a linear regression line. The equation of the line was used to calculate to exact protein concentrations of each sample.

3.7.3 Western blotting – protein separation and membrane transfer

For western blot analysis of proteins, samples were normalised according to their calculated concentrations by combining them with 4x NuPAGE® Lithium Dodecyl Sulphate (LDS) Sample Buffer (NP0007, Invitrogen), 10x NuPAGE® Reducing Agent (NP0004, Invitrogen) and distilled water up to a final volume of 25µl. The LDS sample buffer and reducing agent are used to linearize and reduce the net charge of individual proteins. The samples were then heated to 95°C for 5 minutes, spun down to collect all of the sample mixture and placed back on ice until ready to load onto the gel.

NuPAGE® MOPS running buffer (NP0001, Invitrogen) was prepared according to manufacturer's instructions and the XCell SureLock® Mini-Cell (EI0001, Invitrogen) device assembled by placing a 4-12% NuPAGE® Novex™ Bis-Tris gel alongside a dummy cassette to create a closed circuit. The inner chamber, between the gel and dummy cassette, was filled with MOPS running buffer with extra added to the outer chamber to dissipate heat generated by the electrical current in the system. Wells in the gel were flushed out by pipetting running buffer through them several times and then samples were added. These were flanked by a visible PageRuler™ Prestained Protein

Ladder (SM0671, Fermentas) to assess protein migration and a Novex™ MagicMark™ XP (LC5602, Invitrogen) protein ladder visible only after development of the membrane and used to assess protein band size. Protein separation was initiated at 200V for approximately 50 minutes or until sufficient migration had occurred. While the gel was running, NuPAGE® Transfer Buffer (NP0006, Invitrogen) was diluted according to manufacturer's instructions with methanol (322415, Sigma-Aldrich) added to make up 10% of the total volume. When the protein separation step had finished, the gel was released from its casing and the blot module assembled in the following order from top to bottom in the cathode core: two blotting sponges, filter paper, gel, methanol-activated Polyvinylidene fluoride (PVDF) membrane (0,45µm; LC2005, Invitrogen), filter paper, two blotting sponges (Figure 16). It was then placed inside the XCell SureLock® Mini-Cell and filled with transfer buffer. Protein was transferred from the gel onto the PVDF membrane by applying 36V for 1 hour 45 minutes. Distilled water was added to the outer chamber to dissipate heat as before.

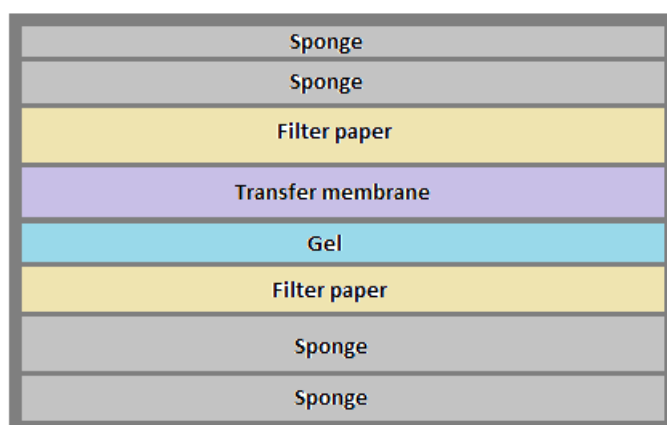


Figure 16 Western blot transfer assembly

3.7.4 Western blotting – detection of proteins

Once proteins were transferred to the membrane, the iBind™ Flex Western Device (SLF2000S, Invitrogen) was used to detect proteins of interest. The associated iBind™ Flex Solution (SLF2020, Invitrogen) was initially used as a blocking buffer applied to the membrane for 5 minutes at room temperature. Following this, the membrane was laid protein side down on an iBind card (SLF1010, Invitrogen) and encased inside the device. 2ml of the primary antibody, diluted in iBind Flex solution, was loaded into the first slot of the device followed by 2ml of the iBind Flex solution as a wash buffer in the second slot. 2ml of the Horseradish Peroxidase (HRP)-linked secondary antibody was added to the third slot and a final 5ml of wash buffer to the fourth slot. The mechanical force exerted by the lid allows for lateral sequential flow of the antibodies and wash solutions over the protein side of the membrane. Once each slot had run dry, ~2 hours 45 minutes, the membrane was washed three times in distilled water to remove non-bound antibodies.

To detect the HRP-linked secondary antibodies, the membrane was incubated with WesternSure™ PREMIUM ECL substrate (926- 95000, Li-Cor) for 5 minutes at room temperature. The membrane was digitally imaged using a C-DiGit Chemiluminescent Western Blot Scanner (3600-00, LiCor) in conjunction with the Image Studio™ software (version 3.1, Li-Cor)

3.8 *In vivo* mouse wound model

Mouse husbandry and wounding procedures were carried out by collaborators; Sabine Werner and her research colleagues. Paraffin embedded samples of wounded tissue were very kindly shipped to our laboratory where all further work was carried out by myself.

Mice were kept under specific pathogen-free conditions and received water and food *ad libitum*. Mouse maintenance and experiments had been approved by the veterinary authorities of Zurich, Switzerland.

For the analysis of the wound healing process, 8- to 12-week-old female mice were anesthetized by intraperitoneal injection of 8g/L of xylazine and 10g/L of ketamine (Streuli Pharma AG, Uznach, Switzerland). The genetic background of the mice used was a mixture of CD-1 and C57BL/6 strains. Two anterior and two posterior full-thickness wounds were generated on both sides of the shaved back lateral to the spine using a 5-mm hole punch (Stiefel, Brentford, UK). Only mice with hair follicles in the telogen phase were wounded and analysed.

At 4 and 7 days post injury, mice were euthanised using carbon dioxide inhalation and then wound biopsy specimens were isolated, including a 2mm surrounding tissue margin. Wounds were fixed overnight in 4% paraformaldehyde in PBS and then processed for paraffin embedding.

3.9 *Ex vivo* mouse wound model

3.9.1 Mouse strains, ethics and animal licenses

All *ex vivo* experiments were carried out using ICR (CD-1) mice purchased from Charles River UK Ltd. and bred in house at the University of Plymouth Animal Facility. Use of these mice, within the remit of the research project, was approved by the local Ethical Review Committee at the University of Plymouth. Appropriate Home Office animal handling qualifications were obtained by myself and all staff involved to ensure that husbandry and sacrifice of the animals was done in accordance with the UK Animal Scientific Handling Act 1986 and in house standards of practice.

3.9.2 Protocol One: Empty wounds on semi-solid

Agar based semi-solid medium was prepared by dissolving 0.75g agar (A1296, Sigma-Aldrich) in 30ml warmed distilled water. This was combined with pre-warmed DMEM F12 (31331-028, Gibco) supplemented with 20% Foetal Bovine Serum (F7524, Sigma-Aldrich), 1% Antibiotic-Antimycotic solution (15240062, Gibco) and 1% multivitamin (M6895, Sigma). The mixture was combined thoroughly until homogenised then divided into 6cm dishes and left to set at room temperature.

Wildtype CD1 litter-mate mice were sacrificed at postnatal day 22 and placed immediately on ice. An iodine solution was used as an initial disinfectant on each mouse before the back skin was removed and washed briefly in pre-warmed HBSS (14175-053, Fisher Scientific) containing Antibiotic-Antimycotic solution and amphotericin B. A final wash was performed using DMEM F12 with the above supplements.

A 3mm punch biopsy tool was used to inflict wounds on three quadrants of the dissected back skin with the fourth quadrant being left as an unwounded control. Each quadrant was then separated, placed into individual semi-solid dishes and maintained at 5% CO₂ and 37°C throughout (Figure 17). Semi-solid was replenished every other day. Images of the wounds were taken using a Leica M80 stereo microscope mounted with a Leica MC170HD camera and processed using LAS V4.4 software.

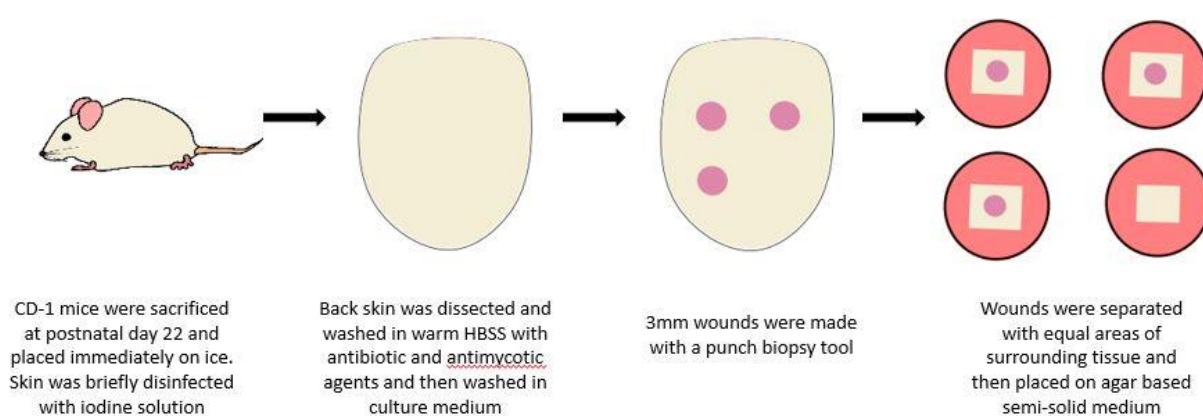


Figure 17 Schematic diagram of the method used in 'Protocol One' of the ex vivo mouse model

3.9.3 Protocol Two: Protein soaked Affi-gel beads

Affi-Gel Blue Gel (1537301, Bio-Rad) beads were prepared by aliquoting 40µl of the gel solution into Eppendorf tubes then adding 1ml PBS to wash away residue. The beads were centrifuged at 8,000rpm for 2 minutes to pellet them at the bottom of the tubes allowing old PBS to be replaced with new. Wash steps were repeated a total of three times. After the final cycle, PBS was removed and any remaining liquid left to evaporate off. The beads were then incubated overnight at 4°C with 50µl of either

rapamycin (5µg/ml), bafilomycin (50nM) or recombinant human Wnt5a protein (50ng/ml).

Wildtype CD1 litter-mate mice were sacrificed at postnatal day 21, their back skin harvested, cleaned and injured using a 3mm punch biopsy tool as described in the previous protocol. Injured tissue was cultured on agar based semi-solid made with supplemented DMEM/F12 media under the same environmental conditions as previously described. Once placed in individual dishes, wounds were filled with the appropriate protein soaked beads above (Protocol as described in Figure 17 with the addition of pre-prepared Affi-gel beads). Semi-solid was replenished every other day. Images of the wounds were taken using a Leica M80 stereo microscope mounted with a Leica MC170HD camera and processed using LAS V4.4 software. Measurements of the wound size was conducted in Adobe Photoshop CC 2018.

3.9.4 Protocol Three: Collagen gels impregnated with protein

Wildtype CD1 litter-mate mice were sacrificed at 2 months old, their back skin dissected, cleaned and injured as before and placed on pre-prepared semi-solid. Collagen gels were made by combining 1200µl rat tail collagen 1 (11519816, Fisher Scientific), 150µl DMEM F12 media supplemented with 20% FBS and 1% AA and 30µl 1M NaOH to neutralise the solution and promote natural cross-linking. Rapamycin (5µg/ml), bafilomycin (50nM) or recombinant human Wnt5a protein (50ng/ml) was added to some of the gel mixtures which were pipetted gently several times to homogenise without creating air pockets and then applied to the wounded tissue to fill the damaged area. After approximately 15 minutes, collagen fibres in the gel had cross-linked sufficiently, forming a plug across the wound. Semi-solid was replenished

every other day. Images of the wounds were taken using a Leica M80 stereo microscope mounted with a Leica MC170HD camera and processed using LAS V4.4 software. Measurements of the wound size was conducted in Adobe Photoshop CC 2018.

3.9.5 Protocol Four: Cell strainers and liquid culture media

Wildtype CD1 litter-mate mice were sacrificed at postnatal day 21. Electronic clippers were used to shave the fur across the back skin of the mice which was then cleaned with sterilising iodine solution 3 times. The skin was dissected and placed immediately in DMEM/F12 media to rinse off the remaining iodine. 3mm punch biopsies were created in the back skin and then placed onto the mesh of individual cell strainers (10737821, Fisher Scientific). Collagen gels were made using the same protocol as before and used to fill the damaged area. The same treatments at the same concentrations were incorporated into the gels with the addition of a Y27632 (10mM) condition. Cell strainers were positioned across the rim of 6 well plates and surrounded by DMEM/F12 media supplemented with 20% FBS and 1% AA so that it reached the height of the epidermis but did not submerge it to maintain an air-liquid interface (Figure 18). Media was changed daily. Images of the wounds were taken using a Leica M80 stereo microscope mounted with a Leica MC170HD camera and processed using LAS V4.4 software. Measurements of the wound size was conducted in Adobe Photoshop CC 2018.

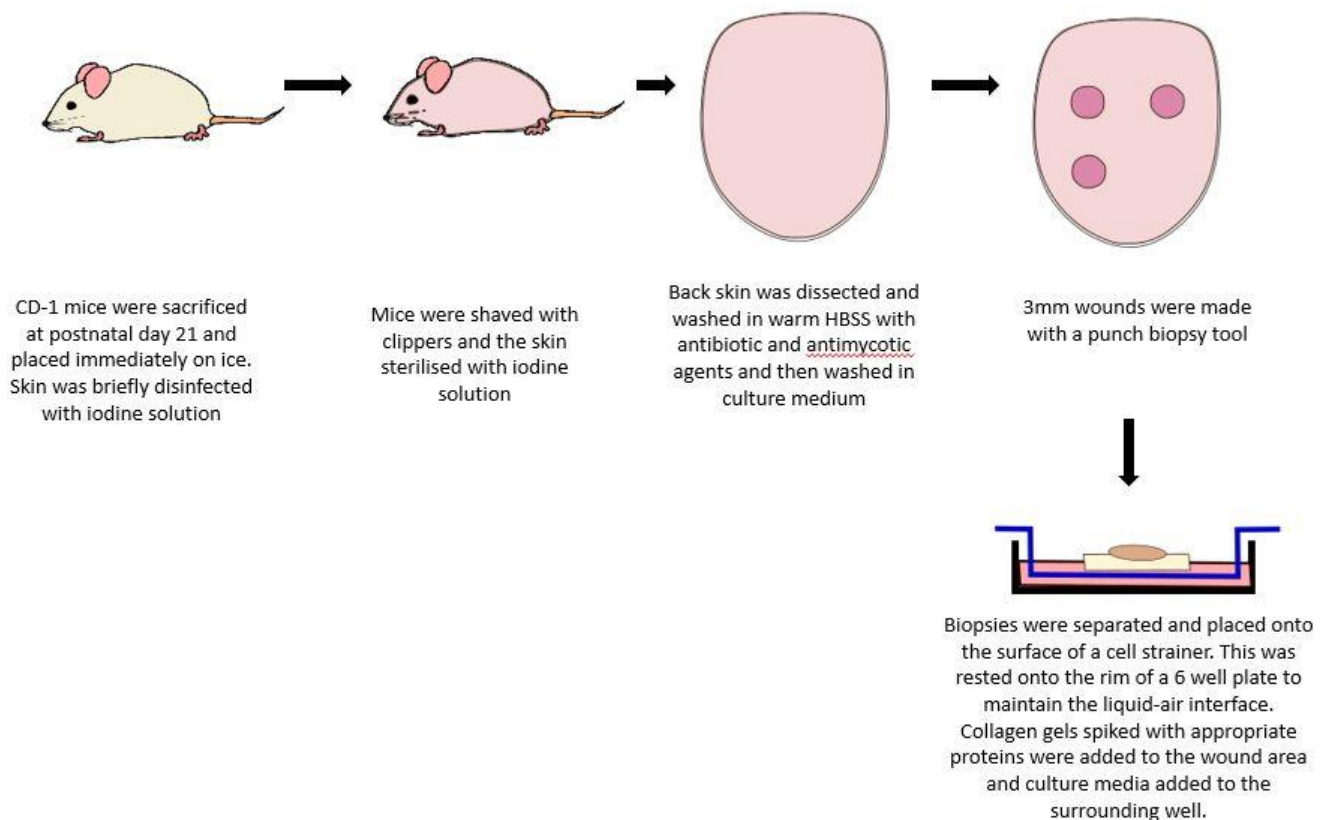


Figure 18 Schematic diagram of the method used in 'Protocol Four' of the ex vivo mouse model

3.9.6 Protocol Five: Blade incisions, cell strainers and liquid culture media

Two female wildtype CD1 mice were sacrificed at three months old. Electronic clippers were used to remove most of the fur across the back skin and then commercially available hair removal cream was used according to manufacturer's instruction to eliminate remaining hair shafts. Mice were washed several times with HBSS until all residual cream had been removed and then sterilising iodine solution was used to disinfect the cleared skin. Forceps were used to gently raise small regions of skin from the body of the mouse and curved dissecting scissors used to snip shallow incisions. Wounds were separated with equal margins of surrounding tissue and then placed onto the surface mesh of a cell strainer. These were placed into 6 well plates containing DMEM/F12 media supplemented with 20% FBS and 1% AA to a volume

sufficient to maintain the air-liquid interface. Pre-prepared collagen gel solutions seeded with human dermal fibroblasts were added to incision site and left to set. Samples were maintained in a 5% CO₂, 37°C incubator with media changed daily. Images of the wounds were taken using a Leica M80 stereo microscope mounted with a Leica MC170HD camera and processed using LAS V4.4 software. Measurements of the wound size was conducted in Adobe Photoshop CC 2018.

3.10 Three-dimensional bioengineered human skin model

3.10.1 Insert based epidermal model

24 well plate hanging cell culture inserts (MCHT24H48, Millipore) with a 0.4µm pored membrane were used to culture neonatal human keratinocytes. To aid attachment, membranes were first coated with 50µl rat tail collagen 1 (11519816, Fisher Scientific) mixed with 1µl 1M NaOH and incubated at 37°C for 30 minutes. Keratinocytes were then seeded onto the membranes and grown in Epilife media supplemented with Human Keratinocyte Growth Supplement, 140µM calcium chloride (C7902, Sigma-Aldrich) and 50µg/ml ascorbic acid (A4403Sigma-Aldrich) until a confluent monolayer was achieved. After 3-6 days, the monolayer of cells was exposed to the air-liquid interface and the concentration of calcium chloride in the media was increased to 1.5mM to encourage the cells to differentiate and stratify upwards. Media was changed three times a week for 14-21 days. The epidermal models were fixed at room temperature in 4% paraformaldehyde.

3.11 Tissue processing and staining

3.11.1 Frozen tissue samples

To cryo-preserve samples, fresh mouse skin was embedded in O.C.T. Compound (Polyvinyl alcohol and polyethylene glycol, 4583, Tissue-Plus SciGen) and snap frozen by immersing in liquid nitrogen. Samples were then stored at -80C.

3.11.2 Paraffin embedded tissue samples

Alternatively, fresh mouse skin was fixed in 4% paraformaldehyde (P6148, Sigma-Aldrich) diluted in phosphate buffered saline solution (PBS)(P4417-100TAB, Sigma-Aldrich) overnight at 4°C. The following morning, paraformaldehyde was removed, replaced with fresh PBS and stored at 4°C.

The fixed tissue was then processed using a HistoCore Pearl tissue processor (Leica) with the program outlined Table 5.

Table 5 Program used for processing paraffin embedded tissue samples

Solution	Time	Temperature	Pump/Vacuum
70% Ethanol	45 minutes	-	Pump + Vacuum
70% Ethanol	45minutes	-	-
70% Ethanol	45 minutes	37°C	-
80% Ethanol	45 Minutes	37°C	-
95% Ethanol	45 Minutes	37°C	-
100% Ethanol	45 Minutes	37°C	-
100% Ethanol	45 Minutes	37°C	-
100% Ethanol	45 Minutes	37°C	-
Xylene	30 Minutes	37°C	-
Xylene	30 Minutes	37°C	-
Paraffin	1 hour	62°C	Vacuum
Paraffin	1 hour	62°C	Vacuum
Paraffin	1 hour	62°C	Vacuum

3.11.3 Tissue sectioning

Frozen tissue was removed from -80°C storage and left to acclimatise at -20°C prior to sectioning the sample. A Leica CM1850 UV cryostat was used to cut sections at a thickness of 10-20µm and collected onto Polysine Microscope Adhesion slides (J2800AMNZ, Thermo Scientific). Slides were left to air dry for 30 minutes to enhance adhesion before being fixed with either 4% paraformaldehyde (158127, Sigma-Aldrich) in PBS or 10% formalin solution (HT50128, Sigma-Aldrich).

Paraffin embedded samples were sectioned at room temperature using a microtome. Sections were cut at 6-10 μm and placed in a 42°C water bath to partially warm the paraffin and relieve any wrinkles or creases that had developed across the sample. They were collected onto Polysine Microscope Adhesion slides as above and air dried at least overnight before further processing.

3.11.4 Histological staining – Hematoxylin and Eosin

Air dried paraffin slides were heated to 60°C to liquefy the wax and then incubated in xylene (534056, VWR) for 10 minutes. A second incubation with fresh xylene was used to ensure all residual paraffin was removed. Tissue was then rehydrated by passing the slides through 100% ethanol, 95% ethanol, 70% ethanol and finally distilled water, incubated for five minutes at each stage. Rehydration of the sample is a key step due to paraffin and xylene being highly hydrophobic which would otherwise prevent sufficient penetration of stains into the tissue.

Both paraffin embedded and frozen slides can be treated in the same manner from this point onwards.

Harris hematoxylin solution (HSS16, Sigma-Aldrich) was added to the slide for three minutes and then washed gently under running tap water until all excess stain was visibly removed. Acid alcohol solution (56694, Sigma-Aldrich) was then added to the slide for 30 seconds to regress the hematoxylin and fix the stain. A further wash in tap water facilitates the bluing step where the slight alkalinity of the water converts the initial soluble red colour of the hematoxylin to an insoluble blue.

Slides are dipped briefly in 95% ethanol and then covered with Eosin Y (230251, Sigma-Aldrich) solution dissolved in 80% ethanol for 2-3 minutes. Final washes are performed in 95% ethanol, 100% ethanol and xylene.

Slides were mounted using Eukitt quick-hardening mounting medium (0389, Sigma-Aldrich) and stored at room temperature.

Images of histological staining was achieved using a Leica DM1000 microscope mounted with a Leica MC170HD camera and LAS V4.4 software.

3.11.5 Immunofluorescence staining

Paraffin embedded samples were deparaffinised as described above (section 3.8.4) prior to immunofluorescence staining being carried out.

Samples were washed three times in PBS, each wash lasting five minutes. Inclusion of 0.1% triton (T) in the washing buffer was dependent on the marker of interest- for proteins known to have nuclear localisation, triton detergent was used to disrupt the cell membrane and enhance penetration of antibodies whereas membrane associated proteins risked being cleaved by triton so it was omitted.

To prevent non-specific binding of antibodies and to reduce background signal, samples were blocked using a solution of PBS/T containing 5% donkey serum (D9663, Sigma-Aldrich), 0.25% cold water fish gelatin (G7765, Sigma-Aldrich) and 0.25% albumin from bovine serum (A2153, Sigma-Aldrich) for two hours at room temperature.

Primary antibodies were diluted in blocking buffer and incubated with the samples overnight at 4°C. Experimental details regarding each antibody can be found in Table 6.

The following morning, samples were washed in PBS/T at room temperature for five minutes. Washing was repeated three times with fresh PBS/T used each time.

Secondary antibodies were then diluted in blocking buffer and incubated with the samples for two hours at room temperature. Due to the light sensitive nature of the secondary antibodies and to avoid bleaching, samples were protected from light from this point onwards. Unbound secondary antibodies were removed by three consecutive washes with PBS/T, as done previously.

To visualise nuclei in the cells, 4'6-diamidino-2-phenylindole (DAPI: D9542, Sigma-Aldrich) was used as a counterstain at 2µg/ml for five minutes.

Samples were mounted and sealed using Dako mounting media (S3023, Dako) and stored at 4°C.

To view the immunofluorescence staining, a Leica DMI6000 confocal microscope with a TCS SP8 attachment was used to capture images at a resolution of 2048 x 2048. LAS AF software from Leica was used to operate the microscope and define imaging parameters. Adobe Photoshop CC was used for post-imaging processing.

Table 6 Experimental details of primary antibodies

Antibody	Host	Company	Product No.	LOT No.	Conc.
Celsr1	Rabbit	Biorbyt	Orb85218	J1793	1:200
Vangl2	Rabbit	Biorbyt	Orb1325		1:200
Vangl2	Goat	Borbyt	Orb19489		1:200
Frizzled 3	Rat	R&D Systems	MAB1001		1:200
Frizzled 6	Goat	R&D Systems	AF1526-SP	IVL0215051	1:200
Phospho-p62	Rat	MBL	D344-3	002	1:200
Nrf2	Rabbit	MBL	PM069	004	1:200
ROR2	Mouse	DHSB			1:10
P62	Rabbit	MBL	PM045	021	1:200
cJun	Rabbit	Cell Signalling	60A8	9	1:200
Wnt5a	Rabbit	R&D Systems	MAB645		1:150
ATG5	Rabbit	Sigma-Aldrich	A0856	067M4801V	1:200
LC3	Rabbit	Cell Signalling	12741S		1:800
Tubulin	Rat	Abcam	Ab6161	GR297372	1:500
LC3	Rabbit	Cell Signalling	D3U4C	4	1:200
Ki67	Rabbit	Abcam	Ab15580	GR3198193-1	1:200
P63	Mouse	Abcam	Ab735	GR234019-1	1:200

3.12 Transmission electron microscopy

Media was removed from the samples and immediately replaced with a fixative solution consisting of 2% glutaraldehyde (G5882, Sigma-Aldrich), 2% paraformaldehyde (P6148, Sigma-Aldrich) and 0.1M PIPES buffer at pH7.2. After 3 x 5 min washes with buffer the cells were post-fixed for 1 hour using 1% osmium tetroxide reduced with 1.5% potassium ferro-cyanide in 0.1M sodium cacodylate. After 3 x 5 min washes in buffer the cells were dehydrated in an ethanol series (70%, 95% and 2 x 100% ethanol – 1 minute each) followed by dipping the coverslips in 100% acetone and

immediately adding a droplet of Spurr resin on top of the cells. The cells were then embedded in Spurr resin using gelatin capsules and the resin cured at 60°C for 12 hours. The coverslips were removed from the resin by dropping the capsules in liquid nitrogen. 60 nm thin sections were produced using an ultramicrotome (Leica UC7) and the sections collected on 100 mesh hexagonal copper EM grids. After contrasting the sections in lead citrate the cells were inspected in a JEOL JEM 1400 transmission electron microscope operated at 120 kV and images taken with a digital camera (Gatan ES1000W).

(Processing and imaging was very kindly carried out by Dr Christian Hacker and Paulina Cherek at the Bioimaging Suite, University of Exeter).

4. Results

RESULTS SECTION I

Characterisation of planar cell polarity and Wnt signalling in the wound environment

I.1 The *in vivo* murine wound model

To tackle the first part of the investigation, it was important to confirm that techniques and models being used throughout the study supported existing knowledge in the field and were therefore suitable tools to investigate novel aspects of wound healing. In order to achieve this, paraffin embedded *in vivo* murine wound model samples were very kindly donated by Sabine Werner and her research group. These mouse models are well established across the wound healing field and provide an excellent platform upon which all aspects of wound healing can be studied.

Samples of wounded back skin were received from wildtype mice sacrificed at four days and seven days post injury. For each time point, four individual specimens were analysed. Histology of the wounds was assessed using haematoxylin and eosin staining to confirm which stage of the wound healing process each sample was in.

I.II Histological assessment of the *in vivo* murine wound model

As expected, the initial haemostasis phase had been achieved by day four with successful clotting and clear formation of a scab across the surface of the wound bed (Figure 19A). Due to the dry, flaky nature of a scab, tissue in this region was brittle and difficult to section without tearing which accounts for the slight distortion across this region in the image.

It is difficult to discern the status of the immune response from histology alone but there is clear evidence that a high number of cells have infiltrated the wound bed, denoted by a dense patch of nuclei in the dermal compartment beneath the scab compared to normal dermal tissue at the periphery of the wound. There is also evidence that the proliferation stage has begun which is marked by a substantial mass of epidermal cells flanking either side of the wound bed. The enlarged images of the left (Figure 19B) and right (Figure 19C) wound borders suggest that the main bulk of proliferation has occurred at the wounds edge and that these cells have begun to migrate beneath the scab to start the re-epithelialisation process. Re-epithelialisation does, however, remain in an early stage with the leading edges of the migrating cells still having some distance to travel before the two sides meet in the middle of the wound bed. This is in accordance with normal progression through the wound healing process, displaying all the features typically expected from a murine wound sample four days post injury.

By day seven, there was a significant increase in re-epithelialisation with keratinocytes forming a complete layer, several cells deep, across the entire wound surface (Figure 20). The initial mass of proliferating cells observed at day four has dispersed across the

tissue indicating that the skin will be transitioning into the final remodelling phase of wound healing.

As the focus of this study was to look specifically at cell changes that occur during migration, it was decided that the day four samples would be more appropriate to use as they captured the phase of wound healing that was of most interest. By day seven, the majority of migration had already occurred and key polarisation events may have been missed.

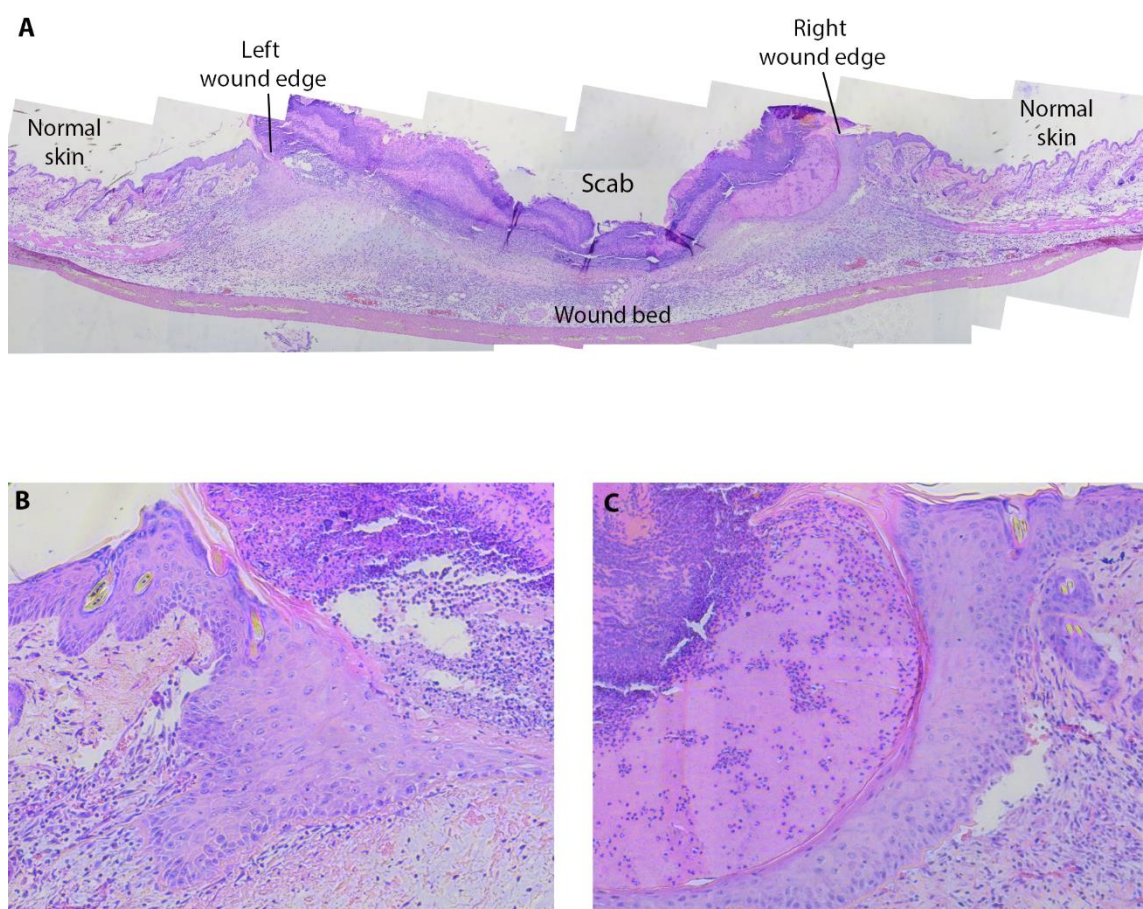


Figure 19 Histological staining of an *in vivo* mouse wound model 4 days post injury

(A) Histology of a murine wound 4 days post injury revealed that a scab had formed across the surface of the wound bed and that the wound site was flanked by enlarged regions of epidermal cells. This indicated that wound healing had proceeded into the proliferative phase where rapid division was occurring in these regions. There was also evidence that the proliferating epidermal cells had begun migrating beneath the scab (B, C) Enlarged images of the left and right wound edges respectively. (n=4)

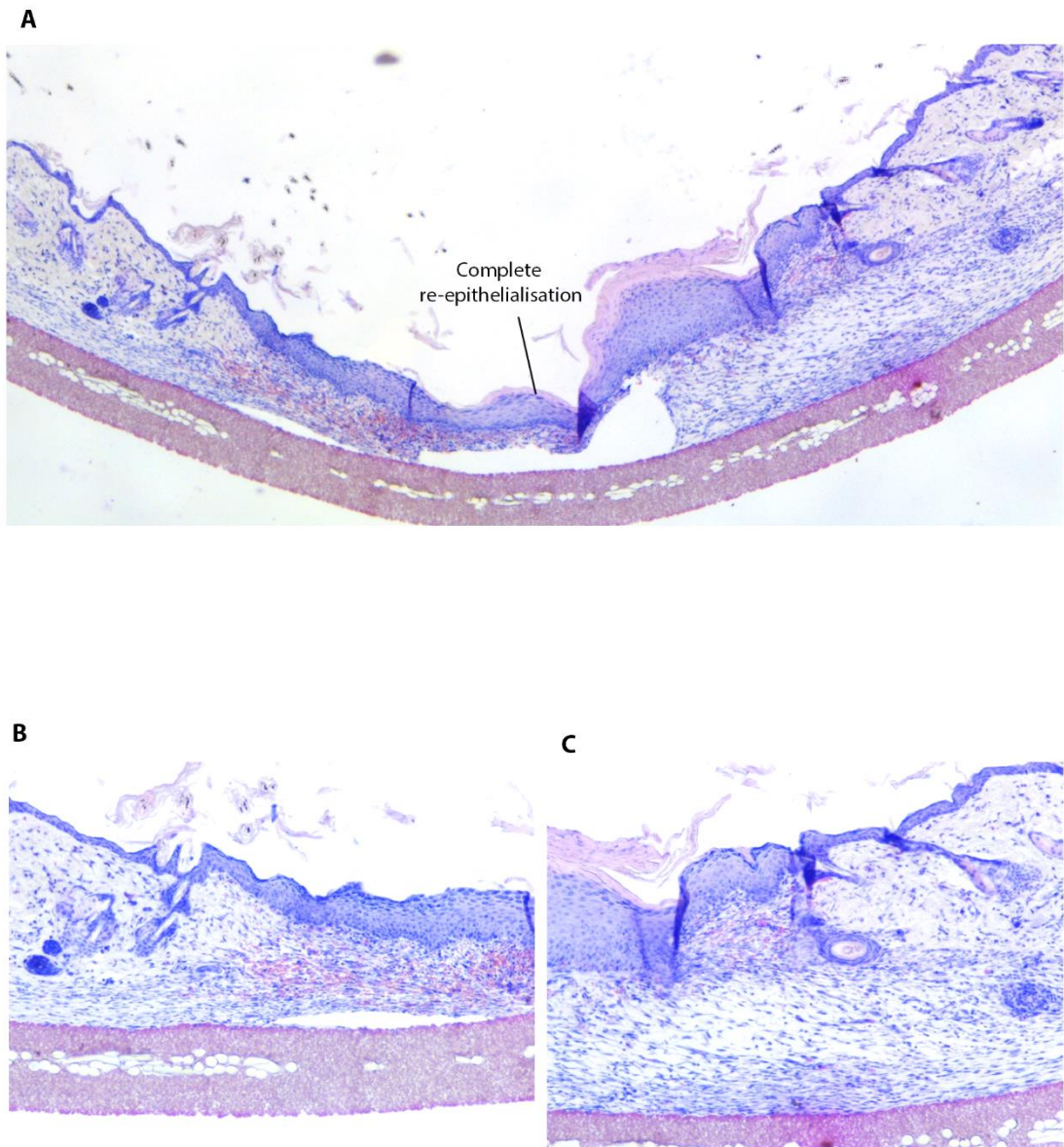


Figure 20 Histological staining of an *in vivo* mouse model 7 days post injury

(A) Histology of a murine wound 7 days post injury revealed that complete re-epithelialisation had occurred, forming a continuous epidermal layer across the wound bed. Evidence of stratification could also be seen. (B, C) Enlarged images of the left and right wound edges respectively. (n=4)

I.III Identification of different cell types at the wound border

Once it had been established that the 4 day samples would be taken forward, further characterisation of the wound was carried out to identify different population of cells at the wound site.

P63 is a transcription factor expressed in proliferating basal keratinocytes. In the skin, this includes interfollicular stem cells, young transit amplifying cells and mature transit amplifying cells ¹⁵¹. As these cells begin to differentiate and move into the suprabasal layer, the expression level of P63 falls to just 25% which coincides with a reduction in their proliferative capability ¹⁵². P63 can therefore be used to help identify the population of proliferating basal cells.

Figure 21 demonstrates that there is high P63 expression in basal cells attached to the basement membrane at both the left and right wound borders but the signal strength of the immunofluorescence staining becomes weaker as the cells move away from this layer. This weaker staining would suggest that these cells have transitioned into more mature migratory cells as the literature describes ¹⁵². As the cells move further towards the wound bed, the expressions falls to nothing, indicating that cell division has ceased in this region.

Images were also taken of skin far away from the site, considered to be unaffected by the wound healing process, to compare any differences between expression at the wound border compared to 'normal' skin (Figure 21E). As expected, P63 was present in the basal layer of normal epidermis as well as in the hair bulb where cycling cells are typically found.

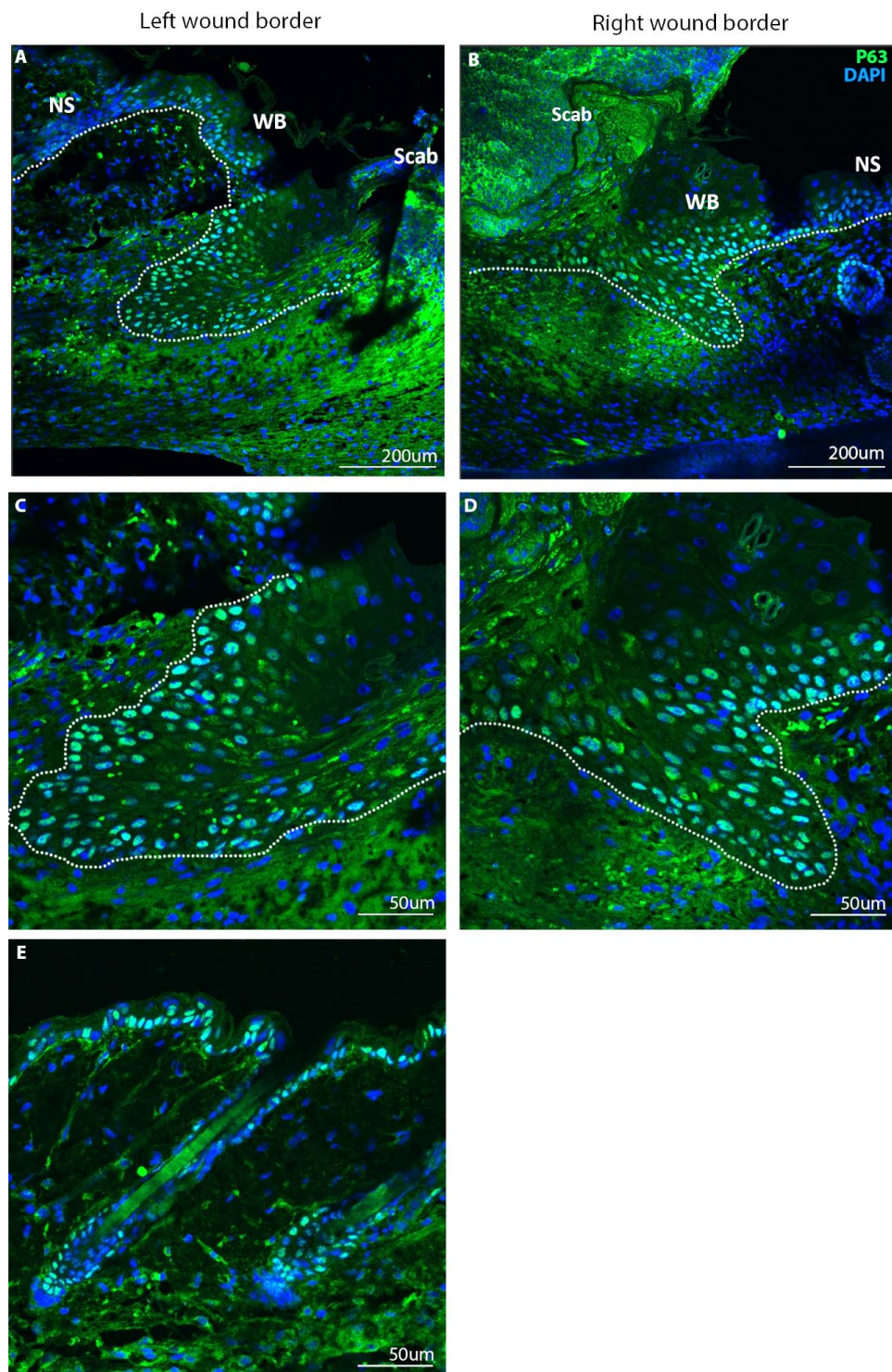


Figure 21 Expression pattern of the proliferation marker P63 in an *in vivo* murine wound model 4 days post injury

Immunofluorescence staining used to characterise the expression pattern of P63 (green) in an in vivo mouse wound sample formalin fixed and paraffin embedded 4 days post injury. (A-D) Images were taken of the proliferative region of cells at the left and right wound edges. Layers of basal keratinocytes within this region displayed strong positive expression. Sections were cut at 8µm. DAPI (blue) was used to counterstain nuclei. NS: Normal Skin, WB: Wound Border. Dotted line indicates the epidermal basement membrane (E) A region away from the wound site displaying P63 expression in normal skin. (n=4)

Ki67 is another marker often used for proliferating cells so was immunofluorescently co-stained with P63 to see whether their expression profiles overlapped. It is common to observe that not all cells positive for P63 are also positive for ki67 and this was certainly the case seen at the wound borders ¹⁸⁵. Figure 22 A&B show the same region at the left side of the wound border. Every cell in the basal layer is positive for P63 but there is only one or two cells positive for ki67. Figure 22 C&D show a similar trend at the right side of the wound border. When this is compared to a region of skin away from the wound (Figure 22E), there appears to be more positive ki67 cells in normal epidermis.

Despite the limited overlap of the two proliferation markers, the P63 staining does provide a strong indication that there is a distinct population of actively dividing cells at the wound border.

We did not deem it necessary to carry out extensive characterisation of the murine wound models because this has been done elsewhere in other studies and the methods used to generate them have been used widely across the field in many peer-reviewed publications ^{182 - 184}. The main purpose of our preliminary characterisation was to identify the region of proliferating epidermal cells which was achieved sufficiently through the histological and immunofluorescence staining.

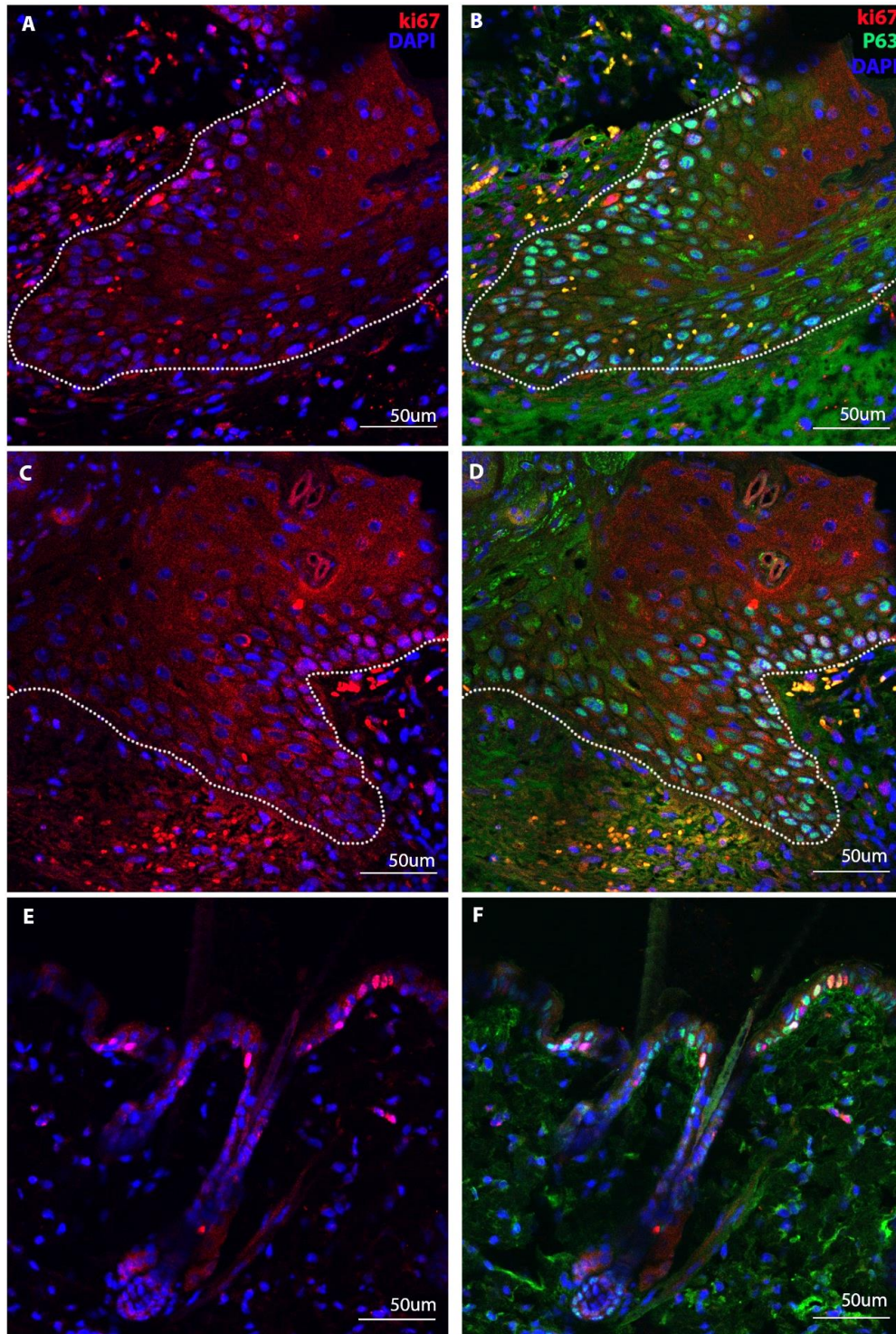


Figure 22 Expression of proliferation markers KI67 and P63 in the proliferative region of an *in vivo* wound model 4 days post injury

Immunofluorescence images showing expression of the proliferation marker KI67 co-stained with P63 at the proliferative region of an in vivo murine wound model formalin fixed and paraffin embedded 4 days post injury. (A, B) Left wound border (C, D) Right wound border (E, F) Uninjured skin. Expression of the two markers at the wound border did not overlap convincingly with just a few of the P63 positive basal cells also displaying positive KI67 expression. A higher degree of overlap between the two markers was observed in uninjured skin. (n=4)

I.IV PCP markers have a distinct expression pattern at the wound border

Since establishing that the murine wound models were appropriate systems to use to study the proliferative stages of wound healing, we next confirmed whether this extended to also include the migratory phase. To do this, we assessed whether cells in our region of interest at the wound border had started to experience Wnt signalling and were therefore eliciting a polarised response through induction of the PCP pathway. Our region of interest was primarily the bulk of proliferating keratinocytes at the wound edges because these cells will succumb to the strongest morphogen gradients emanating from the wound and therefore display the greatest migratory activity.

To investigate this, immunofluorescence staining was used to screen a panel of PCP markers in the *in vivo* models. As mentioned previously, PCP is considered to be under the control of a set of three core transmembrane receptors which are Frizzled, Vangl and Celsr so these were used as a starting point to look for evidence of asymmetric cellular localisation using the same *in vivo* wound models 4 days post injury. If the PCP pathway had indeed been activated in response to injury, we would expect to see polarised expression of these particular markers.

Both Frizzled 3 and Frizzled 6 have previously been implicated in polarisation of adult skin and such studies have identified these two proteins as closely related homologs with a degree of functional redundancy between them ¹⁸⁶.

I.V Frizzled 3 is polarised towards the wound *in vivo* but Frizzled 6 is not

With this in mind, it came as a slight surprise to find that Frizzled 3 showed very pronounced polarised expression at the proximal side of cells towards the direction of migration whereas Frizzled 6 had a weaker, more uniform expression pattern that did not overlap. This phenomenon was seen consistently across all samples where asymmetrical, staining of Frizzled 3 in the leading edge of cells at the left hand side of the wound perfectly mirrored that of the right (Figure 23 and Supplementary Figure 2). Expression of Frizzled 3 seemed to be stronger in spinous layers of cells just beyond the basement membrane where you would expect to find cells that could begin detaching from the surrounding epithelial sheet and begin migration.

The immunofluorescence staining and higher magnification images also showed evidence of structural changes to the cell shape where lamellipodia could clearly be seen projecting outwards towards the wound where the majority of Frizzled 3 expression was concentrated.

The discrepancy in Frizzled 3 and Frizzled 6 staining could suggest that despite their functional redundancy, they may have retained some tissue specific and response specific roles that have remained independent of each other.

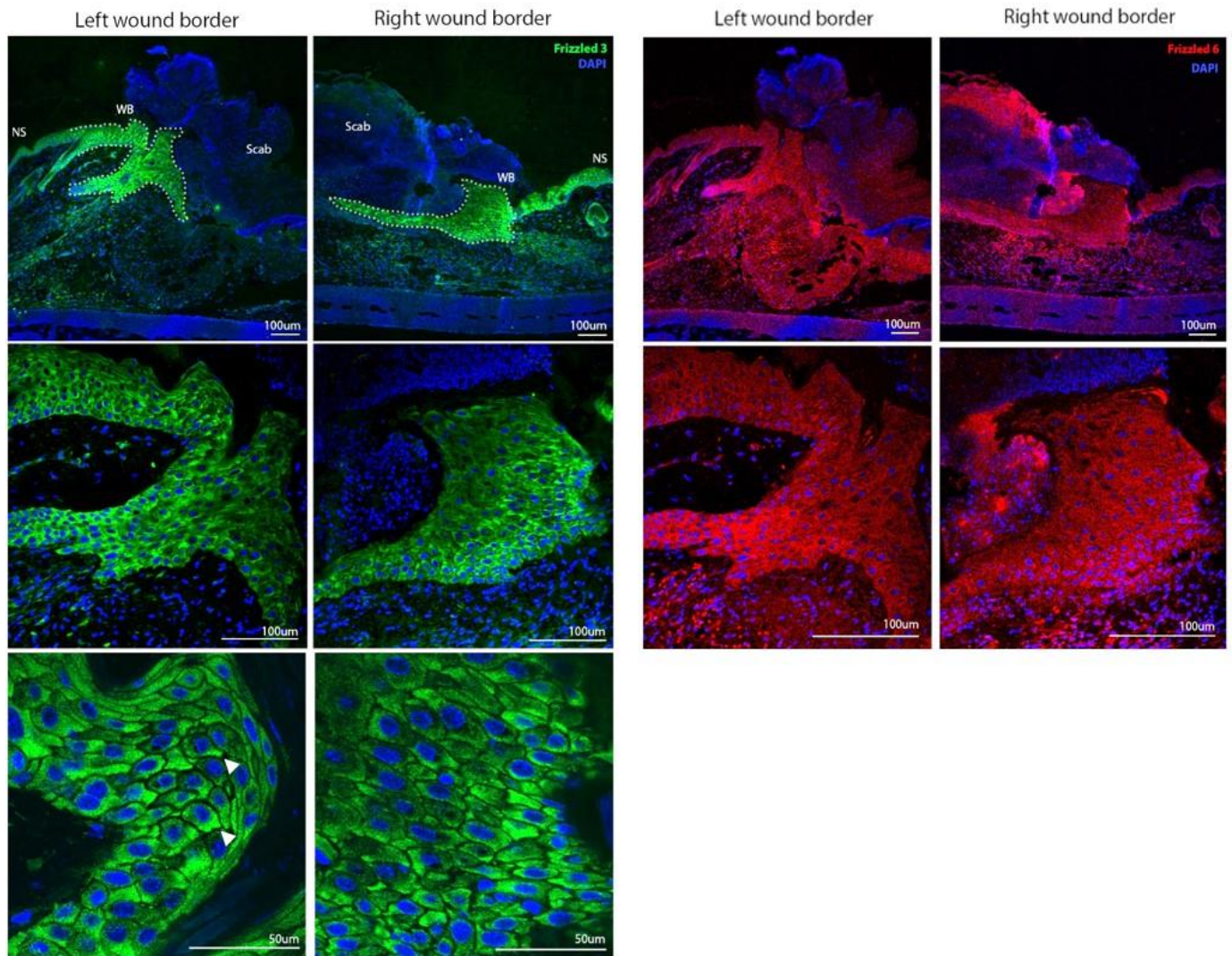


Figure 23 Expression pattern of Frizzled 3 and Frizzled 6 in *in vivo* mouse wound models

Representative images of immunofluorescence staining used to characterise expression patterns of Frizzled 3 (green) and Frizzled 6 (red) receptors in four separate in vivo mouse wound samples formalin fixed and paraffin embedded 4 days post injury. Images were taken of the proliferative regions of cells at the left and right wound edges. Sections were cut at 8µm. DAPI (blue) was used to counterstain nuclei. NS: Normal Skin, WB: Wound Border. Dotted line indicates the region of proliferating cells at the wound edge that are migrating across the wound bed. White arrows highlight polarised expression of Frizzled 3. (n=4)

I.VI Frizzled 3 is also polarised towards the wound *in vitro*

From the immunofluorescence staining carried out on mouse wound samples, it was clear that Frizzled 3 was polarised at the wound border whereas Frizzled 6 was less apparent in both signal strength and asymmetry.

To confirm whether these findings were translatable to human cells, it was decided that the same investigation should be carried out on human keratinocytes by using the well-established and accepted technique of scratch assays²⁰². Here, cells harvested from neonatal foreskin were grown to complete confluency in a cell culture vessel and then 'wounded' by scratching a line across the surface of the dish. As there is no initial blood loss response or presence of immune cells using this technique, the haemostasis and inflammatory phases are essentially bypassed and migration of cells at the scratch border is initiated almost immediately. Despite their drawbacks, scratch assays are frequently used to model wound healing processes *in vitro*.

Figure 24 displays a preliminary example of these cells migrating into the scratch site and was used to determine that time points of 2 hours, 6 hours and 12 hours after the scratch covered a significant window of migration over which the induction of molecular pathways could be sufficiently assessed.

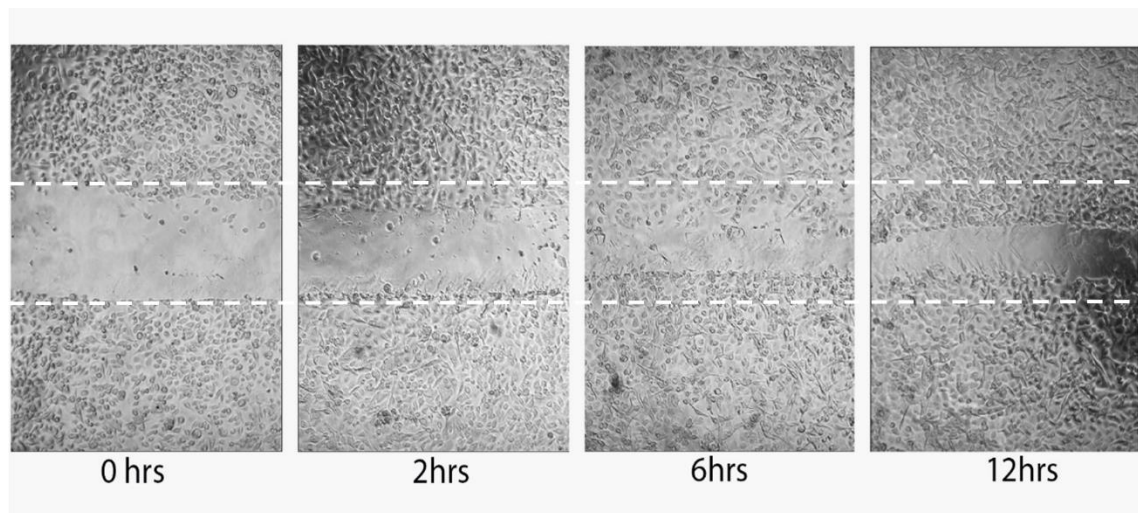


Figure 24 Using scratch assays as an *in vitro* tool to monitor wound closure

Neonatal human epidermal keratinocytes were grown to complete confluency to create a tightly packed monolayer across the surface of the culture vessel. Injury was inflicted on the epidermal sheet by scratching and dislodging a line of cells through the centre of the dish. Cells were followed over time to monitor their behaviour and wound closure ability. Migration began just a few hours post 'injury' with a significant level of closure achieved after 12 hours.

Immunofluorescence staining of Frizzled 3 receptors achieved in the scratch assays showed a similar asymmetric expression pattern with a higher intensity in the leading edge of the keratinocytes, facing the direction they were migrating, at both 6 and 12 hours post 'wound'. At both of these time points cells could be seen migrating into the scratch site, attempting to close the gap that had been created. However, in cells fixed only 2 hours after scratching, there was no evidence of migration and this was coupled with significantly weaker expression with no polarisation which closely matched expression in cells that had not been 'wounded' (Figure 25). This indicates that the upregulation and cellular redistribution of Frizzled 3 receptors in response to injury may take several hours *in vitro* and correlates with the start of migration.

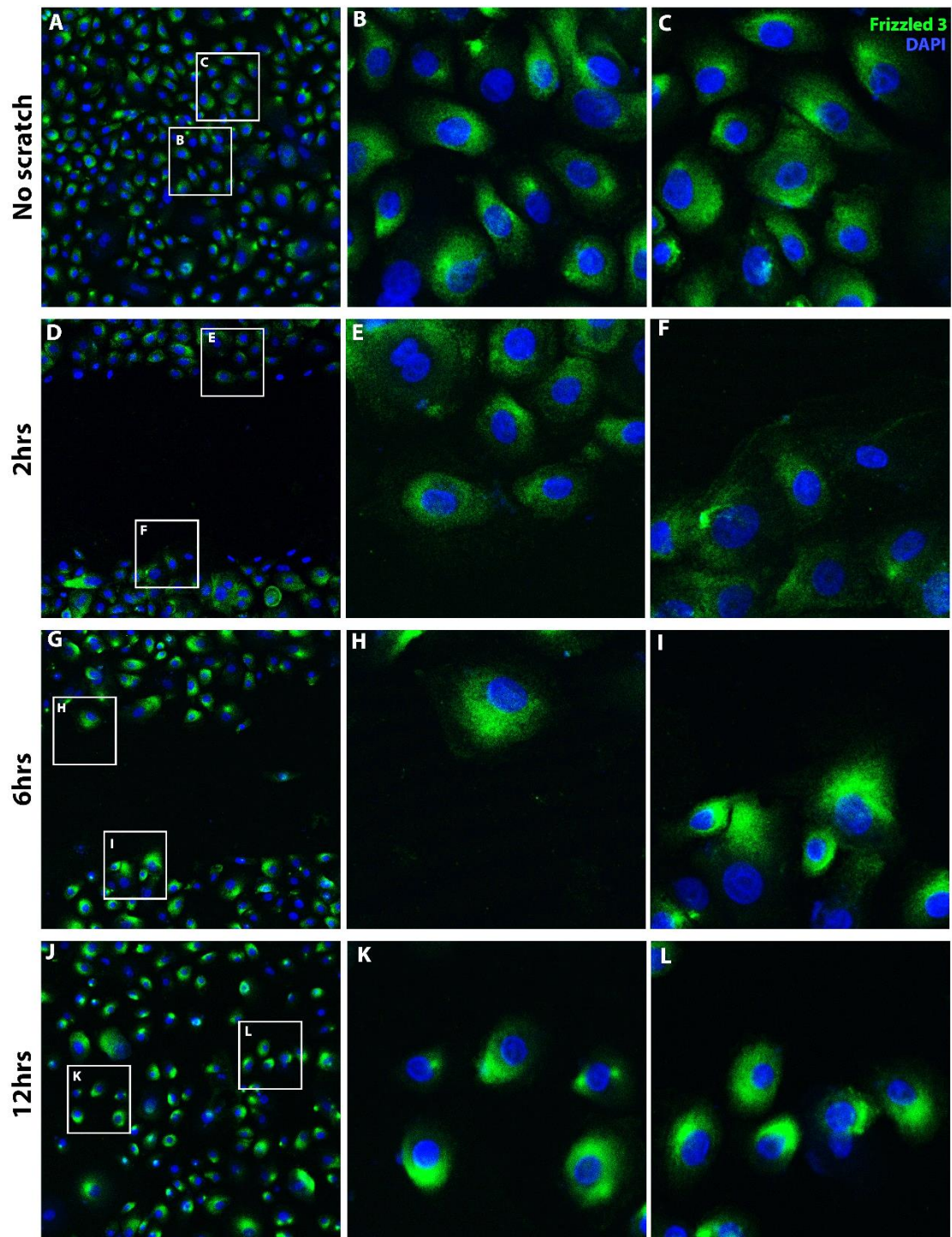


Figure 25 Expression pattern of Frizzled 3 receptors in *in vitro* scratch assays

Immunofluorescence staining used to characterise expression patterns of Frizzled 3 (green) receptors in migrating human keratinocytes that had been grown to complete confluency as a monolayer epidermal sheet and then injured using the scratch assay technique. Images were taken of cells near the scratch border. DAPI (blue) was used to counterstain nuclei.

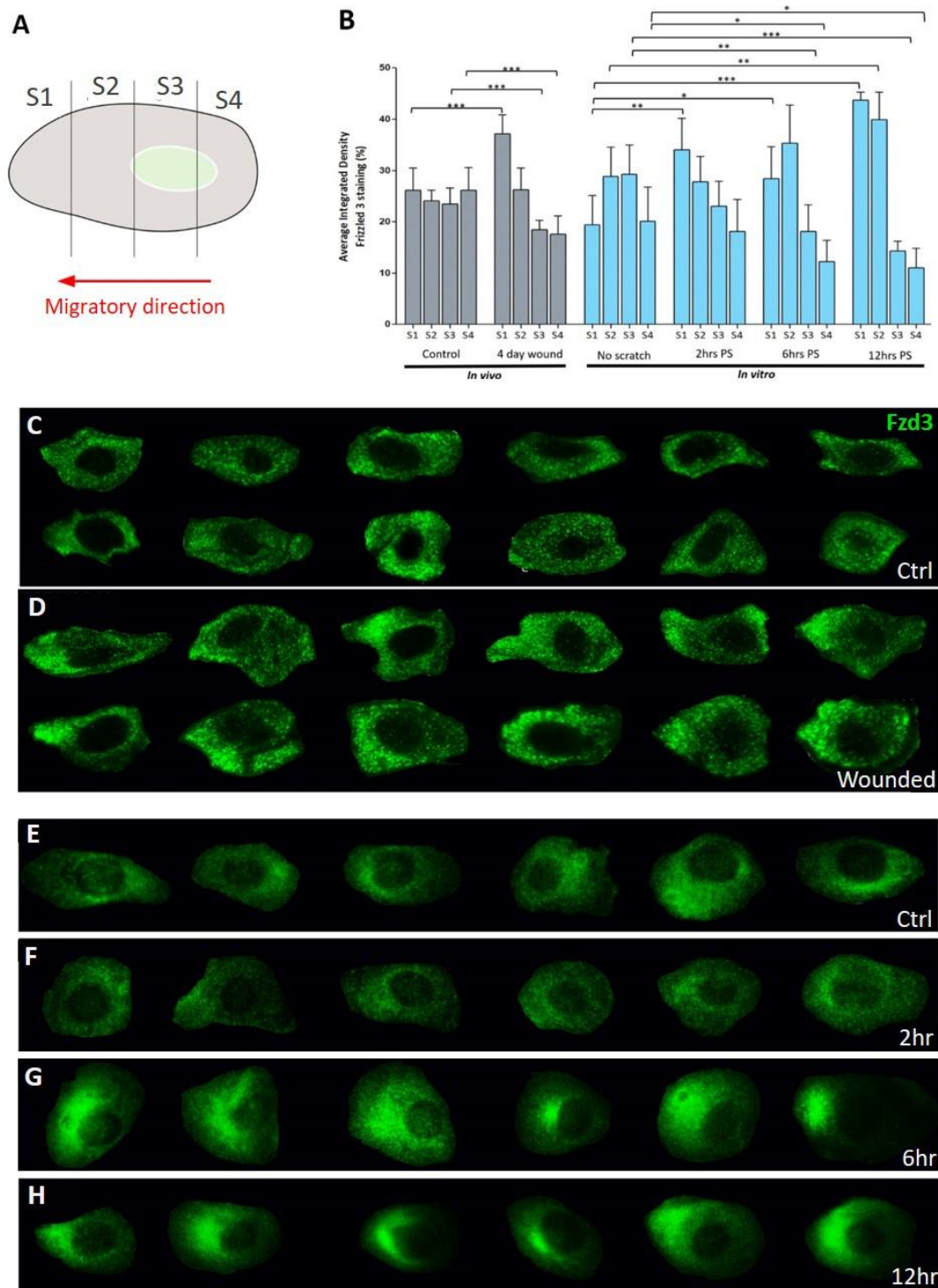


Figure 26 Quantification of polarised Frizzled 3 expression

High magnification images of individual cells were isolated from *in vivo* mouse wounds and *in vitro* scratch assays. (A) *In vivo* cells were orientated parallel to the basement membrane while *in vitro* cells were orientated relative to the position of the scratch and then each was divided into 4 equal segments. S1 represents the leading edge, S2 and S3 represent the middle portions of the cell and S4 represents the trailing end. (B) Fluorescence intensity of Frizzled 3 staining was measured by calculating integrated densities for each cell segment and plotted as a percentage of the total cell fluorescence. (C) *In vivo* images of uninjured keratinocytes and (D) corresponding wounded keratinocytes at the wound border, $n=12$. (E) Un-scratched *in vitro* keratinocytes and (F-H) corresponding scratched keratinocytes at 2, 6 and 12 post scratch (ps), $n=6$. (* = $P < 0.05$, ** = $P < 0.01$, *** = $P < 0.001$)

To statistically assess the significance of wound induced polarisation of Frizzled 3 expression, high magnification images of individual cells were isolated from the *in vivo* and *in vitro* experiments. *In vivo* cells were orientated parallel to the basement membrane so that each cell was assessed relative to the same plane of the wound site. *In vitro* cells were orientated relative to the position of the scratch in the culture vessel (Figure 26C-H). Each cell was then divided into 4 equal segments where segment 1 encapsulated the leading edge, segments 2 and 3 spanned the main body of the cell and segment 4 encapsulated the trailing end (Figure 26A). ImageJ software was used to calculate integrated intensity values for each of these segments to numerically represent the distribution of fluorescence across the whole cell. Average values for each segment were plotted on a graph as a percentage of the total cell fluorescence (Figure 26B).

Significant increases were seen in the fluorescence load of segments 1 and 2 with corresponding reductions in the proportion of fluorescence in segments 3 and 4 in both *in vivo* and *in vitro* cells, supporting the initial observations that expression becomes polarised at the leading edge in response to injury.

I.VII Expression of other PCP receptors at the wound site

We used immunofluorescence staining to assess the expression profiles of Vangl2 and Celsr1 in the same region at the wound border. Owing to the distinct polarisation of Frizzled 3, we expected to see similarly induced asymmetrical distribution of these two receptors as well, particular considering the intracellular antagonism that occurs between Vangl2 and Frizzled to sustain and disseminate polarisation across the area.

However, Vangl2 expression in the murine wound model displayed no evidence of asymmetric membrane localisation, instead presenting as speckled staining throughout the cytoplasm with slight enhancement around the nuclei (Supplementary Figure 1). Celsr1 appeared to show negative staining in all regions of the wound but we did not look into whether this was an antibody issue or if it was a true representation of its expression status (data not shown).

I.VIII A summary of immunofluorescent PCP markers at the wound site

Planar Cell Polarity is already known to be activated in response to injury but we wanted to use the asymmetrical rearrangements of its components to pinpoint where migrating cells resided amongst the mass of cells at the wound border. Frizzled 3 proved to show this most convincingly both *in vivo* and *in vitro* where its expression was consistently restricted to the leading edge lamellipodia of keratinocytes in a group of cells just above the basement membrane. Together with characterisation of proliferating cells, we now had a good sense of where proliferative and migratory regions were in relation to the wound bed 4 days post injury.

I.IX mRNA analysis confirms upregulation of PCP family members in response to injury

The immunofluorescence screening was a useful way to gain an initial assessment of PCP markers in the wound environment compared to their expression in un-injured tissue but we but wanted to strengthen this notion by confirming the result at the

mRNA level to ensure that wounding did upregulate expression of PCP genes in accordance with other publications.

There is a concept described in literature that states that there is a population of cells at the wound border termed 'leaders' that are the first to begin migrating which, after a short period of time, are joined by a population of 'follower' cells ^{190, 191}. There is a brief lag between activation of the two populations which may be for a number of reasons. It might purely be down to proximity to the wound and therefore proximity to the morphogen gradients that initiate migration. Cells closest to the wound are exposed sooner and to higher concentrations of these cues so would theoretically begin migrating before cells further away. There is also a theory that leader cells create signals to their follower counterparts by amplifying the activating cues that they received in order to recruit more cells to the migratory mass ¹⁹².

With this in mind, an experiment was designed primarily to validate the immunofluorescent results at the mRNA level whilst also allowing us to compare any differences between leader and follower populations.

As with previous scratch assays, human epidermal keratinocytes from neonatal donors were grown to full confluency in 10cm² culture dishes. At defined time points of 30 minutes, 2 hours, 6 hours and 12 hours post scratch, cells were collected into three different fractions, as depicted in Figure 27A, and their mRNA was extracted. Fraction 1 was used to capture 'leader' cells directly adjacent to the scratch, Fraction 2 captured 'follower' cells and Fraction 3 represented cells far away from the scratch. A template was made to ensure that the size of each fraction remained consistent for each time

point and across multiple experiments. These fractions were compared to control keratinocytes that were grown to full confluency but remained unscratched.

A panel of primers was designed that included receptors, intracellular components and downstream targets of the planar cell polarity pathway.

Frustratingly, a previously designed primer pair against Frizzled 3 was used alongside the Frizzled 6 primers but they proved to be inconsistent and unreliable in the results that they produced and could therefore not be included. This was particularly disappointing given that the immunofluorescence pattern for Frizzled 3 was far more interesting at the wound border than Frizzled 6. New Frizzled 3 primers were designed at a later date and used in subsequent experiments shown later in the thesis but due to a relatively low yield of mRNA, I did not have enough sample left to repeat the real-time qPCR. I had hoped to repeat the whole experiment again from start to finish to obtain the important results for Frizzled 3 expression but time constraints prevented this.

I also found that a slight limitation with the scratch assays was actually getting the cells to grow to 100% confluency. The keratinocytes maintain a much quicker division rate and healthier morphology when they are passaged regularly. I found that on a few occasions, particularly when a higher passage of cells was used, they struggled to reach the necessary level of confluency before the morphology changed too much and they had to be discarded. I quickly realised that lower passage cells produced much better outcomes but discovering this cost precious time.

Despite this, the overall outcome of the experiment provided additional strong evidence that PCP is upregulated in response to wounding.

Two hours into the healing response, the Frizzled receptors began to show increased expression across all cell fractions which was accompanied by increased activity of downstream PCP effectors such as Rac1 (Figure 27B). This confirmed that polarisation was being induced in cells around the scratch in agreement with previously published papers¹⁹³ and that cytoskeleton rearrangements were beginning to happen to prepare the cell for migration.

As time progressed, we observed a substantial rise in expression across the majority of primers that we tested. Upregulation of Celsr1 and Vangl2 receptors was particularly notable at 12 hours post scratch and we speculate that cells may require them to help maintain polarity in the migrating cells even though immunofluorescence staining did not allude to this. At the final time point, we also observed significant increases in downstream effectors of the PCP pathway including cJun, RhoA and Rac1.

Taken together with the immunofluorescence results, this provided convincing evidence that injury does activate the PCP pathway as literature suggests and that our chosen wound models illicit at least some degree of natural healing response.

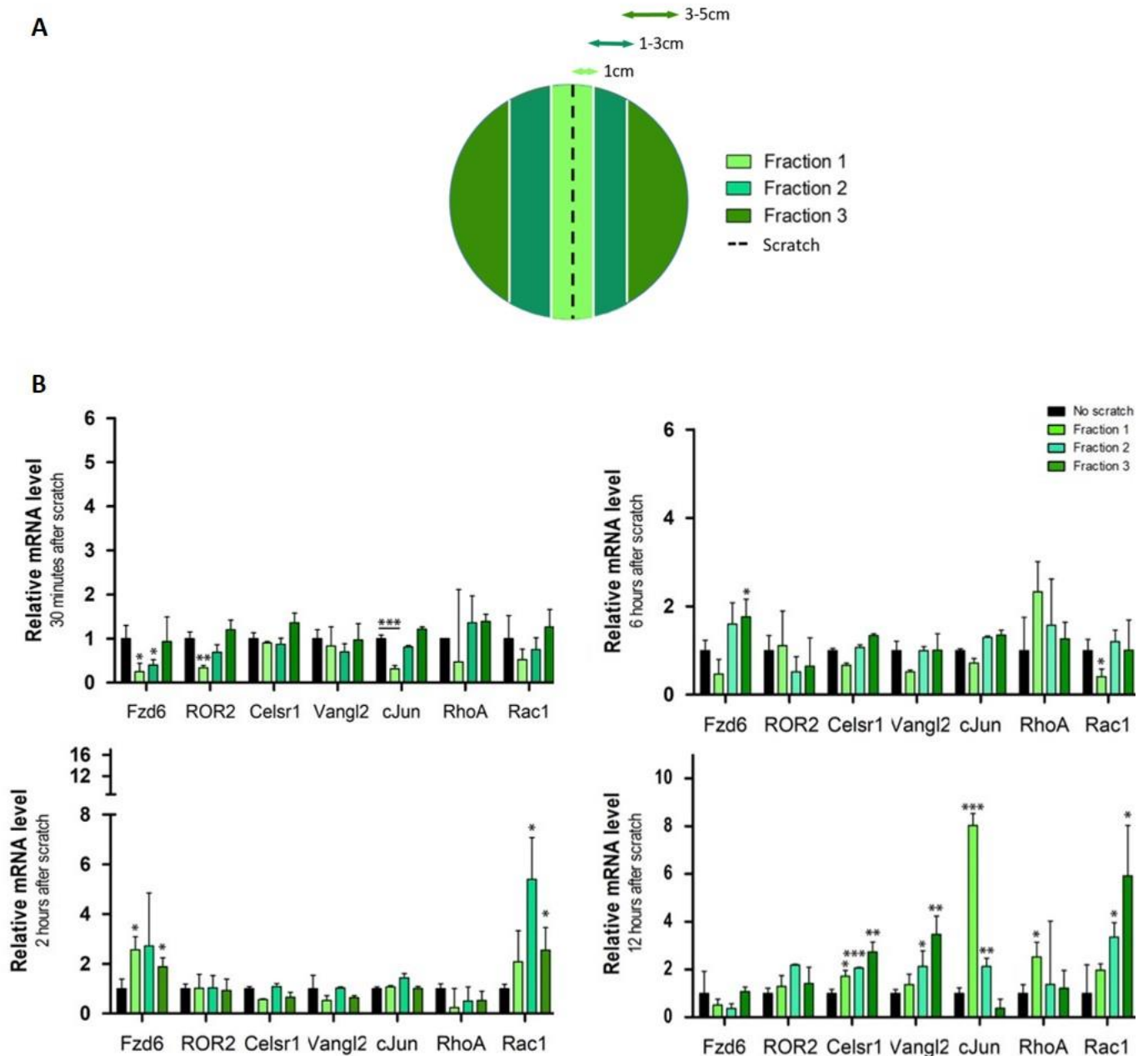


Figure 27 mRNA analysis of PCP components in different populations of keratinocytes following *in vitro* scratch assays

Neonatal human keratinocytes were grown to confluency as a monolayer epidermal sheet and then injured using the scratch assay technique. (A) Dishes were divided into three fractions so that cells could be collected into populations representing 'leader' cells, 'follower' cells and distant cells relative to the scratch that had been inflicted. Fraction 1 captured leader cells that fell within a 1cm margin of the scratch, Fraction 2 captured follower cells within a margin of 1-3cm. Fraction 3 captured the remaining distant cells that fell beyond 3cm from the scratch. (B) Real-Time qPCR analysis was used to assess changes in mRNA expression levels of PCP pathway components in fractions of leader, follower and distant keratinocytes across different time points. There was a clear upregulation of markers in response to injury. (* = $P < 0.05$, ** = $P < 0.01$, *** = $P < 0.001$)

Having established that PCP appears to be both upregulated and polarised in keratinocytes following injury, the next task was to identify and confirm what in the wound environment was causing its activation. Of the 19 known members of the Wnt family, literature suggests that Wnt5a and Wnt11 are the ligands most often associated with Frizzled 3/6 binding^{95, 100, 101}. Using Wnt5a as an initial target, I next investigated whether Wnt5a signals could be identified in the wound models.

I.X Wnt5a signals in the *in vivo* mouse model

Immunofluorescence staining was carried out on the mouse wound models and demonstrated that Wnt5a was highly expressed in the wound bed. It was specific to the dermal compartment beneath the epidermal wound site with no expression present in the surrounding peripheral tissue (Figure 28A-D). To further confirm that Wnt5a signals are produced in response to injury, Figure 28E shows that there is no expression in uninjured mouse skin from the same region.

However, without carrying out further investigation, there was no way of knowing which cells the signals were coming from. There are several different populations of cells recruited to a wound bed so would have needed to co-stain with cell specific markers for dermal fibroblasts, endothelial cells and various immune-related cells to look for overlap in expression. Given that Wnt5a is secreted into the extracellular environment, it would be very difficult to establish exactly where the signal was originating from using immunofluorescence of a fixed tissue.

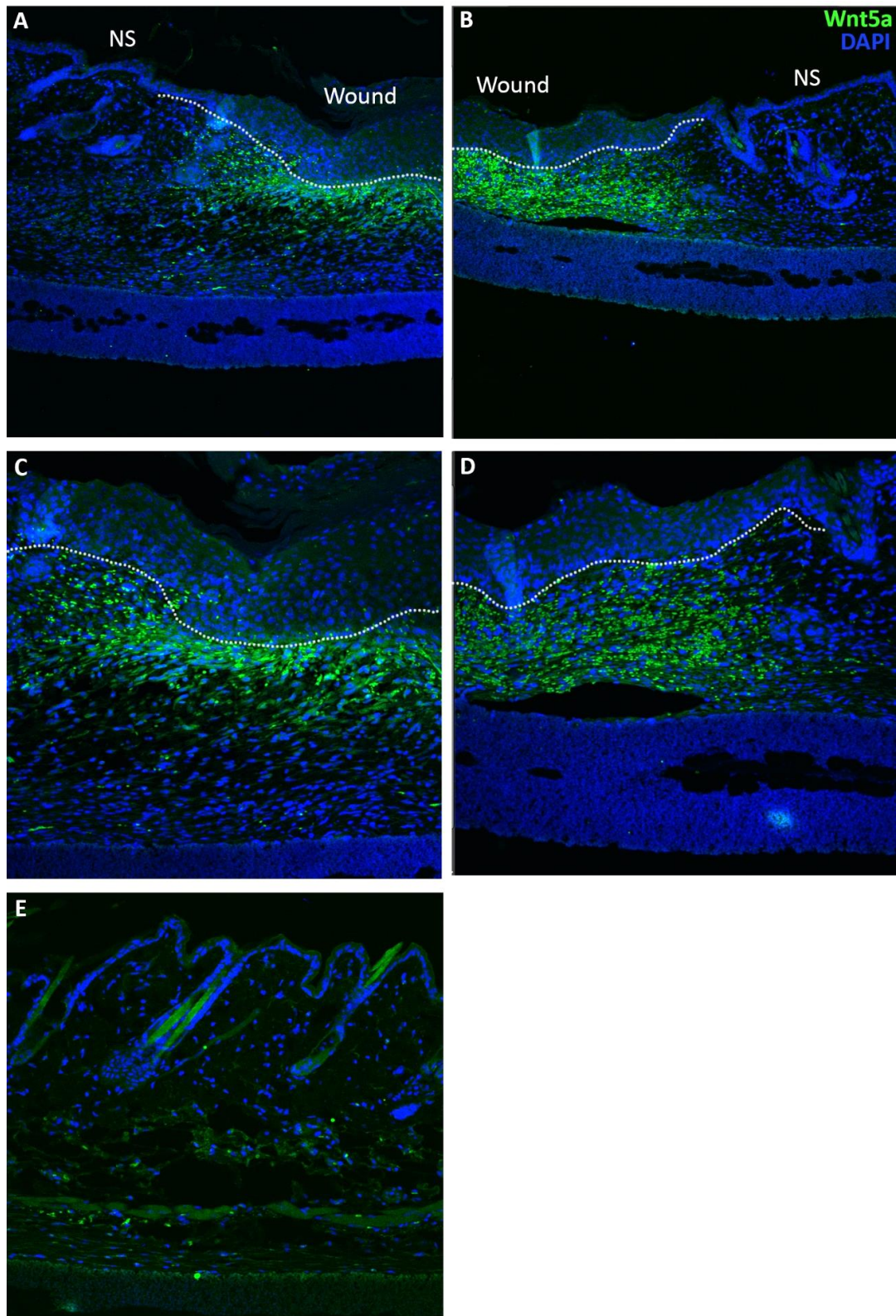


Figure 28 Wnt5a expression in the *in vivo* mouse model

Immunofluorescence staining used to characterise expression of Wnt5a (green) in in vivo mouse wound samples fixed 7 days post injury. Sections were cut at 8µm. DAPI (blue) was used to counterstain nuclei. (A & C) Left wound border. (B & D) Right wound border. (E) Uninjured skin from the same region.

NS: Normal Skin, WB: Wound Border. Dotted line indicates basement membrane.

I.XI Dermal fibroblasts produce Wnt5a in response to scratch assays

To dissect this further, I used the *in vitro* scratch assay technique to isolate individual populations of human cells to see whether they were capable of producing the Wnt5a signal in response to injury.

When using human dermal fibroblasts alone, immunofluorescence results showed a clear increase in the expression of Wnt5a but appeared to be a delayed response, emerging only 24 hours post scratch (Figure 29A).

Wnt5a expression was then analysed at both the mRNA and protein level from 'leader' and 'follower' dermal fibroblasts. These two distinct populations were collected by carrying out the scratch assay in a 10cm culture dish, inflicting the scratch along the vertical midline and then isolating cells within 1cm either side of the scratch as the leader population. The remaining cells that fell outside this margin were collected as the follower population (Figure 29D). Results indicated that there was no discernible upregulation of Wnt5a in response to injury at the mRNA level (Figure 29B) but a small increase in the population of follower cells at the protein level after 24 hours (Figure 29C).

This did not fit with previous results where we had seen activation of PCP much sooner *in vitro*. Two questions arose from these results; first was whether another Wnt ligand was responsible for the earlier activation of PCP at the wound, owing to the known redundancy that exists between Wnt and Frizzled receptors and secondly, whether the scratch alone was sufficient to induce Wnt5a secretion in the HDF cells since they had

now been isolated from the endogenous wound environment. The physical trauma caused by the scratch may not be enough to trigger an endogenous Wnt5a response that would normally occur *in vivo*. We know from other studies that normal dermal fibroblasts at the wound periphery undergo differentiation to become myofibroblasts¹⁹⁹ which experience much stronger tensile forces as they contract to bring the wound edges closer. For this reason, we next investigated whether the HDF cells required both physical damage and tension in order to secrete Wnt5a sooner in the wound environment.

I.XII Stretching forces induce Wnt5a expression in dermal fibroblasts

Suspensions were confirmed by exerting a uniaxial constant strain of 12% on the HDF cells for 6 and 24hr periods. This elicited a much quicker response of Wnt5a upregulation that remained high in comparison to un-stretched cells (Figure 29E) and therefore suggests that HDF cells require multiple factors and triggers to cause Wnt5a secretion at the wound site.

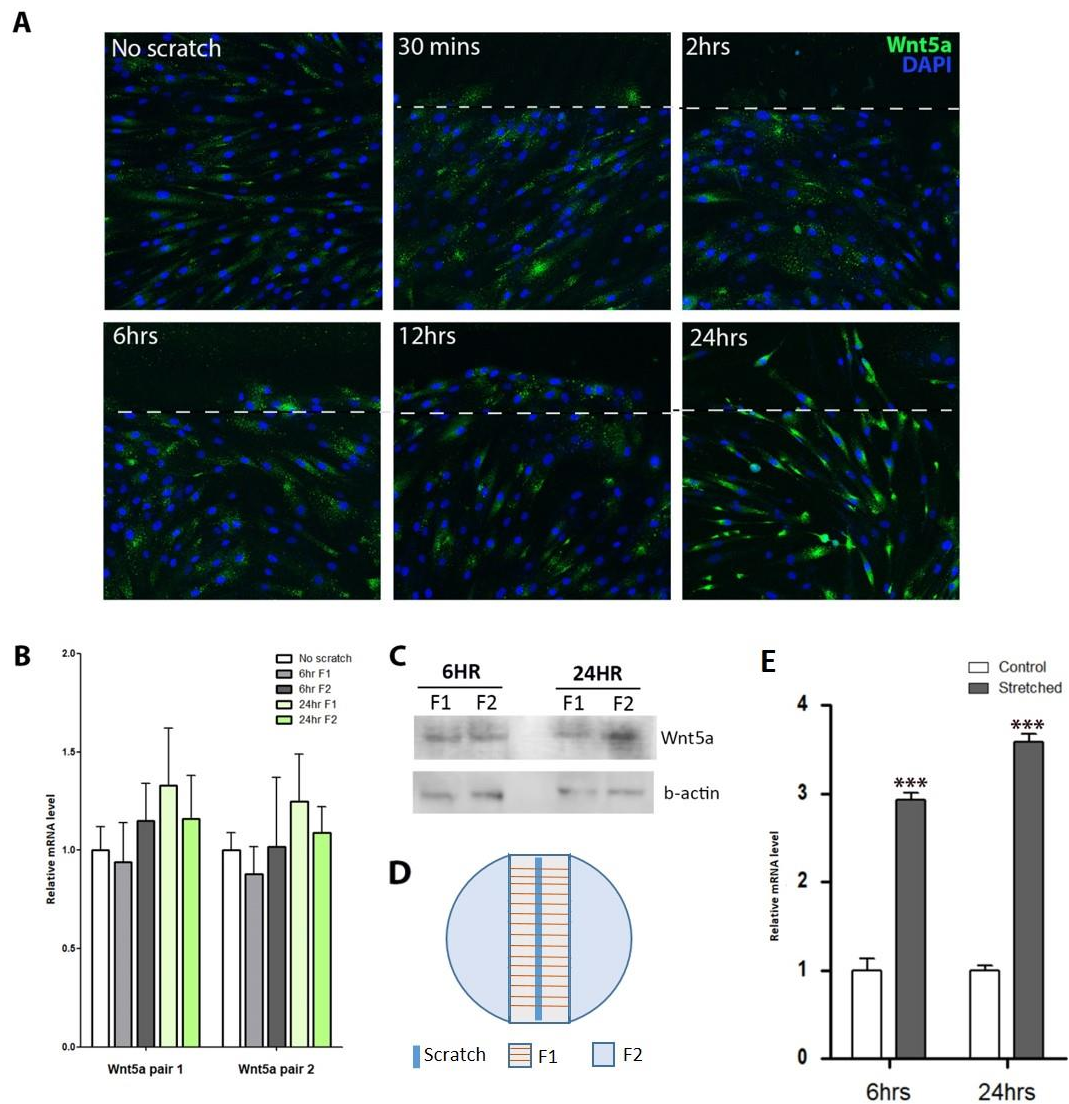


Figure 29 HDF cells secrete Wnt5a in response to *in vitro* injury and tensile forces

(A) Immunofluorescence staining carried out on human dermal fibroblasts that had been grown to confluency and used in a scratch assay showed that there is a gradual increase in the expression of Wnt5a (green) as time since injury increases. After 24 hours, Wnt5a is upregulated by a significant degree. Nuclei are counterstained with DAPI. Dotted white line indicates the initial scratch border. (B) Real-time qPCR analysis was used to assess levels of Wnt5a mRNA expression in populations of leader and follower dermal fibroblasts at 6 and 24 hours post scratch injury. Two different primer pairs, targeting different regions of the gene sequence, were used but no discernible upregulation was seen in response to wounding (F1 = leader, F2 = follower) (C) Western blot analysis of Wnt5a protein levels in the same populations of leader and follower dermal fibroblasts 6 and 24 hours post injury. Bands indicate a small increase in Wnt5a protein in follower cells after 24 hours, consistent with immunofluorescence results. (D) Schematic diagram demonstrating how leader and follower cell population were collected. Dermal fibroblasts were grown to confluency in a 10cm culture dish. A scratch was created along the vertical midline and leader cells collected within a 1cm margin either side of this line. The follower population consisted of the remaining cells. (E) Human dermal fibroblasts were grown on collagen coated silicone stretch chambers and then subjected to a 12% uniaxial constant strain for 6 and 24 hour periods. Real-time qPCR analysis was used to assess expression changes of Wnt5a at the mRNA level. The stretching force was found to induce significant upregulation of Wnt5a during both time periods. (***) = $P < 0.001$)

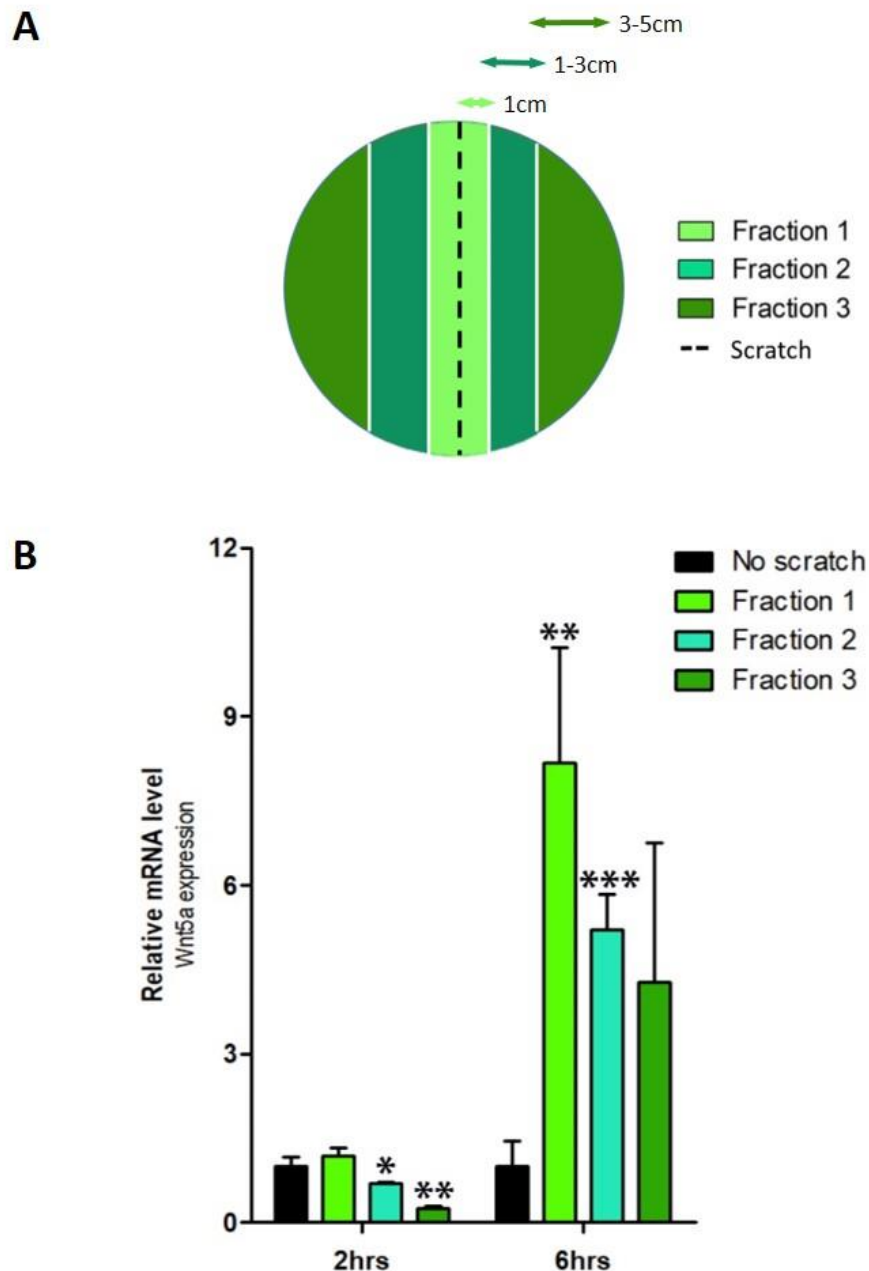


Figure 30 Epidermal keratinocytes secrete Wnt5a in response to *in vitro* injury

Neonatal human keratinocytes were grown to confluency as a monolayer epidermal sheet and then injured using the scratch assay technique. (A) A schematic representation demonstrating how 10cm² cell culture dishes were divided into three fractions so that cells could be collected into populations representing 'leader' cells, 'follower' cells and distant cells relative to the scratch that had been inflicted. Fraction 1 captured leader cells that fell within a 1cm margin of the scratch, Fraction 2 captured follower cells within a margin of 1-3cm. Fraction 3 captured the remaining distant cells that fell beyond 3cm from the scratch. (B) Real-Time qPCR analysis was used to assess changes to mRNA expression levels of Wnt5a in fractions of leader, follower and distant keratinocytes across different time points. Injury was found to induce significant upregulation of Wnt5a in keratinocytes (* = $P < 0.05$, ** = $P < 0.01$, *** = $P < 0.001$)

I.XIII Epidermal keratinocytes produce Wnt5a in response to scratch assays

After gathering evidence that dermal fibroblasts were capable of generating the Wnt5a morphogen gradient, it was logical to assess whether the epidermal keratinocytes could also produce Wnt5a, particularly to see whether migrating leader cells were able to signal to follower populations. A real-time qPCR revealed that 6 hours after *in vitro* injury, Wnt5a expression increased more than 8 fold in leader cells with a gradual reduction in fraction 2 and 3 as the cells got further away from the scratch (Figure 30).

I.XIV Wnt5a treatment upregulates expression of PCP components *in vitro* without prior wounding

It had now been confirmed that Wnt5a was present in the wound environment and was produced by both HDF cells and keratinocytes in response to injury. Our next step was to confirm that it activated the PCP pathway as literature suggests ²⁰⁰.

To test this, we tried to eradicate all other potential wound-associated factors that might upregulate polarity by growing keratinocytes under normal conditions and to a standard confluency. This would alleviate any other triggers such as contact inhibition or nutrient deprivation from overcrowded culture dishes to prevent other factors skewing the results. The cells were treated with human recombinant Wnt5a protein at varying doses to see whether this alone could upregulate the components of the pathway, independently of a scratch being inflicted.

As expected, upregulated expression was seen in both Frizzled 3 and Frizzled 6 receptors. However, there was an absence of response from the other core PCP

membrane components Celsr1 and Vangl2 which may be due to them having no direct interaction with Wnt ligands and therefore no immediate response to the Wnt5a treatment (Figure 31).

As described earlier in the introduction, ROR2 has recently gained interest as a potential co-receptor for Frizzled and may even bind to Wnt directly to enhance polarisation and as an alternative mechanism to activate PCP. The results from this experiment clearly indicate that ROR2 is highly responsive to the presence of Wnt5a. It would be of particular interest to investigate its role in PCP induction in future avenues of research to challenge whether the current model of the PCP pathway is correct, given that we have seen such a distinct response here (Figure 31).

It was also notable that Wnt5a treatment triggered upregulation of the downstream PCP effector Rac1 which plays important roles in cytoskeleton rearrangement. Given what is known about the PCP pathway, this is likely to be an indirect response caused by increased expression of PCP receptors and initiation of polarisation rather than Wnt5a directly influencing its gene regulation (Figure 31).

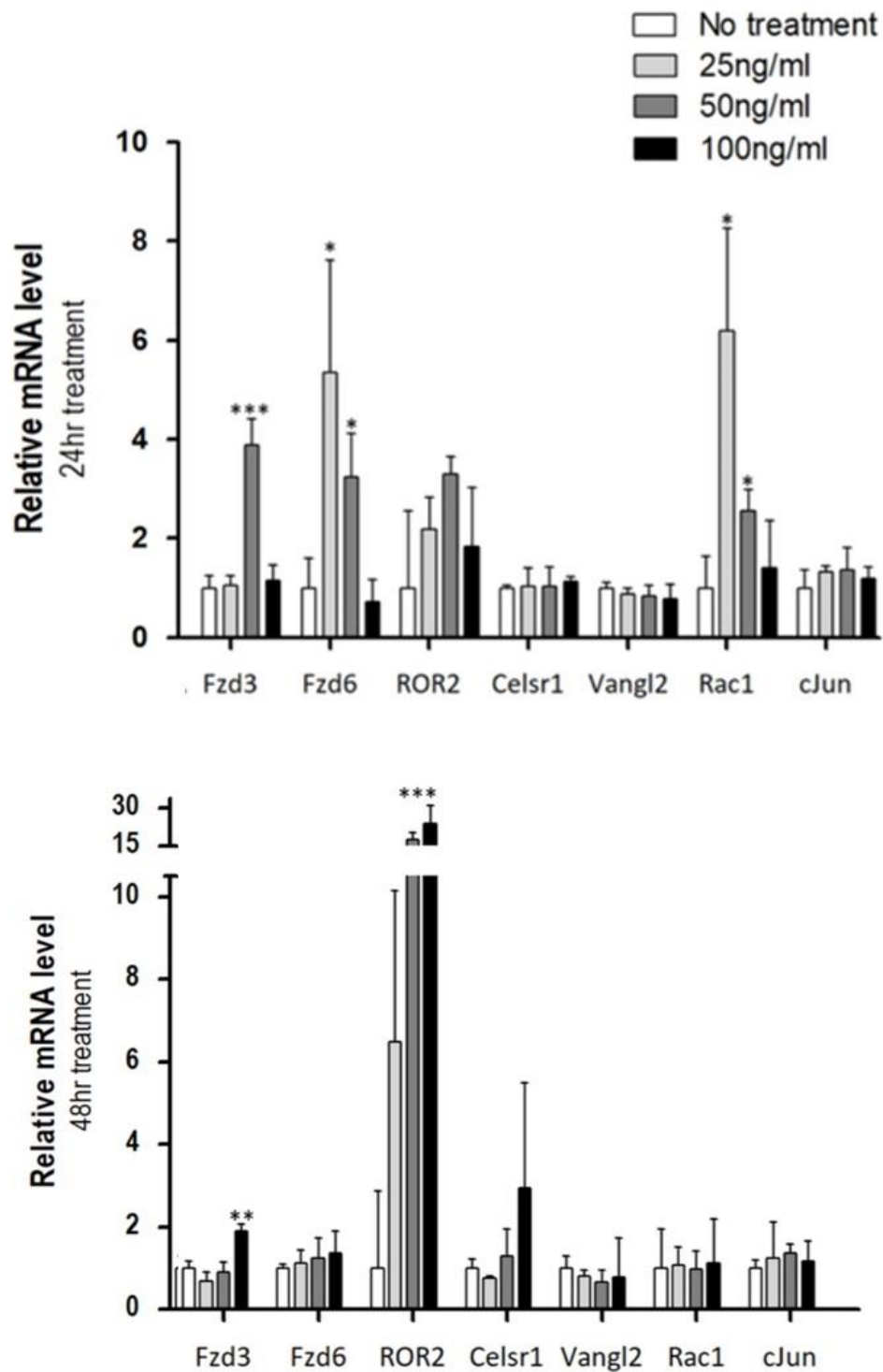


Figure 31 Wnt5a treatment induces upregulation of PCP markers, independent of injury

Real-time qPCRs investigating the effect Wnt5a treatment has on the expression of PCP genes in human epidermal keratinocytes when cells are grown under standard culture conditions to standard confluency. (= $P < 0.05$, ** = $P < 0.01$, *** = $P < 0.001$)*

I.XV Summary of results section 1

The first section of my results has characterised and validated an *in vivo* murine wound model for use throughout the project. The physical morphology of different stages of wound healing were assessed and resulted in 4 days-post injury being chosen as a suitable time point to study migration of cells in the wound environment.

Alongside this, an *in vitro* scratch assay model was characterised to offer an alternative platform upon which finer details of the healing process could be investigated during later stages of the project.

Through immunofluorescent assessment of both of these models, it was confirmed that some members of the planar cell polarity pathway are upregulated and asymmetrically re-distributed in response to injury, most notable of which was the transmembrane receptor Frizzled 3.

This result was confirmed at the mRNA level where significant increases in both receptor and downstream effector expression was seen. These results support the findings of several other publications.

It was then demonstrated that Wnt5a is highly enriched in a wound environment whereas uninjured, healthy skin from the same region shows little to no expression. Both dermal fibroblasts and epidermal keratinocytes are capable of producing a Wnt5a signal in response to *in vitro* injury. Dermal fibroblasts can also release Wnt5a when exposed to tension, demonstrated by simulating the stretching/ contractile forces that would be experienced in the endogenous wound environment.

Finally, it was shown that the presence of Wnt5a ligands, when added to culture medium as recombinant protein, is sufficient to induce upregulation of PCP components in epidermal keratinocytes despite no 'wound' taking place *in vitro*. Efforts were made to eliminate any other triggers that may have influenced the initiation of polarity in the cells, making it likely that the observed changes were due to Wnt5a.

In summary, cutaneous injury triggers the release of Wnt5a from several cell populations in the wound environment. This initiates a signal cascade that subsequently activates planar cell polarity in epidermal cells at the wound periphery.

RESULTS SECTION II

Characterisation of autophagy in the wound environment.

The second results section was used to assess and characterise whether autophagy could be detected in the same populations of migratory cells at the wound borders. For continuity and direct comparison, the same *in vitro* and *in vivo* techniques developed during the first results section were employed in the same fashion. Immunofluorescence staining was carried out using antibodies against the core autophagy components as well as analysis carried out at the protein and mRNA levels in leader and follower epidermal cells.

II.I ATG5 is polarised away from the wound *in vivo*

The first marker tested was ATG5, an autophagy protein that forms part of the final complex involved in elongation and completion of the autophagosome membrane. *In vivo* results from 4 days post injury showed that its expression was present and asymmetrical in the mass of migrating cells at the wound border. Interestingly, staining was concentrated away from the wound at the trailing end of the cell. White arrows in Figure 32 highlight particular cells that show very obvious polarised distribution in the cells.

Of note, cells residing in the inner layers closest to the basement membrane of this region appeared to be negative for ATG5 staining with expression not visible until approximately the spinous layer. Taken together with the P63 result shown previously,

this would suggest that ATG5 is suppressed in proliferating cells and is only activated as the cells begin to mature and migrate towards the wound. This phenomenon occurred in the same population as polarised Frizzled 3 expression but in the opposing half of the cell.

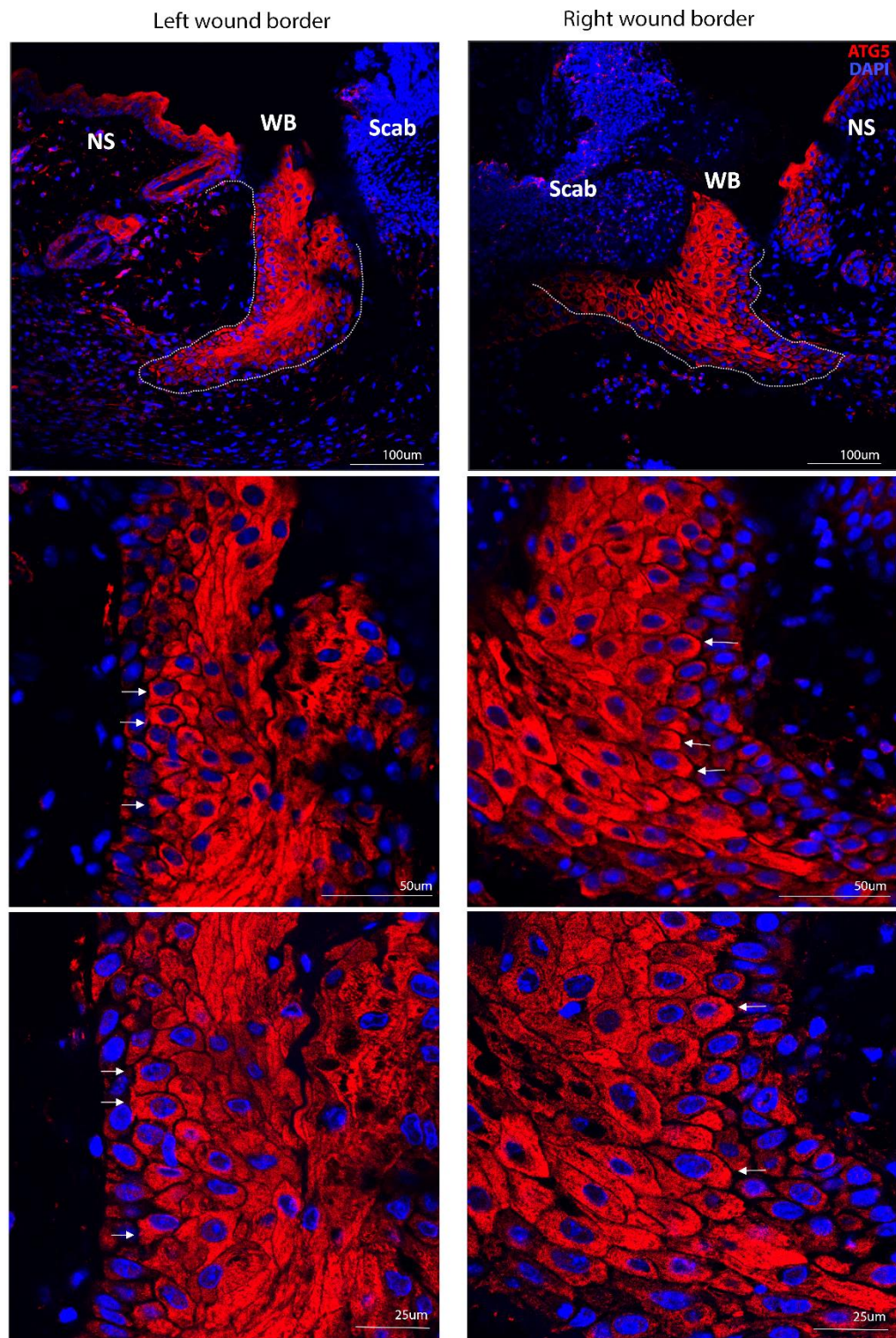


Figure 32 Expression pattern of ATG5 *in vivo*

Immunofluorescence staining used to characterise the expression pattern of ATG5 (red) in an in vivo mouse wound sample formalin fixed and paraffin embedded 4 days post injury. Images were taken of the proliferative region of cells at the left and right wound edges. Sections were cut at 8µm. DAPI (blue) was used to counterstain nuclei. NS: Normal Skin, WB: Wound Border. Dotted line indicates the epidermal basement membrane. White arrows highlight basal cells with clear asymmetrical distribution of ATG5 at their distal side, away from the wound. (n=4)

II.II **ATG5 is polarised away from the scratch *in vitro***

The polarised expression of ATG5 was indeed confirmed *in vitro*. Figure 33 shows that cells fixed at 2 and 6 hours post injury displayed cytoplasmic ATG5 expression almost exclusively in the trailing end of the cell, opposing the migratory direction. This phenomenon not only supported the *in vivo* findings but provided additional evidence that injury does induce autophagic activity and that it is restricted to distal sites within the cell.

There were also some cells with potential staining in the nucleus, particularly at 2 hours, and further reading into this implied that ATG5 has been known to translocate to the nucleus in response to DNA damage ¹⁸⁷. The only cells that this was observed in was those closest to the scratch site and therefore most likely to have been damaged. However, as this was not the focus of the study, it was not looked into further.

By 12 hours, ATG5 expression was greatly reduced in the scratch environment and in uninjured cells it was virtually non-existent. This observation may indicate that ATG5 is upregulated in response to injury but that its activity is short lived.

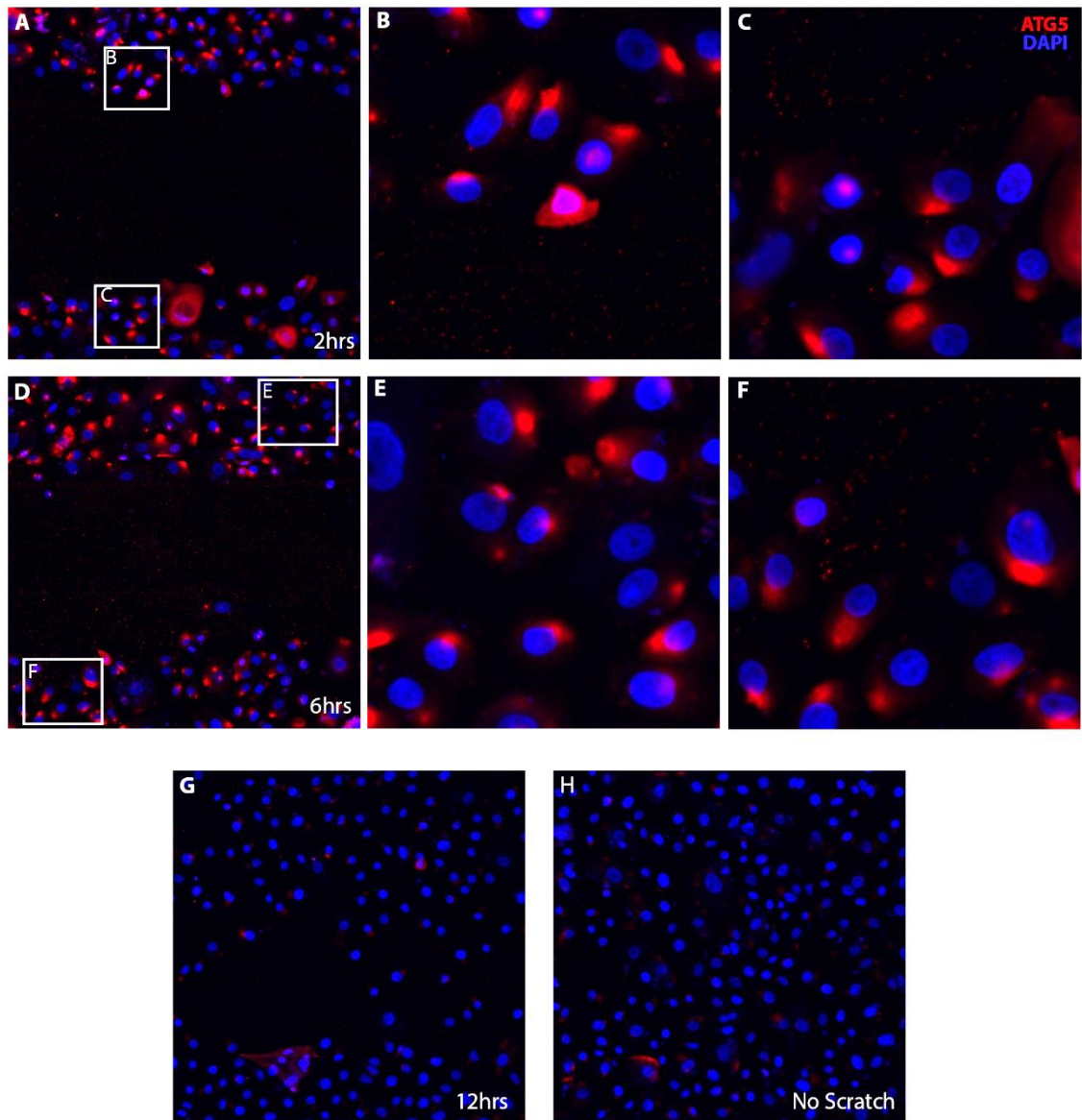


Figure 33 Expression pattern of ATG5 in *in vitro* scratch assays

Immunofluorescence staining used to characterise expression patterns of ATG5 (red) in migrating human keratinocytes that had been grown to confluency as a monolayer epidermal sheet and then injured using the scratch assay technique. Images were taken of cells near the scratch border. DAPI (blue) was used to counterstain nuclei. White boxes indicate cells that have been imaged at higher magnification to emphasise polarised expression opposing the direction of migration.

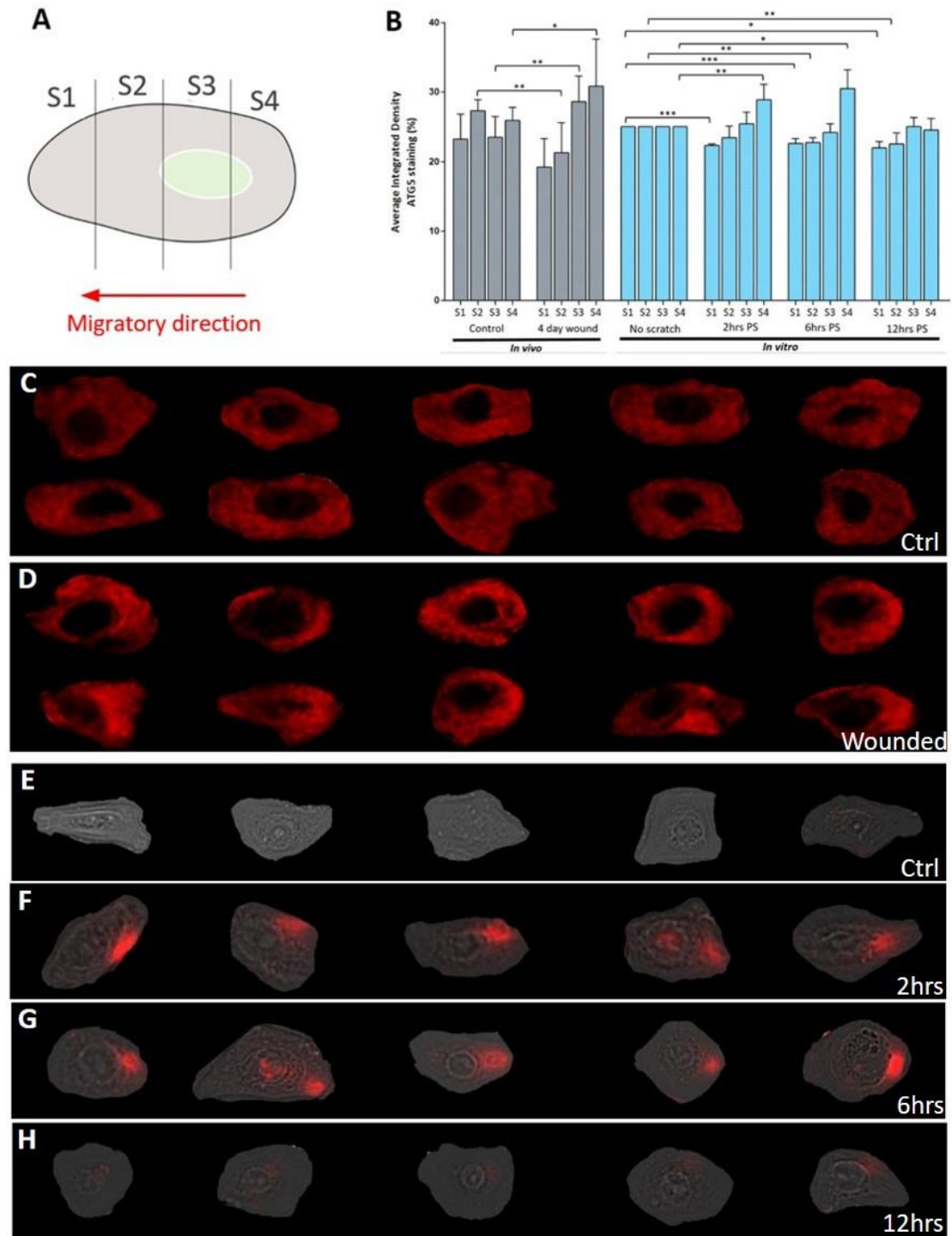


Figure 34 Quantification of polarised ATG5 expression

High magnification images of individual cells were isolated from *in vivo* mouse wounds and *in vitro* scratch assays. (A) *In vivo* cells were orientated parallel to the basement membrane while *in vitro* cells were orientated relative to the position of the scratch and then each was divided into 4 equal segments. S1 represents the leading edge, S2 and S3 represent the middle portions of the cell and S4 represents the trailing end. (B) Fluorescence intensity of ATG5 staining was measured by calculating integrated densities for each cell segment and plotted as a percentage of the total cell fluorescence. (C) *In vivo* images of uninjured keratinocytes and (D) corresponding wounded keratinocytes at the wound border, $n=10$. (E) Un-scratched *in vitro* keratinocytes and (F-H) corresponding scratched keratinocytes at 2, 6 and 12 post scratch (ps), $n=5$. (* = $P < 0.05$, ** = $P < 0.01$, *** = $P < 0.001$)

As previously explained for Frizzled 3 staining, the distribution of ATG5 expression was statistically analysed by measuring intensity density values for *in vivo* and *in vitro* cells across the 4 segments indicated in Figure 34A. For *in vivo* cells, a significant rise in the proportion of fluorescence in segments 3 and 4 was seen which corresponded to significantly more fluorescence in segment 4 of *in vitro* cells compared to unscratched cells. Both of these results provided statistical evidence that ATG5 polarises towards the trailing end of the cell (Figure 34B).

II.III Asymmetrical localisation of ATG16L is not as pronounced as ATG5

ATG16L is another protein involved in the same complex as ATG5 during autophagy so was included in the panel of markers that was initially screened to look for evidence of active autophagy. Considering the asymmetry seen in ATG5 staining, it was assumed that a similar pattern would be observed with ATG16L but this wasn't the case.

Although strong expression was present in the cytoplasm of cells at the wound border, it was much more ubiquitous in its location with little evidence of asymmetry (Figure 35). At this stage, it was difficult to explain why this was the case as most of the literature pertains to them working in conjunction with each other as part of a larger unit so should therefore be co-localised during active autophagy.

The lack of polarisation was confirmed through analysis of fluorescence intensity distribution where no significant differences were measured between wounded and unwounded tissue across any of the four cell segments (Figure 36).

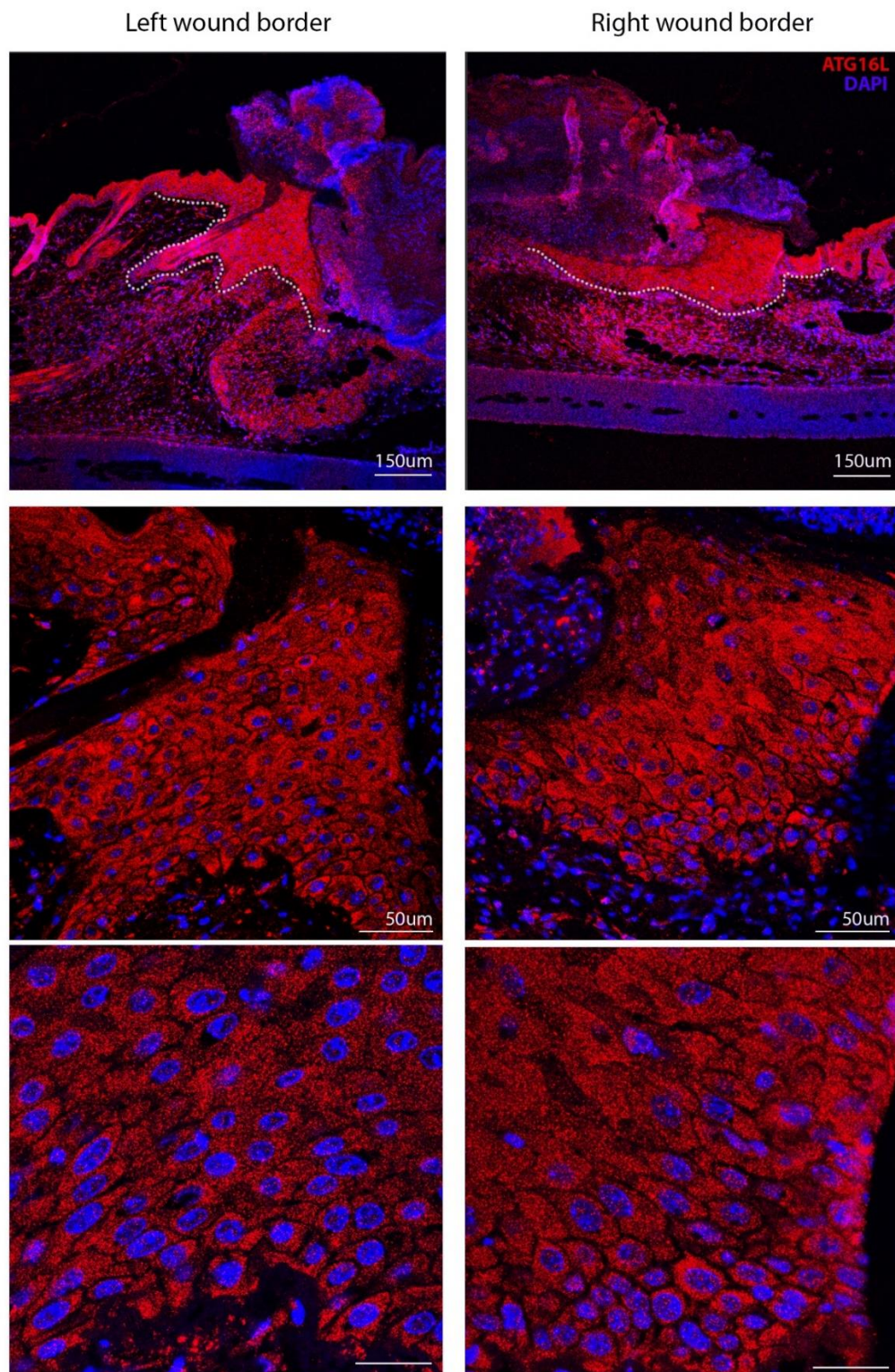


Figure 35 Expression pattern of ATG16L *in vivo*

Immunofluorescence staining used to characterise the expression pattern of ATG16L (red) in an in vivo mouse wound sample formalin fixed and paraffin embedded 4 days post injury. Images were taken of the proliferative region of cells at the left and right wound edges. Sections were cut at 8µm. DAPI (blue) was used to counterstain nuclei. NS: Normal Skin, WB: Wound Border. Dotted line indicates the region of proliferating cells at the wound edge that are migrating across the wound bed. Expression appears to be present throughout this region although little evidence of asymmetric patterning was observed. (n=4)

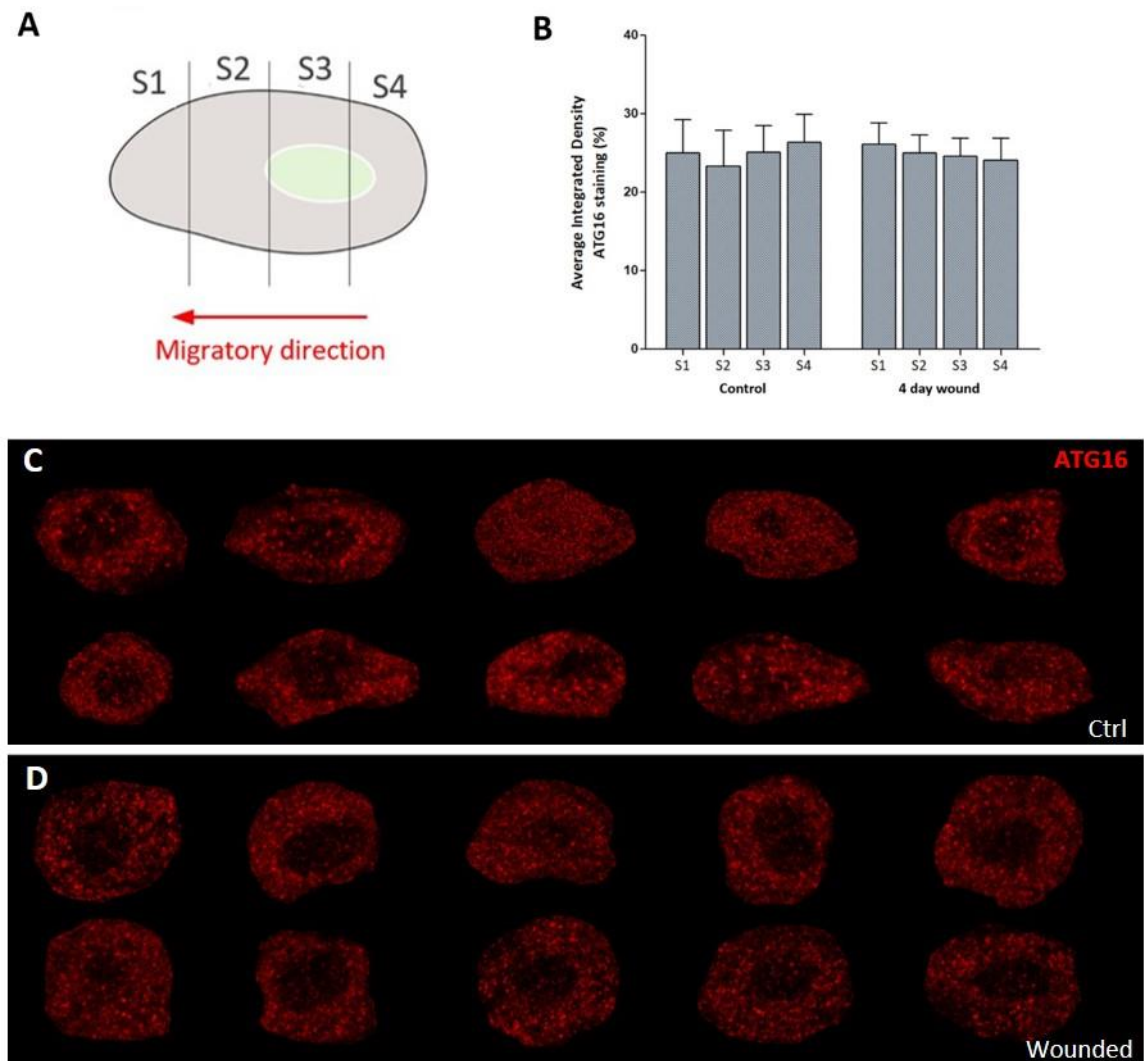


Figure 36 Quantification of unpolarised ATG16 expression

High magnification images of individual cells were isolated from *in vivo* mouse wounds (A) *In vivo* cells were orientated parallel to the basement membrane and then divided into 4 equal segments. S1 represents the leading edge, S2 and S3 represent the middle portions of the cell and S4 represents the trailing end. (B) Fluorescence intensity of ATG16 staining was measured by calculating integrated densities for each cell segment and plotted as a percentage of the total cell fluorescence. (C) *In vivo* images of uninjured keratinocytes and (D) corresponding wounded keratinocytes at the wound border, $n=10$ (* = $P < 0.05$, ** = $P < 0.01$, *** = $P < 0.001$)

II.IV LC3 is clustered around the nucleus away from the wound *in vivo*

One role of the complex that ATG5 and ATG16L form part of is to convert LC3-I to LC3-II which then decorates the autophagosome membrane. The LC3 molecules are believed to aid in elongation and membrane fusion events as well as mediating interactions with target cargo. It is a commonly used marker for active autophagy in many cell types. LC3 can typically be difficult to visualise in cells due to it being a small protein and often gives punctate staining that can only be seen clearly at higher magnifications. Initial imaging at low magnification suggested that LC3 expression was very weak, almost negative, in the region of interest at the wound border which was somewhat disappointing. However, the higher magnification images in Figure 37 and Figure 38 revealed that there was staining present and that it appeared to cluster around the periphery of the nucleus in most cells. At a first glance, the expression appeared more uniformly dispersed around the cell compared to some of the more distinct patterns observed with ATG5 but closer evaluation of the images did hint that some cells, highlighted by the white arrows in Figure 37, had more concentrated staining behind the nucleus at the distal side of the cell in relation to the wound. This complemented the observation of ATG5 expression, adding to evidence that autophagy markers are present and clustered away from the wound.

This was confirmed through measurement of fluorescence intensity across the different sections of the cell where there was a statistically significant decrease in the proportion of expression in segment 1 between injured and un-injured tissue and a corresponding increase in segments 3 and 4, supporting polarised distribution towards the trailing end (Figure 39).

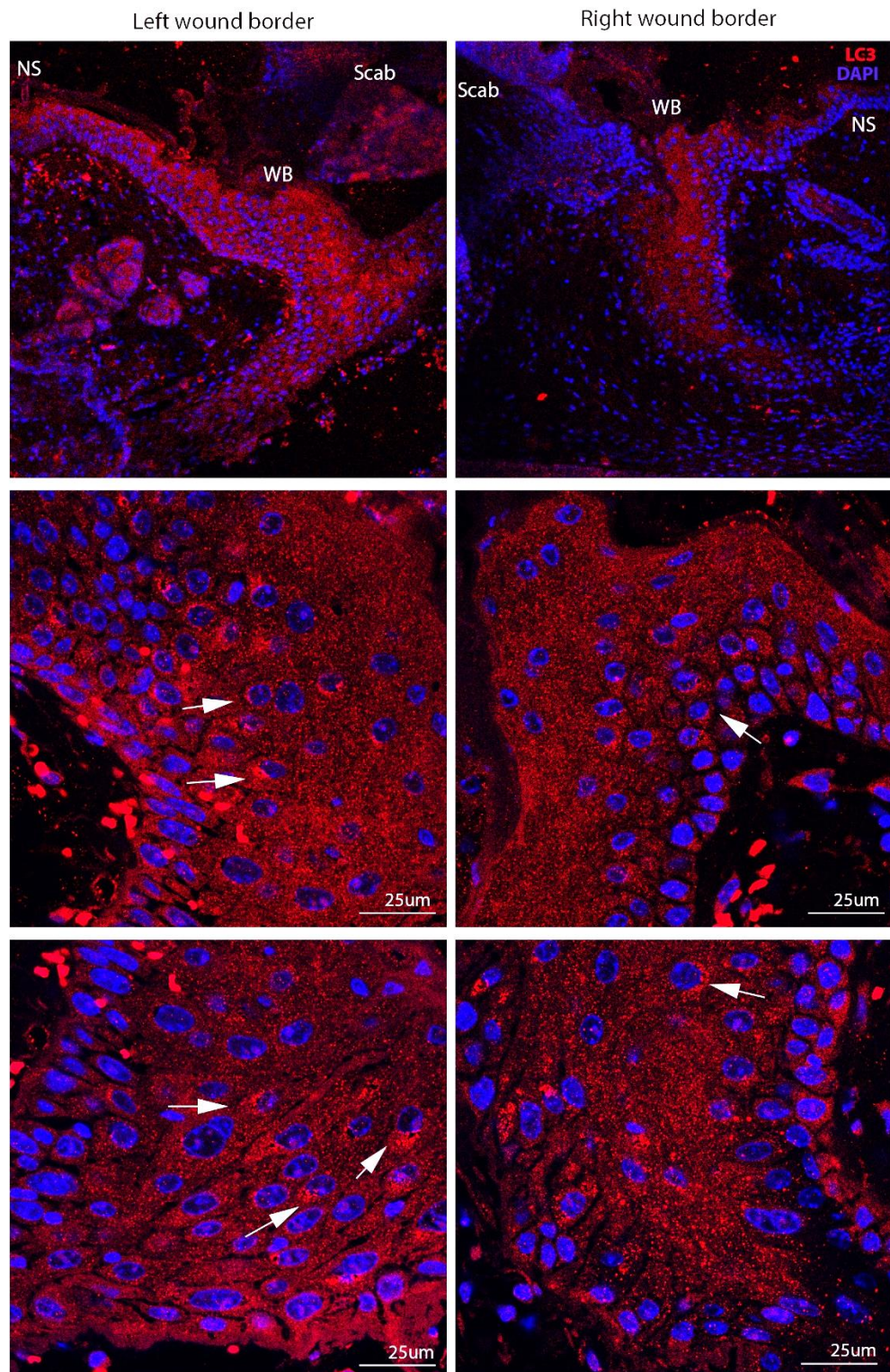


Figure 37 Expression pattern of LC3 *in vivo*

Immunofluorescence staining used to characterise the expression pattern of LC3 (red) in an in vivo mouse wound sample formalin fixed and paraffin embedded 4 days post injury. Images were taken of the proliferative region of cells at the left and right wound edges. Sections were cut at 8µm. DAPI (blue) was used to counterstain nuclei. White arrows indicate cells that have a higher concentration of LC3 expression behind the nucleus at the distal side of the cell.

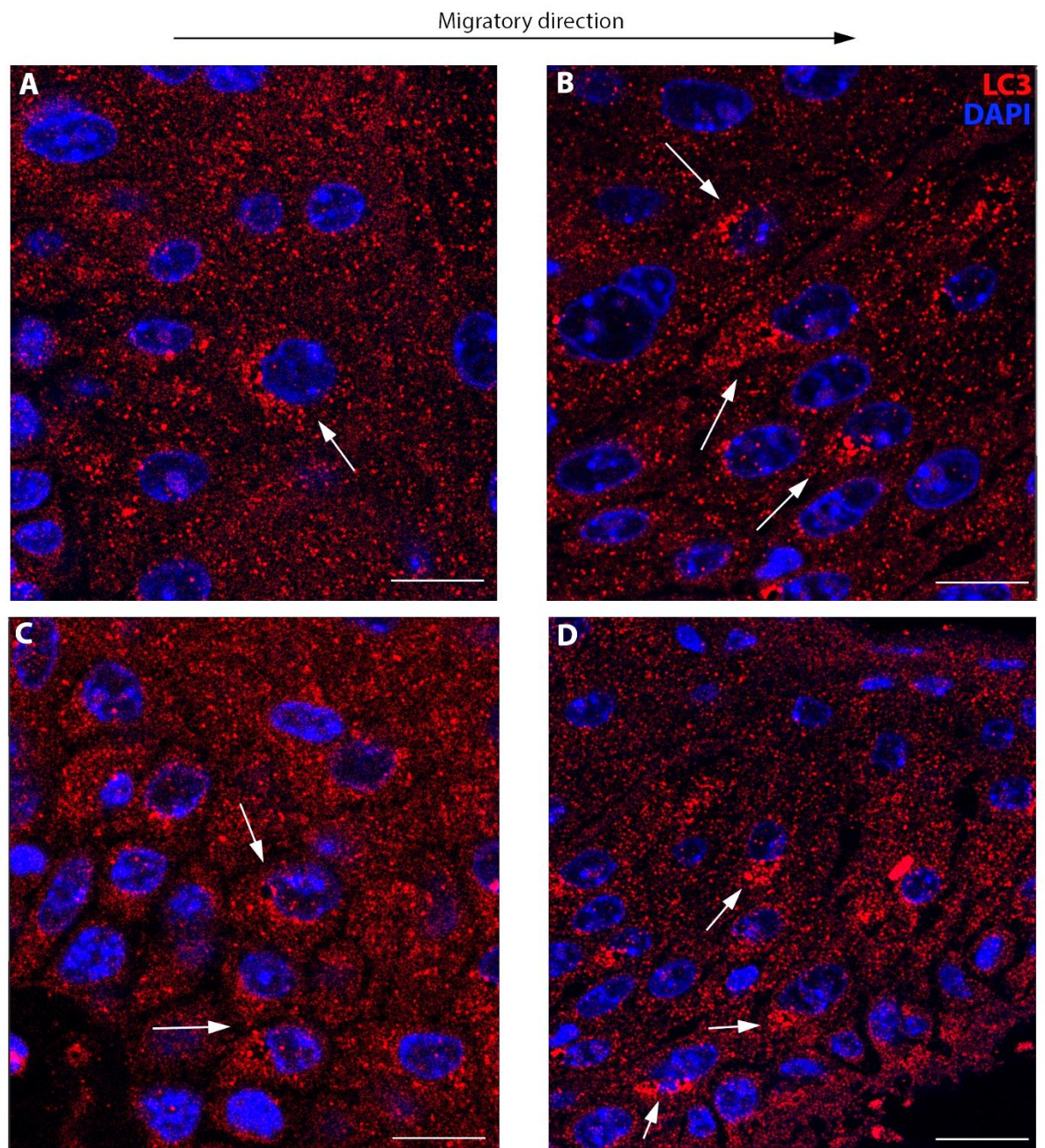


Figure 38 Expression pattern of LC3 *in vivo*

*Higher magnification images of LC3 (red) staining in keratinocytes at the border of an *in vivo* murine wound model 4 days post injury. DAPI (blue) was used to counterstain nuclei. White arrows highlight accumulation of LC3 puncta behind the nucleus. Scale bar = 10μm.*

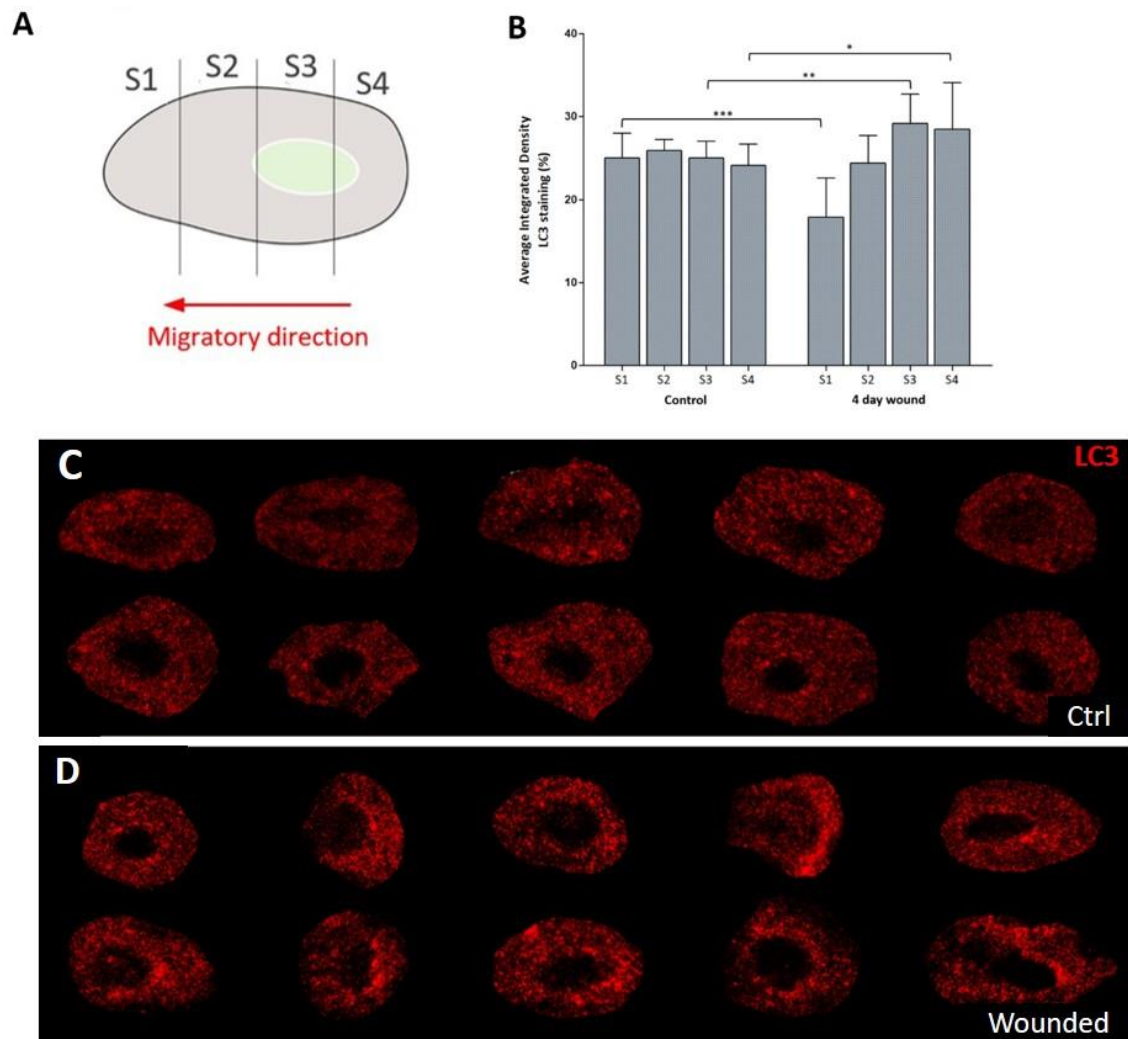


Figure 39 Quantification of polarised LC3 expression

High magnification images of individual cells were isolated from *in vivo* mouse wounds (A) *In vivo* cells were orientated parallel to the basement membrane and then divided into 4 equal segments. S1 represents the leading edge, S2 and S3 represent the middle portions of the cell and S4 represents the trailing end. (B) Fluorescence intensity of LC3 staining was measured by calculating integrated densities for each cell segment and plotted as a percentage of the total cell fluorescence. (C) *In vivo* images of uninjured keratinocytes and (D) corresponding wounded keratinocytes at the wound border, $n=10$ (* = $P < 0.05$, ** = $P < 0.01$, *** = $P < 0.001$)

II.V Total p62 is polarised towards the wound *in vivo*

Total p62 was included in the panel of autophagy markers that were tested because although it is not involved in nucleation, formation or elongation of the autophagosome, it plays a key role in sequestering target molecules. Its location in the cell would therefore help indicate where active autophagy was occurring.

Interestingly, its expression did not match what had been seen with previous autophagy markers, instead being localised in close proximity to the cell membrane in the leading edge lamellipodia towards the wound bed and migratory direction (Figure 40).

However, one comparable feature of the expression pattern was that cells in the basal layer showed virtually no staining, an observation also seen in the ATG5 images.

Considering the normal architecture of the epidermis, this is a logical phenomenon because highly proliferating cells will reside in this unstained basal region while cells that have broken free of the basement membrane will be free to migrate into the wound site. If autophagy is indeed involved in cytoskeletal rearrangements that aid migration, you would not expect them to be expressed in stem-like cells.

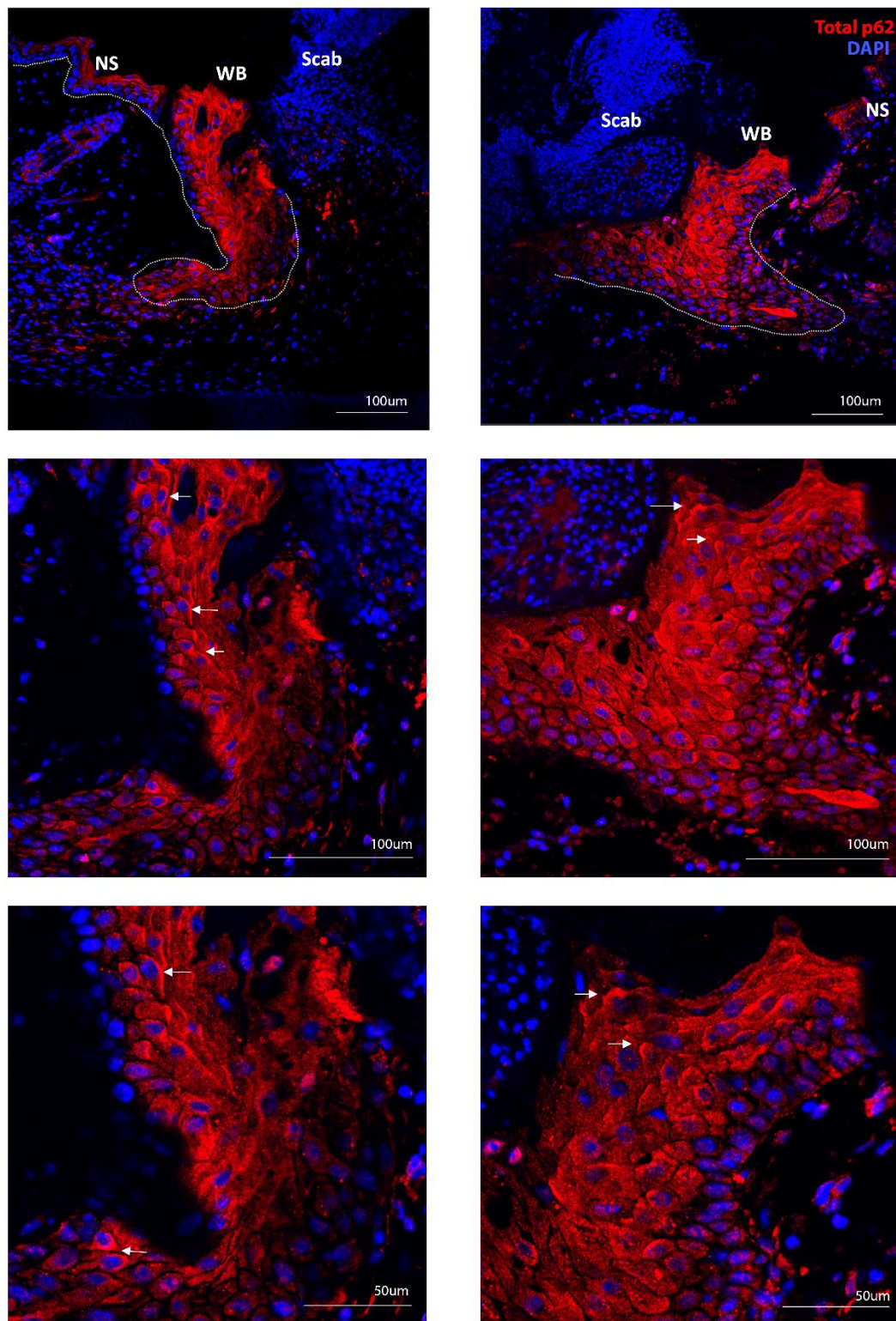


Figure 40 Expression pattern of total p62 *in vivo*

Immunofluorescence staining used to characterise the expression pattern of total p62 (red) in an in vivo mouse wound sample formalin fixed and paraffin embedded 4 days post injury. Images were taken of the proliferative region of cells at the left and right wound edges. Sections were cut at 8µm. DAPI (blue) was used to counterstain nuclei. NS: Normal Skin, WB: Wound Border. Dotted line indicates epidermal basement membrane. White arrows highlight expression concentrated near the cell membrane towards the wound bed. (n=4)

II.VI Total p62 is polarised towards the scratch *in vitro*

Again, this result was confirmed *in vitro* using scratch assays. The bottom panel in Figure 41 shows total p62 expression 6 hours after the scratch. It clearly depicts three cells that have broken away from the main group of cells and are migrating upwards into the scratch site. It also shows that staining in these cells has very defined polarisation of total p62 towards the direction that they are migrating. This contrasts with the expression in cells 2 hours after the scratch as well as unscratched control cells which both have positive staining but throughout the whole cell rather than polarised. This also suggests that redistribution of total p62 to one side of the cell is in response to wounding.

This is consistent with the findings *in vivo* and supports the notion that despite other autophagy markers localising to the distal side, total p62 does in fact congregate on the proximal side of the cells.

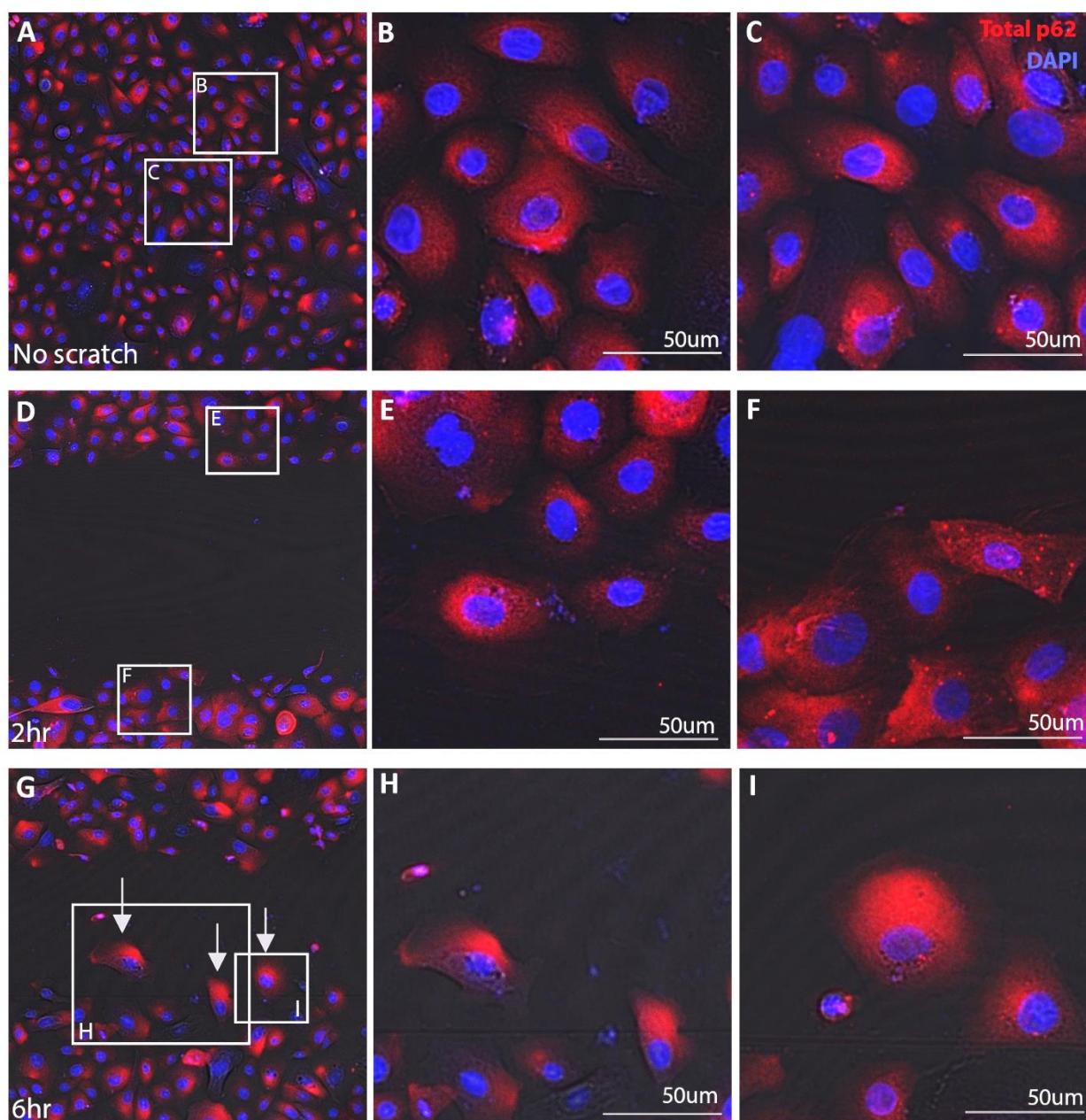


Figure 41 Expression pattern of total p62 *in vitro*

Immunofluorescence staining used to characterise expression patterns of total p62 (red) in migrating human keratinocytes that had been grown to confluency as a monolayer epidermal sheet and then injured using the scratch assay technique. Images were taken of cells near the scratch border. DAPI (blue) was used to counterstain nuclei. Bright field images have been overlaid to indicate where cell borders lie. White arrows highlight migrating cells with distinct polarised expression of total p62 at the proximal side of the cell.

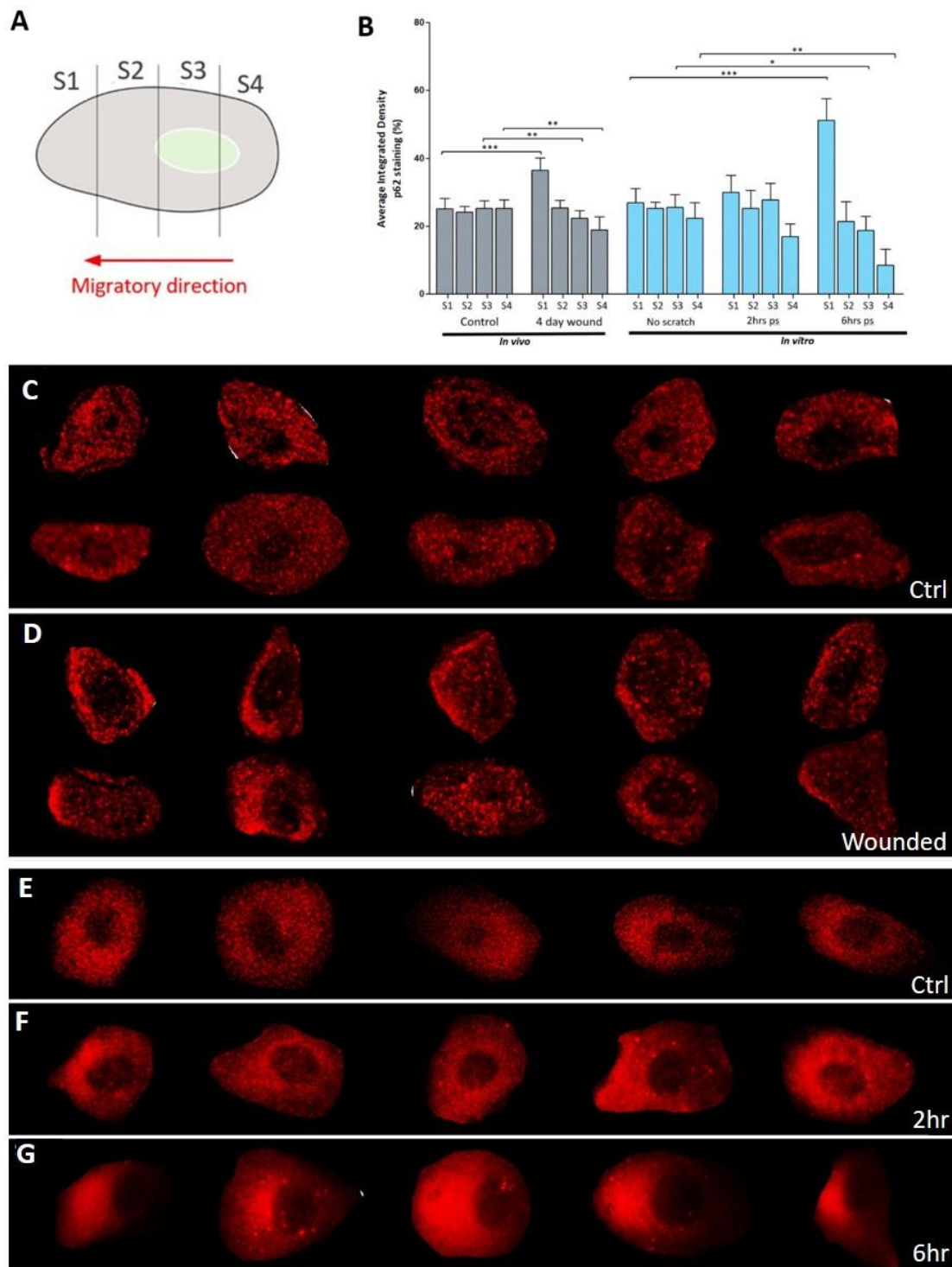


Figure 42 Quantification of polarised p62 expression

High magnification images of individual cells were isolated from *in vivo* mouse wounds and *in vitro* scratch assays. (A) *In vivo* cells were orientated parallel to the basement membrane while *in vitro* cells were orientated relative to the position of the scratch and then each was divided into 4 equal segments. S1 represents the leading edge, S2 and S3 represent the middle portions of the cell and S4 represents the trailing end. (B) Fluorescence intensity of p62 staining was measured by calculating integrated densities for each cell segment and plotted as a percentage of the total cell fluorescence. (C) *In vivo* images of uninjured keratinocytes and (D) corresponding wounded keratinocytes at the wound border, $n=10$. (E) Unscratched *in vitro* keratinocytes and (F-G) corresponding scratched keratinocytes at 2 and 6 hours post scratch (ps), $n=5$. (* = $P < 0.05$, ** = $P < 0.01$, *** = $P < 0.001$)

These results were statistically proved by measuring the fluorescence intensity distribution across different segments of the *in vivo* and *in vitro* cells. In both instances, injury caused a significant redistribution of expression towards segment 1 at the leading edge of the cell (Figure 42).

II.VII Phosphorylated p62 is polarised away from the wound *in vivo*

The phosphorylation status of p62 is pivotal to the way that it functions and is necessary for its interaction with a number of different molecules, including ubiquitinated cargo destined for autophagic degradation (discussed previously in introduction). We were curious to know whether total p62 had a similar expression pattern to its phosphorylated, active form so an antibody that detects phosphorylation at serine 403 was included in the screening panel. Results appeared to display almost the exact opposite. As with LC3, expression was concentrated around the periphery of the nucleus but only on the distal side in many cells (Figure 43). It was promising to discover that both LC3 and phosphorylated p62 co-localise in cells at the wound border in this way as most literature reports that they are tethered to the autophagosome membrane and should be present in close proximity to each other during active autophagy. The polarised expression was more obvious in basal stem-like cells with a handful of examples seen in cells closer to the wound in the migratory region.

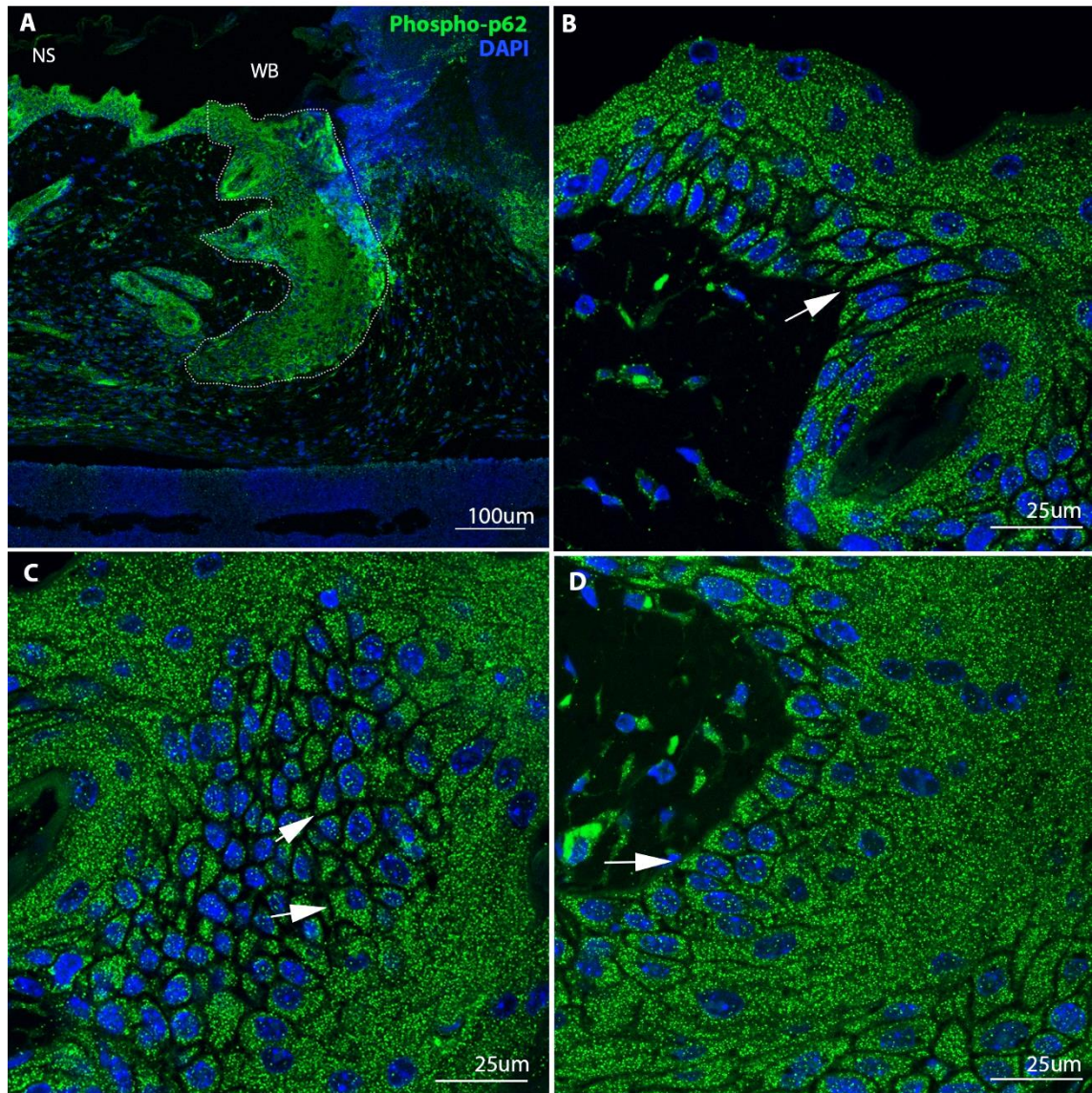


Figure 43 Expression pattern of phosphorylated p62 *in vivo*

Immunofluorescence staining used to characterise the expression pattern of phosphorylated p62 (green) in an in vivo mouse wound sample formalin fixed and paraffin embedded 4 days post injury. Images were taken of the proliferative region of cells at the left wound edge. Sections were cut at 8µm. DAPI (blue) was used to counterstain nuclei. NS: Normal Skin, WB: Wound Border. Dotted line indicates the region of proliferating cells at the wound edge that are migrating across the wound bed. White arrows highlight expression at the distal side of the cell. (n=4)

II.VIII Phosphorylated p62 is polarised away from the scratch *in vitro*

As with other autophagy markers that had displayed asymmetric expression, polarised distribution of phosphorylated p62 was confirmed by looking at cells *in vitro*.

The unscratched control condition had some staining but the signal was relatively weak and had a speckled, punctate appearance across the cells. As expected, the expression became consistently polarised in all of the cells 2 hours post scratch, again at the distal side in the very tips of the trailing edge. This pattern persisted in the cells 6 hours after the scratch but became less pronounced by 12 hours.

Again, both of these results were numerically confirmed by measuring the distribution of fluorescence intensity across different segments of the cells. Injury was seen to cause a significant redistribution of phosphorylated p62 expression in segment 4 of the cells, at the trailing end, both *in vivo* and *in vitro* (Figure 45).

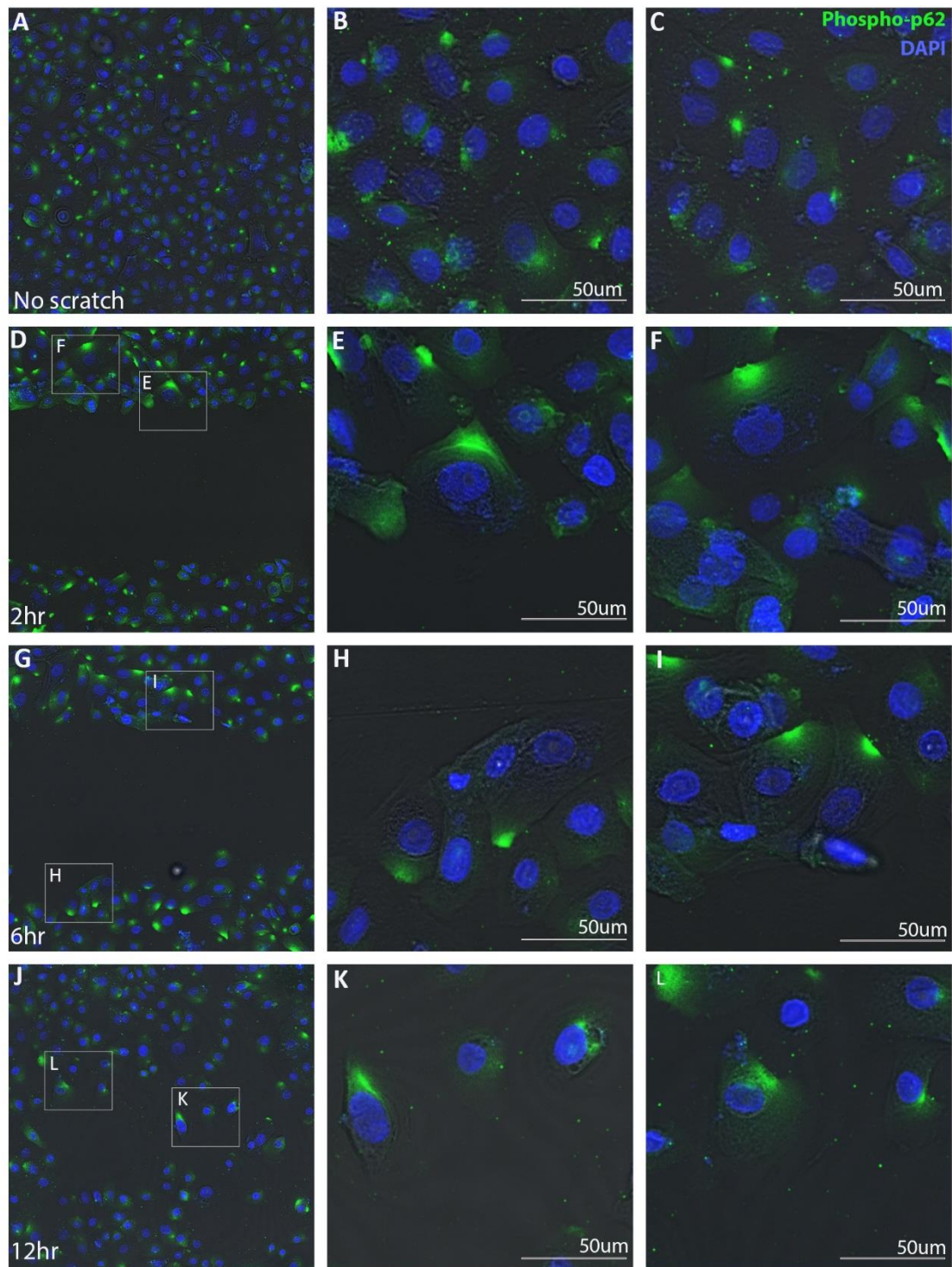


Figure 44 Expression pattern of phosphorylated p62 *in vitro*

Immunofluorescence staining used to characterise expression patterns of phosphorylated p62 (green) in migrating human keratinocytes that had been grown to complete confluency as a monolayer epidermal sheet and then injured using the scratch assay technique. Images were taken of cells near the scratch border. DAPI (blue) was used to counterstain nuclei. White boxes indicate cells that have been imaged at higher magnification to emphasise polarised expression in the most distal tip of cells.

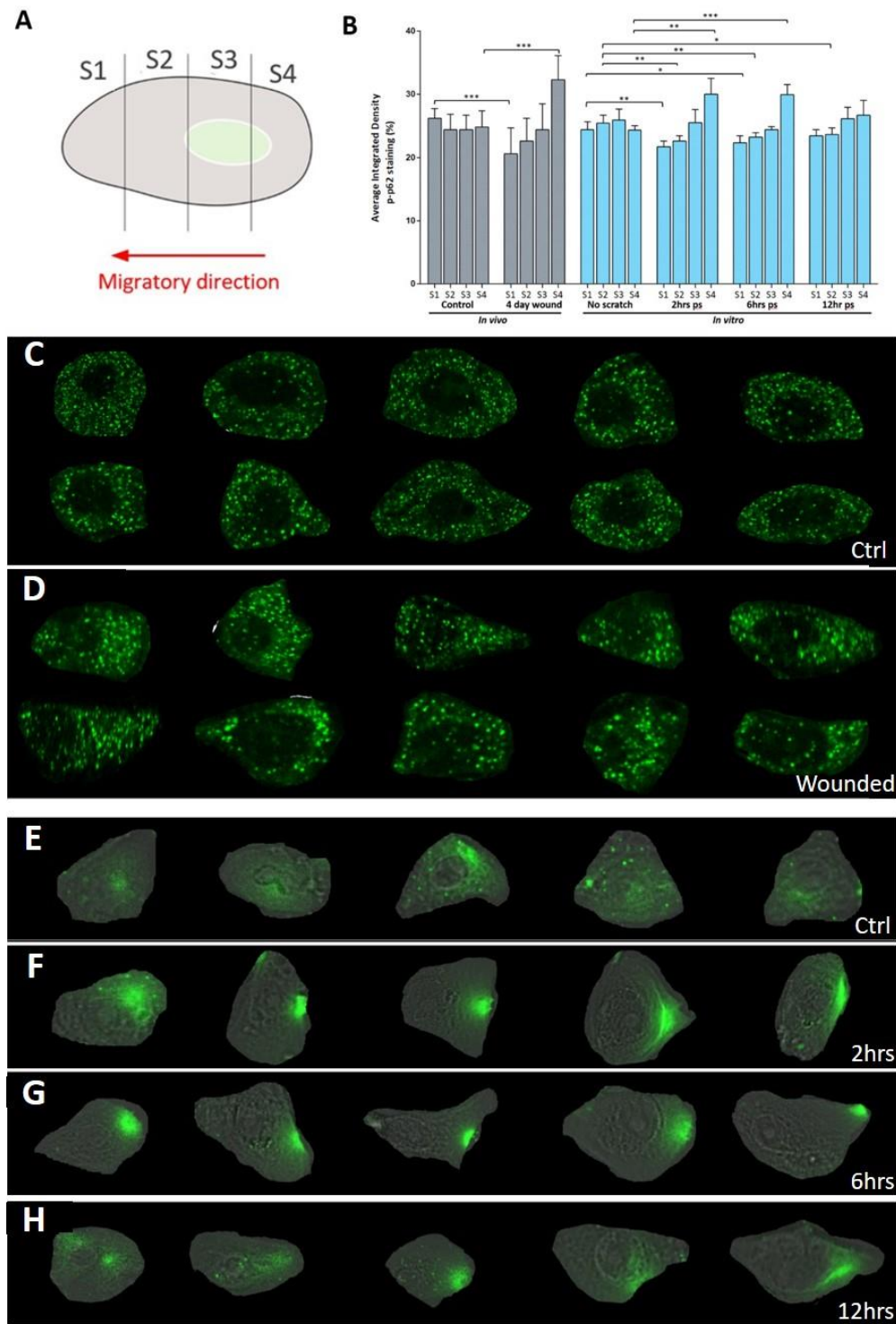


Figure 45 Quantification of polarised phosphorylated p62 expression

High magnification images of individual cells were isolated from *in vivo* mouse wounds and *in vitro* scratch assays. (A) *In vivo* cells were orientated parallel to the basement membrane while *in vitro* cells were orientated relative to the position of the scratch and then each was divided into 4 equal segments. S1 represents the leading edge, S2 and S3 represent the middle portions of the cell and S4 represents the trailing end. (B) Fluorescence intensity of phosphorylated p62 staining was measured by calculating integrated densities for each cell segment and plotted as a percentage of the total cell fluorescence. (C) *In vivo* images of uninjured keratinocytes and (D) corresponding wounded keratinocytes at the wound border, $n=10$. (E) Un-scratched *in vitro* keratinocytes and (F-H) corresponding scratched keratinocytes at 2, 6 and 12 hours post scratch (ps), $n=5$. (* = $P < 0.05$, ** = $P < 0.01$, *** = $P < 0.001$)

II.IX Transmission electron microscopy confirms location of autophagosomes towards the trailing end of human keratinocytes

Information gathered from the immunofluorescence results indicated that autophagosomes were likely to be forming in the distal half of cells in response to injury. Transmission electron microscopy was carried out on human neonatal keratinocyte scratch assays to obtain images of much high magnification and much greater detail to help confirm and assess a more precise location.

Figures 46-49 display a selection of cells taken from the immediate scratch border and cells residing several rows behind the scratch at 2, 6, 12 and 24 hours after the scratch was inflicted.

Across all time points autophagosomes could be seen forming behind the nucleus, in a region closely matching the location of both LC3 and phosphorylated p62 expression. Their clustered nature in the distal half of the cells supported the notion that injury induces autophagy in a specific region of the cell.

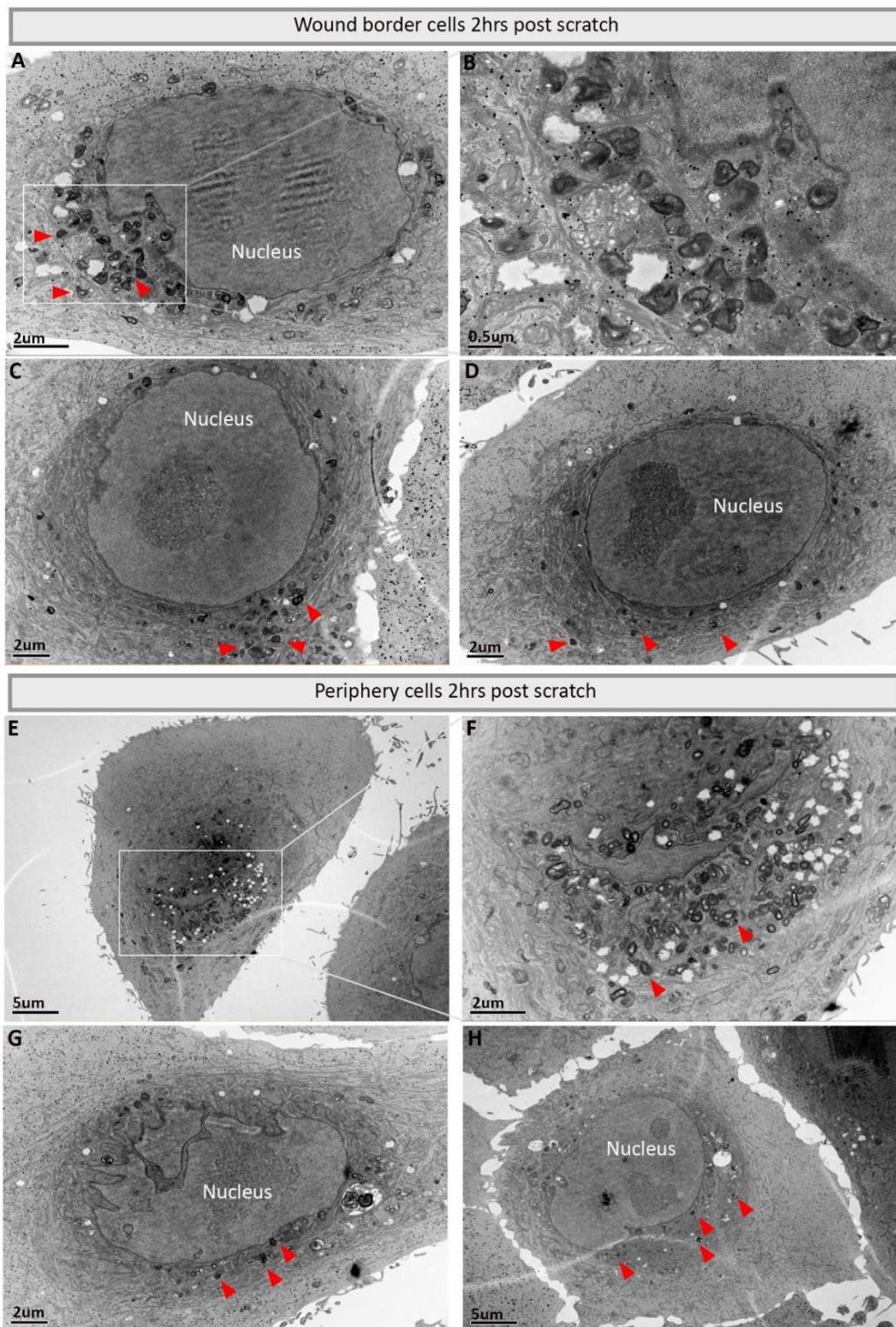


Figure 46 Transmission electron microscopy of autophagosomes in human keratinocytes 2 hours post scratch

Human neonatal keratinocytes grown to complete confluency on collagen I coated glass coverslips were used for a scratch assay. Transmission electron microscopy was used to visualise the location of autophagosomes within cells at the immediate scratch border and within cells several rows away from the scratch 2 hours post injury. Red arrowheads indicate examples of autophagosomes. The scratch is orientated directly above each image. Samples were kindly processed and imaged by Dr Christian Hacker, University of Exeter

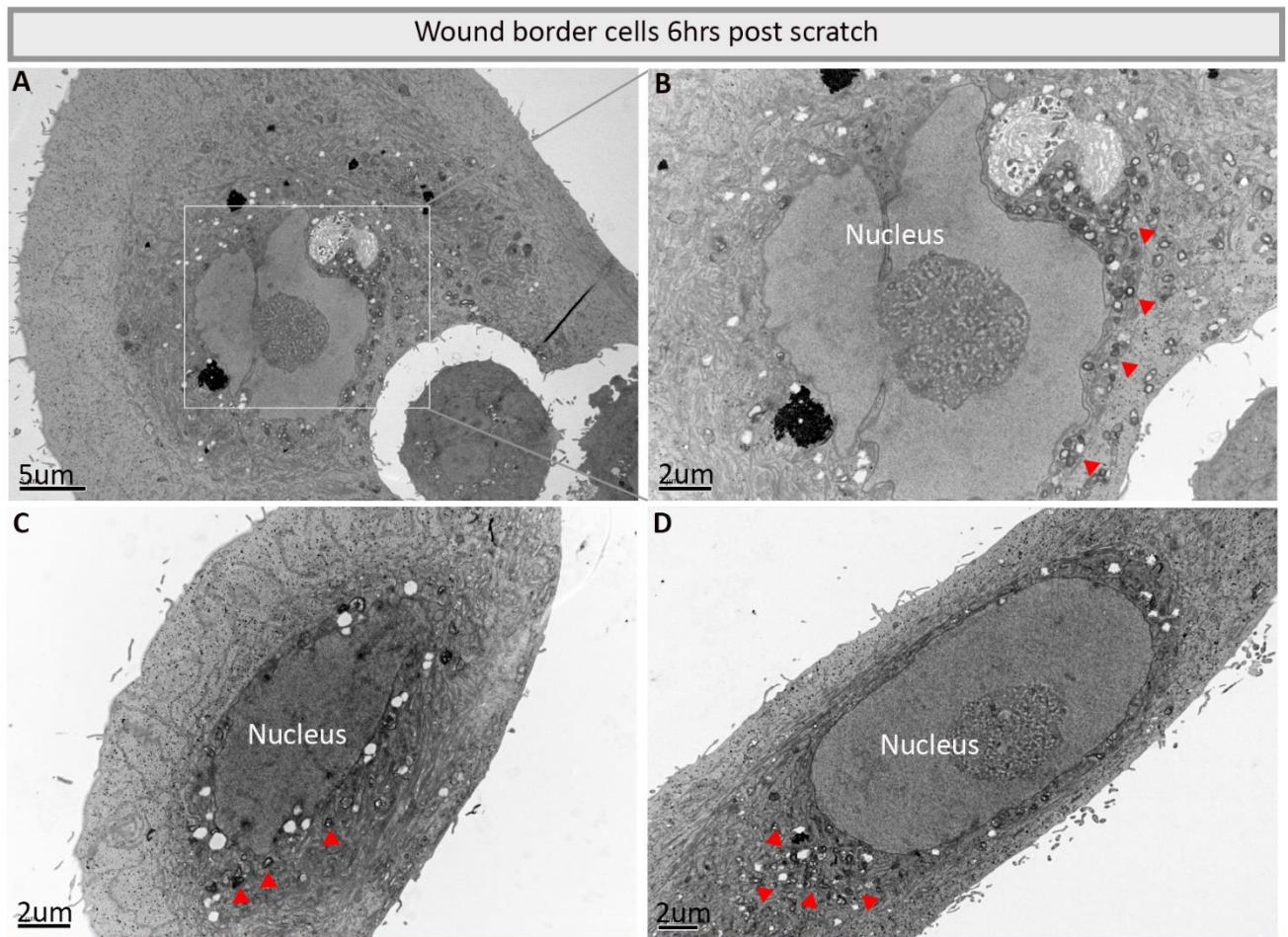


Figure 47 Transmission electron microscopy of autophagosomes in human keratinocytes 6 hours post scratch

Human neonatal keratinocytes grown to complete confluency on collagen I coated glass coverslips were used for a scratch assay. Transmission electron microscopy was used to visualise the location of autophagosomes within cells at the immediate scratch border and within cells several rows away from the scratch 6 hours post injury. Red arrowheads indicate examples of autophagosomes. The scratch is orientated directly above each image. Samples were kindly processed and imaged by Dr Christian Hacker, University of Exeter

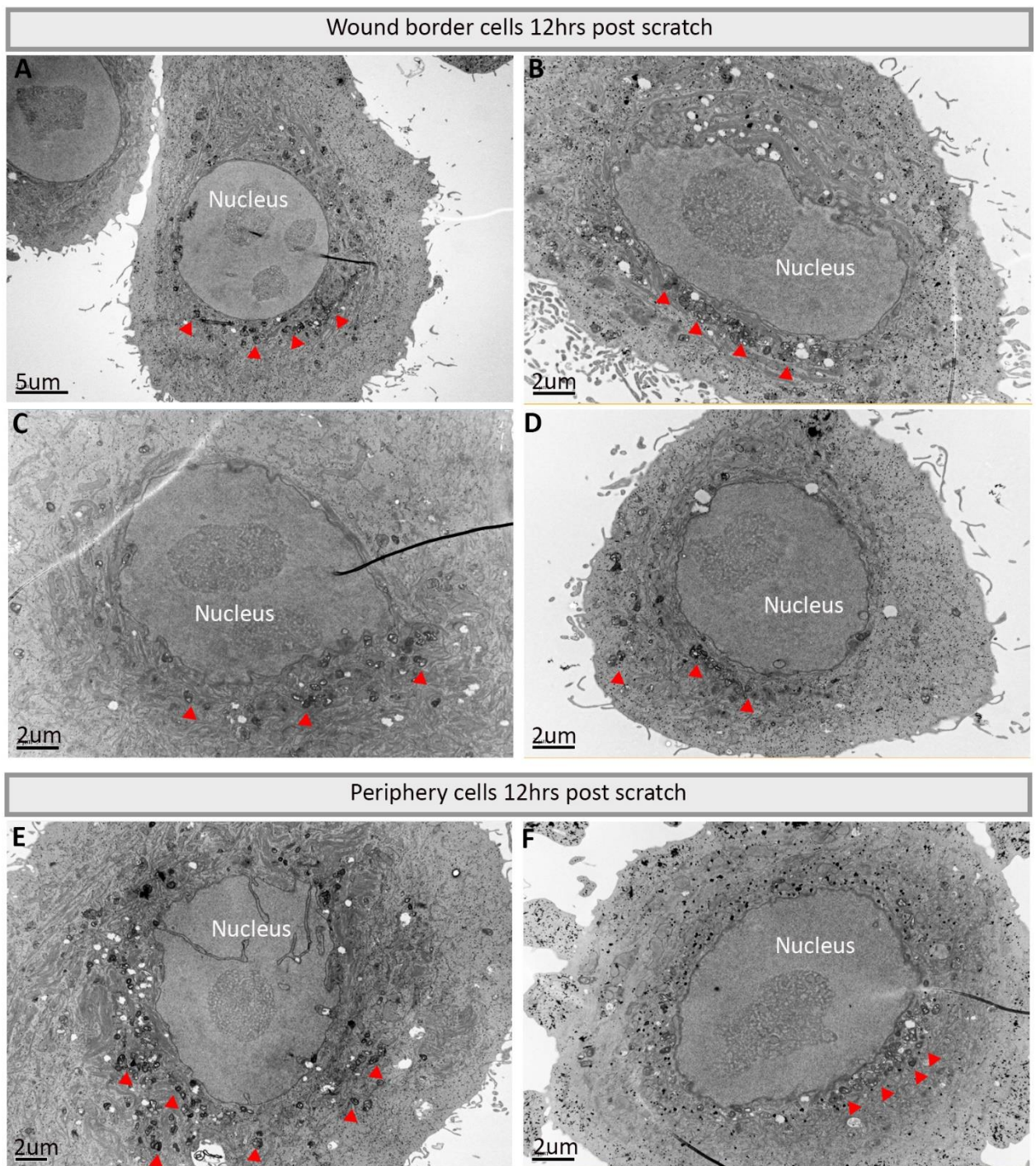


Figure 48 Transmission electron microscopy of autophagosomes in human keratinocytes 12 hours post scratch

Human neonatal keratinocytes grown to complete confluency on collagen I coated glass coverslips were used for a scratch assay. Transmission electron microscopy was used to visualise the location of autophagosomes within cells at the immediate scratch border and within cells several rows away from the scratch 12 hours post injury. Red arrowheads indicate examples of autophagosomes. The scratch is orientated directly above each image. Samples were kindly processed and imaged by Dr Christian Hacker, University of Exeter

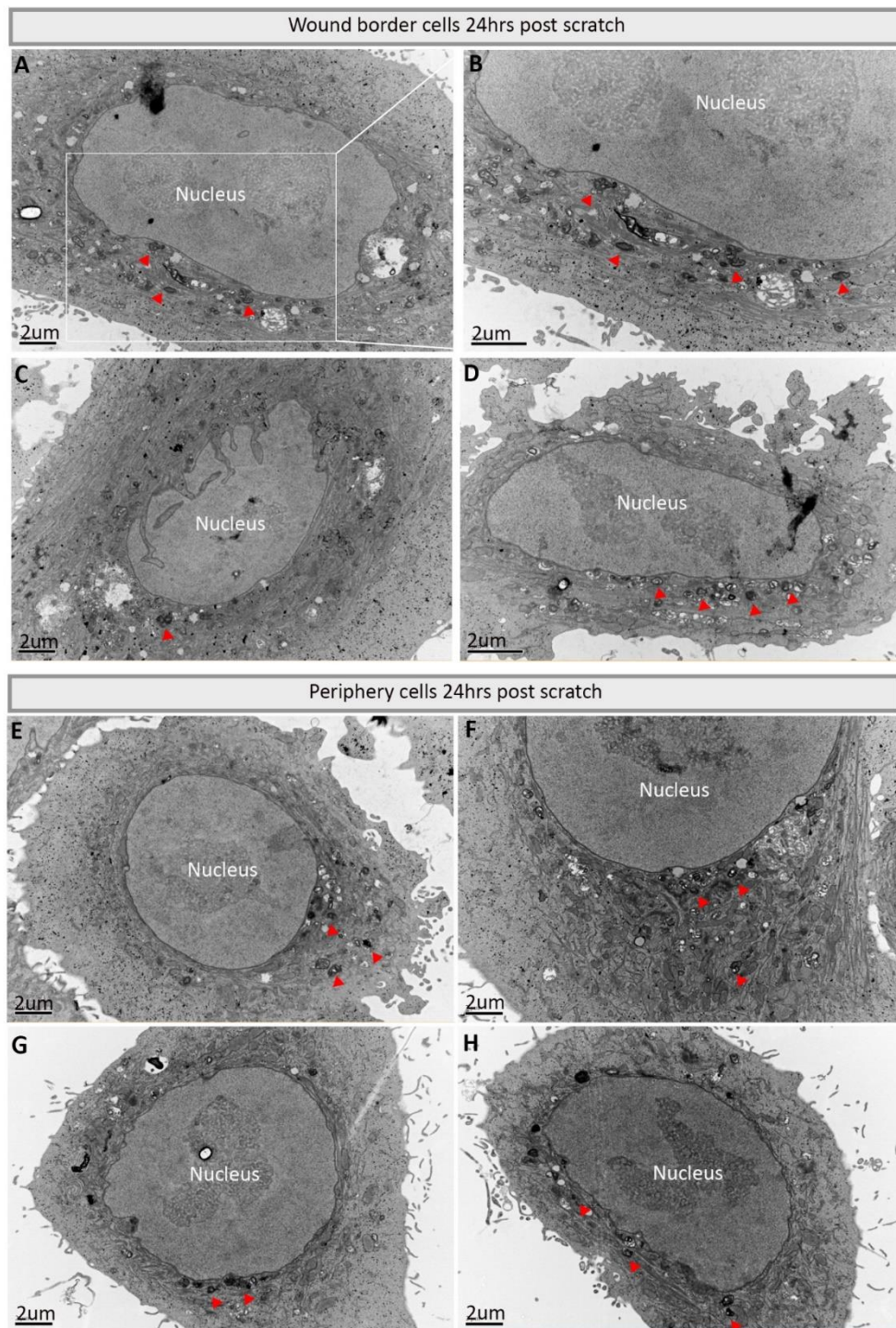


Figure 49 Transmission electron microscopy of autophagosomes in human keratinocytes 24 hours post scratch

Human neonatal keratinocytes grown to complete confluency on collagen I coated glass coverslips were used for a scratch assay. Transmission electron microscopy was used to visualise the location of autophagosomes within cells at the immediate scratch border and within cells several rows away from the scratch 24 hours post injury. Red arrowheads indicate examples of autophagosomes. The scratch is orientated directly above each image. Samples were kindly processed and imaged by Dr Christian Hacker, University of Exeter

II.X mRNA analysis confirms upregulation of core autophagy genes in response to injury

As previously analysed with the PCP markers, *in vitro* scratch assays were conducted using human epidermal keratinocytes to assess injury induced changes to the expression of core autophagy genes at the mRNA level. Cells were collected into three different fractions, as depicted in Figure 50A, and their mRNA was extracted. Fraction 1 was used to capture 'leader' cells directly adjacent to the scratch, Fraction 2 captured 'follower' cells and Fraction 3 represented cells far away from the scratch. A template was made to ensure that the size of each fraction remained consistent for each time point and across multiple experiments. These fractions were compared to control keratinocytes that were grown to full confluency but remained unscratched.

LC3 was found to be highly upregulated in the population of cells immediately adjacent to the scratch, in the fraction designated as 'leader' cells. This was consistently observed across all time points assessed (Figure 50).

Other markers, particularly ATG3 and Beclin1, also showed significant upregulation in response to injury.

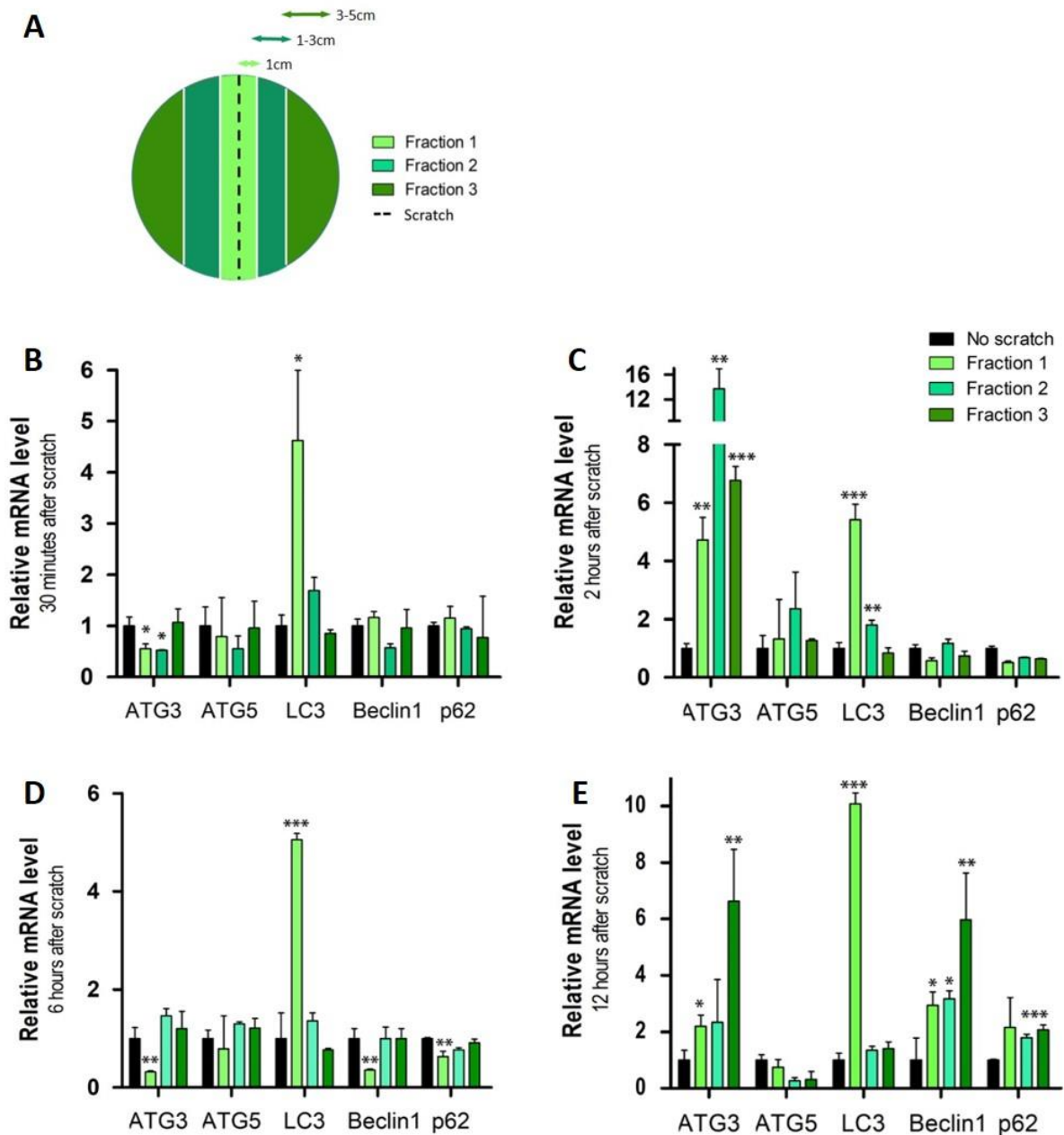


Figure 50 mRNA analysis of core autophagy genes in different populations of keratinocytes following *in vitro* scratch assays

Neonatal human keratinocytes were grown to confluency as a monolayer epidermal sheet and then injured using the scratch assay technique. (A) Dishes were divided into three fractions so that cells could be collected into populations representing 'leader' cells, 'follower' cells and distant cells relative to the scratch that had been inflicted. Fraction 1 captured leader cells that fell within a 1cm margin of the scratch, Fraction 2 captured follower cells within a margin of 1-3cm. Fraction 3 captured the remaining distant cells that fell beyond 3cm from the scratch. (B) Real-Time qPCR analysis was used to assess changes in mRNA expression levels of PCP pathway components in fractions of leader, follower and distant keratinocytes across different time points. There was a clear upregulation of markers in response to injury. (* = $P < 0.05$, ** = $P < 0.01$, *** = $P < 0.001$)

II.XI Summary of results section II

The second results section employed the same *in vitro* and *in vivo* techniques developed in the previous section to investigate whether autophagy may be associated with injury.

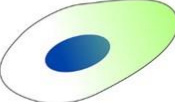
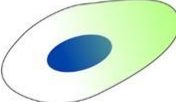


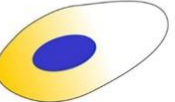
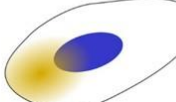


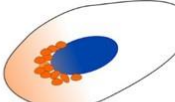
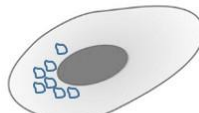
Results from these preliminary screening experiments have not only provided a strong indication that autophagic activity is present at the wound site but that components of its pathway appear to be localised to the trailing end of migrating cells.

This was first highlighted through immunofluorescence staining which revealed that ATG5, LC3 and phosphorylated p62 had stronger expression in wounded samples compared to unwounded control samples both *in vivo* and *in vitro*. mRNA analysis of epidermal keratinocytes subjected to *in vitro* scratch assays supported this result by showing statistically relevant upregulation of autophagy genes in response to injury compared to uninjured cells.

Immunofluorescence results also indicated that injury caused autophagy markers to localise to the distal region of migrating cells, opposing their migratory direction. This was in direct contrast to the localisation of upregulated PCP markers at the leading edge and was supported by higher densities of autophagosome structures observed in transition electron microscopy images of keratinocytes at the borders of scratch assays.

These were the first pieces of evidence to suggest that there was indeed substance to our hypothesis that targeted autophagy plays a role in the wound healing response. We concluded that although our current data was limited, we had sufficient evidence needed to continue pursuing the role of autophagy in wound healing.

The expression patterns and localisation findings from sections I and II are summarised in Figure 51.

Direction of migration →		
	In vivo	In vitro
Frizzled 3		
Total p62		
ATG5		
Phospho-p62		
LC3		
TEM		

Inconclusive markers


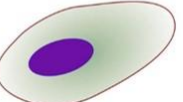

Frizzled 6	
Vangl2	
ATG16L	

Figure 51 Schematic diagram summarising expression patterns and localisation of autophagy and PCP markers *in vivo* and *in vitro*

Polarised localisation of both autophagy and PCP markers was observed at the wound borders. Evidence of clustered Frizzled 3 and total p62 protein was seen at the leading edge of cells while ATG5, phosphorylated p62 and LC3 expression was clustered at the trailing end of cells, opposing their direction of migration. Transition electron microscopy (TEM) also showed a higher density of autophagosome structures in the trailing end of cells in relation to the migratory direction

RESULTS SECTION III

Investigating the molecular mechanisms that control activation of autophagy in a wound environment

So far, the project had identified the activation of PCP in migrating cells at the wound border- a response to injury that is widely known, but had also identified that autophagy is activated in the same population of cells- a phenomenon that is less well known and understood.

The next results section aimed to unravel more details regarding the purpose of autophagy in migrating cells at the wound site as well as some of the control mechanisms in place that regulate its activation under certain conditions.

III.I Wnt5a treatment upregulates expression of autophagy genes *in vitro* without prior wounding

Given that both PCP and autophagy appear to be upregulated in the same population of migrating keratinocytes and across the same time period, we first asked whether there may be a relationship between the two pathways in terms of the activating signals that they respond to in the wound environment. We have previously shown that the presence of Wnt5a is sufficient to upregulate PCP genes and is released as a signalling cue in the wound so we tested whether the addition of Wnt5a to the culture media of keratinocytes could have any effect on autophagy genes. The same experimental parameters were repeated as described in previous Wnt5a treatments,

where efforts were made to eliminate any other injury associate triggers.

Keratinocytes were grown under standard culture conditions at a standard cell density to avoid nutrient starvation and contact inhibition.

mRNA levels from keratinocytes treated with varying concentrations of Wnt5a were compared to untreated cells through real-time qPCR analysis. Results showed a clear upregulation of ATG3, ATG5, ATG7 and LC3 in response to all Wnt5a doses at both 24 and 48 hours of treatment (Figure 52B, C).

Protein levels from the same experiment were also assessed by Western Blotting. This confirmed that LC3 and ATG5 protein increased in a dose dependent manner, in line with the qPCR results (Figure 52).

The western blot analysis also allowed us to make the distinction between total p62 protein and its phosphorylated, active form through the use of an antibody targeting phosphorylation at serine 403. While we had seen no evidence of upregulated p62 at the mRNA level, we observed the significant finding that Wnt5a treatment very clearly induced phosphorylation of p62 whereas no bands were detected in untreated control cells. When levels of phosphorylation were at their highest, there appeared to be a corresponding depletion of total p62, perhaps suggesting that all newly synthesised p62 is quickly phosphorylated when Wnt5a signals are present in the environment (Figure 52).

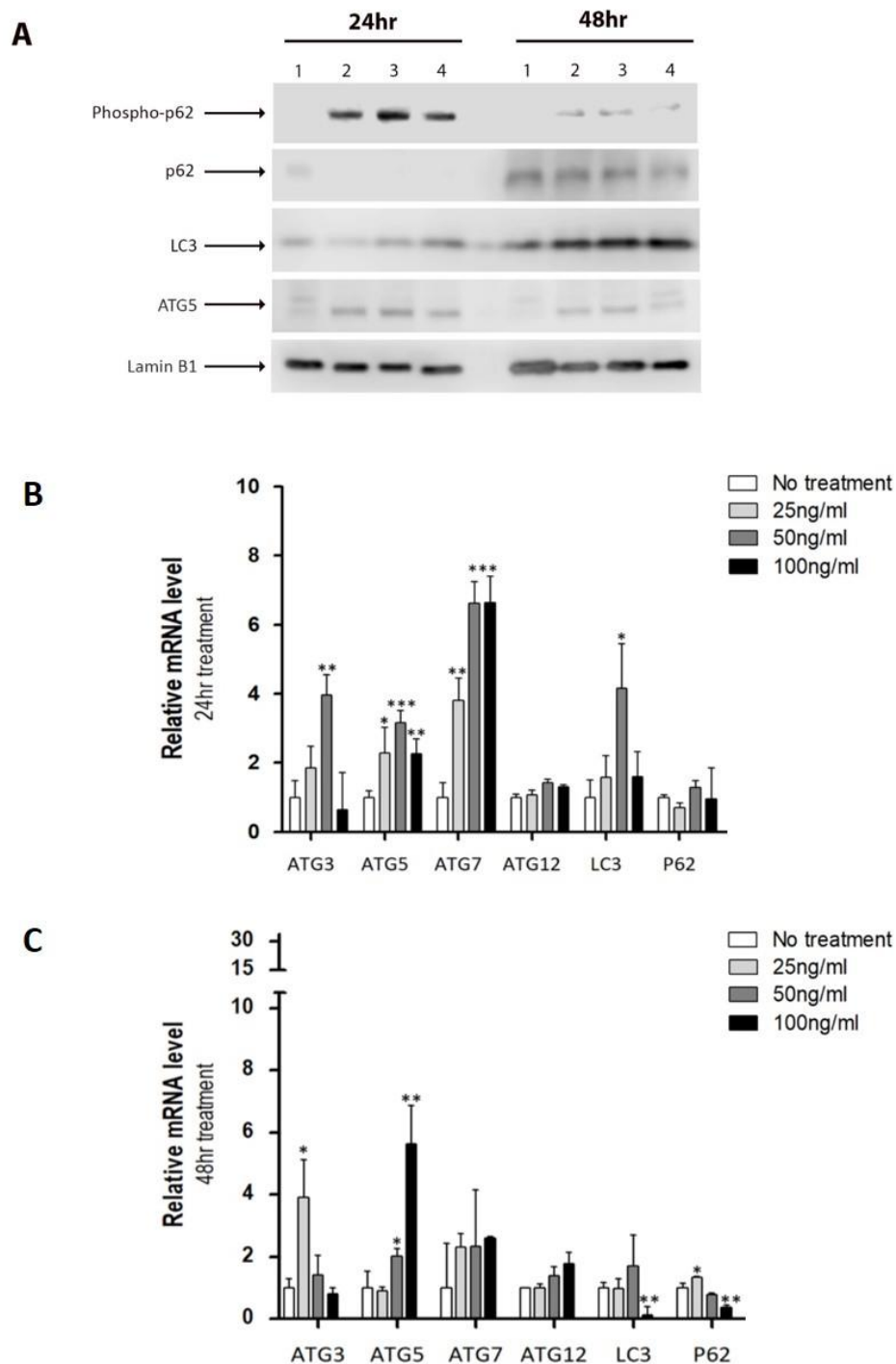


Figure 52 Wnt5a treatment induces upregulation of autophagy markers, independent of injury

(A) Western Blot analysis of autophagy components after neonatal human keratinocytes were treated with increasing doses of recombinant human Wnt5a protein for 24 or 48 hours. Lane 1: No treatment, Lane 2: 25ng/ml Wnt5a, Lane 3: 50ng/ml Wnt5a, Lane 4: 100ng/ml Wnt5a (B, C) Real-time qPCRs investigating the effect of Wnt5a treatment on the expression of autophagy genes in human epidermal keratinocytes. (* = $P < 0.05$, ** = $P < 0.01$, *** = $P < 0.001$)

III.II Wnt3a does not activate PCP or autophagy pathways in human keratinocytes

We now had some evidence to suggest a link between PCP and autophagy via Wnt5a cues so we next wanted to confirm whether this joint activation of both pathways was restricted to the non-canonical mechanisms of Wnt signalling. To achieve this, we treated keratinocytes with recombinant Wnt3a protein to see whether this gave us the same upregulation of PCP and autophagy components as was seen with Wnt5a.

Wnt3a was chosen as it is known to activate the canonical Wnt pathway whereby β -catenin enters the nucleus (discussed previously) but should not activate PCP.

Figure 53 confirms that there were no significant differences in PCP or autophagy expression between treated or untreated conditions. This further hints at a possible interaction between the two pathways whereby Wnt5a plays a necessary and crucial role in inducing autophagy at wound sites.

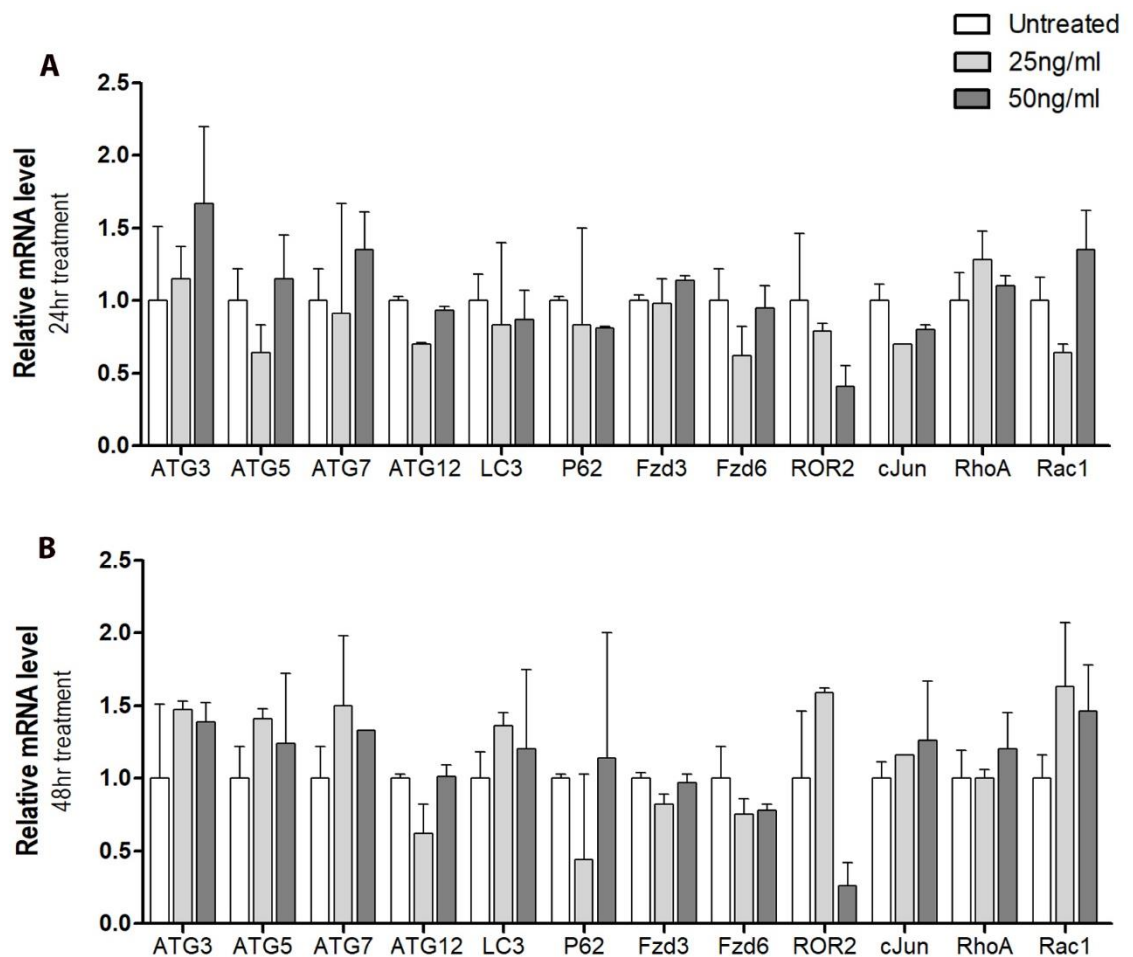


Figure 53 Wnt3a does not activate PCP or autophagy

Real-time qPCRs investigating the effect of human recombinant Wnt3a protein treatment over 24 and 48 hours on the expression of PCP and autophagy genes in human epidermal keratinocytes. No significant expression changes were observed between treated and untreated cells (= $P < 0.05$, ** = $P < 0.01$, *** = $P < 0.001$)*

III.III Wnt5a acts via Frizzled 3 to activate autophagy

The obvious next step was to elucidate what the mechanism of this shared activation might be. We had established that Wnt5a but not Wnt3a can activate both PCP and autophagy in keratinocytes and we knew from prior publications that Wnt5a acts via Frizzled 3/Frizzled 6 receptors ¹⁹⁸. From our initial immunofluorescence staining, Frizzled 3 appeared to show a stronger response to injury both *in vivo* and *in vitro* so we hypothesised that in the context of wound healing, Frizzled 3 likely plays a more prominent role than Frizzled 6. For this reason, we sought to knock down Frizzled 3 receptors through the use of siRNA and then treated the keratinocytes with 50ng/ml Wnt5a protein as before to test whether this inhibited the upregulation of autophagy. We could then decipher whether Wnt5a had to act via Frizzled 3 to upregulate autophagy or whether it activated the pathway through an alternative mechanism.

An siRNA targeting the transcripts of Renilla Luciferase (RLUC) was used as a negative control for this experiment alongside siRNA targeting Frizzled 3 transcripts. RLUC is found exclusively in the cnidarian *Renilla reniformis* and is often used as a negative control across many systems that lack this specific enzyme because it should theoretically have no biological effect on the cells.

It was first confirmed that knock down of Frizzled 3 had been successfully achieved but were surprised to find that Frizzled 6 had also been significantly reduced. There should be no overlap in the reactivity of the siRNA and, if anything, we expected the expression of Frizzled 6 to increase in order to compensate for loss of Frizzled 3 due to their reported redundancy (Figure 54A).

The specificity of the siRNA was checked by aligning its documented target sequence against copies of the human sequences for Frizzled 3 and Frizzled 6 (Supplementary figure 3). There was 100% overlap with the Frizzled 3 sequence but only 47% overlap with the Frizzled 6 sequence, suggesting that there should be minimal cross-reactivity.

The overall trend in the results was that cells treated with siRLUC + Wnt5a showed upregulation in most of the autophagy markers whereas cells treated with siFzd3 + Wnt5a failed to show any response to the Wnt5a signal. This implied that there is a crucial interaction between Wnt5a and Frizzled 3 that is needed to orchestrate the activation of autophagy in keratinocytes.

A scratch assay was carried out using the same treatments to knock down expression of Frizzled 3 receptors and then introduced an exogenous Wnt5a signal to show that migration in these cells was hindered (Figure 54B). Although we could not separate the influence of polarisation over autophagy, there were clearly fewer cells inside the scratch region after 24 hours when compared to cells treated with siRLUC + Wnt5a (Figure 54C).

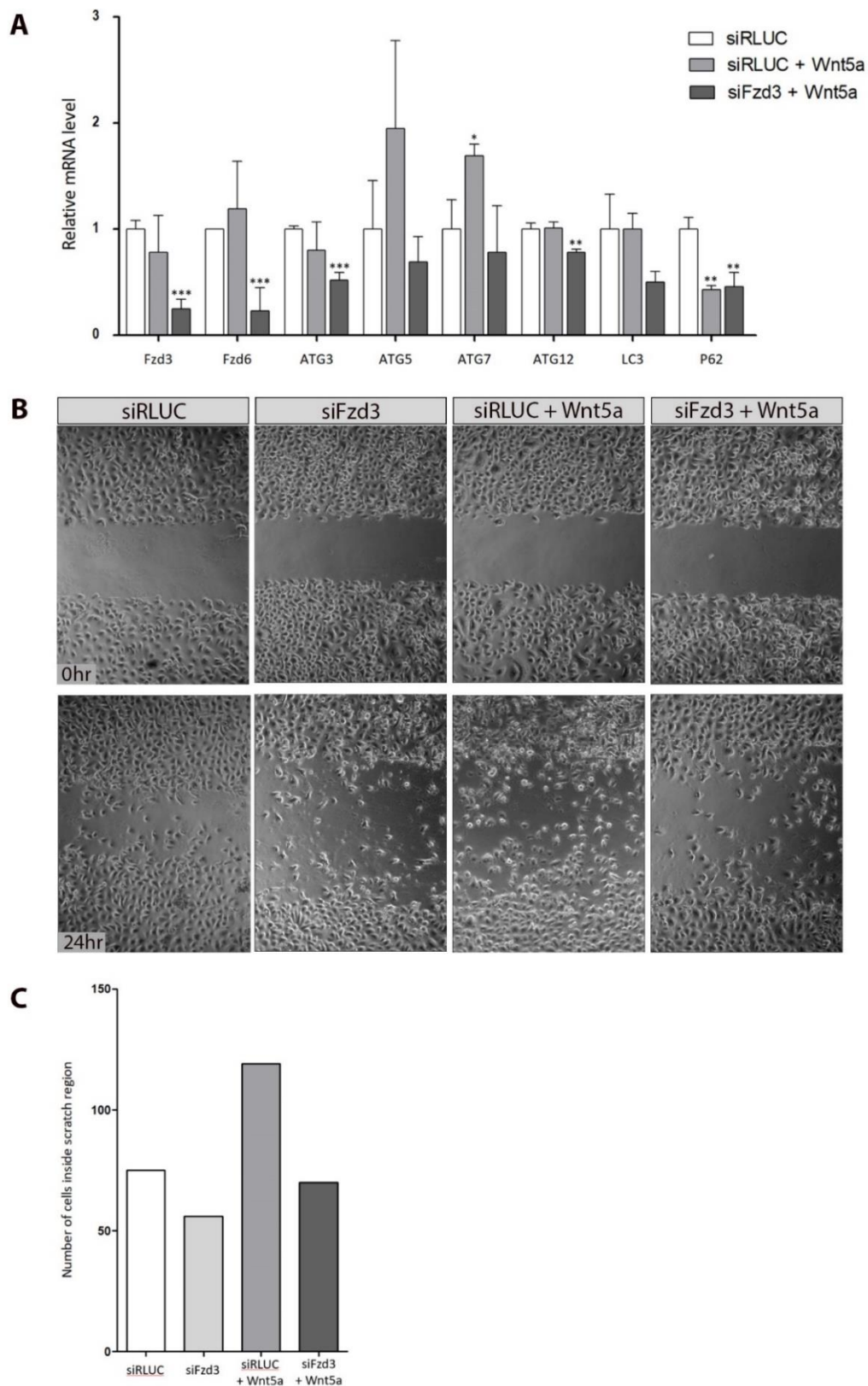


Figure 54 Wnt5a acts via Frizzled 3 to regulate autophagy in keratinocytes

(A) Human neonatal keratinocytes were treated with siRNAs to knock down expression of either RLUC or Frizzled 3 receptors and then exposed to exogenous Wnt5a signals. A real-time qPCR highlighted the requirement of Frizzled 3 receptors to activate autophagy in response to Wnt5a signals (* = $P < 0.05$, ** = $P < 0.01$, *** = $P < 0.001$). (B) The same treatment conditions were used in a scratch assay which indicated that migration of keratinocytes is delayed when they are unable to respond to Wnt5a signals. (C) Quantification of cells inside the scratch region after 24hrs

III.IV Investigating ROCK as a potential mediator of autophagy in the wound environment

We had established that Wnt5a needed to interact with Frizzled 3 to induce autophagy as part of the wound healing response but the mechanism used to relay Wnt5a signals to autophagy machinery was yet to be elucidated. It remained unclear whether autophagy was a direct pathway initiated by Wnt5a-Frizzled 3 binding or whether it was initiated as an indirect consequence of the PCP pathway being activated. Many components of the PCP pathway have multiple roles in a cell so there was a strong possibility that it was actually one of these molecules responsible for activating autophagy rather than Wnt5a itself.

Each of these possibilities were dissected in more detail to seek out which molecules were likely to be the strongest candidates for mediating the potential link between autophagy and PCP in the context of wound healing. A literature search was conducted to scope out any papers that mentioned PCP components in conjunction with autophagy. A key paper published by Gurkar *et al.* in Nature Communications had identified ROCK as a critical regulator of Beclin1 mediated autophagy during periods of metabolic stress¹⁵⁵. Here, they describe how nutrient deprivation activates the kinase function of ROCK causing it to bind to and phosphorylate Beclin1. This results in Beclin1 being released from its complex with Bcl2 to take its place in the PI3PC3-CI complex and begin forming phagophore membranes.

It was certainly plausible that a similar system was at play in the wound environment where Wnt5a signals could activate the PCP pathway which in turn would activate downstream ROCK to cause both cytoskeletal changes and autophagic behaviour in migrating cells. ROCK is known to interact with numerous proteins to regulate

cytoskeleton remodelling including actin filament stabilisation, assembly of the actin network and actomyosin fibres, actin-membrane linkage and microtubule dynamics^{156–159}. Some of these interactions are outlined in Figure 55A along with our hypothesised interaction with Beclin1.

Based on this theory, we conducted a series of experiments using Y27632, a highly potent inhibitor of ROCK that acts by competing with ATP for its catalytic binding site (Figure 55A). Our aim here was to investigate whether inhibition of ROCK (and therefore its associated kinase activity) could prevent the activation of Wnt5a induced autophagy. These experiments were designed to seek out the crucial information that would reveal how the two pathways were intrinsically linked.

When human epidermal keratinocytes from neonatal donors were treated with human recombinant Wnt5a protein, the same significant upregulation of autophagy markers was observed at the mRNA level, consistent with findings from earlier experiments (Figure 56). A rapamycin treatment was included in the tested conditions to prove that the keratinocytes were eliciting normal responses to known autophagic cues.

Rapamycin is a lipophilic macrolide antibiotic that induces autophagy by stabilising the Raptor – mTOR unit and prevents it associating with the ULK1 complex (this mechanism is discussed in detail in the introduction and illustrated in Figure 55B).

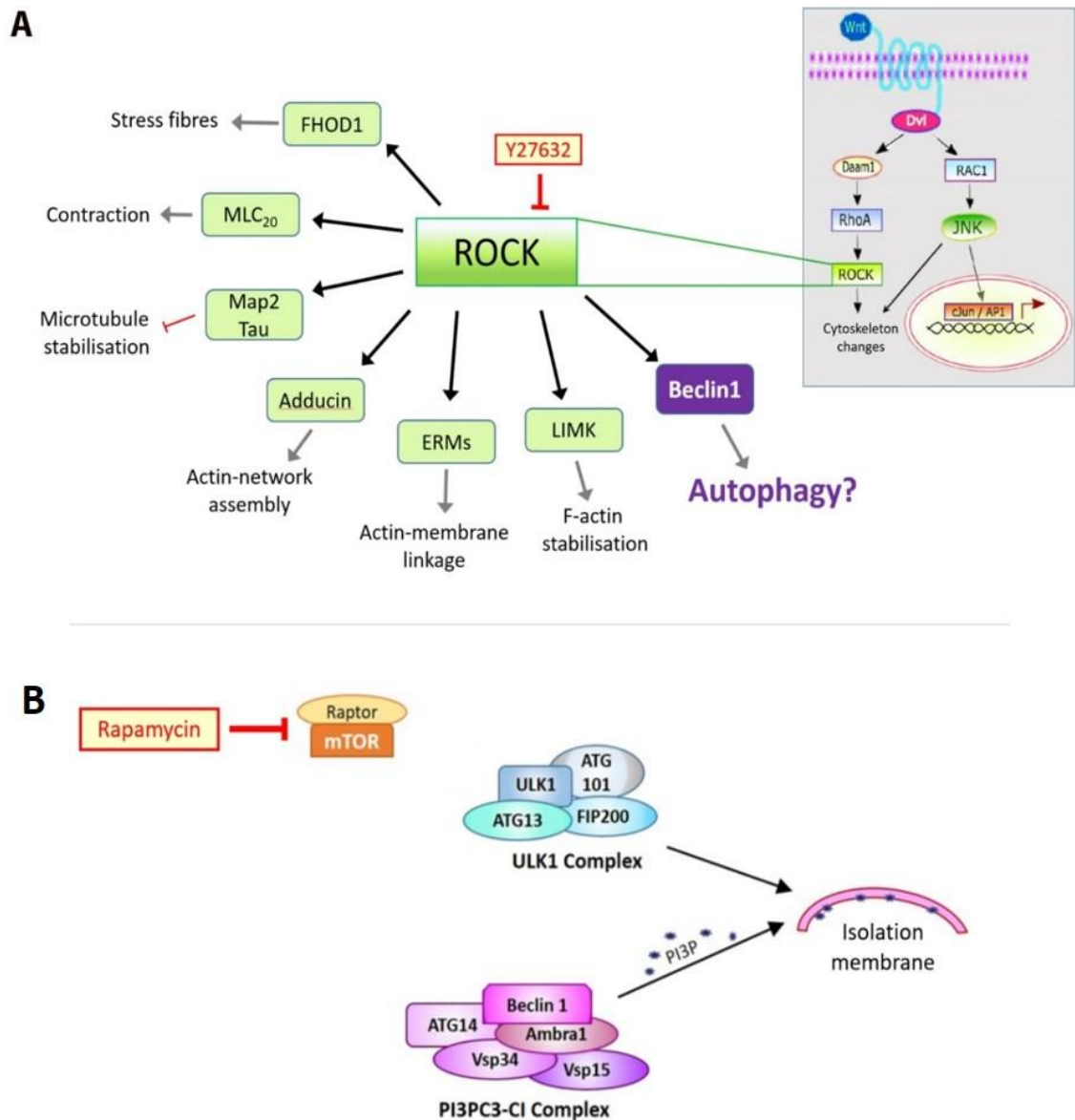


Figure 55 Mechanisms of Y27632, Bafilomycin and Rapamycin

(A) Diagram illustrating some of the substrates that interact with ROCK, often becoming activated through phosphorylation to cause a range of downstream cytoskeletal rearrangements that enable a cell to migrate. An interaction between ROCK and the autophagy protein Beclin 1 has been proposed where ROCK uses its kinase function to activate Beclin 1 and initiate nucleation of phagophore membranes. Y27632 is an inhibitor of ROCK that competes with other substrates for its catalytic binding site. By doing so, it prevents ROCK from phosphorylating its target downstream effectors. (B) Rapamycin is a common antibiotic that can also be used to initiate autophagy. It interacts with the Raptor-mTOR unit, stabilising and preventing it from associating with the ULK1 complex. In a similar mechanism to starvation induced autophagy, the free ULK1 complex is then able to nucleate a phagophore membrane.

Rapamycin also inhibits the kinase activity of mTOR – both of these factors actively promote autophagy. While rapamycin treatment did cause significant upregulation of the autophagy markers compared to untreated cells, Wnt5a appeared to elicit a much stronger response.

The most important condition used in this experiment was the combined treatment of Wnt5a protein alongside Y27632. The addition of the ROCK inhibitor irrefutably restricted the Wnt5a induced autophagy with all markers showing significantly reduced expression compared to cells treated only with Wnt5a. This crucial finding convincingly supports the notion that ROCK plays a key role in mediating activation of autophagy in the presence of Wnt5a signals (Figure 56).

Another significant finding from these results was that the addition of exogenous Wnt5a protein to the surrounding culture media triggered the cells to begin expressing their own Wnt5a, presumably creating a feedback loop to amplify the signal to nearby cells as suggested in the ‘leader’ and ‘follower’ model. However, when the Wnt5a treatment was combined with Y27632, no such amplification was observed (Figure 56). This indicates that ROCK may also contribute to the maintenance of Wnt5a in the wound environment through mediating a pathway involved in its feedback loop.

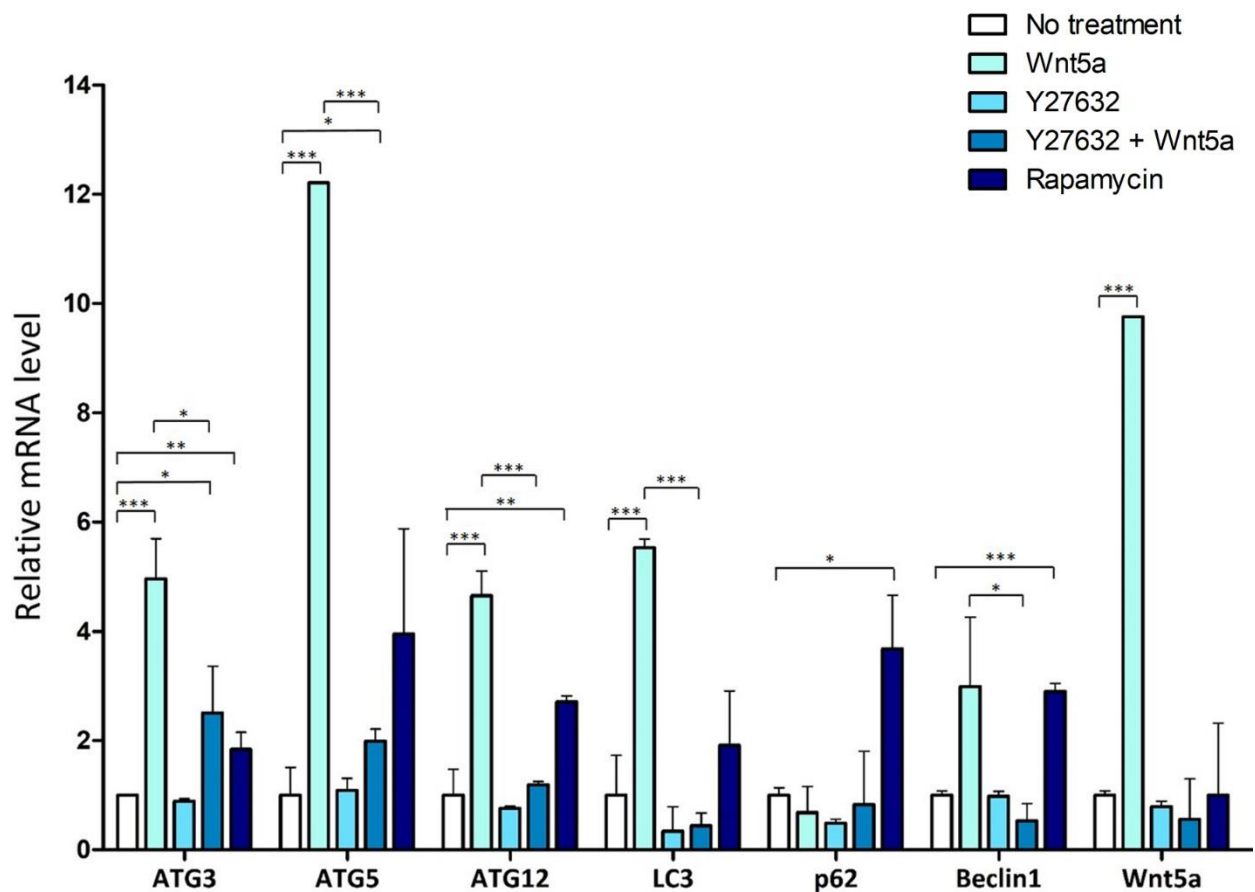


Figure 56 Y27632 prevents Wnt5a induced autophagy in keratinocytes

Real-time qPCR analysis showed that when human keratinocytes from neonatal donors were treated with Wnt5a protein it caused a significant increase in expression of autophagy markers and this was to a greater extent than the upregulation seen in cells treated with rapamycin which is traditionally used to induce the autophagy pathway. When the activity of ROCK was inhibited with Y27632, Wnt5a treatment had no effect on the expression of autophagy markers. (* = $P < 0.05$, ** = $P < 0.01$, *** = $P < 0.001$).

To follow this up, another scratch assay was performed to compare untreated injuries against those treated with Y27632. Contrary to our expectations, inhibition of ROCK accelerated the closure rate with 214 cells inside the scratch margins after 12 hours while the control condition had only 51 cells. (Figure 57A, B).

Upon further investigation, reports were found describing how ROCK inhibitors such as Y27632 can prolong the replicative lifespan of keratinocytes *in vitro* by promoting rapid proliferation whilst suppressing differentiation and stratification, keeping them in an immature state for longer periods of time²⁰¹. This increased rate of cell division would provide an explanation as to why scratches appeared to close more rapidly in the presence of Y27632 despite the treatment preventing activation of autophagy. Indeed, there is evidence of this occurring in the scratch assay experiment at the 6hr time point where dividing cells have been highlighted with white arrows in the Y27632 condition while no examples were seen in the control condition (Figure 57).

With this in mind, we cannot conclusively comment on whether blocking the initiation of autophagy through inhibiting ROCK has any affect on the migratory rate of the cells without conducting further experiments. The sheer number of new cells generated through Y27632 treatment pushes the wound margins inwards without necessarily requiring any migration of the cells. To uncover the true effect of limited autophagy on migration, we will need to conduct time lapse imaging and subsequent migratory track analysis on scratch assay experiments in the future. We may also look at treatments that postpone progression through the cell cycle to prevent the increased proliferation and isolate the rate of migration as a single measurable parameter.

Despite the enhanced closure rate, immunofluorescence staining provided clear evidence that there was a marked absence of Beclin 1 expression in the trailing end of Y27632 treated cells compared to the control condition (Figure 57C). The polarised redistribution of Frizzled 3 receptors in response to the scratch was also unaffected under either treatment condition.

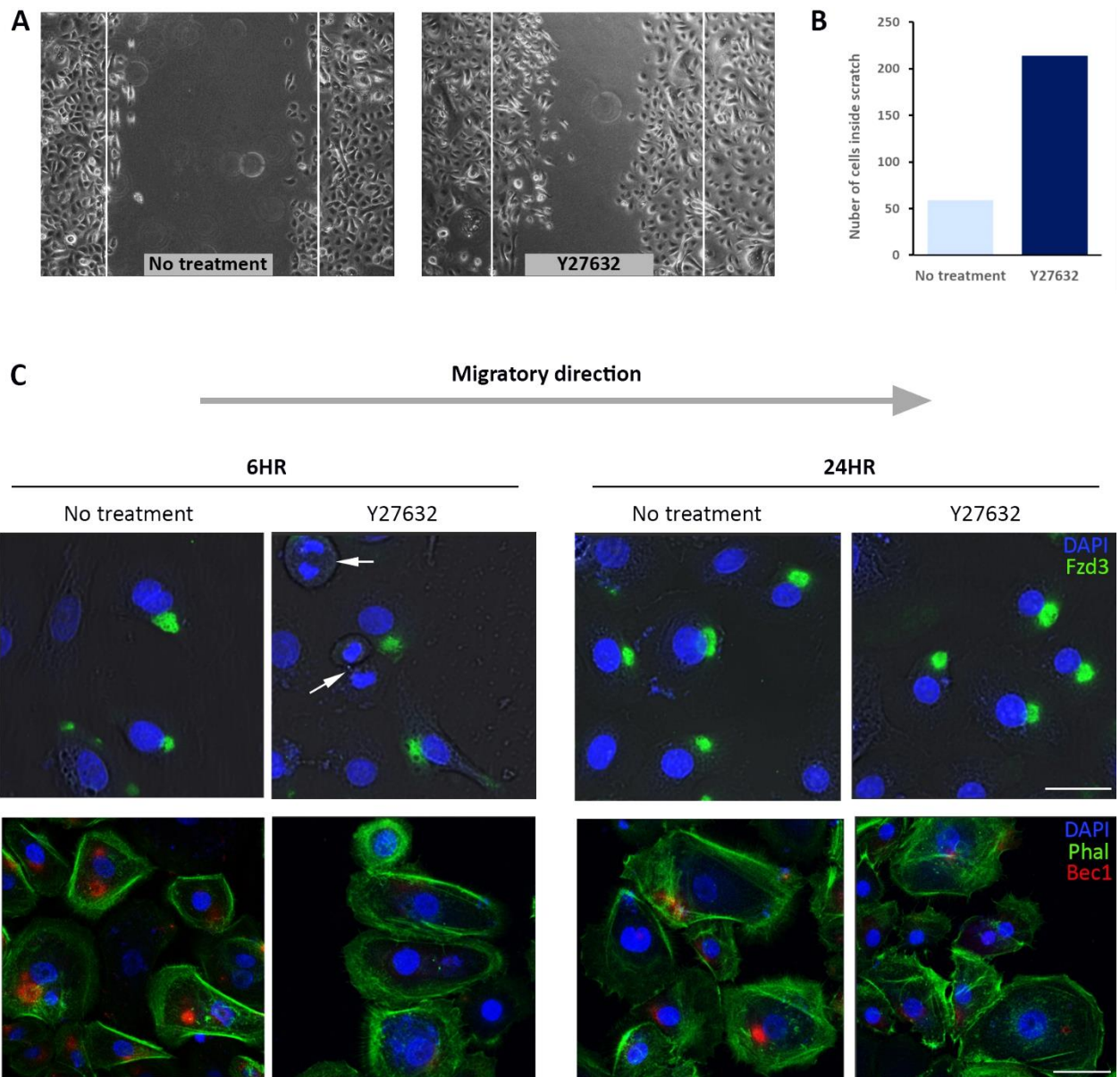


Figure 57 Y27632 treatment has no effect on activation of PCP in response to injury but does prevent activation of autophagy *in vitro*

Human keratinocytes from neonatal donors were grown to full confluency as a monolayer epidermal sheet and then injured using the scratch assay technique. Y27632 was added to the injured cells to inhibit the activity of ROCK. (A) Images of the scratch assays taken 12 hours post injury. Y27632 treatment caused an increase in wound closure rate compared to untreated cells. (B) Quantification of cells within the scratch margins after 12 hours (C) Immunofluorescence staining used to characterise expression patterns of Frizzled 3 (green) receptors in the top panel. Actin filaments (green, phalloidin) and Beclin1 (red) are shown in the bottom panel. DAPI (blue) was used to counterstain nuclei. Images were taken of cells near the scratch border. White arrows indicate actively dividing cells. Scale bar = 50µm

III.V Summary of results section III

This section has aimed to understand more about the regulatory mechanisms surrounding autophagy in the wound environment. Through collating the results, we have shown that Wnt5a is released into the wound and surrounding tissue by both dermal fibroblasts residing in the dermis as well as keratinocytes in the epidermis. The resultant chemotactic morphogen gradient is capable of inducing cellular rearrangements in keratinocytes by activating the planar cell polarity pathway which in turn, promotes their directed migration towards the wound. At the same time, Wnt5a signals also induce upregulation of autophagy, irrespective of whether the cells have been exposed to injury and these signals must be channelled through Frizzled 3 receptors for autophagic behaviour to occur.

Moreover, we have shown that the downstream PCP effector, ROCK, may be a key mediator involved in relaying Wnt5a signals to autophagy machinery by using its kinase ability to activate Beclin 1 and initiate phagophore assembly.

DISCUSSION OF SECTIONS I-III

Cutaneous injury is often an inevitable and unavoidable occurrence that will happen during our lifetime. Fortunately, most of these wounds will heal without excessive intervention and cause minimal impact to our overall health. However, clinical environments are often presented with more severe wounds that have occurred through traumatic events, are associated with surgical incisions or arise through medical complications such as chronic, diabetic wounds. The UK's National Health Service is estimated to face over 2.2 million wounds annually; these result in 10.9 million community nurse visits, 7.7 million GP visits and 3.4 million hospital outpatient visits. This puts a tremendous amount of strain on what is already a limited pool of resources and is estimated to incur costs of £5 billion each year ¹⁶⁵.

The purpose of this study was to unravel molecular events that occur within and around a wound site, providing both the scientific community and clinicians with a better understanding of the mechanisms at play during the healing process. Advancing knowledge in this field could lead to novel treatment strategies that not only benefit patients on a personal level but could have huge financial impacts on global health systems.

The main focus of the project was to investigate some of the molecular pathways specifically activated in migrating epidermal cells surrounding the wound border. By employing several molecular techniques across both human and murine wound models, we quickly established that the well-known cellular process of autophagy was

significantly upregulated in response to injury. This pathway has been extensively investigated across many systems in the context of other biological functions but is surprisingly understudied in the wound environment. As a general rule, autophagy is considered to play an essential role in maintaining cellular homeostasis where it recognises damaged, malfunctioning molecules and destroys them through fusion with lysosomes containing hydrolytic enzymes. It is often studied in the context of nutrient deprivation where it targets surplus material to degrade and recycle its energy elsewhere in the cell to keep essential pathways functioning. In the medical field, decades of research have been conducted on deregulation of the autophagy pathway and the effect it has when cells are unable to clear dangerous entities. This forms a significant sector of research on neurodegenerative disease where Lewy bodies accumulate in affected neurons often leading to their demise and subsequent onset of conditions such as Alzheimer's and dementia. Taking into consideration the extent to which autophagy is understood as a process, it is surprising how little is known about its role in wounding.

Further to our discovery that autophagy is activated at wound sites, immunofluorescence staining revealed that many of its pathway components were exclusively expressed in the trailing end of migrating epidermal cells. This distinct, asymmetrical expression pattern was seen consistently across *in vivo* murine wound models as well as *in vitro* scratch assays using human derived keratinocytes. It would be sensible to assume that some degree of autophagy is triggered by the cellular damage sustained during an injury to expel organelles that have become irreparable under its role in maintaining cellular homeostasis but this process would likely occur throughout the cell. The specific localisation that was observed in the

migrating cells instead indicates that injury induced autophagy plays an additional role above and beyond its homeostatic role that is exclusive to the wound healing process.

Drawing upon existing knowledge in the field, Planar Cell Polarity is another molecular pathway known to be activated in epidermal keratinocytes in response to injury. It is responsible for creating asymmetric distribution of cell components including lipids, proteins, RNA and organelles in response to chemotactic morphogen gradients to facilitate directional migration towards a given cue. In the context of wound healing, these signalling cues are known to take the form of Wnt ligands that are detected by their Frizzled receptor counterparts and direct cells towards the wound bed.

With this in mind, similar molecular techniques were employed to confirm that the asymmetrical expression pattern presented by autophagy markers was perfectly mirrored by some, but not all, of the asymmetrically redistributed PCP pathway components. Of the ten Frizzled receptor family members, Frizzled 3 and Frizzled 6 are most often associated with PCP, with widely reported functional redundancy between the two. However, immunofluorescence staining highlighted a distinct discrepancy between the expression profiles of each receptor. While Frizzled 3 displayed clear evidence of polarised expression at the leading edge of migrating cells, Frizzled 6 showed a much more ubiquitous expression pattern throughout the whole cell leading us to conclude that the two receptors may have retained some independent tissue and context specific roles with Frizzled 3 playing a more prominent role in wound healing.

Furthermore, asymmetrical distribution of autophagy markers was found to coincide with asymmetrical localisation of PCP markers at opposing sides of cells residing in a

distinct population of keratinocytes in the proliferative region of the wound border. More specifically, this population consisted of cells that had detached from the basement membrane of the epidermis and started their migratory journey towards the wound bed.

The overlap in activation and subsequent polarisation of both pathways in response to injury led us to investigate whether there was a yet unknown link between the two. Wnt5a shares a well-studied interaction with Frizzled 3 receptors to trigger activation of the PCP pathway but its influence over the autophagy pathway was previously unexplored. Through real-time qPCR analysis, we have proved that the presence of recombinant human Wnt5a protein in the surrounding environment is sufficient to induce activation of both PCP as well as autophagy pathways in epidermal keratinocytes completely independently of a wound being inflicted. This experiment isolated the effect of Wnt5a, excluding all other wound associated signals to confirm that it plays a crucial role in activating both pathways during the healing process.

To confirm that activation of the autophagy pathway was intrinsically linked only to the non-canonical branch of Wnt signalling, a similar experiment was conducted instead adding recombinant human Wnt3a protein to the surrounding environment. Wnt3a is known to interact with other Frizzled family members to activate the canonical form of Wnt signalling. A real-time qPCR revealed that Wnt3a had no effect on the expression of PCP or autophagy components.

The next stage of the study investigated where Wnt5a ligands were secreted from in the wound environment in order to activate polarisation and autophagy in surrounding keratinocytes.

Human dermal fibroblasts were found to require both physical trauma through infliction of an injury as well as tensile, stretching forces to elicit a substantial upregulation of Wnt5a expression. These are environmental conditions that fibroblasts would naturally experience at the periphery of a wound and suggests that the cells are capable of responding to numerous triggers in order to initiate and control migration.

Epidermal keratinocytes also showed evidence of upregulated Wnt5a expression in response to physical trauma. Moreover, the signal secreted by keratinocytes was found to be perpetuated through an apparent feedback loop that sustained expression of Wnt5a in the wound environment as well as activated regions of epidermis further from the site. The precise mechanism through which this operates was not looked into further.

The study also confirmed that the interaction between Frizzled 3 receptors and Wnt5a ligands was necessary to activate the planar cell polarity pathway, in agreement with existing knowledge, but this same interaction was also essential in activating autophagy in a Wnt enriched environment. The use of siRNA to knock-down Frizzled 3 activity allowed us to restrict the keratinocytes ability to respond to exogenous Wnt5a signals by limiting the number of receptors available for interaction. As a consequence, no evidence of autophagy induction was witnessed despite surplus concentrations of Wnt5a present in the extracellular environment. Indeed, the absence of Frizzled 3

receptors from siRNA knock-down caused substantial interruption to the migration of keratinocytes *in vitro*. Existing knowledge would attribute this to the cells reduced ability to become polarised and therefore unable to perform directed migration towards the scratch site but emerging evidence from the study was beginning to suggest that this phenomenon may be due to more factors than previously thought.

The requirement of this interaction was not necessarily indicative of autophagy being a direct downstream pathway targeted by Wnt5a-Frizzled 3 binding and may rather represent the origin of a more complex cascade of events that culminates in activation of autophagy.

A paper published by Gurkar *et al*¹⁵⁵ proved to play a pivotal role in helping us to understand the relationship between PCP and autophagy induction in the context of wound healing. As part of this study, we proposed a theory that the mechanism postulated by Gurkar's group may also be relevant to the process of wound healing whereby ROCK uses its kinase function to phosphorylate Beclin 1 thereby releasing it from its complex with Bcl2 and triggering activation of autophagy. This event may act as the catalyst to begin nucleation of autophagosomes in polarised, migrating cells.

We have demonstrated that the presence of Y27632 in culture media (a robust inhibitor of ROCK that competes with ATP for its catalytic binding site and therefore impedes its kinase function) causes significant retardation to autophagy activation despite an abundance of Wnt5a available to the keratinocytes. These results highlighted that ROCK was a highly likely candidate responsible for mediating Wnt5a induced autophagy in the wound environment (Figure 58).

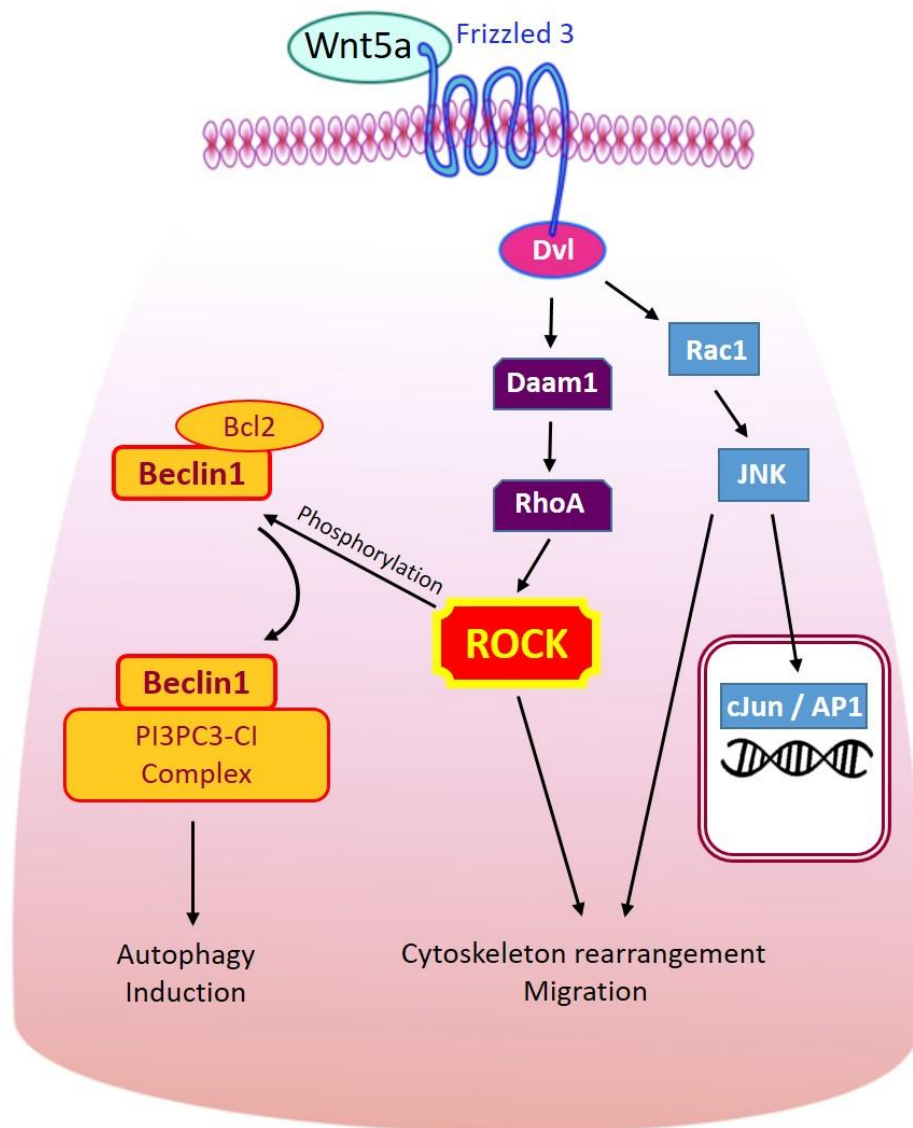


Figure 58 Proposed mechanism for the joint activation of Wnt5a mediated PCP and autophagy in migrating epidermal cells at the periphery of a wound

Results obtained over the course of this study have alluded to a proposed novel mechanism that causes activation of the autophagy pathway as an indirect target of Wnt signalling in a wound environment. We hypothesise that the occurrence of Wnt5a-Frizzled binding induces normal activation of the Planar Cell Polarity pathway leading to already known cytoskeletal and other cellular rearrangements to facilitate directed migration. However, in parallel, we propose that the activation of ROCK as part of PCP also triggers its kinase function to phosphorylate Beclin1 thus initiating autophagy concurrently with PCP. Although the exact role of this activated autophagy remains to be elucidated, we speculate that it is involved in facilitating cellular rearrangement during the migratory phase of wound healing.

The final aim of the project was to understand the role played by Wnt5a induced autophagy in the wound. The asymmetrical expression profile of autophagy components offered some clues as to what the autophagosomes might have been targeting, given the known architecture of a migrating cell and the molecular events that occur in its trailing end. We had hoped to further pinpoint the sites of active autophagy at the trailing end of cells by carrying out electron microscopy analysis of migrating human keratinocytes that had been injured through the use of a scratch assay. Indeed, the experiment was conducted, the samples appropriately fixed and then delivered to our collaborators at the University of Exeter who began processing the cells. Unfortunately this work was halted due to University closure and lockdown conditions during the COVID-19 pandemic. As such, the images were received very close to the thesis submission date so time did not allow a comprehensive analysis to be carried out but is currently an ongoing avenue of work.

Over the course of this study, a number of new publications came to light that supported the results we were obtaining and provided new information that helped guide our theory towards a logical role for autophagy. Of particular interest was work presented by Kenific *et al* in the Journal of Cell Science¹⁶⁶ who demonstrated that selective autophagy mediated by the cargo receptor NBR1 targets focal adhesions in migrating cells to facilitate their turnover, subsequently enabling the cell to migrate across its underlying substrate through rapid assembly and disassembly of adhesion points.

They also identified ubiquitinated active RhoA as a target of p62-mediated autophagic degradation in migrating cells. Active RhoA interacts with ROCK to initiate

phosphorylation and eventual activation of myosin II which then results in contraction and tensional forces exerted on actin stress fibres. Through targeting RhoA for cellular degradation at restricted sites, autophagy controls loss of tension in regions of cells where focal adhesions are disassembling. This leads to tension at the leading edge of the cell (where newly formed focal adhesions are found) to become the dominant force and creates propulsion in the forward direction.

Elucidating a role for autophagy in the wound environment was the final aim of the study but progress on this section was significantly hindered by the complications caused by COVID-19. However, this paper had presented two examples of selective autophagy that promoted migration and were both highly likely to exist in cells at the wound periphery. Moreover, both examples targeted components that would reside in the trailing end of cells and were therefore even more likely candidates for the Wnt5a-induced autophagy reported in this study.

Kenific did not discuss these forms of selective autophagy in the context of wound healing and also stated that much remains to be learned with regards to how selective autophagy is regulated and what pathways lead to induction of selective autophagy in migrating cells. We have presented evidence that may begin to answer some of these questions by identifying molecular interactions that occur between the injury associated, Wnt5a-mediated PCP pathway and activation of Beclin-1 mediated autophagy with ROCK playing a pivotal role.

Furthermore, the proposed molecular relationship between the two pathways fits the logic that when a cell experiences a chemotactic morphogen gradient and undergoes

significant cellular rearrangement to prepare itself for migration, all the necessary pathways required to facilitate this event should be intrinsically linked to make the response more effective. In this case, keratinocytes must become polarised through asymmetric distribution of its components, rearrange its cytoskeleton and modulate cell-matrix interactions by controlling focal adhesion and integrin turnover. By using the Wnt5a signal to orchestrate a molecular cascade that encompasses each of these processes simultaneously, the cell can elicit a more rapid response to injury.

RESULTS SECTION IV

IV.I Investigating the cell cycle status of cells at the wound order using the Fluorescence-acquired Ubiquitination Cell Cycle Indicator reporter system.

Throughout the project, we had noticed that in the majority of real-time qPCRs conducted, almost all of the markers that we tested showed an initial down-regulation in expression immediately following injury when compared to expression in uninjured cells. Following this brief down-regulation, we then often observed the expected expression increase in response to injury (Examples are shown in (Figure 27 and Figure 50).

This raised some questions as to why this was occurring so we developed a small side project to investigate some of the possible causes.

Naturally, it is these cells that are at risk of experiencing the most severe trauma and therefore most likely to acquire some degree of cellular damage. If the damage is deemed too great for the cell to overcome, it may become necrotic or apoptotic - a form of programmed cell death used to eradicate harmful or unwanted cells ¹⁹⁴. If this is the case, these cells are unlikely to respond to the activating cues of the healing process in the manner that we would expect and is therefore a potential reason for down rather than upregulation that was seen.

It is also possible that cells at the immediate wound front enter cellular senescence triggered by the damage they have sustained. Senescence is a cellular response usually associated with aging that causes cells to lose their proliferative capability and enter an irreversible state of dormancy¹⁹⁵. Each of these possibilities would disrupt the natural progression of cells through the cell cycle, often leading to cell cycle arrest or their complete exit from the mitotic process.

In order to investigate the cell cycle status of cells in the different fractions, we used the Fluorescence-acquired Ubiquitination Cell Cycle Indicator (FUCCI) system in the form of lentivirus vector reporters, developed by Sakaue-Sawano *et al*¹⁵³. This is an elegant system that utilises the oscillating expression of proteins that mark cell-cycle transitions to generate either red or green fluorescent signals in live cells.

In its first iteration, the protein Geminin coupled with green fluorescent protein (GFP) is degraded during the G₁ phase while a second protein, Chromatin Licensing and DNA Replication Factor 1 (Cdt1) coupled with red fluorescent protein (RFP) is degraded during S, G₂ and M phases. The alternating degradation of these fluorophore complexes during the cell cycle allow the detection of G₁ cells through the expression of RFP while G₂ and M cells are detected through the expression of GFP. There is a brief period during the S phase where both Geminin and Cdt1 are active, resulting in both RFP and GFP being expressed at the same time so cells in this phase are visualised as yellow.

A drawback that was discovered with this system was that it provided no way of distinguishing between quiescent cells in the G₀ phase (a reversible, dormant state where cells transiently exit the cell cycle) from cells in the G₁ phase as Cdt1 is

expressed in both instances so both populations appear red. To tackle this problem, a modification was made to incorporate a Ki67 promoter into the construct. Ki67 is expressed only in cycling cells and absent in G_0 cells so would restrict expression of the fluorophore complexes, rendering G_0 cells colourless and therefore distinguishable from G_1 cells (Figure 59B). The resultant constructs used for the dual lentiviral infection of keratinocytes are shown in Figure 59A. The virus containing the constructs also harbours antibiotic resistance genes allowing us to keep the cells under permanent antibiotic selection to eradicate any uninfected cells from the culture.

Once infected, keratinocytes were used to generate time lapse data that followed cells over the first 24 hours of a scratch assay. This experimental set up would provide us with vital information regarding the cell cycle status of leader, follower and distant cells to see whether this could explain the initial downregulation of PCP and autophagy markers that was observed at the scratch border.

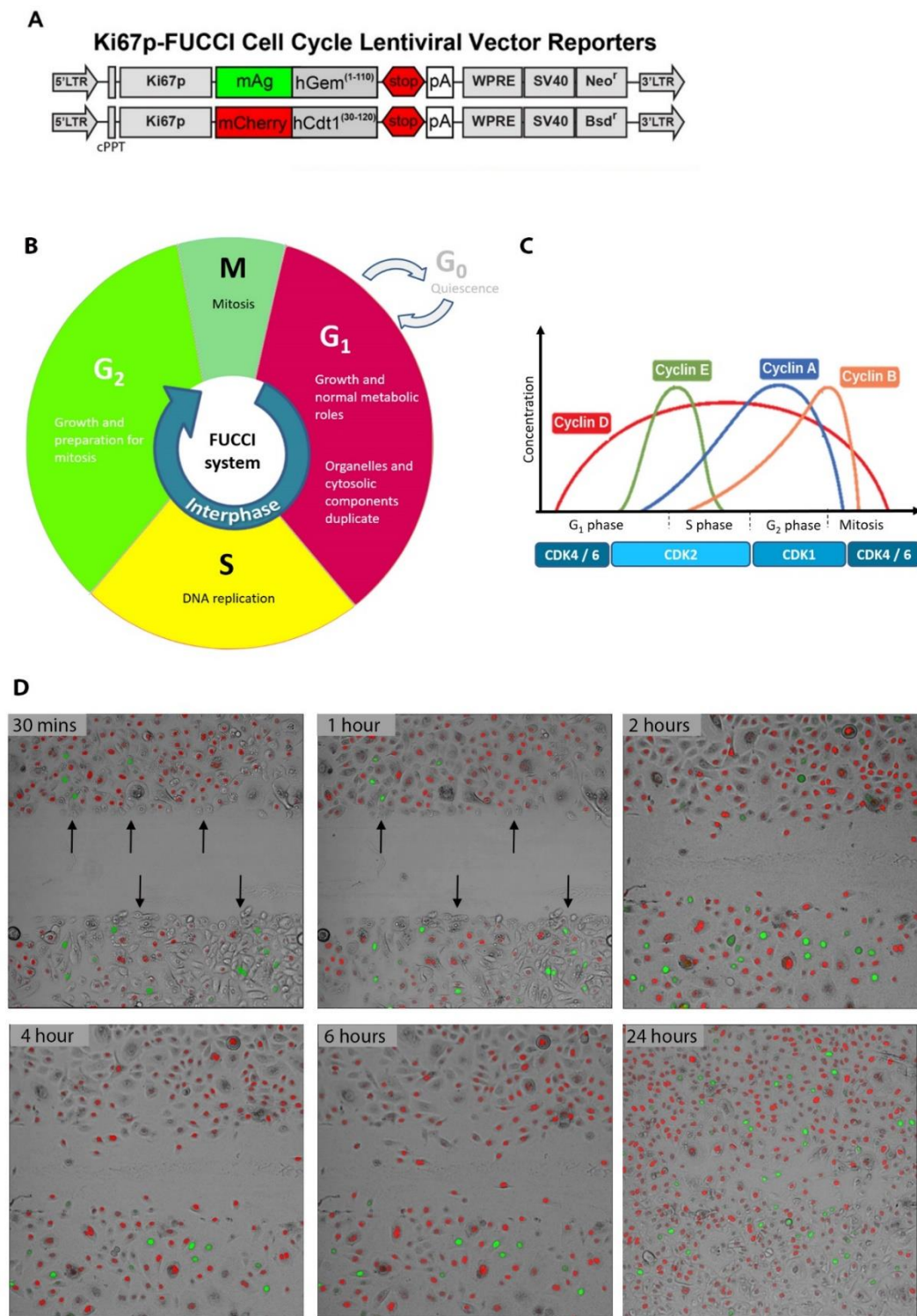


Figure 59 Using the FUCCI reporter system to analyse cell cycle status in scratch assays

Lentiviral infection was used to incorporate a fluorescent cell cycle indicator into neonatal human keratinocytes which were then grown to confluency and used in a scratch assay to assess cell cycle status at the immediate wound border and surrounding periphery. (A) Schematic diagram outlining the constructs used for lentiviral infection. (B) Schematic diagram displaying different phases of the cell cycle and the colour that they are represented by in the FUCCI system. (C) Expression profiles of cyclins and CDKs throughout the different phases of the cell cycle. (D) Static images taken during a time lapse series of FUCCI infected keratinocytes that were used in a scratch assay. Black arrows indicate cells at the immediate wound border that have turned colourless in response to injury.

Figure 59D shows representative static images of the FUCCI scratch assay captured at various points throughout the time lapse series. It became apparent that there was indeed a unique population of cells directly adjacent to the scratch that became colourless within the first 30 minutes and retained this status for at least the first hour. This phenomenon was only seen in one or two cell layers immediately adjacent to the scratch border. According to the colour outputs of the FUCCI system, this implied that the cells had become quiescent and entered the G_0 state. This status is usually associated with long term dormancy but by 2 hours, the colourless cells had developed a red fluorescence indicating that they had re-entered the cell cycle at G_1 . This also confirmed that the cells were still infected with the FUCCI constructs and eliminated the possibility of them being rogue, uninfected cells. There are very few publications that describe such short lived periods of quiescence but the time over which the cells remain colourless did coincide with downregulated expression of PCP and autophagy markers.

By delving further into literature surrounding this topic, it became clear that contact inhibition and certain stress conditions (both of which apply to the nature of scratch assays) can force cells into a transient G_0 like state that is separate from the traditional prolonged phase of quiescence associated with stem cell maintenance ¹⁵⁴.

As with the rest of the cell cycle, there is a heavy reliance on cyclin-dependent kinase (CDK) activity to regulate progression through the normal cycle as well as this transition to the transient G_0 state. The decision to briefly exit the cell cycle is made at the end of mitosis and is predominantly determined by either a build-up of CDK2 activity that favours progression onto the next round of division or suppression of CDK2 that favours transient G_0 .

IV.II Analysis of CDKs and cyclins suggest that colourless cells at the scratch border enter a transient G₀-like state

To confirm whether the colourless cells seen at the FUCCI scratch border were briefly entering G₀, fractions of leader, follower and distant cells were collected as before and used to perform a real-time qPCR to assess levels of CDKs and cyclins. Figure 59C briefly outlines the cyclic activity of these proteins throughout the cell cycle.

Cyclin D, CDK4 and CDK6 are most active during the G₁ phase, followed by increased activity of Cyclin E and CDK2 as cells begin their transition to S phase. As the cell prepares for division in G₂, Cyclin A and CDK1 are upregulated with a final increase of Cyclin B during M phase.

Consistent with the time lapse observations, expression of all proteins was reduced at the 30 minute time point with this trend becoming much more significant by 2 hours when compared to unscratched cells. As expected, the fraction of leader cells displayed the largest fold change in downregulation which supports the possibility of them entering a transient G₀ state immediately following injury. Further evidence that this may be the case came from a very large induction of both Cyclin E1 and CDK2 in the later time points which are known to work in conjunction with each other to kick start re-entry into the cell cycle and the transition from G₁ to S phase¹⁹⁶ (Figure 60).

To summarise, the real-time qPCR did indicate that leader cells might enter a transient G₀ state through reduced expression of all cell cycle proteins but it was unclear whether the subsequent increase in Cyclin E1 and CDK2 was responsible for drawing this population back into the cell cycle or whether it served to increase overall proliferation at the periphery of the scratch. From this experiment alone, we could not

say with certainty that the observed colourless phase was short lived and reversible in this sub-population of cells.

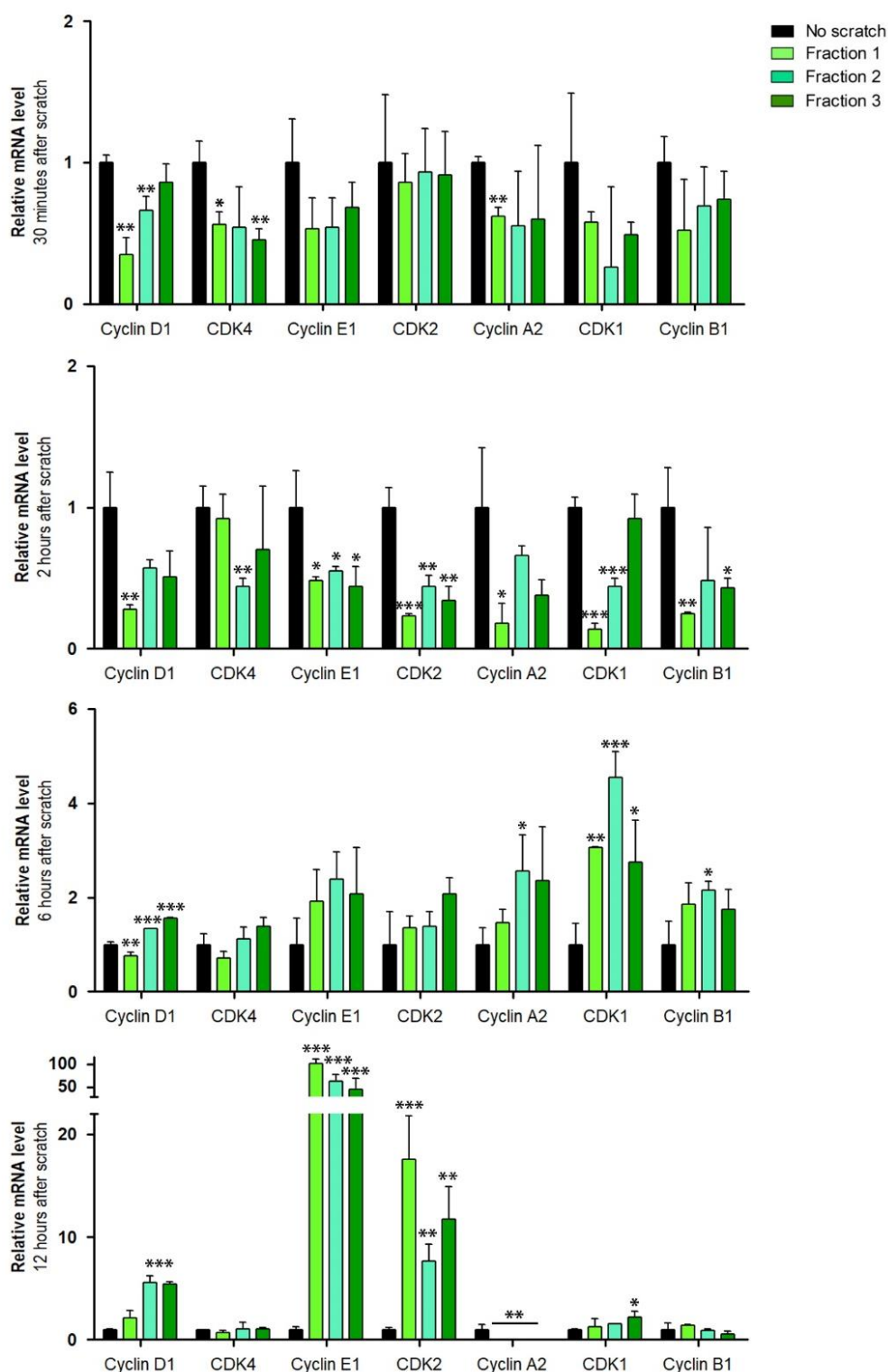


Figure 60 Cyclin and CDK mRNA expression in leader vs follower cells

Neonatal human keratinocytes were grown to confluency as a monolayer epidermal sheet and then injured using the scratch assay technique. Real-Time qPCR analysis was used to assess changes in mRNA expression levels of cyclins and CDKs associated with various stages of the cell cycle in fractions of leader, follower and distant keratinocytes across different time points. An initial down regulation in all cell cycle markers was observed during early time points which was followed by a subsequent and very significant upregulation of Cyclin E1 and CDK2 at later time points (* = $P < 0.05$, ** = $P < 0.01$, *** = $P < 0.001$)

IV.III Colourless cells at the wound border are not senescent

To help confirm that the cells hadn't terminally exited the cell cycle, an assay was used to rule out the possibility of senescence. Here, senescence-associated β -galactosidase activity was used as a biomarker for assessing the senescent state of keratinocytes at the scratch border. During the assay, all cells were treated with the chromogenic substrate 5-bromo-4-chloro-3-indolyl-beta-d-galactopyranoside (X-Gal). Only senescent cells with increased β -galactosidase activity are capable of cleaving this substrate which generates a blue stain within the cells and allows them to be detected. The pH at which the assay is carried out is critical in obtaining accurate results. A pH of 6.0 is necessary to sufficiently suppress low level lysosomal β -galactosidase activity that is present in cycling cells to ensure that non-senescent cells are not detected by mistake. When a lower pH is used, the assay produces false positive results where all cells are stained blue.

In this experiment, Fucci infected keratinocytes were used to generate scratches and then fixed at defined time points so that the senescence assay could be carried out. This experimental design allowed us to directly compare colourless Fucci infected cells with the presence of β -galactosidase activity. For each time point, the senescence assay was carried out at pH4.5 as the control condition to ensure reagents were working correctly and at pH6.0 as the true experimental condition. Figure 61 indicates that although the row of colourless cells adjacent to the scratch was once again observed, there was no corresponding evidence of senescence. We can therefore conclude with relative certainty that this sub-population of colourless cells are not senescent.

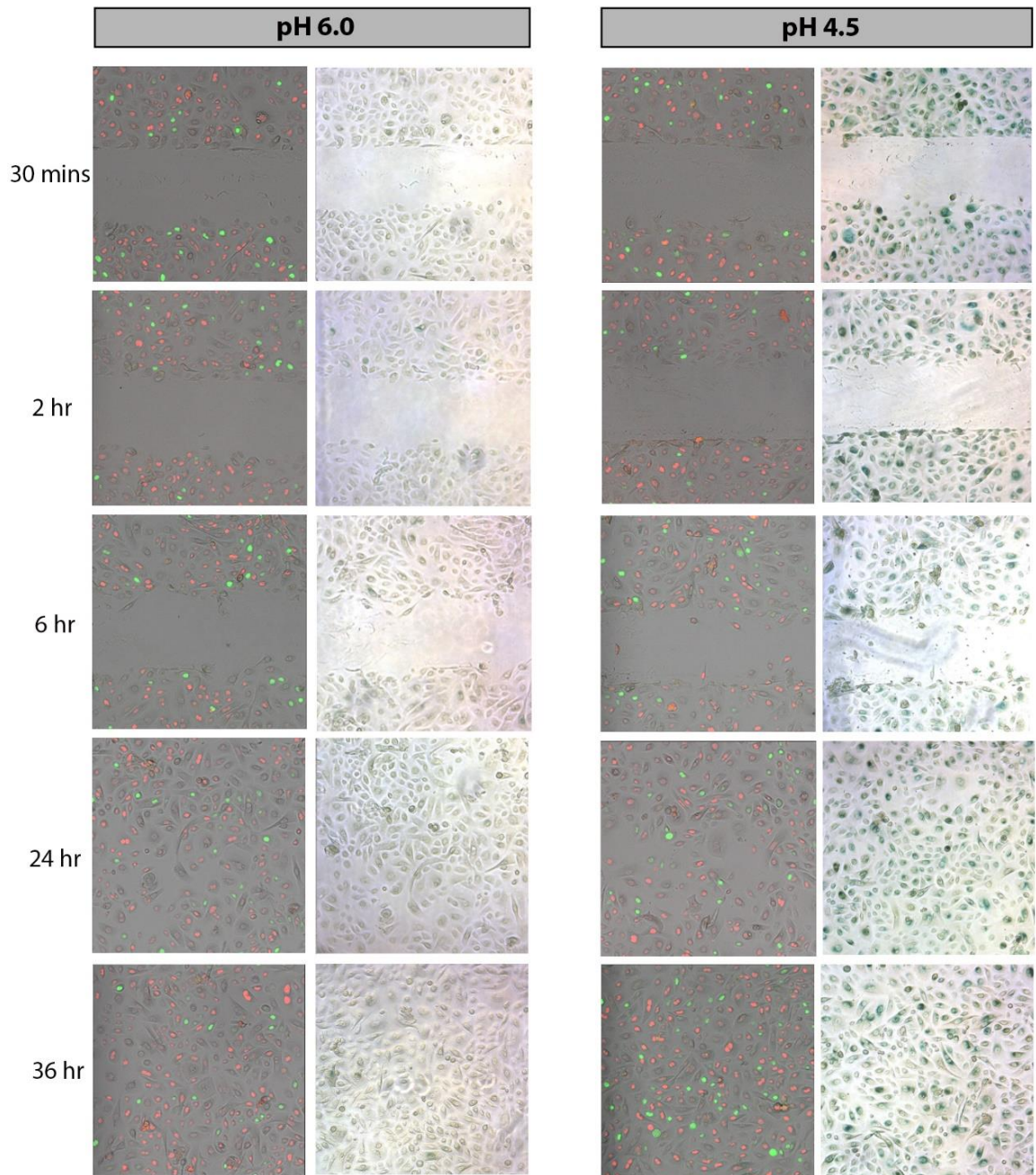


Figure 61 Senescence at the scratch border

The detection of β -galactosidase activity was used to determine whether colourless Fucci infected cells at the wound border had entered senescence. The left hand panel shows results from the true experimental condition carried out at pH 6.0 while the right hand panel shows results from the positive control condition carried out at pH4.5. There was no evidence that cells at the wound border become senescent.

Considering that the results were pointing towards cells at the immediate wound border entering a transient state of G_0 and that this corresponded to downregulation of autophagy and polarisation responses, we next asked whether this restricted the cells ability to migrate until they had re-entered the cell cycle.

To achieve this, time lapse imaging was used to generate migratory tracks of cells during the first two hours and then between 4 -6 hours after the scratch. Using the TrackMate plugin in conjunction with Image J and MATLAB software, it was possible to create compass plots that depict the angle at which each cell migrated in relation to the scratch as well as the displaced distance from its origin. The data from red, green and colourless cells was separated into individual plots for each time point where the length of arrow indicates the distance travelled and its angle indicates the overall migratory direction.

During the first 2 hours, 59.5% of the cells analysed were red and 24.4% were green. Movement of both groups appeared to be random with no specific migration towards the scratch and little difference between the average distances that they travelled (30.6 μ m for red cells and 25 μ m for green cells). The remaining 16.1% of cells were colourless and intriguingly, almost all of them migrated away from the scratch. However, with an average distance of just 4.3 μ m, this is likely to be a negligible result. Having said this, the relatively short distance that colourless cells travelled in comparison to red and green cells fits nicely with the proposition that they are in a more dormant state with restricted migratory capability (Figure 62A).

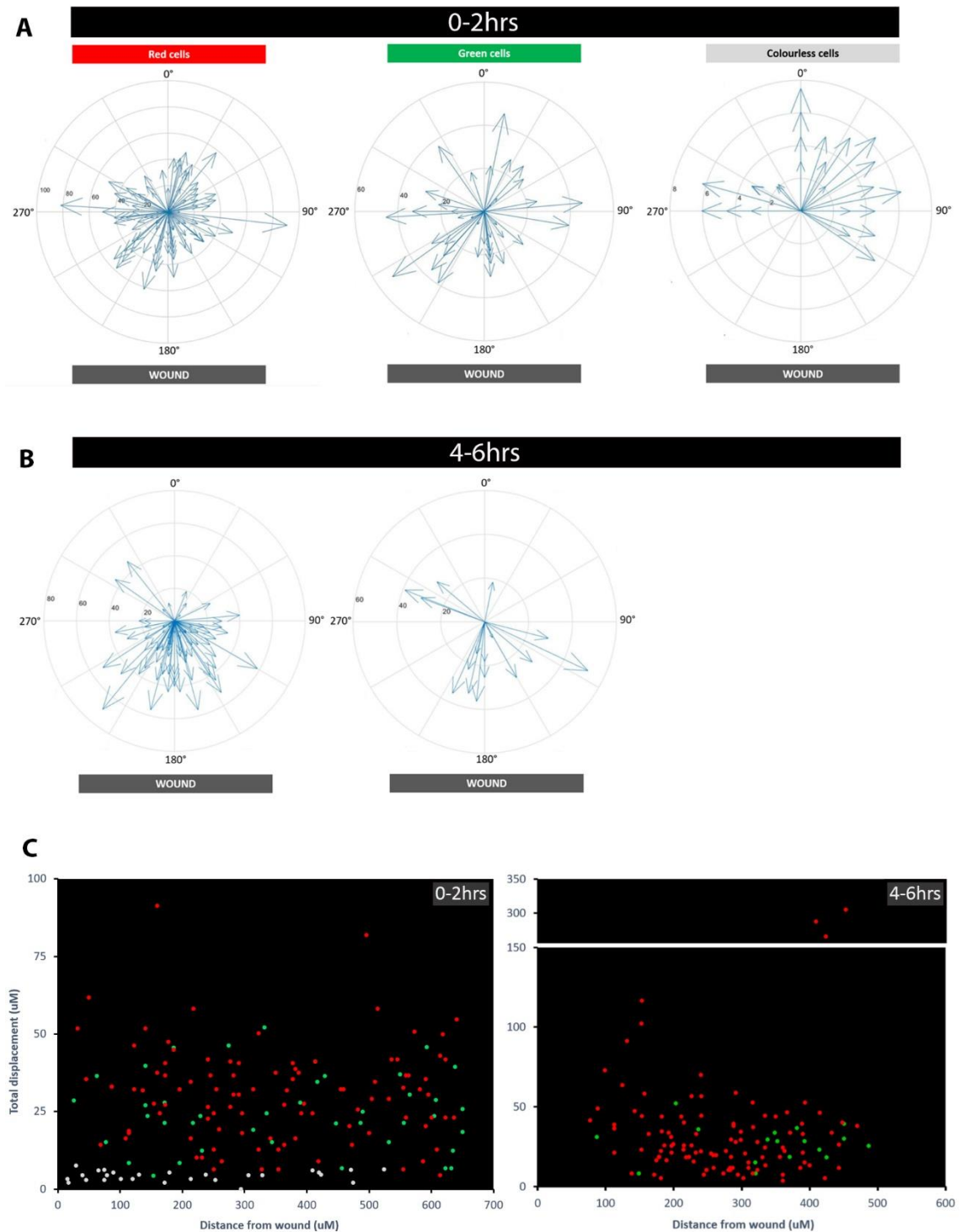


Figure 62 Migratory direction and displaced distance travelled by wounded keratinocytes

Time lapse images of keratinocytes carrying the Fucci reporter were carried out for 2 hour periods immediately following the scratch and 4 hours later were used to generate migratory tracks of each cell. (A) Compass plots depicting the trajectory angle and displaced distance travelled by red, green and colourless cells during the first 2 hours. Length of arrow is relative to distance travelled, scratch is orientated directly downwards at 180° . (Red cells: $n=100$, mean distance = $30.60\mu\text{m}$; Green cells: $n=41$, mean distance = $25\mu\text{m}$; Colourless cells: $n=27$, mean distance = $4.32\mu\text{m}$). (B) Compass plots of red and green cell trajectories 4-6 hours after the scratch. There were no colourless cells during this time point. (Red cells: $n=105$, mean distance = $36.71\mu\text{m}$; Green cells: $n=16$, mean distance = $27.10\mu\text{m}$). (C) Displaced distance travelled by each cell plotted against its starting position relative to the scratch.

The later time lapse series ran between 4-6 hours after the scratch and revealed that all of the colourless cells initially at the scratch border had disappeared leaving none that could be tracked. There was a significantly higher proportion of red cells to green (86.8% to 13.2% respectively) and considering that G_0 cells always re-enter the cell cycle at G_1 , it is likely that the colourless cells had already undergone this transition despite the colour change not being observed during the time lapse period.

The biggest finding from the second set of compass plots came from a much more refined directional migration towards the scratch from both red and green cells. This was accompanied by increases in the distance both groups of cells travelled with red cells migrating an average of $36.71\mu\text{m}$ over 2 hours and green cells $27.1\mu\text{m}$ (Figure 62B).

We also looked at whether there was a relationship between how far a cell migrated and its proximity to the scratch by plotting the two variables against each other for each time series (Figure 62C). This showed the same trend where most colourless cells were clustered close to the scratch with little movement while red and green cells were dispersed across a much larger area from the scratch and migrated various distances. During the second time series, there appeared to be a group of red cells close to the scratch border that migrated a much greater distance than cells further away which adds strength to the existence of a leader population. Despite not having the evidence to prove it, it would be interesting to find out whether these are the same cells that were initially colourless, an experiment that would be useful to carry out in the future.

Summary and discussion of results section IV

An additional area explored as part of this thesis was the unexplained delay, or downregulation, in expression of both PCP and autophagy markers in cells at the immediate wound border for a very short period following injury. Our study demonstrates that this phenomenon is likely due to a very brief and transient G_0 like state that was highlighted by a colourless output from keratinocytes infected with a fluorescent cell cycle indicator system. This event was validated using real-time qPCR analysis which indicated that there was a significant reduction in expression of all cell cycle associated cyclins and CDKs. We also show that this unexplained event terminates through a rapid surge of cyclin E1 and CDK2 expression which triggers this population to re-enter the cell cycle at G_1 . However, the mechanism behind this sudden increase and subsequent restoration of cell division was not studied further.

We subsequently demonstrated that while keratinocytes are in this transient quiescence-like state, their ability to migrate is severely restricted. This may be related to the absence of PCP or autophagy expression, leaving the cells blind to the migratory cues and unable to perform the necessary cellular rearrangements until they have re-entered the normal phases of the cell cycle.

Investigating the purpose of this phase was beyond the scope of the project and will require further experimental work in the future. However, given the circumstances under which this observed phenomenon occurs, it is likely to be associated with G_1 cell cycle arrest; a known damage response mechanism that allows time for cells to repair

critical damage before DNA replication takes places, thereby avoiding propagation of genetic lesions to progeny cells ¹⁹⁷.

RESULTS SECTION V

Optimisation and use of an *ex vivo* murine wound model

As mentioned previously, neither wound healing model employed during this project allowed us to perfectly recapitulate the wound healing process. While the *in vivo* mouse model was a useful tool to study the wound environment in three dimensions and encompassed all the relevant cell types, it was regrettable that we did not hold the Home Office Project Licence needed to inflict cutaneous injury on mice in our in-house animal facility. For this reason, we only had access to specimens prepared elsewhere under a project licence held by Sabine Werner's research group which were then paraffin embedded and shipped to our laboratory. Although they proved to be invaluable during the preliminary data collection stage, the scope of the project could have been greatly enhanced had we had the ability to manipulate wounds *in vivo* through topical application of various treatments or through the use of transgenic/conditional knockout mice.

An alternative method to address this issue was to use *in vitro* scratch assays as they provided a greater flexibility over influencing cell behaviour, made the results more applicable to humans and were less expensive and time consuming to conduct. However, their major drawback was the absence of a haemostasis or inflammatory phase and the array of cells and signalling associated with them prior to migration occurring.

V.I Protocol One – Empty punch biopsy wounds

Towards the end of my time in the laboratory, I attempted to find a solution that incorporated the benefits of both models while still falling within the legal restrictions of my Home Office Personal Licence. Background reading around the matter highlighted *ex vivo* organ culture as a potential way forward that would allow more detailed investigation into the link between autophagy and PCP using a more realistic 3D wound environment. Sacrificing the mice through approved Schedule 1 methods, immediately harvesting and injuring their back skin and maintaining the tissue in optimum survival conditions may prolong the life span of cells in the wound environment long enough to elicit natural responses to injury, providing us with a more accurate platform upon which we could perform manipulation at various stages of the healing process.

To test this concept, four wildtype CD1 mice were sacrificed at postnatal day 22, their back skin dissected and 3mm circular wounds inflicted on the tissue using a punch biopsy tool. Four wounds were made in each piece of tissue (Figure 63A) which were then separated and placed immediately on pre-prepared semisolid made from DMEM/F12 media supplemented with 20% FBS and 1% multivitamin. Care was taken to ensure that the same sized region of surrounding skin was left around each wound to make sure that the volume of tissue contributing to the healing was consistent.

The four wounds from each mouse were snap frozen by embedding in OCT compound and submerging in liquid nitrogen at 24, 48, 72 and 96 hours post injury. Histology was assessed using haematoxylin and eosin staining to confirm whether the *ex vivo* samples displayed similar morphology to the *in vivo* wound models. Figure 63B&C

show representative images of the wound area 24 hours after the punch biopsy.

Although this protocol lent itself to producing uniform wounds of equal width with clearly defined edges in each sample, it was difficult to maintain a uniform depth throughout each tissue. The two example images in Figure 63 highlight this issue where the panniculus carnosus muscle layer remains intact in one sample but has been breached in the other. This poses problems when using the system to determine the rate of wound closure due to its contractile function bringing the wound edges together. Where there were discrepancies between samples, it would be difficult to discern whether closure differences were due to treatment conditions or degree of contractile force. Owing to the contribution of dermal fibroblasts, the thickness of the dermal tissue beneath the wound bed would also affect the rate of closure making it impossible to accurately compare different wounds and treatments.

The histology also revealed that there were no signs of proliferation at the wound borders, even 96 hours after injury, along with no evidence of migration suggesting that the protocol was not sufficient to keep the cells alive and eliciting normal behaviour.

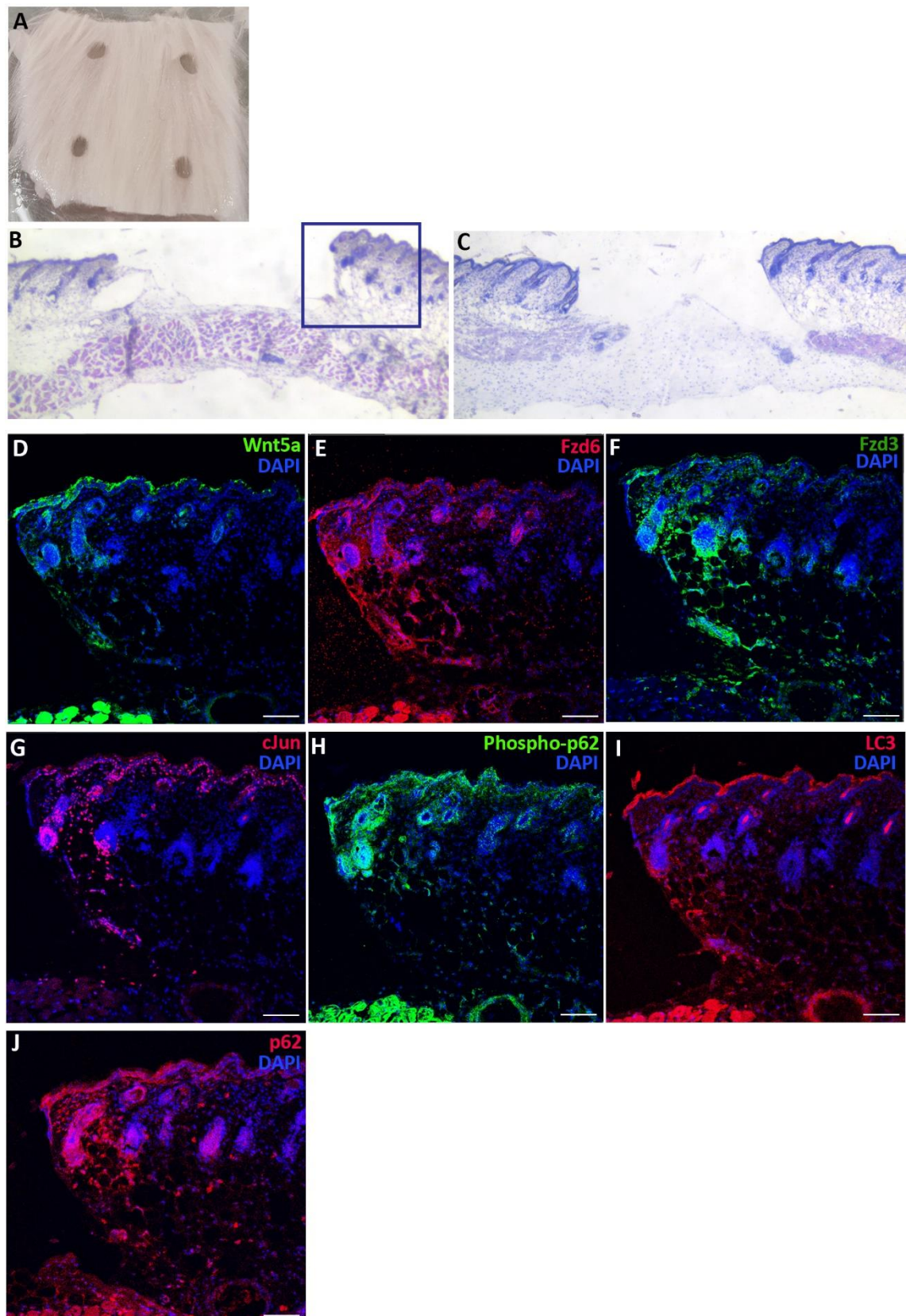


Figure 63 *Ex vivo* wound model at 24 hours post injury- protocol one

Back skin from 22 day old CD1 mice was dissected and injured using a 3mm punch biopsy tool to create *ex vivo* wound models. (A) Photographic demonstration of the technique used prior to the wounds being separated and placed on semi-solid. (B, C) Cross-sections of wounded tissue frozen 24 hours after injury were stained with

haematoxylin and eosin to assess their histology. The two examples show how the punch biopsy technique produced inconsistent wound depths with the panniculus carnosus intact in some samples (B) but breached in others (C). There was also little evidence of proliferation at the wound borders and no migration of keratinocytes into the wound bed. (D-G) The cross-sections were stained with autophagy or PCP antibodies and counterstained with DAPI to assess whether the ex vivo models elicited similar wound responses to in vivo tissue. Higher magnification images are shown of the right wound border from the sample shown in (B). All markers showed increased epidermal expression towards the wound bed. A significant increase was also observed in hair follicles near the wound, consistent with previously shown in vivo wounds. (Scale bar = 100um, n=4)

Despite the drawbacks identified and the lack of proliferation, we checked to see whether any of the wound healing pathways of interest had been activated at the wound borders. We used the same PCP and autophagy antibodies that had been used in the panel of markers for the *in vivo* samples so that we could directly compare expression between those and our *ex vivo* samples. The immunofluorescence results showed that there was increased dermal and epidermal expression of components from both pathways at the wound border and that this decreased in a linear fashion as distance from the wound increased (Figure 63D-J). This proved that there was at least some similarity in how the cells behaved *in vivo* and *ex vivo* so modifications were made to the protocol in an attempt to overcome the initial problems and achieve a more accurate representation of wound healing in the *ex vivo* system.

We hypothesised that a potential reason for the lack of proliferation and migration was due to the absence of a clot and granulation tissue which usually provide a substrate across which the cells can move. There is also an abundance of signalling molecules usually produced by these components of the wound so their absence may account for the differences between the two systems. The obvious solution was to

artificially add signalling proteins and a matrix into the punch biopsy wound to mimic the stages of healing that were missing.

V.II Protocol Two – Incorporation of protein soaked Affi-Gel Blue agarose beads

Affi-Gel blue affinity gel is a beaded, crosslinked agarose gel covalently coupled to the Cibacron blue dye F3GA. This dye functions as an ionic, hydrophobic, aromatic or sterically active binding site that allows a wide range of proteins to be captured and absorbed with a capacity of more than 11mg/ml. It is traditionally used in purifying serum proteins by removing the albumin component or to purify enzymes such as kinases and dehydrogenases but has also been used to deliver proteins to specific tissue locations. The slow release delivery of proteins such as Wnt5a directly from the wound bed would provide an ideal method of mimicking the normal signals that are present in the wound environment and may trigger more realistic behaviour in cells at the wound periphery.

To test this approach, a further four wildtype CD1 mice were sacrificed at postnatal day 21, their back skin harvested and injured with punch biopsies as before.

Immediately following their placement onto semi-solid media, pre-soaked Affi-gel blue beads loaded with either Wnt5a, rapamycin or bafilomycin were inserted into the wound bed. The wounds were imaged on consecutive days for 1 week to monitor the rate of closure. While we expected the Wnt5a soaked beads to enhance wound closure by increasing directional migration, both rapamycin and bafilomycin also decreased the wound size to a greater extent than the empty control wound (Figure 64C). The

rapamycin result fitted the logic that autophagy is needed as part of the healing process and by artificially activating the pathway, it is possible to increase the closure rate. However, that same logic would dictate that when autophagic degradation is blocked through bafilomycin treatment, the wound closure should be hindered. The histology of each condition was assessed at 168 hours post injury to confirm whether the increased rate of healing was due to enhanced migration but again, there was no evidence that the *ex vivo* tissue was comparable to the wound borders observed *in vivo* (Figure 64B).

Although the beads appeared to be effective in delivering the exogenous signals throughout the duration of the experiment, issues arose in their practicality where inserting them accurately into the wound bed without obscuring the wound edges became difficult. Figure 64A shows how some of the beads became trapped on the surrounding fur, potentially causing detrimental effects to the origin of the directional cue in the case of Wnt5a and also making it difficult to measure the size of the wound when the edges were not clearly visible. This made the task of measuring the wounds somewhat ambiguous and definitely needed to be improved upon.

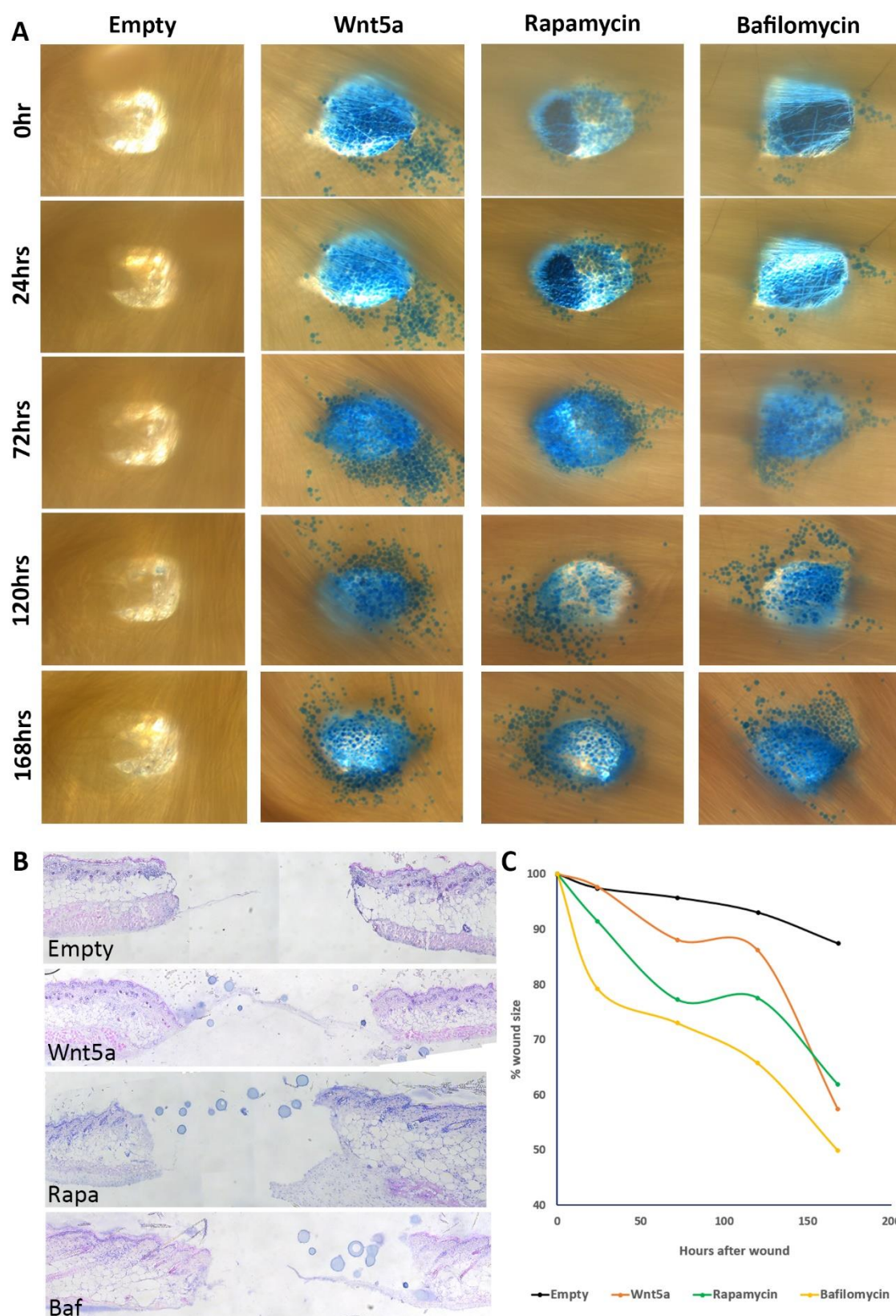


Figure 64 *Ex vivo* wound model - protocol two with Affi-Gel beads

Back skin from 21 day old wildtype CD1 litter-mate mice was dissected and injured using a 3mm punch biopsy tool to create *ex vivo* wound models as previously described in the first protocol. Affi-Gel beads soaked with treatments of either Wnt5a, rapamycin or bafilomycin were placed inside the wound bed and rates of wound closure monitored. (A) Transverse images of the wounds. Beads in the wound bed obscured the

wound borders making it difficult to accurately monitor their closure (B) Cross-sections of wounded tissue frozen 168 hours after injury were stained with haematoxylin and eosin to assess their histology. The punch biopsies were more uniform across each sample than the previous attempt but had created full thickness wounds leaving no underlying substrate for cells to migrate across. There was still no evidence of proliferation or migration. (C) Quantification of the closure rate for each treatment. (n=4)

V.III Protocol Three – Collagen gels impregnated with proteins

The next amendment made to the protocol was to incorporate a collagen gel into the void created by the punch biopsy. As collagen is a natural component of the dermis and is secreted by dermal fibroblasts as part of the granulation tissue, it was chosen as a suitable material to pack the wound that would help mimic the natural wound environment and provide a surface over which keratinocytes could migrate. It is also a versatile material that can be used to form gels of varying rigidity through the addition of different crosslinking agents and can harbour proteins or treatments of choice by adding them to the collagen solution prior to it setting.

To test this amendment, six male wildtype CD1 litter-mates were sacrificed at two months with their back skin harvested and injured as previously described. The same treatments were used as before; each mouse had an empty wound, a wound filled with just collagen and wounds containing either Wnt5a, rapamycin or bafilomycin incorporated into the collagen gel. Again, wound closure was monitored and imaged daily. Figure 65 shows representative images from one of these mice.

This approach was far more successful in terms of keeping the wound edges visible and clearly defined, making it much easier to obtain accurate measurements at each time

point. This was the first iteration of the protocol where wound closure could convincingly be observed.

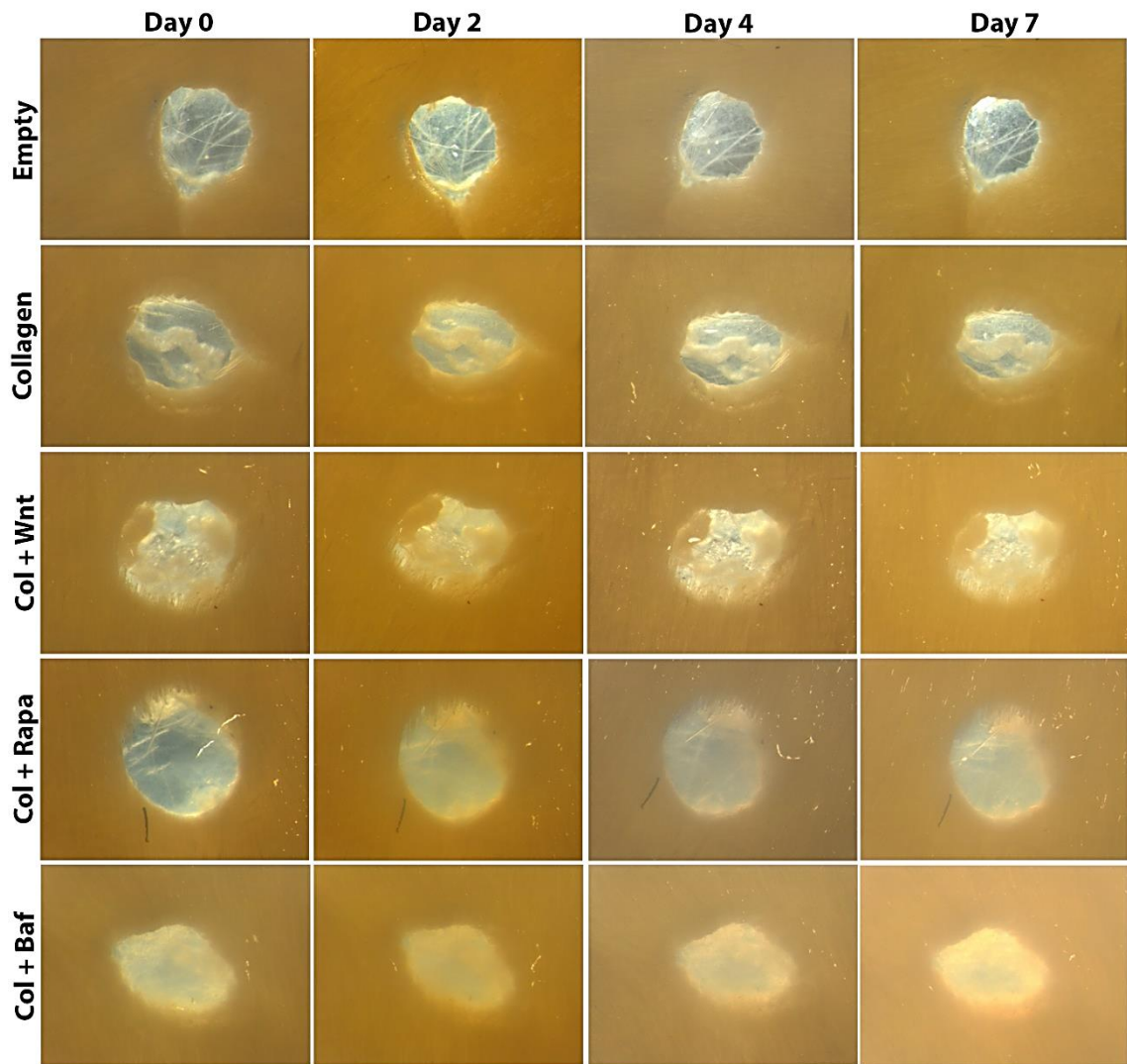


Figure 65 *Ex vivo* wound model - collagen gels impregnated with protein

Back skin from 2 month old wildtype CD1 litter-mate mice was dissected and injured using a 3mm punch biopsy tool to create *ex vivo* wound models as previously described in the first protocol. Treatments of either Wnt5a, rapamycin or bafilomycin were delivered to the wound bed by incorporating them into collagen gels. The gels also provided a substrate over and through which cells could migrate and utilised a material that would naturally be present in the wound as part of the secreted granulation tissue. Samples were cultured on the surface of an agar based semi-solid made with supplemented DMEM/F12. Transverse images are shown of each treatment taken across the duration of the experiment.

Analysis of the measurements indicated that although the mice were litter-mates of the same sex, sacrificed at the same age and their skin taken from the same anatomical location, there was still a significant degree of variation across the group (Figure 66A).

When the raw data was represented as Tukey's box and whisker plots, each wound condition shared a substantial degree of overlap with no significant differences at any time point. However, under closer inspection of the data, a clear trend could be seen in the rate of wound closure for each given mouse. The empty wounds and bafilomycin treated wounds consistently performed worse than their Wnt5a and rapamycin treated counterparts in every mouse; but when the six litter-mates were averaged, this trend was obscured. To better represent this result, the empty wound for each mouse was used as the baseline rate of closure for that individual and all other treatments for the same mouse were then normalised against this value. This method of analysis allows for direct comparisons of each treatment whilst accounting for variation in the overall healing ability amongst the population.

When the normalised closure rates were averaged and graphically represented, it became clear that wounds filled with the collagen gel impregnated with Wnt5a protein healed at a quicker rate than any other condition.

However, the rapamycin treatment appeared to have little effect, causing similar closure rates to those containing only collagen. This suggests that enhancing the rate of autophagy alone without having a relevant guidance cue to enhance migration has no influence on how quickly the wound closes. Conversely, bafilomycin caused a

substantial hindrance to the overall closure rate with bafilomycin treated wounds performing much worse than the empty baseline ones. We concluded that bafilomycin may therefore be interfering with endogenous autophagy occurring at the wound borders, having a consequential impact on the cells ability to migrate (Figure 66B).

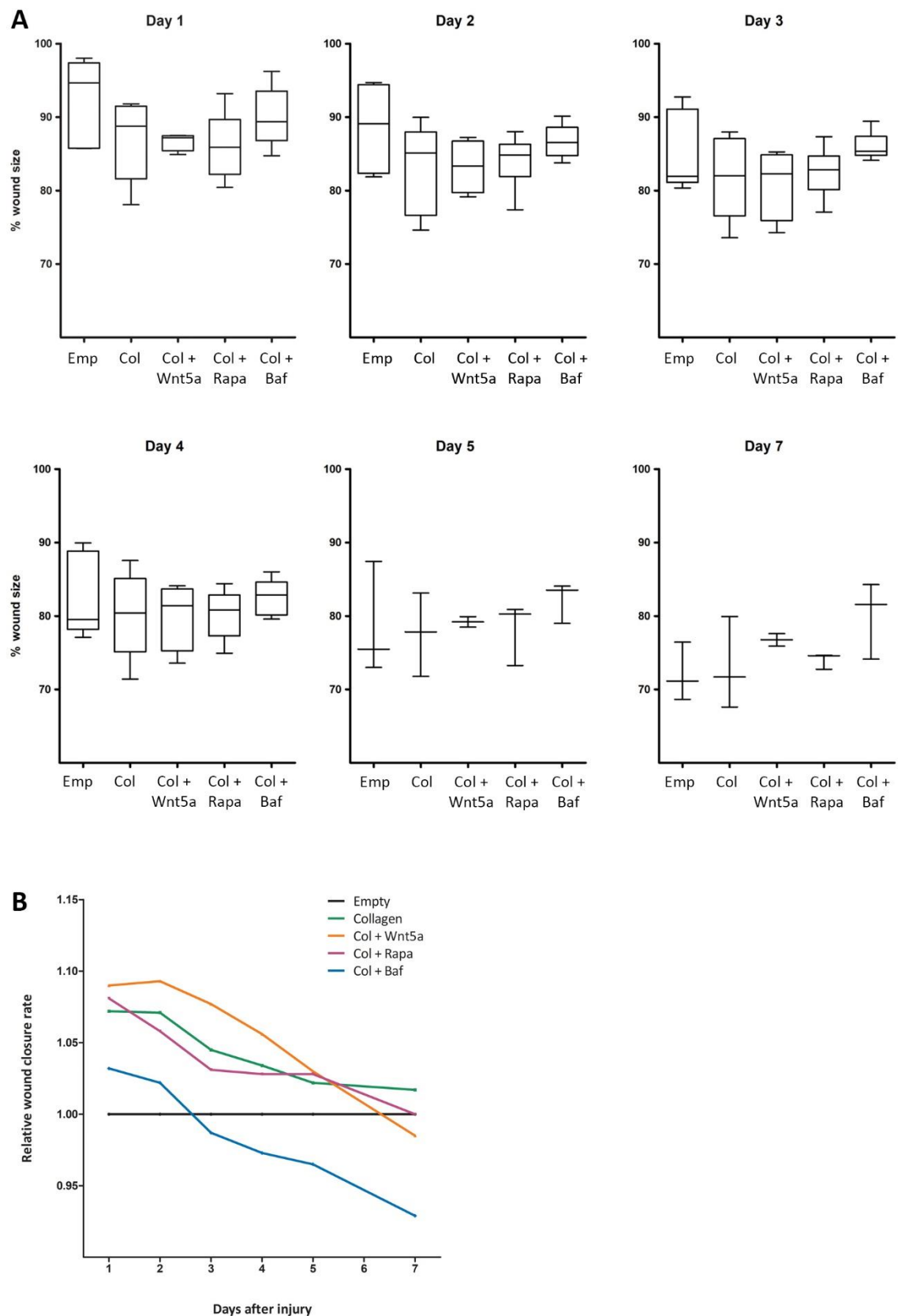


Figure 66 *Ex vivo* wound model - collagen gel measurements

Back skin from 2 month old wildtype CD1 litter-mate mice was dissected and injured using a 3mm punch biopsy tool to create *ex vivo* wound models as previously described in the first protocol. Treatments of either Wnt5a, rapamycin or bafilomycin were delivered to the wound bed by incorporating them into collagen gels. The gels also

provided a substrate over and through which cells could migrate and utilised a material that would naturally be present in the wound as part of the secreted granulation tissue. Samples were cultured on the surface of an agar based semi-solid made with supplemented DMEM/F12 (A) Tukey's box and whisker plots were used to represent the raw data for closure rates given by each treatment. (C) To accommodate variation between individual mice in the population, relative closure rates were calculated by normalising the measurements to the empty wound for each mouse. Wnt5a treatment provided the greatest healing enhancement with bafilomycin treatment causing significant hindrance to the closure rate. (n=6)

Although successful improvements had been made to the *ex vivo* protocol by incorporating the collagen gels and using them as a vehicle to deliver treatments to the wound area, the skin tissue was still not behaving in an endogenous manner. A key indicator that this was the case was the slowing of the closure rate in all treatment conditions despite the wounds having only reduced to 70 -80% of their original size. We suspected that this was due to experimental limits of how long cells within the tissue could stay alive under the culture conditions being used.

We had initially based our protocol on existing *ex vivo* tissue culture techniques described in relevant publications but realised that using semi-solid created several problems for the wound models. First was that the tissue rested across the surface of the pre-set semi-solid to maintain the natural air-liquid interface between the dermal and epidermal compartments rather than the tissue being embedded directly into it. This would have restricted the availability of media to the cells where depletion of nutrients at the surface of the semi-solid may have elicited unnatural behaviour in the wounded tissue. This would include starvation responses, including the activation of autophagy irrespective of injury which may have skewed the results. We had foreseen this problem and had been replenishing the semi-solid every other day by preparing fresh media and transferring the samples across to the new dishes. This consequently

caused the second problem where the act of moving the tissue unavoidably created distortion to the wound, even when the greatest care was taken not to stretch or compress the sample. As a result, the shape of the wound was unavoidably altered slightly and had knock on effects on the reliability and comparability of the measurements from day to day.

V.IV Protocol four – cell strainers and liquid media

As an alternative approach to the semi-solid, we wanted to give the skin tissue direct exposure to standard DMEM/F12 culture media supplemented with 20% FBS to maximise its nutrients availability and prolong survival of the cells. However, it was important that the samples were not fully submerged beneath the surface of the media because an air-liquid interface needed to be maintained to allow natural stratification and differentiation of the keratinocytes to occur alongside re-epithelialisation. This was achieved by using 50ml Falcon tube cell strainers. Their nylon mesh contains 40µm pores and are normally used to isolate primary cells to obtain uniform single-cell suspensions from tissue but this feature also provided a perfect platform that we could use to elevate the wound samples. The cell strainers conveniently rested on the rim of 6 well plates which meant that the skin could be placed on the mesh at the beginning of the experiment and the media in the surrounding well changed easily without any disturbance to the wound itself. The pore size of the mesh allowed free circulation between the media and tissue whilst maintaining air exposure to the skins surface by manually regulating the volume of media placed into each well.

To test the new method, nine wildtype CD1 litter-mates were sacrificed at postnatal day 21 and wounded as before. Five of these mice were male and four were female. Another amendment made at this stage was to shave the mice using clippers to shorten the fur around the punch site to increase the definition of the wound edges. The wounds were imaged daily with representative photos from a male and female mouse shown in Figure 67 and Figure 68 respectively.

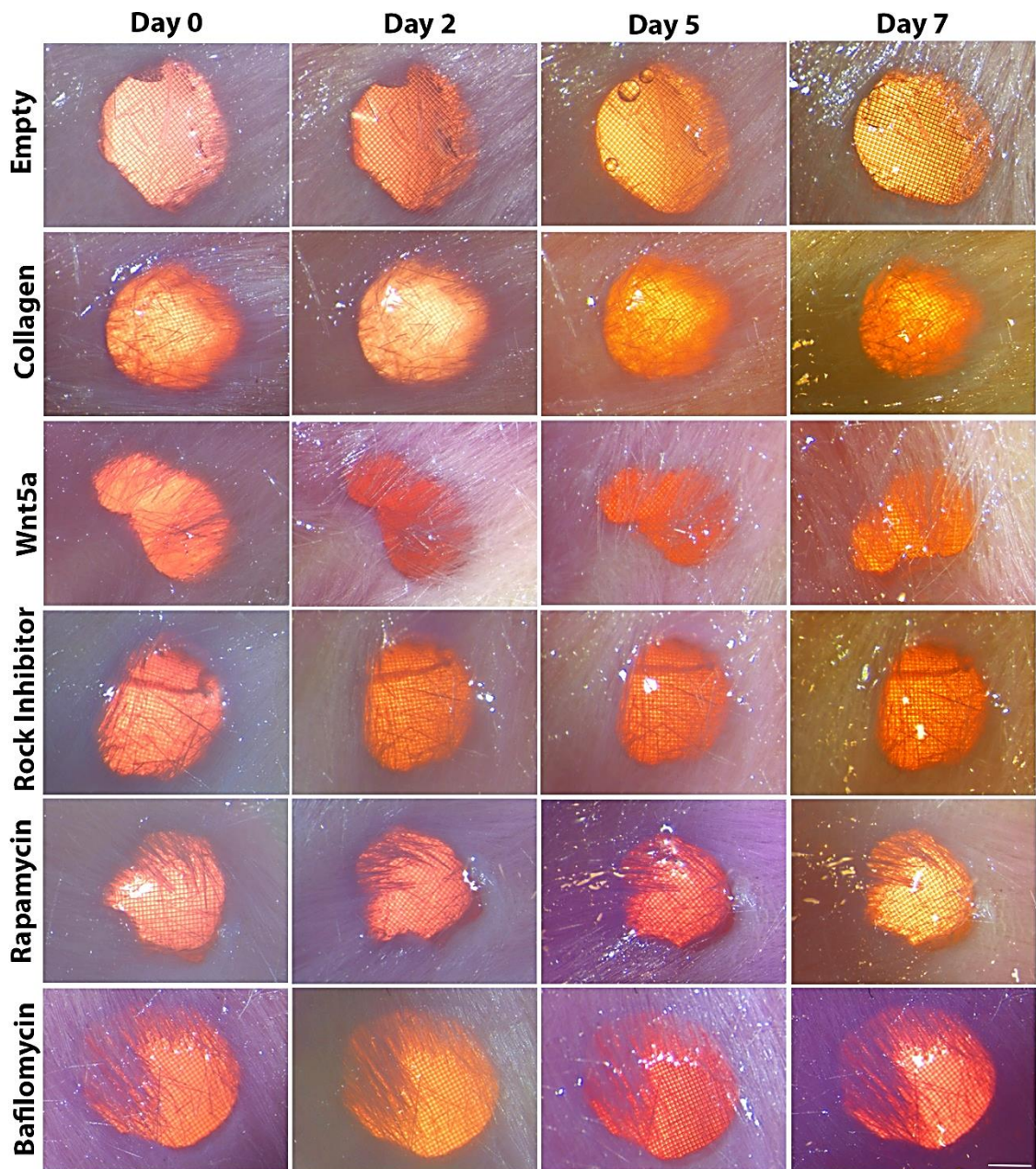


Figure 67 *Ex vivo* wound model - cell strainer male mouse

Back skin from 21 day old wildtype CD1 litter-mate mice was dissected and injured using a 3mm punch biopsy tool to create *ex vivo* wound models as previously described in the first protocol. Treatments of either Wnt5a, Rock inhibitor (Y27632), rapamycin or bafilomycin were delivered to the wound bed by incorporating them into collagen gels as before. Tissue was cultured on the surface on cell strainer mesh in DMEM/F12 media. Transverse images of the wounds from a male mouse are shown. Scale bar = 1000 μ m.

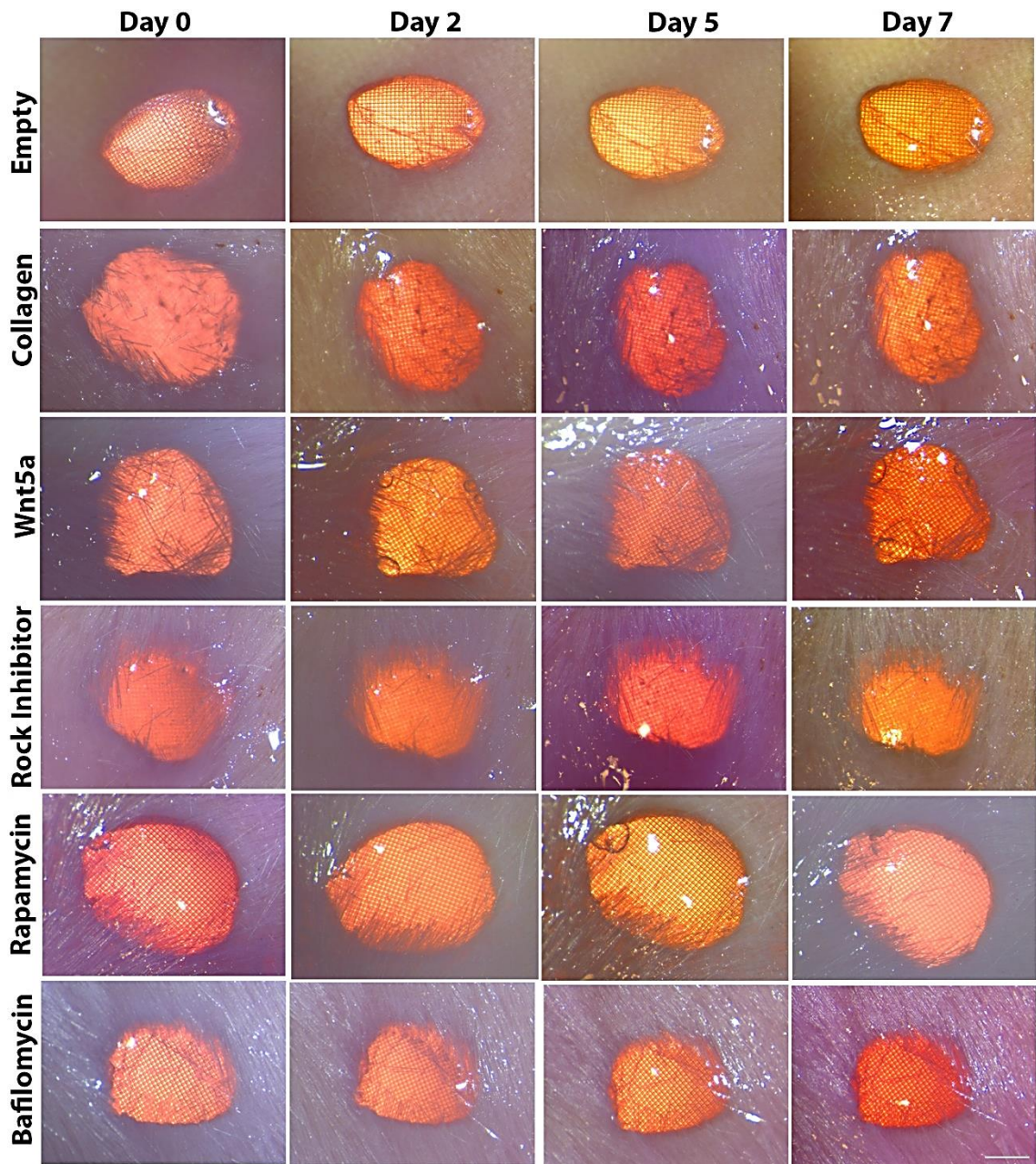


Figure 68 *Ex vivo* wound model - cell strainer female mouse

Back skin from 21 day old wildtype CD1 litter-mate mice was dissected and injured using a 3mm punch biopsy tool to create *ex vivo* wound models as previously described in the first protocol. Treatments of either Wnt5a, Rock inhibitor (Y27632), rapamycin or bafilomycin were delivered to the wound bed by incorporating them into collagen gels as before. Tissue was cultured on the surface on cell strainer mesh in DMEM/F12 media. Transverse images of the wounds from a female mouse are shown. Scale bar = 1000 μ m.

The same method as the previous protocol was used to analyse the measurements where Tukey's box and whisker plots were used to visualise the raw data. As discussed in section 1.5 of the introduction, there are anatomical differences between male and female skin which affects the physiology of healing so data for the two cohorts remained separated at this point.

Again, there was a large degree of overlap across the different treatments when the data was collectively presented in this way (Figure 69). However, the graphs do highlight the distinct differences in the ability to close the wound between male and female mice which is particularly evident in the Wnt5a, rapamycin and bafilomycin treatments where females consistently outperformed the males (Figure 69).

By calculating the relative closure rates for each individual by normalising its treated wound measurements to its corresponding empty wound, we were able to combine the data for males and females. The results confirmed what had been seen in the previous experiment where exogenous Wnt5a treatment caused positive enhancement to the closure rate, presumably due to heightened migratory signals and quicker polarisation responses in the surrounding cells.

Interestingly, treatment with the ROCK inhibitor, Y27632, caused the most pronounced increase in wound closure. Our proposed theory suggested that it was ROCK that mediated the link between Wnt5a induced PCP activation and autophagy via phosphorylation and subsequent activation of Beclin 1. By preventing the interaction between the two pathways, we expected to interfere with wound induced autophagy and hence reduce the tissues ability to heal but this appeared not to be the case.

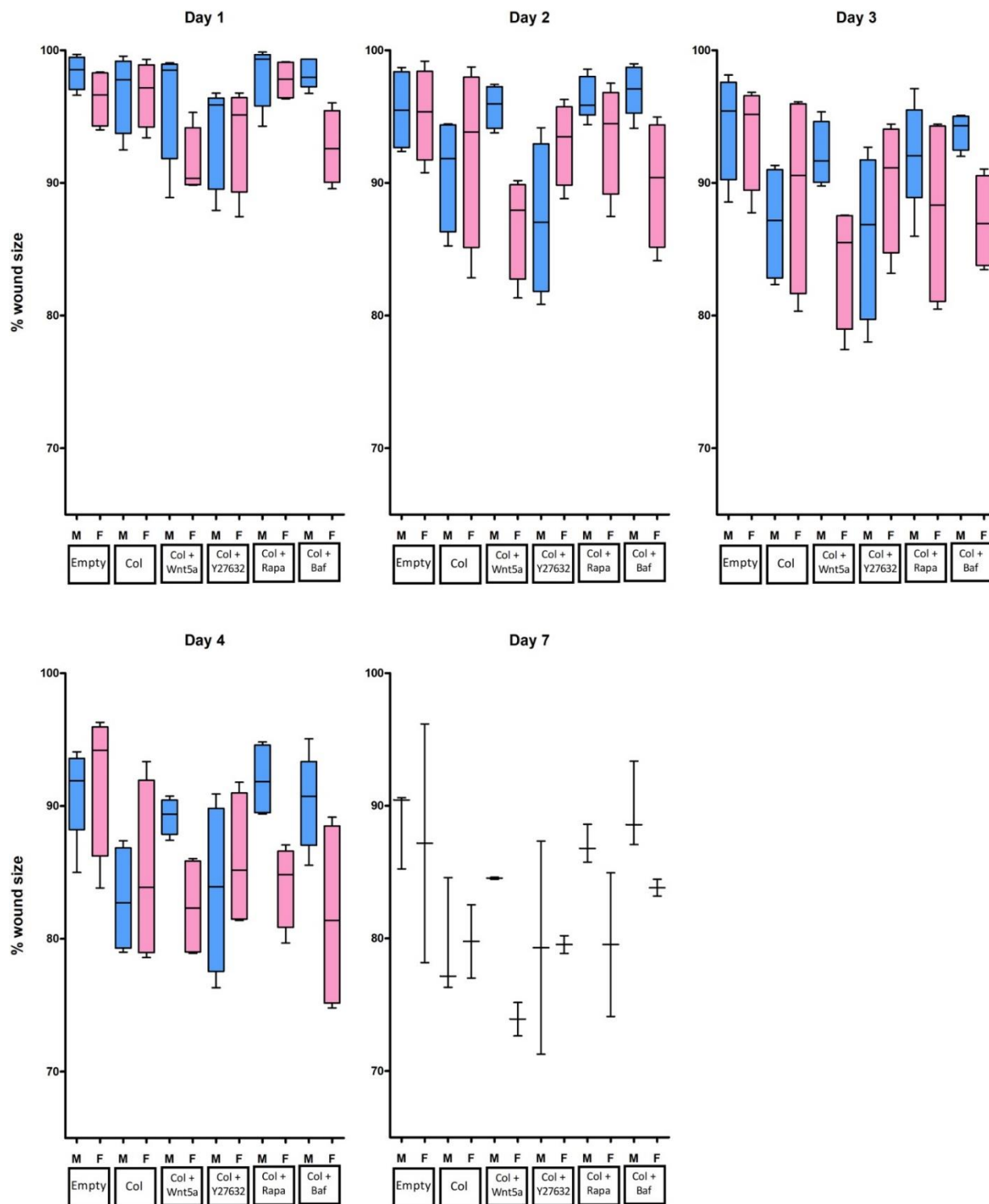


Figure 69 *Ex vivo* wound model - cell strainer box and whisker plots of raw data

Back skin from postnatal day 21 wildtype CD1 litter-mate mice was dissected and injured using a 3mm punch biopsy tool to create *ex vivo* wound models as previously described in the first protocol. Treatments of either Wnt5a, rapamycin, bafilomycin or Y27632 were delivered to the wound bed by incorporating them into collagen gels. Tissue was cultured on the surface of cell strainer mesh in supplemented DMEM/F12 media. Tukey's box and whisker plots were used to represent the raw data for closure rates given by each treatment. Data from male and female mice were plotted separately and highlighted the discrepancies in healing rates between the two sexes despite being treated under the same conditions and can be attributed to anatomical differences (n=9 (5 male, 4 female))

Further reading revealed that several other groups had reported similar findings where Y27632 had been found to effectively increase the proliferative capabilities of keratinocytes and prolonged their viability during *in vitro* experiments when added to the culture media ^{160, 161}. As a consequence, the use of Y27632 in the context of wound healing became much more complex and made it difficult to isolate the individual roles of ROCK. While earlier experiments proved that inhibition of ROCK does interfere with Wnt5a induced autophagy, it concurrently causes excessive proliferation of keratinocytes making it difficult to ascertain whether reduced autophagic behaviour does hinder the tissues healing capability because it is masked by the positive effects of increase cell division.

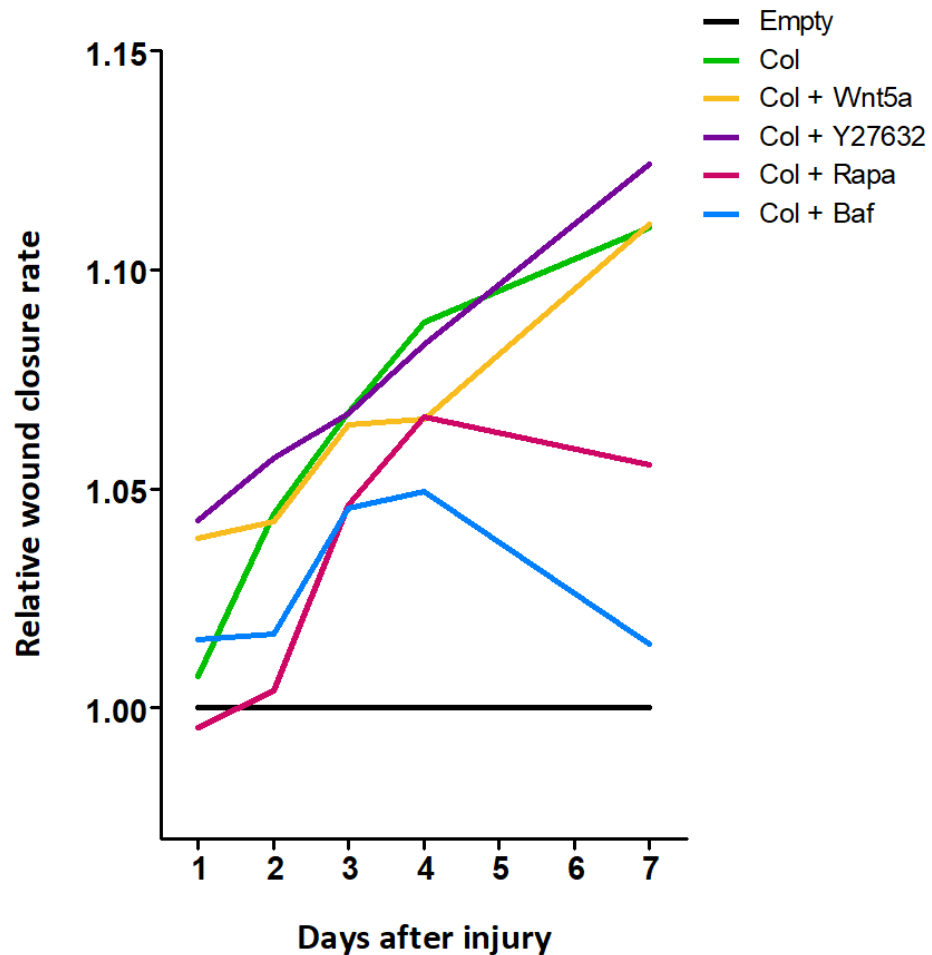


Figure 70 *Ex vivo* wound model - cell strainer relative closure rates

Back skin from postnatal day 21 wildtype CD1 litter-mate mice was dissected and injured using a 3mm punch biopsy tool to create *ex vivo* wound models as previously described in the first protocol. Treatments of either Wnt5a, rapamycin, bafilomycin or Y27632 were delivered to the wound bed by incorporating them into collagen gels. Tissue was cultured on the surface of cell strainer mesh in supplemented DMEM/F12 media. To accommodate variation between individual mice in the population, relative closure rates were calculated by normalising the measurements to the empty wound for each mouse and then plotting the average. Wnt5a and Y27632 treatment caused significant enhancement of wound closure compared to empty wounds. (n=9)

V.V Protocol five: blade incisions with collagen embedded fibroblasts

In a final attempt to optimise the protocol for our needs, it was decided that use of the punch biopsy tool would be abandoned. We were not aiming to produce full thickness wounds but maintaining a uniform pressure to penetrate the skin to the same depth on each sample proved to be a challenge and often resulted in puncturing a hole straight through the tissue instead. To achieve more consistent superficial wounds, forceps were used to gently lift a small section of the skin with curved dissecting scissors used to snip a shallow incision.

It was also decided that clipping the fur around the wound site wasn't sufficient enough to fully visualise small scale changes that were occurring at the wound edges. Commercially available hair removable cream was chosen as an alternative because it would eradicate the fur without causing excessive damage to the surface of the skin. Once the fur had been removed and the incision made, the wound was filled with collagen gel.

No treatments were added at this stage, instead testing whether the presence of dermal fibroblasts embedded into the collagen gel could help achieve more realistic healing behaviour from the surrounding cells. The logic behind this idea was that granulation tissue naturally fills the wound bed *in vivo* and the cells within it secrete a complex array of extracellular matrix components that were currently missing from our model as the wound bed was only being filled with collagen. We hoped that by embedding dermal fibroblasts into the collagen packing material, they would begin remodelling the gel and secreting their own extracellular components to better mimic

a natural wound environment. As this was an entirely new approach, just two female wildtype CD1 mice were sacrificed at 3 months old and used in a preliminary test.

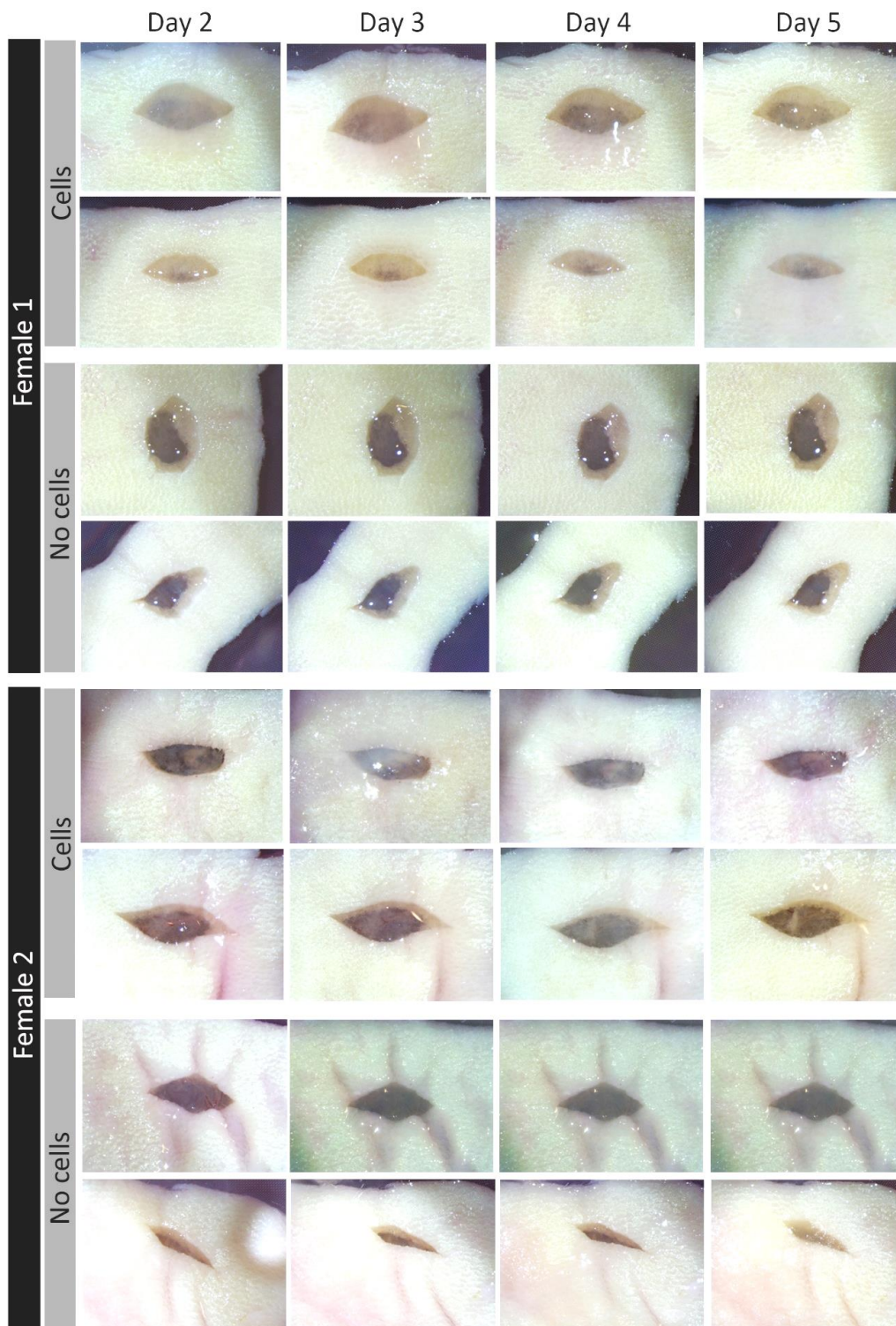


Figure 71 *Ex vivo* wound model – blade incisions with embedded fibroblasts

Fur was removed from the back skin of 3 month old wildtype CD1 litter-mate mice. The back skin was then dissected and injured using curved dissection scissors to make a shallow incision at the surface of the skin. The superficial ex vivo wounds were filled with a collagen gel either with or without human dermal fibroblasts embedded into it. Tissue was cultured on the surface of cell strainer mesh in DMEM/F12 media. Transverse images of the wounds taken on consecutive days following injury are shown.

Aerial view images of each wound are depicted in Figure 71. The new technique made it much easier to observe the outline of the wound and also simplified the administration of collagen gel directly into the incision without being obstructed by the surrounding fur.

Measurements of the wound size over five days indicated that the addition of dermal fibroblasts had a significant positive effect on the healing capability of the model (Figure 72). However, there are several roles played by fibroblasts that this could be attributed to. Further investigation would tell us whether the embedded fibroblasts were producing their own extracellular matrix into the surrounding collagen gel and whether this was having an impact on the behaviour of surrounding cells in the wound. Moreover, the introduction of fibroblasts into a collagen gel is widely reported to cause contraction and shrinkage as they latch onto collagen fibres and draw them together as they remodel their surrounding environment ^{162, 163}. This contraction would give the illusion of wound closure but may not be a true representation of the skins healing status.

Histology of the tissue indicated that this technique was a vast improvement on previous attempts. The incisions were not full thickness and had left enough underlying dermal tissue to create a wound bed from which endogenous wound signals would be released. There was clearer evidence of thickened epidermis at the wound border in the majority of samples suggesting that the new conditions promoted

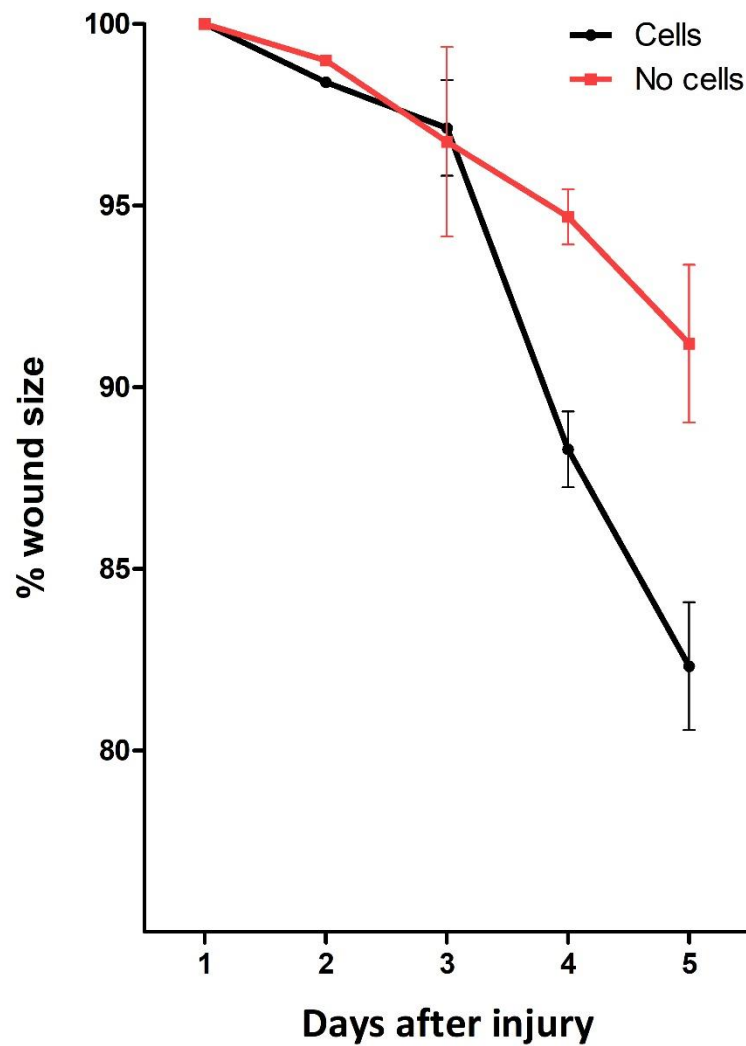


Figure 72 *Ex vivo* wound model – dermal fibroblasts embedded into collagen gel packing material significantly improves healing rates

Superficial ex vivo incision wounds were filled with a collagen gel either with or without human dermal fibroblasts embedded into it. Tissue was cultured on the surface of cell strainer mesh in DMEM/F12 media. Wound size was measured over five days. The inclusion of dermal fibroblasts had a significant positive impact on the speed at which the wound closed compared to those packed only with collagen. [n= 4 (2 female mice each with 4 wounds made in their back skin – 2 with only collagen, 2 with collagen plus cells)].

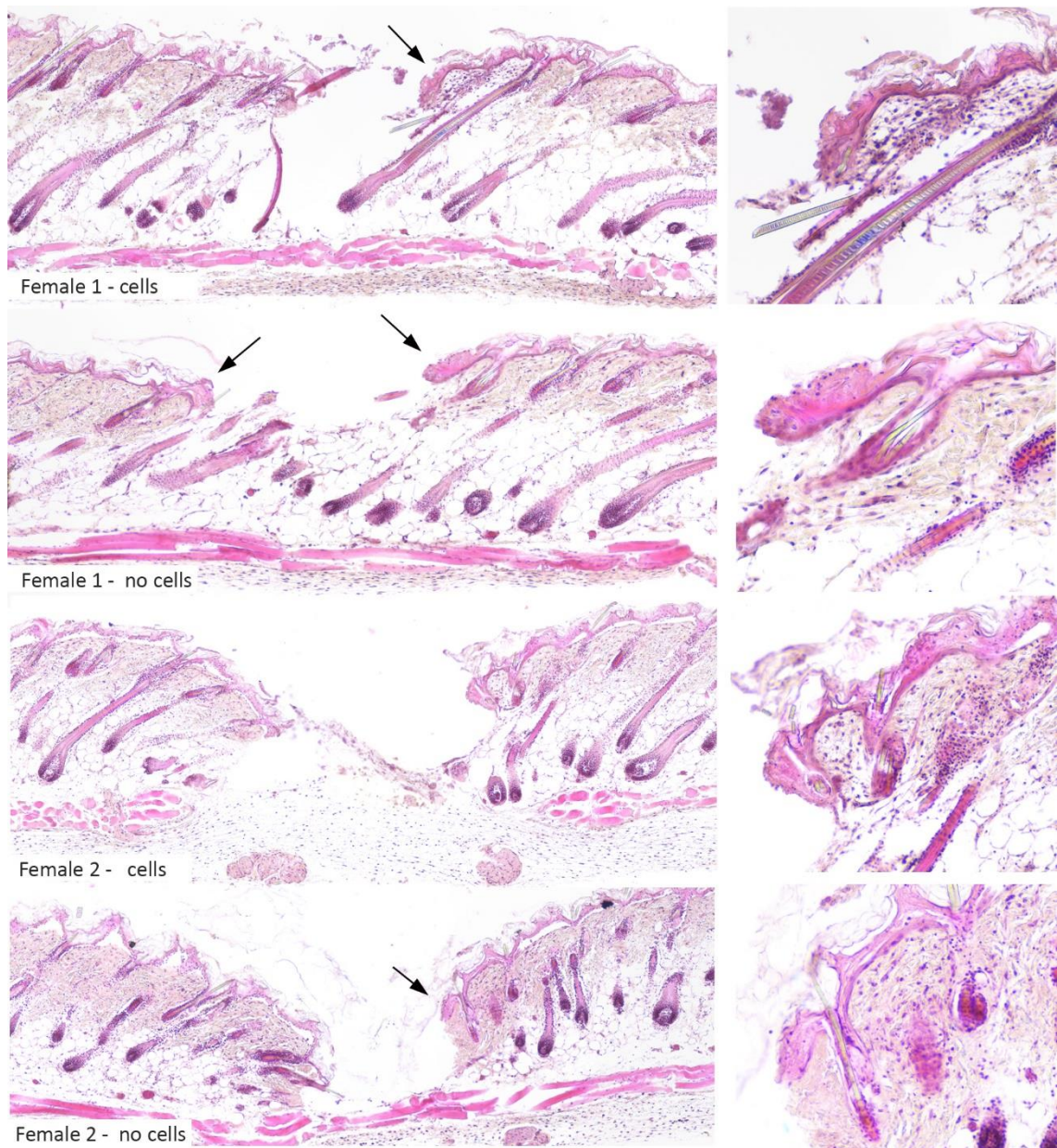


Figure 73 *Ex vivo* wound model - histology of superficial incisions filled with fibroblast embedded collagen gel

Superficial ex vivo incision wounds were filled with a collagen gel either with or without human dermal fibroblasts embedded into it. Tissue was cultured on the surface of cell strainer mesh in DMEM/F12 media. Hematoxylin and eosin staining was used to assess histology of the wounded tissue fixed five days after injury. The right hand panel shows enlarged images of the right wound border. Black arrows indicate thickened regions of epidermis at the wound edge.

wound induced proliferation to a much greater extent than previous models (Figure 73). It was unfortunate that unforeseen circumstances due to COVID-19 caused this experiment to be cut short with all samples being fixed sooner than anticipated. Had the tissue been allowed to continue thriving in the culture conditions, we may have achieved a more enlarged proliferative region that closely resembled the *in vivo* mouse model.

Immunofluorescence staining was used to provide further evidence that this thickened region of epidermis was due to proliferation of keratinocytes at the wound border. For consistency, KI67 and P63 antibodies were used to identify proliferating basal cells in the same manner used during earlier characterisation of the *in vivo* model. Although wounds both with and without fibroblasts in their collagen showed positive expression of P63 in epidermal cells towards the wound edge, there was an increased number of KI67 positive keratinocytes in wounds containing additional fibroblasts (Figure 74). The expression of both markers alluded to stronger proliferative activity at the wound borders compared to uninjured skin further away, was therefore indicative of a natural response to injury and brought us closer to achieving an accurate *ex vivo* wound model that could be used for future wound healing studies.

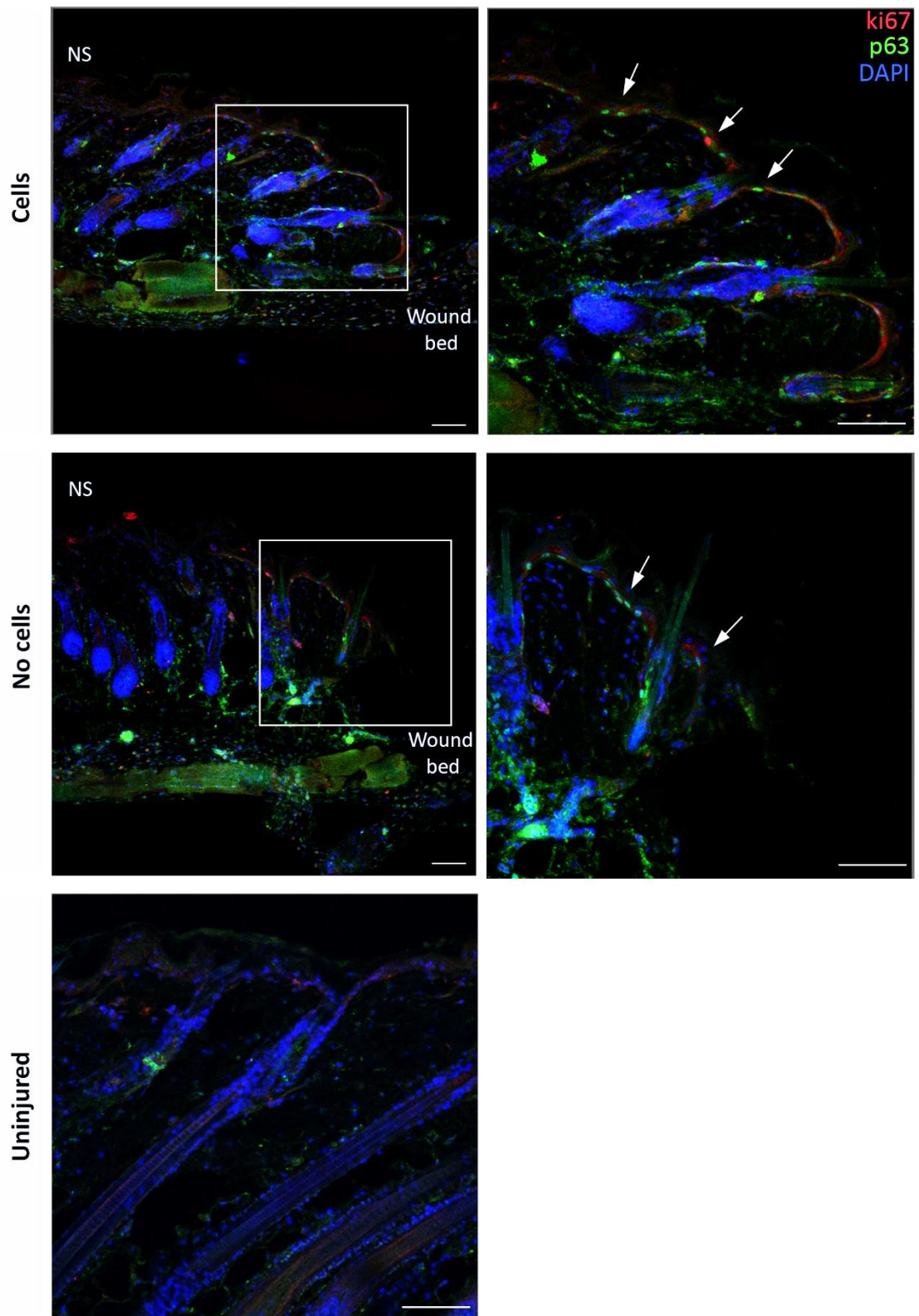


Figure 74 Ex vivo wound model – KI67 and P63 expression in superficial incisions filled with fibroblast embedded collagen gel

Superficial ex vivo incision wounds were filled with a collagen gel either with or without human dermal fibroblasts embedded into it. Tissue was cultured on the surface of cell strainer mesh in DMEM/F12 media. The right hand panel shows enlarged images of the right wound border. Black arrows indicate thickened regions of epidermis at the wound edge.

RESULTS SECTION VI

Optimisation and use of a three-dimensional bioengineered human skin model

VI.1 The concept of an artificially created human skin model

In parallel with the development of a murine *ex vivo* wound model, we began conducting experiments to create a three dimensional human skin model. This concept aimed to reconstruct the major components of the skin using raw materials and primary cell lines to achieve a live but artificially created tissue that behaved like human skin and could be used to study wound healing in a more detailed, three dimensional manner that the *in vitro* scratch assay could not provide. The two separate approaches to develop a wound healing platform were done in conjunction with one another because the *ex vivo* murine model was a more simple concept to achieve and was more likely to be successful over a relatively short time period but still raised issues over its applicability to humans and the clinical setting. While the artificial human skin model was a much more complex avenue to pursue, it would eventually provide a far more suitable platform upon which molecular aspects of wound healing could be studied.

Several commercially available human skin models were already in existence on the market but due to their novel nature, they were extremely expensive and unfortunately not a tool we could invest in for this project. For obvious reasons, the

exact protocol used by these companies was closely guarded but other groups had attempted to duplicate the results for their own work so we fortunately had a starting point to work from.

VI.II Development of an insert based epidermis model

As previously described at length in the introduction, human skin is divided into several complex multicellular compartments so it was a seemingly impossible task to accurately recreate each of these components and get them interacting with one another properly. The most important aspect to this project was to achieve a fully differentiated, fully stratified epidermis that contained stem-like, proliferative cells in its basal layers and mature keratinocytes in its outer layers. A wound could then be inflicted upon the tissue allowing us to investigate the mechanisms of PCP and autophagy in a natural, three dimensional, human environment. For this reason, we first concentrated on developing an epidermis only model rather than tackling a full thickness model from the outset. This allowed us to optimise the protocol and conditions needed to produce an accurate, stratified epidermal component before incorporating other features like the dermis.

Several experiments were carried out using hanging cup inserts to culture human neonatal keratinocytes across the surface of a 0.4 μ m pored membrane. Cells were submerged on the insert and grown until a monolayer had formed, at which point the membrane was raised to expose the cells to the air-liquid interface and induce differentiation in the keratinocytes. The concentration of calcium chloride added to the culture media at the point of exposure was also optimised to mimic endogenous differentiation cues.

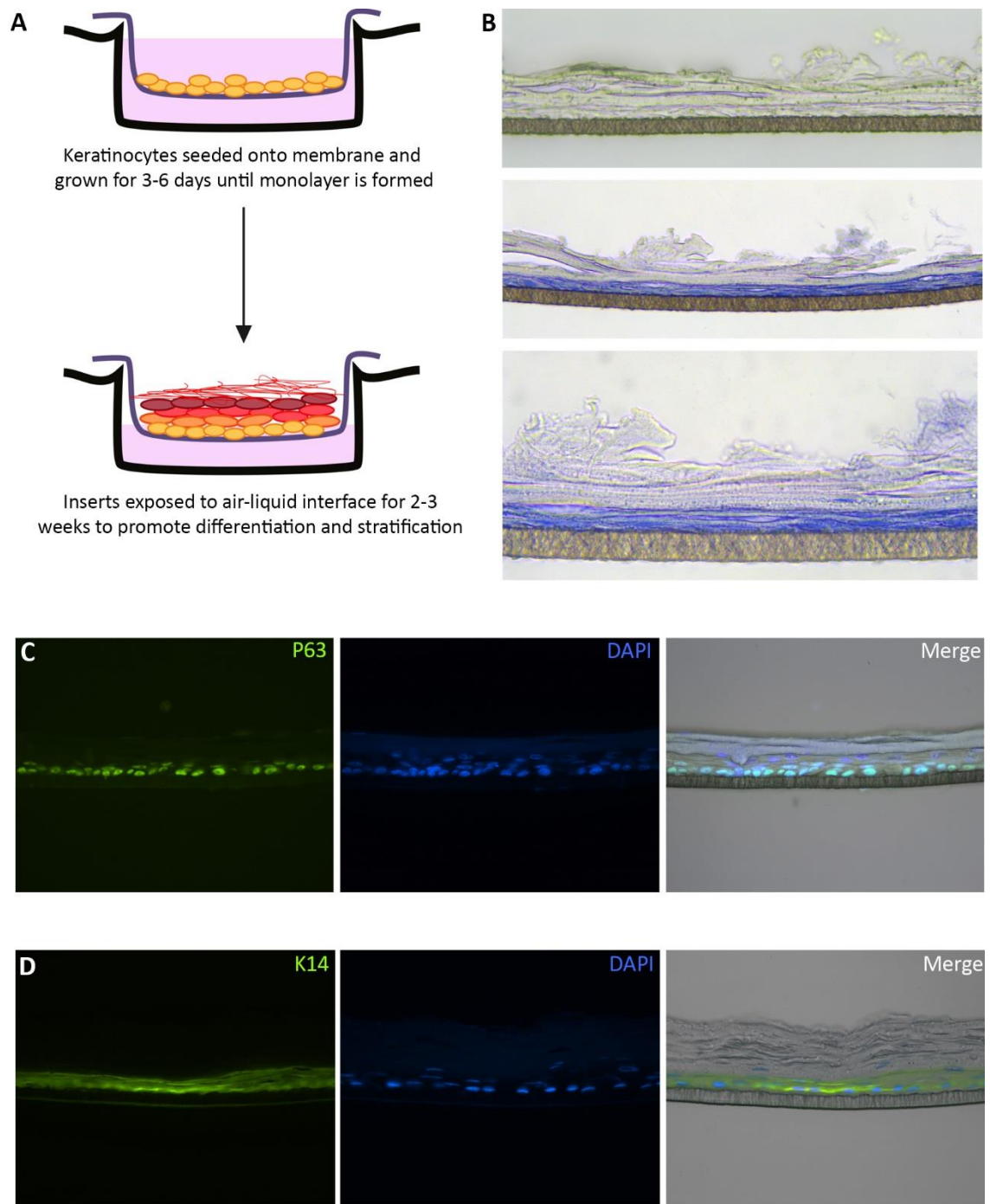


Figure 75 Insert based human epidermis model

(A) A schematic diagram illustrating the method used to generate an insert based human epidermis model. Neonatal human keratinocytes were cultured in a hanging cup on the surface of its membrane containing $0.4\mu\text{m}$ pores. Once a monolayer had formed across the span of the membrane, cells were exposed to the air-liquid interface and cultured in a calcium chloride enriched Epilife media to encourage differentiation and stratification. After 14 days, inserts were fixed in 4% paraformaldehyde. (B) Histology of the epidermal model indicated that intact nuclei resided only in the basal layers. Upper layers lacked any nuclear staining suggesting that cells in this region were more differentiated and morphologically different to the basal cells. (C&D) Correct architecture of the stratified layers was confirmed through immunofluorescence staining with antibodies against P63 and K14. Proliferating, immature keratinocytes were restricted to the basal layers of the model with the expression pattern of both markers closely resembling that of healthy human skin. Nuclei were counterstained with DAPI.

It took between 3 and 6 days to achieve a monolayer across the surface of the insert, depending on the passage of cell used and the number seeded. Exposure to the air-liquid interface was usually maintained for 14 – 21 days to reach full stratification (Figure 75A).

The histology staining depicted in Figure 75B demonstrates the extent of stratification that could be achieved with a 14 day air exposure. Hematoxylin staining was concentrated in the basal layers where you would expect intact nuclei of undifferentiated keratinocytes to reside while the upper layers lacked evidence of nuclei, suggesting that the tissue had undergone the morphological changes associated with later stage differentiation and become more cornified in this region.

Immunofluorescence staining was used to confirm that the stratified layers had the correct organisation and revealed that P63 expression along with K14 was restricted only to basal layers of cells immediately adjacent to the insert membrane in accordance with the expression pattern found in healthy human skin.

VI.III Development of a dermal compartment model

The first iteration of the protocol used to generate a dermal compartment for the 3D human skin model followed the same principle that was used in the *ex vivo* mouse model. Human dermal fibroblasts were incorporated into a collagen gel which was then pipetted into a hanging cup insert, left to set and cultured in DMEM. To compensate for the shrinkage and contraction that occurred as the fibroblasts remodelled the gel, a larger starting volume was needed compared to what had previously been prepared during the *ex vivo* experiments. We found that this made it

more difficult to achieve a homogenous gel with fibroblasts equally dispersed because it required more vigorous pipetting which consequently introduced air bubbles into the mixture. We also wanted to avoid excessive mixing in case it was damaging the fibroblasts and affecting their viability. As a solution, it was decided that half of the desired number of fibroblasts would be incorporated into the collagen gel prior to it setting while the remaining half would then be seeded onto the surface of the gel once it had solidified. These surface fibroblasts should then attach to the gel and naturally migrate into its core resulting in their dispersal without the risk of introducing too many air pockets or too much damage.

Figure 76A demonstrates how the fibroblasts had attached to the collagen gel and acquired a typical elongated morphology by day 2. In the days that followed, the fibroblasts were seen to be migrating downwards into the gel. This phenomenon was visualised by microscopically descending through the different focal planes of the gel. By the fifth day, few cells remained clearly visible at the surface of the gel.

The morphology of the fibroblasts one week after initial seeding had become dendritic with long, slender extensions; a characteristic appearance associated with healthy *in situ* mesenchymal cells in connective tissue (Figure 76B) ¹⁶⁴.

Finally, hematoxylin and eosin staining of fixed cross sections demonstrated how well disseminated the fibroblasts were across the gel. The eosin staining showed varying degrees of light and dense regions within the collagen, particularly in the vicinity of fibroblasts which may indicate remodelling and ECM secretion.

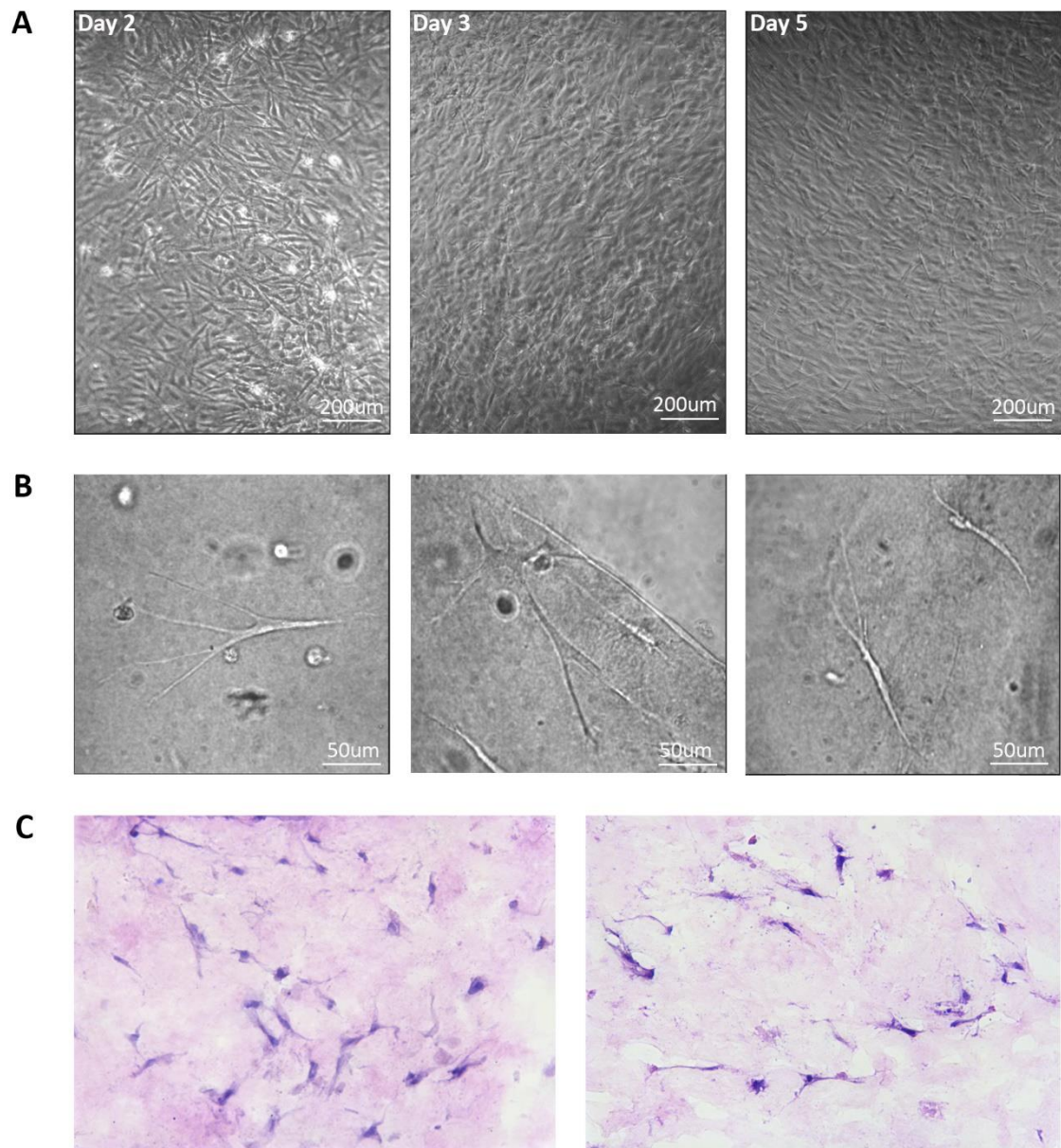


Figure 76 Development of the dermal compartment

A dermal model was created by preparing a collagen gel with human dermal fibroblasts incorporated into the mixture. Once solidified, further fibroblasts were seeded on to the surface of the gel (A) Fibroblasts had attached and acquired a normal, elongated morphology by day 2. Over subsequent days, fibroblasts migrated downwards into the core of the gel. Images were taken of the focal plane directly in line with the surface of the gel. At later time points, fewer cells remained clearly visible, with the majority now residing in lower focal planes deeper within the gel. Scale bar = 200µm (B) A week after the initial seeding, fibroblasts had acquired a dendritic shape with branched extensions. Scale bar = 50µm (C) Hematoxylin and eosin staining of dermal models fixed and cross-sectioned 7 days after seeding. Fibroblasts were well dispersed and the varied densities of eosin staining suggested that other ECM components may have been secreted in the vicinity of the cells.

VI.IV Development of a full thickness skin model

We now had relatively accurate but stand-alone protocols in place to create both an epidermal and dermal compartment so the next stage was to marry the two together to give a working full thickness human skin model.

The individual protocols remained largely the same with the dermal compartment being created in a hanging cup insert using a combination of incorporated fibroblasts and surface seeded fibroblasts which were then cultured for 5-7 days. One day prior to keratinocytes being added, the media was switched to enhanced Epilife to allow the collagen gel to absorb and acclimatise to the change hence maximising the survival rate of the epidermal layer. Once the keratinocytes had been seeded onto the surface of the gel, the submerged culture time and air-liquid interface period remained the same as before (Figure 77A).

Several repeats were carried out using this protocol and although each model had regions of well stratified epidermis with normal architecture, this was frequently found to be inconsistent. Some models produced patchy epidermis where the keratinocytes reached the expected layer height in some areas but then diminished, reducing to only a few layers of undifferentiated basal cells (Figure 77C). Other models resulted in an epidermis with better uniformity in its thickness, tighter cell junctions and better organised layers despite the same protocol and cell types being used (Figure 77D,E).

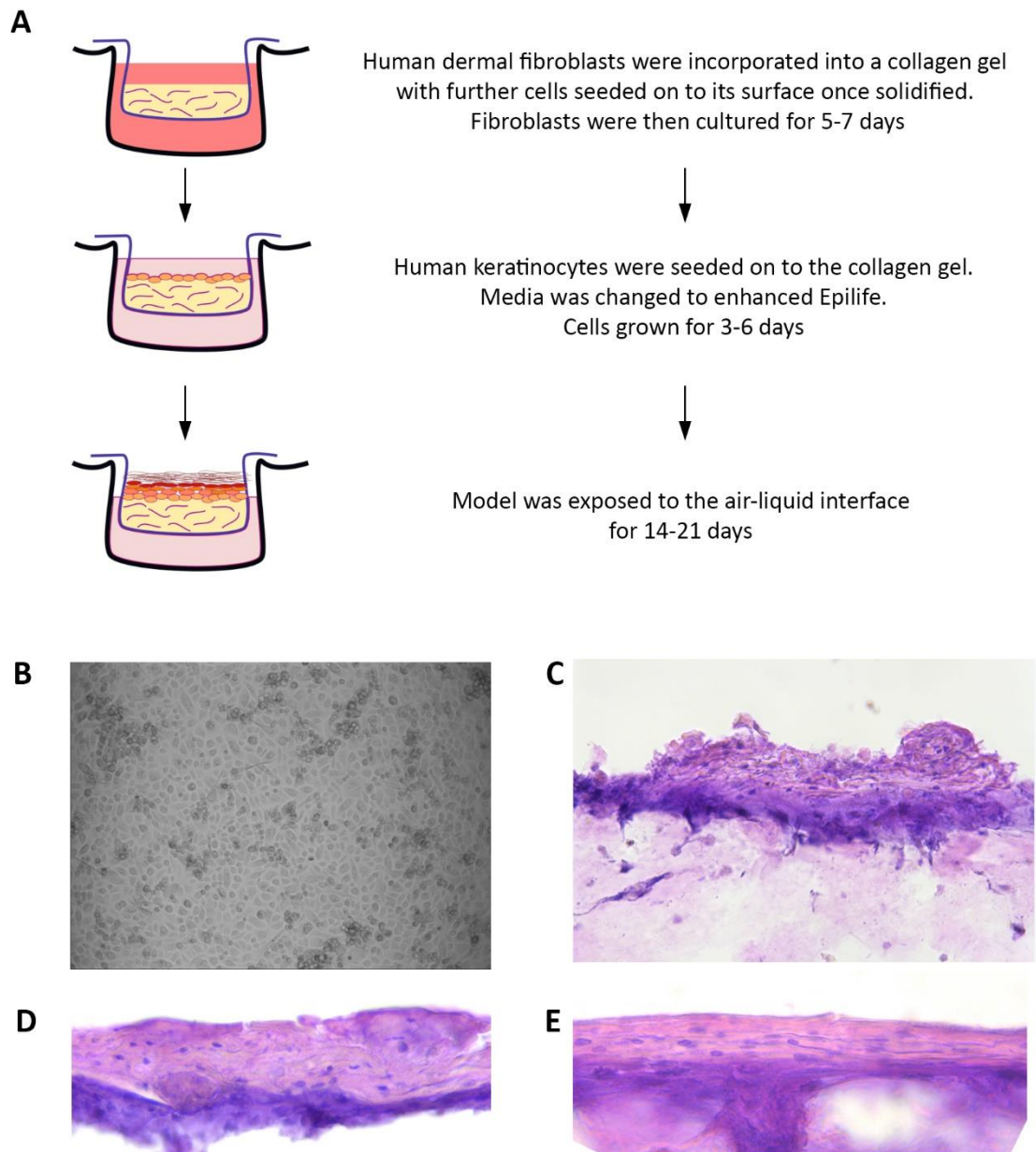


Figure 77 Full thickness human skin model

(A) Schematic diagram demonstrating how the two separate protocols used to achieve an epidermal model and dermal model were merged together to create a full thickness human skin model. (B) Neonatal human keratinocytes were grown until a confluent monolayer had formed across the surface of the collagen gel. Gels were checked frequently to assess when this point had been reached. (C) Histology staining revealed that some models produced patchy epidermis where regions of full stratification and differentiation were spread sporadically across the surface of the gel whereas (D,E) other models resulted in a much more uniform epidermis that had tighter cell junctions and a more accurate architecture despite the same protocol and cells being used for all models.

VI.V Assessment of the bioengineered, full thickness skin model and its suitability for use in the wound healing field

The work carried out on the bioengineered human skin model was done so in a very preliminary manner and with some degree of success. A model was produced that morphologically resembled interfollicular human skin but a huge amount of work still remained to be done to further optimise the protocol and begin introducing other cutaneous components that were currently missing. The volume of work that it would amount to led to this aspect of the project being handed over to a colleague who continued the line of experiments with it eventually forming a large portion of her PhD project.

The model has since been developed where human collagen I and collagen III have replaced the previously used collagen derived from rat tail in the dermal compartment. An additional step has also been introduced where the surface of the fibroblast loaded gel is coated with a solution containing human collagen IV and laminin both of which are important molecules that make up a substantial part of the basement membrane in healthy skin. Better attachment of the keratinocytes is now achieved through using this coating.

A significant amount of work has also been done on characterisation of the model, assessing cell behaviour, viability and longevity and looking at epidermal-mesenchymal interactions and signalling occurring between different layers of the model. It was regrettable that I did not conduct more characterisation of the preliminary model myself as it would have been useful to discuss these points in more detail.

Furthermore, the group has since invested in a 3D bioprinter which has opened up a vast number of new applications where models can be precisely printed and manipulated to fit the requirements of the experiment. The accuracy of this system naturally reduces the inconsistency that was arising from the preliminary protocol and has resulted in a platform with substantial potential.

In terms of its suitability for the wound healing field, its entirely human derived components make it a superior choice over the *ex vivo* murine model, as does its automated accuracy and reproducibility. Its three dimensional architecture and multicellular tissues also give it benefits over *in vitro* scratch assays.

While it forms an elegant platform for studies requiring homeostatic healthy skin, its downfall still resides in the absence of a blood supply and immune response as these are crucial steps in the wound healing process. Without these initial responses present, it is very difficult to artificially engineer a natural wound environment that elicits a proper response to injury from the surrounding cells. Moreover, the lack of any cutaneous appendages abolishes the contribution played by hair follicles and their stem cell niches, adding to the missing features of the wound healing process.

It is extremely unfortunate that none of the tested wound models can currently rival the use of *in vivo* animal models and the knowledge that we can gain from them. We are still faced with a significant challenge in being able to embody all of the relevant stages of wound healing into one model if we want to study the process as a whole.

5. Impact of the study and future work

This study has uncovered several avenues of research that can be pursued further, however the majority of future work related to this project should focus on investigating the precise role of Wnt5a-induced autophagy in the wound environment.

I propose that the first line of work should aim to better characterise the nature of the autophagic activity through analysing the accumulation of autophagosomes visualised by electron microscopy imaging. This should be supported through the use of a system such as a GFP-LC3 reporter and high magnification/resolution imaging to further analyse and quantify LC3 positive puncta in different regions of migratory vs. static keratinocytes to help define their localisation within each cell.

The accumulation of autophagy components already observed at the trailing end of cells is not necessarily indicative of increased autophagic activity and may rather indicate reduced turnover of autophagosomes that has arisen through defects in their fusion with lysosomes or following insufficient degradation of the target cargo. In conjunction with better defining the localisation of autophagosomes in migrating cells, the rate of autophagic flux should also be assessed to ensure that the increased expression of autophagy markers does correlate with completion of the pathway and total destruction of the cargo.

This could be achieved by blocking autophagic sequestration at specific steps of the process (i.e. blocking nucleation of new phagophore membranes) and then measuring the expression of particular markers beyond this point. If their expression decreases, it

would indicate that the pathway does reach completion and that the autophagosome-lysosome unit undergoes destruction.

Depending on the outcome of these experiments and whether the results supported the hypothesis that autophagy targets focal adhesions in migrating cells, further work should be carried out to follow up this line of investigation.

Live cell imaging using a system such as paxillin-mCherry-labelled focal adhesions co-expressed with a GFP-LC3 reporter would be a useful experiment to assess whether autophagosome accumulation is enriched at focal adhesion sites. I would perform this in healthy, untreated keratinocytes to begin with to understand the normal turnover rate of focal adhesions in naturally migrating cells and compare this to autophagy deficient keratinocytes to assess whether their turnover rate is constrained and if this has an impact on their ability to migrate.

A significant drawback of the study has been with restrictions on the use of transgenic/conditional knock-out mice to help elucidate the role of autophagy in wound healing. If a project license could be obtained for this in the future and funding was not limited, I would propose that wounding was carried out on autophagy deficient mice and their progress through the healing process compared against wild-type counterparts, again to help define the role of autophagy.

6. Supplementary material

Table 7 Composition of Dulbecco's Modified Eagle's medium

Component	Concentration (mg/L)
Amino Acids	
<i>Glycine</i>	30.0
<i>L-Arginine hydrochloride</i>	84.0
<i>L-Cystine 2HCl</i>	63.0
<i>L-Histidine hydrochloride-H₂O</i>	42.0
<i>L-Isoleucine</i>	105.0
<i>L-Leucine</i>	105.0
<i>L-Lysine hydrochloride</i>	146.0
<i>L-Methionine</i>	30.0
<i>L-Phenylalanine</i>	66.0
<i>L-Serine</i>	42.0
<i>L-Threonine</i>	95.0
<i>L-Tryptophan</i>	16.0
<i>L-Tyrosine</i>	72.0
<i>L-Valine</i>	94.0
Inorganic Salts	
<i>Calcium Chloride</i>	264.0
<i>Ferric Nitrate</i>	0.1
<i>Magnesium Sulfate</i>	200.0
<i>Potassium Chloride</i>	400.0
<i>Sodium Bicarbonate</i>	3700.0
<i>Sodium Chloride</i>	6400.0
<i>Sodium Phosphate monobasic</i>	141.0
Vitamins	
<i>Choline Chloride</i>	4.0
<i>D-Calcium Pantothenate</i>	4.0
<i>Folic Acid</i>	4.0
<i>Niacinamide</i>	4.0
<i>Pyridoxine Hydrochloride</i>	4.0
<i>Riboflavin</i>	0.4
<i>Thiamine Hydrochloride</i>	4.0
<i>i-Inositol</i>	7.2
Other components	
<i>D-Glucose (Dextrose)</i>	25.0
<i>Phenol Red</i>	15.0
<i>Sodium Pyruvate</i>	110.0

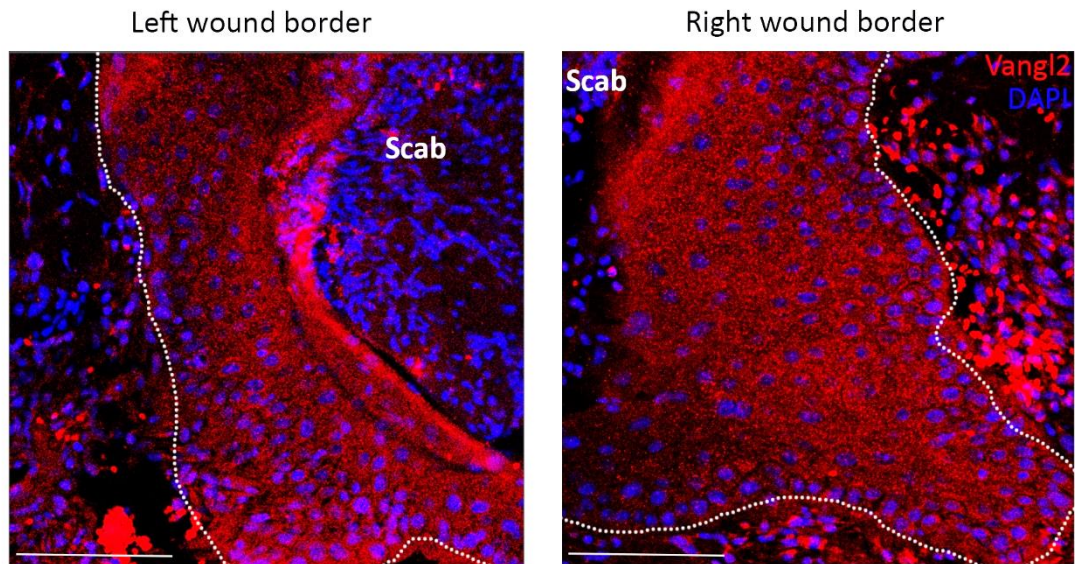
Table 8 Composition of Epilife media

Component	Concentration (mg/L)
Amino Acids	
<i>Glycine</i>	<i>Classified</i>
<i>L-Alanine</i>	<i>Classified</i>
<i>L-Arginine hydrochloride</i>	<i>Classified</i>
<i>L-Asparagine-H₂O</i>	<i>Classified</i>
<i>L-Aspartic acid</i>	<i>Classified</i>
<i>L-Cysteine</i>	<i>Classified</i>
<i>L-Glutamic acid</i>	<i>Classified</i>
<i>L-Glutamine</i>	<i>Classified</i>
<i>L-Histidine hydrochloride-H₂O</i>	<i>Classified</i>
<i>L-Isoleucine</i>	<i>Classified</i>
<i>L-Leucine</i>	<i>Classified</i>
<i>L-Lyysine hydrochloride</i>	<i>Classified</i>
<i>L-Methionine</i>	<i>Classified</i>
<i>L-Phenylalanine</i>	<i>Classified</i>
<i>L-Proline</i>	<i>Classified</i>
<i>L-Serine</i>	<i>Classified</i>
<i>L-Threonine</i>	<i>Classified</i>
<i>L-Tryptophan</i>	<i>Classified</i>
<i>L-Tyrosine</i>	<i>Classified</i>
<i>L-Valine</i>	<i>Classified</i>
Vitamins	
<i>Choline chloride</i>	<i>Classified</i>
<i>D-Pantothenic acid</i>	<i>Classified</i>
<i>Folic acid</i>	<i>Classified</i>
<i>Myo-Inositol</i>	<i>Classified</i>
<i>Niacinamide</i>	<i>Classified</i>
<i>Pyridoxal hydrochloride</i>	<i>Classified</i>
<i>Riboflavin</i>	<i>Classified</i>
<i>Thiamine hydrochloride</i>	<i>Classified</i>
<i>Vitamin B12</i>	<i>Classified</i>
<i>d-Biotin</i>	<i>Classified</i>
Inorganic salts	
<i>Ammonium molybdate</i>	<i>Classified</i>
<i>Ammonium metavanadate</i>	<i>Classified</i>
<i>Calcium chloride</i>	<i>Classified</i>
<i>Cupric sulfate</i>	<i>Classified</i>

<i>Magnesium chloride</i>	<i>Classified</i>
<i>Manganese chloride</i>	<i>Classified</i>
<i>Manganese sulfate</i>	<i>Classified</i>
<i>Nickelous chloride</i>	<i>Classified</i>
<i>Potassium chloride</i>	<i>Classified</i>
<i>Sodium bicarbonate</i>	<i>Classified</i>
<i>Sodium chloride</i>	<i>Classified</i>
<i>Sodium meta silicate</i>	<i>Classified</i>
<i>Sodium phosphate dibasic</i>	<i>Classified</i>
<i>Sodium selenite</i>	<i>Classified</i>
<i>Tin chloride</i>	<i>Classified</i>
<i>Zinc sulfate</i>	<i>Classified</i>
Other components	
<i>Adenine.HCl</i>	<i>Classified</i>
<i>D-Glucose</i>	<i>Classified</i>
<i>Etanolamine</i>	<i>Classified</i>
<i>HEPES</i>	<i>Classified</i>
<i>O-Phosphorylethanolamine</i>	<i>Classified</i>
<i>Phenol red</i>	<i>Classified</i>
<i>Putrescine 2HCl</i>	<i>Classified</i>
<i>Sodium pyruvate</i>	<i>Classified</i>
<i>Thymidine</i>	<i>Classified</i>

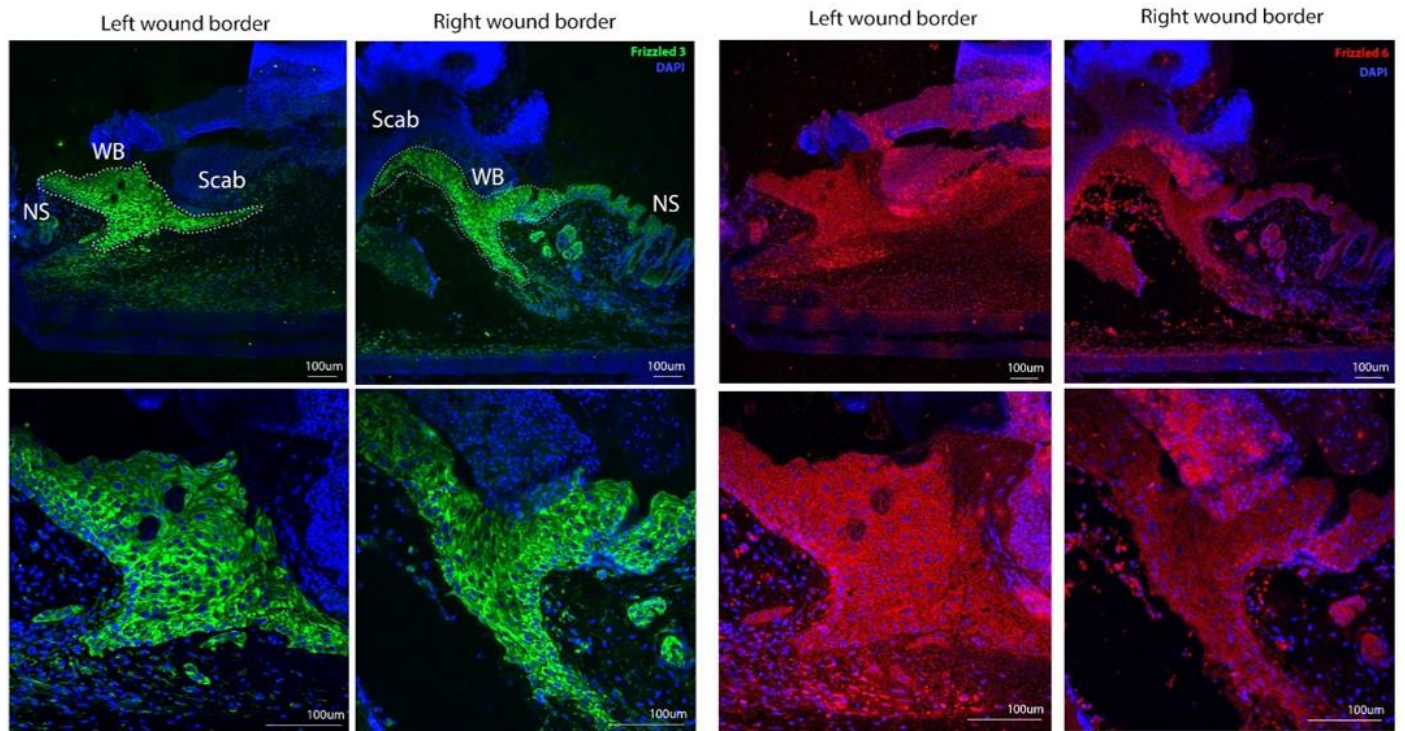
Table 9 Composition of Human Keratinocyte Growth Supplement

Component	Concentration (mg/L)
Protiens	
<i>Human recombinant EGF</i>	<i>Classified</i>
<i>Insulin</i>	<i>Classified</i>
<i>Transferrin</i>	<i>Classified</i>
Other components	
<i>Bovine pituitary extract</i>	<i>Classified</i>
<i>Hydrocortisone</i>	<i>Classified</i>



Supplementary Figure 1 Expression pattern of Vangl2 receptors in an *in vivo* murine wound model 4 days post injury

Immunofluorescence staining used to characterise the expression pattern of Vangl2 receptors (red) in an in vivo mouse wound sample formalin fixed and paraffin embedded 4 days post injury. Images were taken of the proliferative region of cells at the left and right wound edges. Little evidence of polarised membrane expression could be identified and staining appeared to be concentrated more around the nuclei. Sections were cut at 8µm. DAPI (blue) was used to counterstain nuclei. Dotted line indicates the epidermal basement membrane. Scale bar = 100µm



Supplementary Figure 2 Expression pattern of Frizzled 3 and Frizzled 6 in *in vivo* mouse wound models.

Representative images of immunofluorescence staining used to characterise expression patterns of Frizzled 3 (green) and Frizzled 6 (red) receptors in four separate in vivo mouse wound samples formalin fixed and paraffin embedded 4 days post injury. Images were taken of the proliferative regions of cells at the left and right wound edges. Sections were cut at 8µm. DAPI (blue) was used to counterstain nuclei. NS: Normal Skin, WB: Wound Border. Dotted line indicates the region of proliferating cells at the wound edge that are migrating across the wound bed. (n=4)

Frizzled 3

1	-----	0
1	gcgaaagctcgtctgctgggaggcgccgcccggcggttcctcgccgct	50
1	-----	0
51	ccgggtacctgaggagcgcggcgcccgccggcaggcggtgcagcccc	100
1	-----	0
101	ccaccccttgaggcaggcgccggggtctgaggatagcatttctcaagac	150
1	-----	0
151	ctgacttatggagcacttgtaacctgagatatttcagttgaaggaagaaa	200
1	-----	0
201	tagctcttctcctaagatggaatctgtggtttgggaatgtggtgatcaa	250
1	-----	0
251	cttgatatgttgccaaatgtgccccatgtaataaaatgaaagaagaga	300
1	-----	0
301	caagatgatgtcattttcccatattgtgaacacaaaaaacgcctttt	350
1	-----	0
351	gtgagaccaagctaacaacctctgacggctggaagagtatttaactgtt	400
1	-----	0
401	tgaagaatttaacagtaagatacagaagaagaccttcgagctgagacct	450
1	-----	0
451	gcaggtgtataaatatctaaaaacatattgaatagcctgatcatctga	500
1	-----CTTCAGACCCAGGAAGGATGGCTATGACTTGGATTGTTCTCTC	45
501	atctccttcagaccaggaaggatggctatgacttggtgtgtctctc	550
46	TTTGCCCTTGACTGTGTTCATGGGCGATATAGGTGGGCACAGTTTGT	95
51	tttggcccttgactgtgtcatgggcatataggtgggcacagttgttt	600
96	TCTTGTGAACCTATTACCTTGAGGATGTGCGAAGATTGCCTTATAATC	145
601	tcttgtaacctattaccttgaggatgtgccaagattgccttataatac	650
146	TACCTTCATGCCTAATCTTCTGAATCATTATGACCAACAGACAGCAGCTT	195
651	taccttcagcctaactcttctgaatcattatgaccaacagacagcagctt	700
196	TGGCAATGGAGCCATTCCACCCTATGGTGAATCGGATTGTTCTCGGAT	245
701	tggcaatggagcattccaccctatggatctggattgtctcgggat	750
246	TTCCGGCCTTTCTTTGTGCACTACGCTCCTATTGTATGGAATATGG	295
751	ttccggccttttcttgtgctactcagctctatttgtatggaatagg	800
296	ACGTGTCACACTTCCCTGTCGTAGGCTGTGTGAGCGGCTTACAGTGAGT	345
801	acgtgtcacacttccctgtctaggctgtgtcagcgggcttacagtgagt	850
346	GTTGCAAGCTCATGGAGATGTTGGTGTCTTGGCTGAAGATATGGAA	395
851	gttgaagctcatggagatgttgggtcttctggcctgaagatatggaa	900
396	TGCAGTAGGTTCCAGATTGTGATGAGCCATATCCTCG-----	433
901	tgcatgaggttccagattgtgatgagcctatctcagctgtgtgatct	950
434	-----	433
951	gaatttagctggagaaccaactgaaggagcccagtgagtcagtgagag	1000

Frizzled 6

1	-----	0
1	attcttgactcctgaaatccgaaggaagtggttcttttagagccagcg	50
1	-----CTTC-----AGACCCAGGA-----	14
51	ccaagagcttcaaaaatccttctaagtaattgacccaggactcattttc	100
15	AGGATGGC-----TATGACTTGGATTGT-----CTTC	41
101	aggaaagcctgaaatgagtaaaatagtgaaatgaggaattgaacattt	150
42	TCTCTTTGGC-----CCTTGA	57
151	tatctttggatgggatcttctgaggatgcaagagtgattcatcgaagc	200
58	C-TGTG-----TTC-----ATGG-----	69
201	catgtggtaaaatcaggaatttgaagaaatggaatgtttacattttg	250
70	--GGCAT-----ATAGGTGGGCACAGTTTGTCTTCTTG	100
251	ttgacgtgtatttttctacccctcctgaaggggcacagtccttcacactg	300
101	TGAACCTATTACCTGAGGATGTGCCAAGAT-----TTGCCTTATA	141
301	tgaaccaattac-----tggtccagatgtatgaaatggcc-taca	341
142	ATACTACCTTCATGCCTAATCTTCTGAATCATTATGACCAACAGACAGCA	191
342	acatgacgttttccctaatctgagggatcattatgaccagagattggtc	391
192	GCTTTGGCAATGGAGCCATTCACCCTATGGTGAATCGGATTGTTCTCG	241
392	gctgtggaaatggagcattttctcctcctgcaaatctggaatgttcacc	441
242	GGATTTCGGCCTTTCTTTGTGCACTACGCTCCTATTGTATGGAAT	291
442	aaacattgaaacttctcctgcaagcattgtaccacactgcatagaac	491
292	ATGGACGTGTACACTTCCCTGTCGTAGGCTGTGTGAGCGGCTTACAGT	341
492	aaattcatgtggttccacctgtgtgtaaaccttgtgagaagaattatctt	541
342	GAGTGTTCGAAGCTCATGGAGATGTTGGTGTTC--TTGGCTGAAGATA	390
542	gattgcaaaaaaattgaattgacacttttg-gatccgatggcctgaggagc	590
391	TGGAATGCAGTAGGTTCCAGATTGTGATGAGCCATATCCTCG-----	433
591	ttgaatgtgacagattacaatactgtgatgagactgttctt-gtaacttt	639
434	-----	433
640	tgatccacacacagaatttcttggtcctcagaagaaaaacagaacaagtcc	689
434	-----	433
740	caaggatataagtttctgggaattgaccagtgctgcctccatgcccaa	789
434	-----	433
790	catgtattttaaagtgtgatgactagattgcaaaaagttttattggaa	839
434	-----	433
840	cagtttcaatattttgtcttctgtgcaactctgttcacattccttactttt	889
434	-----	433
890	ttaattgatgttagaagattcagataccagagagaccaattatatatta	939
434	-----	433
940	ctctgtctgttacagcattgtatcttcttactgtacttcatggattttgc	989
434	-----	433
990	taggcgatgacacagcctgcaataaggcagatgagaagctagaacttggt	1039
434	-----	433

Supplementary Figure 3 Alignment of siRNA target sequence with Fzd3 and Fzd6 human genome sequences

7. References

1. Bekkers, S., Bot, A. G. J., Makarawung, D., Neuhaus, V. & Ring, D. The National Hospital Discharge Survey and Nationwide Inpatient Sample: The Databases Used Affect Results in THA Research. *Clin. Orthop. Relat. Res.* **472**, 3441–3449 (2014).
2. Alonso, L. & Fuchs, E. Stem cells of the skin epithelium. *Proc. Natl. Acad. Sci. U. S. A.* **100** Suppl, 11830–5 (2003).
3. LEBLOND, C. P. CLASSIFICATION OF CELL POPULATIONS ON THE BASIS OF THEIR PROLIFERATIVE BEHAVIOR. *Natl. Cancer Inst. Monogr.* **14**, 119–50 (1964).
4. Omary, M. B., Coulombe, P. A. & McLean, W. H. I. Intermediate Filament Proteins and Their Associated Diseases. *N. Engl. J. Med.* **351**, 2087–2100 (2004).
5. Fuchs, E. Keratins and the Skin. *Annu. Rev. Cell Dev. Biol.* **11**, 123–154 (1995).
6. Blanpain, C. & Fuchs, E. Epidermal Stem Cells of the Skin. *Annu. Rev. Cell Dev. Biol.* **22**, 339 (2006).
7. Fuchs, E. & Cleveland, D. W. A Structural Scaffolding of Intermediate Filaments in Health and Disease. *Science (80-.).* **279**, 514–519 (1998).
8. Byrne, C., Tainsky, M. & Fuchs, E. Programming gene expression in developing epidermis. *Development* (1994).
9. Lechler, T. & Fuchs, E. Asymmetric cell divisions promote stratification and differentiation of mammalian skin. *Nature* (2005). doi:10.1038/nature03922
10. Nickoloff, B. J. *et al.* Jagged-1 mediated activation of notch signaling induces complete maturation of human keratinocytes through NF-kappaB and PPARGamma. *Cell Death Differ.* **9**, 842–55 (2002).
11. Kypriotou, M., Huber, M. & Hohl, D. The human epidermal differentiation complex: Cornified envelope precursors, S100 proteins and the ‘fused genes’ family. *Experimental Dermatology* (2012). doi:10.1111/j.1600-0625.2012.01472.x
12. Sandilands, A., Sutherland, C., Irvine, A. D. & McLean, W. H. I. Filaggrin in the frontline: role in skin barrier function and disease. *J. Cell Sci.* (2009). doi:10.1242/jcs.033969
13. Candi, E., Schmidt, R. & Melino, G. The cornified envelope: A model of cell death in the skin. *Nature Reviews Molecular Cell Biology* (2005). doi:10.1038/nrm1619
14. Kalinin, A., Marekov, L. N. & Steinert, P. M. Assembly of the epidermal cornified cell envelope. *J. Cell Sci.* **114**, (2001).
15. Candi, E. *et al.* Transglutaminase cross-linking properties of the small proline-rich 1 family of cornified cell envelope proteins. Integration with loricrin. *J. Biol. Chem.* **274**, 7226–37 (1999).
16. Jarnik, M., Kartasova, T., Steinert, P. M., Lichti, U. & Steven, A. C. Differential expression and cell envelope incorporation of small proline-rich protein 1 in different cornified epithelia. *J. Cell Sci.* **109**, (1996).
17. Steinert, P. M., Candi, E., Kartasova, T. & Marekov, L. Small proline-rich proteins are cross-bridging proteins in the cornified cell envelopes of stratified squamous epithelia. *J. Struct. Biol.* **122**, 76–85 (1998).
18. Feingold, K. R. The Importance of Lipids in Cutaneous Function. *J. Lipid Res.* (2007). doi:10.1194/jlr.e700004-jlr200

19. Nemes, Z., Marekov, L. N., Fesus, L. & Steinert, P. M. A novel function for transglutaminase 1: Attachment of long-chain α -hydroxyceramides to involucrin by ester bond formation. *Proc. Natl. Acad. Sci.* (2002). doi:10.1073/pnas.96.15.8402
20. López, O., Cócera, M., Wertz, P. W., López-Iglesias, C. & de la Maza, A. New arrangement of proteins and lipids in the stratum corneum cornified envelope. *Biochim. Biophys. Acta - Biomembr.* (2007). doi:10.1016/j.bbamem.2006.11.023
21. Lavker, R. M. & Gedeon Matoltsy, A. Formation of horny cells: The fate of cell organelles and differentiation products in ruminal epithelium. *J. Cell Biol.* (1970). doi:10.1083/jcb.44.3.501
22. Morioka, K. *et al.* Extinction of Organelles in Differentiating Epidermis. *Acta Histochem. Cytochem.* **32**, 465–476 (1999).
23. Fischer, J. & Meyer-Hoffert, U. Regulation of kallikrein-related peptidases in the skin - from physiology to diseases to therapeutic options. *Thromb. Haemost.* **110**, 442–9 (2013).
24. Ishida-Yamamoto, A. *et al.* Epidermal lamellar granules transport different cargoes as distinct aggregates. *J. Invest. Dermatol.* (2004). doi:10.1111/j.0022-202X.2004.22515.x
25. Kishibe, M. Physiological and pathological roles of kallikrein-related peptidases in the epidermis. *J. Dermatol. Sci.* (2019). doi:10.1016/j.jdermsci.2019.06.007
26. Has, C. & Nyström, A. Epidermal Basement Membrane in Health and Disease. *Curr. Top. Membr.* **76**, 117–170 (2015).
27. Behrens, D. T. *et al.* The epidermal basement membrane is a composite of separate laminin- or collagen IV-containing networks connected by aggregated perlecan, but not by nidogens. *J. Biol. Chem.* **287**, 18700–9 (2012).
28. Yurchenco, P. D. Basement membranes: Cell scaffoldings and signaling platforms. *Cold Spring Harb. Perspect. Biol.* **3**, 1–27 (2011).
29. Bruckner-Tuderman, L. Secondary modifiers and the phenotypic variability of junctional epidermolysis bullosa. *Acta Derm. Venereol.* **88**, 436 (2008).
30. Woodley, D. T. Distinct Fibroblasts in the Papillary and Reticular Dermis: Implications for Wound Healing. *Dermatologic Clinics* **35**, 95–100 (2017).
31. Cormack, D. The integumentary system. *Ham's Histol.* 450–474 (1987).
32. Sorrell, J. M. & Caplan, A. I. Fibroblast heterogeneity: More than skin deep. *Journal of Cell Science* **117**, 667–675 (2004).
33. Meigel, W. N., Gay, S. & Weber, L. Dermal architecture and collagen type distribution. *Arch. dermatological Res. = Arch. fur dermatologische Forsch.* **259**, 1–10 (1977).
34. Zimmermann, D. R., Dours-Zimmermann, M. T., Schubert, M. & Bruckner-Tuderman, L. Versican is expressed in the proliferating zone in the epidermis and in association with the elastic network of the dermis. *J. Cell Biol.* **124**, 817–825 (1994).
35. Gonzaga da Cunha, M., Cury Rezende, F., Gonzaga da Cunha, A. L., Machado, C. A. & Fonseca, F. L. A. Anatomical, Histological And Metabolic Differences Between Hypodermis And Subcutaneous Adipose Tissue. *Int. Arch. Med.* **10**, (2017).
36. Kruglikov, I. L. & Scherer, P. E. Dermal Adipocytes: From Irrelevance to Metabolic Targets? *Trends in Endocrinology and Metabolism* **27**, 1–10 (2016).
37. Festa, E. *et al.* Adipocyte lineage cells contribute to the skin stem cell niche to drive hair cycling. *Cell* **146**, 761–771 (2011).
38. Rivera-Gonzalez, G., Shook, B. & Horsley, V. Adipocytes in skin health and disease. *Cold*

Spring Harb. Perspect. Med. **4**, (2014).

39. Schmidt, B. A. & Horsley, V. Intradermal adipocytes mediate fibroblast recruitment during skin wound healing. *Dev.* **140**, 1517–1527 (2013).
40. Gilaberte, Y., Prieto-Torres, L., Pastushenko, I. & Juarraz, Á. Anatomy and Function of the Skin. in *Nanoscience in Dermatology* 1–14 (Elsevier Inc., 2016). doi:10.1016/B978-0-12-802926-8.00001-X
41. Mort, R. L., Jackson, I. J. & Elizabeth Patton, E. The melanocyte lineage in development and disease. *Development (Cambridge)* **142**, 620–632 (2015).
42. Romani, N., Clausen, B. E. & Stoitzner, P. Langerhans cells and more: Langerin-expressing dendritic cell subsets in the skin. *Immunological Reviews* **234**, 120–141 (2010).
43. Birbeck, M. S., Breathnach, A. S. & Everall, J. D. An Electron Microscope Study of Basal Melanocytes and High-Level Clear Cells (Langerhans Cells) in Vitiligo. *J. Invest. Dermatol.* **37**, 51–64 (1961).
44. Valladeau, J. *et al.* Langerin, a novel C-type lectin specific to langerhans cells, is an endocytic receptor that induces the formation of Birbeck granules. *Immunity* **12**, 71–81 (2000).
45. Kaplan, D. H. Ontogeny and function of murine epidermal Langerhans cells. *Nature Immunology* **18**, 1068–1075 (2017).
46. Krishnaswamy, G., Ajitawi, O. & Chi, D. S. The Human Mast Cell: An Overview. in *Mast Cells* 013–034 (Humana Press). doi:10.1385/1-59259-967-2:013
47. Johnson, K. O. The roles and functions of cutaneous mechanoreceptors. *Current Opinion in Neurobiology* **11**, 455–461 (2001).
48. Hodge, B. D. & Brodell, R. T. *Anatomy, Skin, Sweat Glands. StatPearls* (2018).
49. Brodell, L. A. & Rosenthal, K. S. Skin structure and function: The body's primary defense against infection. *Infectious Diseases in Clinical Practice* **16**, 113–117 (2008).
50. PM, E. The skin barrier as an innate immune element. *Semin. Immunopathol.* **3**, (2007).
51. Elwood, J. M. & Jopson, J. Melanoma and sun exposure: an overview of published studies. *Int. J. cancer* **73**, 198–203 (1997).
52. Schulz, I., Mahler, H. C., Boiteux, S. & Epe, B. Oxidative DNA base damage induced by singlet oxygen and photosensitization: recognition by repair endonucleases and mutagenicity. *Mutat. Res.* **461**, 145–56 (2000).
53. Meyskens, F. L., Farmer, P. & Fruehauf, J. P. Redox regulation in human melanocytes and melanoma. *Pigment cell Res.* **14**, 148–54 (2001).
54. D'Orazio, J., Jarrett, S., Amaro-Ortiz, A. & Scott, T. UV radiation and the skin. *International Journal of Molecular Sciences* **14**, 12222–12248 (2013).
55. Scott, T. L. *et al.* Pigment-independent cAMP-mediated epidermal thickening protects against cutaneous UV injury by keratinocyte proliferation. *Exp. Dermatol.* **21**, 771–7 (2012).
56. Coelho, S. G. *et al.* Short- and long-term effects of UV radiation on the pigmentation of human skin. *J. Investig. dermatology. Symp. Proc.* **14**, 32–5 (2009).
57. Beattie, P. E., Dawe, R. S., Ferguson, J. & Ibbotson, S. H. Dose-response and time-course characteristics of UV-A1 erythema. *Arch. Dermatol.* **141**, 1549–1555 (2005).
58. Holick, M. F. Sunlight and vitamin D for bone health and prevention of autoimmune diseases, cancers, and cardiovascular disease -- Holick 80 (6): 1678S -- American Journal

- of Clinical Nutrition. *Am. J. Clin. Nutr.* **80**, 1678S-1688S (2004).
59. Landmann, L. The epidermal permeability barrier. *Anatomy and Embryology* **178**, 1–13 (1988).
 60. Robson, M. C., Steed, D. L. & Franz, M. G. Wound healing: biologic features and approaches to maximize healing trajectories. *Curr. Probl. Surg.* **38**, 72–140 (2001).
 61. Velnar, T., Bailey, T. & Smrkolj, V. *The Wound Healing Process: an Overview of the Cellular and Molecular Mechanisms. The Journal of International Medical Research* **37**, (2009).
 62. Strecker-McGraw, M. K., Jones, T. R. & Baer, D. G. Soft tissue wounds and principles of healing. *Emerg. Med. Clin. North Am.* **25**, 1–22 (2007).
 63. Martin, P. Wound healing - Aiming for perfect skin regeneration. *Science (80-.).* **276**, 75–81 (1997).
 64. Opneja, A., Kapoor, S. & Stavrou, E. X. Contribution of platelets, the coagulation and fibrinolytic systems to cutaneous wound healing. *Thrombosis Research* **179**, 56–63 (2019).
 65. Machlus, K. R., Thon, J. N. & Italiano, J. E. Interpreting the developmental dance of the megakaryocyte: a review of the cellular and molecular processes mediating platelet formation. *Br. J. Haematol.* **165**, 227–36 (2014).
 66. Heldin, C. H. & Westermark, B. Mechanism of action and in vivo role of platelet-derived growth factor. *Physiological Reviews* **79**, 1283–1316 (1999).
 67. Gleissner, C. A., Von Hundelshausen, P. & Ley, K. Platelet chemokines in vascular disease. *Arteriosclerosis, Thrombosis, and Vascular Biology* **28**, 1920–1927 (2008).
 68. Ross, R., Glomset, J., Kariya, B. & Harker, L. A platelet dependent serum factor that stimulates the proliferation of arterial smooth muscle cells in vitro. *Proc. Natl. Acad. Sci. U. S. A.* **71**, 1207–1210 (1974).
 69. Richardson, M. Acute wounds: an overview of the physiological healing process. *Nurs. Times* **100**, 50–3
 70. Lawrence, W. T. Physiology of the acute wound. *Clin. Plast. Surg.* **25**, 321–40 (1998).
 71. Hart, J. Inflammation. 1: Its role in the healing of acute wounds. *J. Wound Care* **11**, 205–9 (2002).
 72. Springer, T. A. Traffic signals for lymphocyte recirculation and leukocyte emigration: the multistep paradigm. *Cell* **76**, 301–14 (1994).
 73. Flanagan, M. The physiology of wound healing. *J. Wound Care* **9**, 299–300 (2000).
 74. Diegelmann, R. F. & Evans, M. C. Wound healing: an overview of acute, fibrotic and delayed healing. *Front. Biosci.* **9**, 283–9 (2004).
 75. Ramasastry, S. S. Acute wounds. *Clinics in Plastic Surgery* **32**, 195–208 (2005).
 76. Goldman, R. Growth factors and chronic wound healing: past, present, and future. *Adv. Skin Wound Care* **17**, 24–35
 77. Vaughan, M. B., Howard, E. W. & Tomasek, J. J. Transforming growth factor-beta1 promotes the morphological and functional differentiation of the myofibroblast. *Exp. Cell Res.* **257**, 180–9 (2000).
 78. Li, B. & Wang, J. H. C. Fibroblasts and myofibroblasts in wound healing: Force generation and measurement. *J. Tissue Viability* **20**, 108–120 (2011).
 79. Tomasek, J. J., Gabbiani, G., Hinz, B., Chaponnier, C. & Brown, R. A. Myofibroblasts and

- mechano-regulation of connective tissue remodelling. *Nat. Rev. Mol. Cell Biol.* **3**, 349–63 (2002).
80. Clark, R. A. F., An, J. Q., Greiling, D., Khan, A. & Schwarzbauer, J. E. Fibroblast Migration on Fibronectin Requires Three Distinct Functional Domains. *J. Invest. Dermatol.* **121**, 695–705 (2003).
 81. Haapasalmi, K. *et al.* Keratinocytes in human wounds express alpha v beta 6 integrin. *J. Invest. Dermatol.* **106**, 42–8 (1996).
 82. Gipson, I. K., Spurr-Michaud, S. J. & Tisdale, A. S. Hemidesmosomes and anchoring fibril collagen appear synchronously during development and wound healing. *Dev. Biol.* **126**, 253–62 (1988).
 83. Giannone, G. *et al.* Periodic lamellipodial contractions correlate with rearward actin waves. *Cell* **116**, 431–43 (2004).
 84. Wolgemuth, C. W. Lamellipodial contractions during crawling and spreading. *Biophys. J.* **89**, 1643–1649 (2005).
 85. Oberringer, M., Meins, C., Bubel, M. & Pohlemann, T. In vitro wounding: effects of hypoxia and transforming growth factor beta1 on proliferation, migration and myofibroblastic differentiation in an endothelial cell-fibroblast co-culture model. *J. Mol. Histol.* **39**, 37–47 (2008).
 86. Koolwijk, P. *et al.* Cooperative effect of TNFalpha, bFGF, and VEGF on the formation of tubular structures of human microvascular endothelial cells in a fibrin matrix. Role of urokinase activity. *J. Cell Biol.* **132**, 1177–88 (1996).
 87. Namiki, A. *et al.* Hypoxia induces vascular endothelial growth factor in cultured human endothelial cells. *J. Biol. Chem.* **270**, 31189–95 (1995).
 88. Gaudry, M. *et al.* Intracellular pool of vascular endothelial growth factor in human neutrophils. *Blood* **90**, 4153–61 (1997).
 89. Banks, R. E. *et al.* Release of the angiogenic cytokine vascular endothelial growth factor (VEGF) from platelets: significance for VEGF measurements and cancer biology. *Br. J. Cancer* **77**, 956–64 (1998).
 90. Zhang, H.-Y. & Phan, S. H. Inhibition of myofibroblast apoptosis by TGFbeta1. *Am J Respir Cell Mol Biol* **21**, 658–665 (1999).
 91. P., B. Wound healing and the role of fibroblasts. *J. Wound Care* **22**, 407–412 (2013).
 92. Witte, M. B. & Barbul, A. General principles of wound healing. *Surg. Clin. North Am.* **77**, 509–28 (1997).
 93. Toy, L. W. Matrix metalloproteinases: their function in tissue repair. *J. Wound Care* **14**, 20–2 (2005).
 94. Mendes, J. J. & Neves, J. *Open access publishing The Journal of Diabetic Foot Complications Diabetic Foot Infections: Current Diagnosis and Treatment. The Journal of Diabetic Foot Complications* **4**, (2012).
 95. Logan, C. Y. & Nusse, R. The Wnt signaling pathway in development and disease. *Annu. Rev. Cell Dev. Biol.* **20**, 781–810 (2004).
 96. van Amerongen, R., Mikels, A. & Nusse, R. Alternative wnt signaling is initiated by distinct receptors. *Sci. Signal.* **1**, re9 (2008).
 97. MacDonald, B. T., Tamai, K. & He, X. Wnt/ β -Catenin Signaling: Components, Mechanisms, and Diseases. *Developmental Cell* **17**, 9–26 (2009).
 98. Tellkamp, F., Vorhagen, S. & Niessen, C. M. Epidermal polarity genes in health and

- disease. *Cold Spring Harb. Perspect. Med.* **4**, (2014).
99. Muroyama, A. & Lechler, T. Polarity and stratification of the epidermis. *Seminars in Cell and Developmental Biology* **23**, 890–896 (2012).
 100. Devenport, D. The cell biology of planar cell polarity. *Journal of Cell Biology* **207**, 171–179 (2014).
 101. Caddy, J. *et al.* Epidermal Wound Repair is Regulated by the Planar Cell Polarity Signaling Pathway. *Dev. Cell* **19**, 138–147 (2010).
 102. Strutt, D. The planar polarity pathway. *Current Biology* **18**, (2008).
 103. Axelrod, J. D. Progress and challenges in understanding planar cell polarity signaling. *Semin. Cell Dev. Biol.* **20**, 964–71 (2009).
 104. Strutt, H., Warrington, S. J. & Strutt, D. Dynamics of core planar polarity protein turnover and stable assembly into discrete membrane subdomains. *Dev. Cell* **20**, 511–25 (2011).
 105. Komiya, Y. & Habas, R. Wnt Secretion and Extra-Cellular Regulators. **4**, 68–75 (2008).
 106. Wallingford, J. B. & Habas, R. The developmental biology of Dishevelled: an enigmatic protein governing cell fate and cell polarity. *Development* **132**, 4421–36 (2005).
 107. Marlow, F., Topczewski, J., Sepich, D. & Solnica-Krezel, L. Zebrafish Rho kinase 2 acts downstream of Wnt11 to mediate cell polarity and effective convergence and extension movements. *Curr. Biol.* **12**, 876–84 (2002).
 108. Habas, R., Kato, Y. & He, X. Wnt/Frizzled activation of Rho regulates vertebrate gastrulation and requires a novel Formin homology protein Daam1. *Cell* **107**, 843–54 (2001).
 109. Chrzanowska-Wodnicka, M. & Burridge, K. Rho-stimulated contractility drives the formation of stress fibers and focal adhesions. *J. Cell Biol.* **133**, 1403–1415 (1996).
 110. Wu, J. & Mlodzik, M. The Frizzled Extracellular Domain Is a Ligand for Van Gogh/Stbm during Nonautonomous Planar Cell Polarity Signaling. *Dev. Cell* **15**, 462–469 (2008).
 111. Fuchs, E. Scratching the surface of skin development. *Nature* **445**, 834–842 (2007).
 112. Stern, C. D. Neural induction: old problem, new findings, yet more questions. *Development* **132**, 2007–2021 (2005).
 113. Dikic, I. & Elazar, Z. Mechanism and medical implications of mammalian autophagy. *Nature Reviews Molecular Cell Biology* **19**, 349–364 (2018).
 114. Lamb, C. A., Yoshimori, T. & Tooze, S. A. The autophagosome: Origins unknown, biogenesis complex. *Nature Reviews Molecular Cell Biology* **14**, 759–774 (2013).
 115. Zachari, M. & Ganley, I. G. The mammalian ULK1 complex and autophagy initiation. *Essays in Biochemistry* **61**, 585–596 (2017).
 116. Kim, J., Kundu, M., Viollet, B. & Guan, K. L. AMPK and mTOR regulate autophagy through direct phosphorylation of Ulk1. *Nat. Cell Biol.* **13**, 132–141 (2011).
 117. Rabanal-Ruiz, Y., Otten, E. G. & Korolchuk, V. I. MTORC1 as the main gateway to autophagy. *Essays in Biochemistry* **61**, 565–584 (2017).
 118. Bach, M., Larance, M., James, D. E. & Ramm, G. The serine/threonine kinase ULK1 is a target of multiple phosphorylation events. *Biochem. J.* **440**, 283–291 (2011).
 119. Itakura, E., Kishi, C., Inoue, K. & Mizushima, N. Beclin 1 forms two distinct phosphatidylinositol 3-kinase complexes with mammalian Atg14 and UVRAG. *Mol. Biol. Cell* **19**, 5360–72 (2008).

120. Russell, R. C. *et al.* ULK1 induces autophagy by phosphorylating Beclin-1 and activating VPS34 lipid kinase. *Nat. Cell Biol.* **15**, 741–750 (2013).
121. Dooley, H. C. *et al.* WIPI2 Links LC3 Conjugation with PI3P, Autophagosome Formation, and Pathogen Clearance by Recruiting Atg12-5-16L1. *Mol. Cell* **55**, 238–252 (2014).
122. Dossou, A. S. & Basu, A. The emerging roles of mTORC1 in macromanaging autophagy. *Cancers* **11**, (2019).
123. Cheng, X. *et al.* Pacer Mediates the Function of Class III PI3K and HOPS Complexes in Autophagosome Maturation by Engaging Stx17. *Mol. Cell* **65**, 1029–1043.e5 (2017).
124. Yamamoto, A., Masaki, R. & Tashiro, Y. Characterization of the isolation membranes and the limiting membranes of autophagosomes in rat hepatocytes by lectin cytochemistry. *J. Histochem. Cytochem.* **38**, 573–580 (1990).
125. Ravikumar, B., Moreau, K., Jahreiss, L., Puri, C. & Rubinsztein, D. C. Plasma membrane contributes to the formation of pre-autophagosomal structures. *Nat. Cell Biol.* **12**, 747–757 (2010).
126. Hailey, D. W. *et al.* Mitochondria Supply Membranes for Autophagosome Biogenesis during Starvation. *Cell* **141**, 656–667 (2010).
127. Zaffagnini, G. & Martens, S. Mechanisms of Selective Autophagy. *Journal of Molecular Biology* **428**, 1714–1724 (2016).
128. Rogov, V., Dötsch, V., Johansen, T. & Kirkin, V. Interactions between Autophagy Receptors and Ubiquitin-like Proteins Form the Molecular Basis for Selective Autophagy. *Molecular Cell* **53**, 167–178 (2014).
129. Bjørkøy, G. *et al.* p62/SQSTM1 forms protein aggregates degraded by autophagy and has a protective effect on huntingtin-induced cell death. *J. Cell Biol.* **171**, 603–614 (2005).
130. Zaffagnini, G. *et al.* p62 filaments capture and present ubiquitinated cargos for autophagy. *EMBO J.* **37**, (2018).
131. Turco, E. *et al.* FIP200 Claw Domain Binding to p62 Promotes Autophagosome Formation at Ubiquitin Condensates. *Mol. Cell* **74**, 330–346.e11 (2019).
132. Jain, A. *et al.* p62/SQSTM1 is a target gene for transcription factor NRF2 and creates a positive feedback loop by inducing antioxidant response element-driven gene transcription. *J. Biol. Chem.* **285**, 22576–22591 (2010).
133. Zhang, D. D. & Hannink, M. Distinct Cysteine Residues in Keap1 Are Required for Keap1-Dependent Ubiquitination of Nrf2 and for Stabilization of Nrf2 by Chemopreventive Agents and Oxidative Stress. *Mol. Cell. Biol.* **23**, 8137–8151 (2003).
134. Rada, P. *et al.* SCF/ β -TrCP promotes glycogen synthase kinase 3-dependent degradation of the Nrf2 transcription factor in a Keap1-independent manner. *Mol. Cell. Biol.* **31**, 1121–33 (2011).
135. Wu, T. *et al.* Hrd1 suppresses Nrf2-mediated cellular protection during liver cirrhosis. *Genes Dev.* **28**, 708–722 (2014).
136. Komatsu, M. *et al.* The selective autophagy substrate p62 activates the stress responsive transcription factor Nrf2 through inactivation of Keap1. *Nat. Cell Biol.* **12**, 213–223 (2010).
137. Ichimura, Y. *et al.* Phosphorylation of p62 Activates the Keap1-Nrf2 Pathway during Selective Autophagy. *Mol. Cell* **51**, 618–631 (2013).
138. Gurtner, G. C., Wong, V. W., Sorkin, M., Glotzbach, J. P. & Longaker, M. T. Surgical approaches to create murine models of human wound healing. *Journal of Biomedicine*

and *Biotechnology* **2011**, (2011).

139. Abdullahi, A., Amini-Nik, S. & Jeschke, M. G. Animal models in burn research. *Cellular and Molecular Life Sciences* **71**, 3241–3255 (2014).
140. Gerber, P. A. *et al.* The top skin-associated genes: A comparative analysis of human and mouse skin transcriptomes. *Biological Chemistry* **395**, 577–591 (2014).
141. Cibelli, J. *et al.* Strategies for improving animal models for regenerative medicine. *Cell Stem Cell* **12**, 271–274 (2013).
142. Zomer, H. D. & Trentin, A. G. Skin wound healing in humans and mice: Challenges in translational research. *Journal of Dermatological Science* **90**, 3–12 (2018).
143. Levy, V., Lindon, C., Zheng, Y., Harfe, B. D. & Morgan, B. A. Epidermal stem cells arise from the hair follicle after wounding. *FASEB J.* **21**, 1358–1366 (2007).
144. The hair cycle TL - 119. *J. Cell Sci.* **119 VN**-, 391–393 (2006).
145. Ansell, D. M., Kloepper, J. E., Thomason, H. A., Paus, R. & Hardman, M. J. Exploring the hair growth-wound healing connection: Anagen phase promotes wound re-Epithelialization. *J. Invest. Dermatol.* **131**, 518–528 (2011).
146. Ito, M. *et al.* Wnt-dependent de novo hair follicle regeneration in adult mouse skin after wounding. *Nature* **447**, 316–320 (2007).
147. Rittié, L., Sachs, D. L., Orringer, J. S., Voorhees, J. J. & Fisher, G. J. Eccrine sweat glands are major contributors to reepithelialization of human wounds. *Am. J. Pathol.* **182**, 163–171 (2013).
148. Hedges, S. B., Dudley, J. & Kumar, S. TimeTree: A public knowledge-base of divergence times among organisms. *Bioinformatics* **22**, 2971–2972 (2006).
149. Waterston, R. H. *et al.* Initial sequencing and comparative analysis of the mouse genome. *Nature* **420**, 520–562 (2002).
150. Doeing, D. C., Borowicz, J. L. & Crockett, E. T. Gender dimorphism in differential peripheral blood leukocyte counts in mice using cardiac, tail, foot, and saphenous vein puncture methods. *BMC Clin. Pathol.* **3**, (2003).
151. Lehrer, M. S., Sun, T. T. & Lavker, R. M. Strategies of epithelial repair: Modulation of stem cell and transit amplifying cell proliferation. *J. Cell Sci.* **111**, 2867–2875 (1998).
152. King, K. E. *et al.* Unique domain functions of p63 isoforms that differentially regulate distinct aspects of epidermal homeostasis. *Carcinogenesis* **27**, 53–63 (2006).
153. Sakaue-Sawano, A. *et al.* Visualizing Spatiotemporal Dynamics of Multicellular Cell-Cycle Progression. *Cell* **132**, 487–498 (2008).
154. Spencer, S. L. *et al.* The proliferation-quiescence decision is controlled by a bifurcation in CDK2 activity at mitotic exit. *Cell* **155**, 369 (2013).
155. Gurkar, A. U. *et al.* Identification of ROCK1 kinase as a critical regulator of Beclin1-mediated autophagy during metabolic stress. *Nat. Commun.* **4**, 1–13 (2013).
156. Somlyo, A. P. & Somlyo, A. V. Ca²⁺ sensitivity of smooth muscle and nonmuscle myosin II: Modulated by G proteins, kinases, and myosin phosphatase. *Physiological Reviews* **83**, 1325–1358 (2003).
157. Matsui, T. *et al.* Rho-kinase phosphorylates COOH-terminal threonines of ezrin/radixin/moesin (ERM) proteins and regulates their head-to-tail association. *J. Cell Biol.* **140**, 647–657 (1998).
158. Kimura, K. *et al.* Regulation of the association of adducin with actin filaments by Rho-associated kinase (Rho-kinase) and myosin phosphatase. *J. Biol. Chem.* **273**, 5542–5548

(1998).

159. Amin, E. *et al.* Rho-kinase: Regulation, (dys)function, and inhibition. *Biological Chemistry* **394**, 1399–1410 (2013).
160. Anderson, E. D. *et al.* Prolonging culture of primary human keratinocytes isolated from suction blisters with Rho kinase inhibitor Y-27632. *PLoS ONE*. **13**(9):e0198862 (2018)
161. Gandham, V. *et al.* Effects of Y27632 on keratinocyte procurement and wound healing. *Clinical and Experimental Dermatology* **38** (7), 782-786 (2013)
162. Zhang, T *et al.* Investigating Fibroblast-Induced Collagen Gel Contraction Using a Dynamic Microscale Platform. *Front. Bioeng. Biotechnol.*, (2019)
163. Bell, *et al.* Production of a tissue-like structure by contraction of a collagen lattices by human fibroblasts of different proliferative potential in vitro. *Proc. Natl. Acad. Sci. U.S.A.* **76**, 1274-1278 (1979)
164. Omagari, N. *et al.* Three dimensional arrangement of fibrocytes in the dermal papilla of the human sole skin. *Okajimas Folia Anat Jpn* **67**, 195-202 (1990)
165. Guest, J. F. *et al.* Health economic burden that wounds impose on the National Health Service in the UK. *BMJ Open*. **5**(12) (2015)
166. Kenific, C.M. *et al.* Autophagy in adhesion and migration. *Journal of Cell Science*. **129**: 3685-3693 (2016)
167. Yu, J *et al.* Updating the Wnt pathways. *Biosci Rep*. **34**: (5) (2014)
168. Popp, T. *et al.* Wnt5a/ β -catenin signalling drives calcium-induced differentiation of human primary keratinocytes. *J Invest Dermatol* **134**: 2183-2191 (2014)
169. Schmidt-Ullrich, R. *et al.* Molecular principles of hair follicle induction and morphogenesis. *Bioessays*. **27**: 247-261 (2005)
170. Van der Veen, C. *et al.* A comprehensive guide for the recognition and classification of distinct stages of hair follicle morphogenesis. *Invest Dermatol*. **113**: 523-532 (1999)
171. Mahanty, S. *et al.* Keratinocyte differentiation promotes ER stress-dependent lysosome biogenesis. *Cell Death and Disease*. **10**: 269 (2019)
172. Yoshihara, N. *et al.* The significant role of autophagy in the granular layer in normal skin differentiation and hair growth. *Arch. Dermatol. Res*. **307**, 159–169 (2015).
173. Murase, D. *et al.* Autophagy has a significant role in determining skin color by regulating melanosome degradation in keratinocytes. *Journal of Investigative Dermatology*. **133**: (10) 2416-2424 (2013)
174. Eckhart, E. *et al.* Autophagic control of skin aging. *Front. Cell Dev. Biol.* (2019)
175. Mintern, J. D. *et al.* Differential use of autophagy by primary dendritic cells specialized in cross-presentation. *Autophagy* **11**: (6) 906-917
176. Tripathi, S. *et al.* Hypertrophic scars and keloids: a review and current treatment modalities. *Biomedical Dermatology* **4**: (11) (2020)

177. Shinkuma, S. Dystrophic epidermolysis bullosa: a review. *Clin Cosmet Investig Dermatol* **8**: 275-284 (2015)
178. Gonzaga da Cunha, M. *et al.* Hypodermis and subcutaneous adipose tissue – two different structures. *Surg Cosmet Dermatol* **6** (4) 355-359 (2014)
179. Lu, C., Fuchs, E. Sweat gland progenitors in development, homeostasis and wound repair. *Cold Spring Harb Perspect Med.* **4** (2) (2014)
180. D’Orazio, J. *et al.* UV Radiation and the Skin. *Int J Mol Sci* **14** (6) 12222-12248 (2013)
181. Cui, C-Y. *et al.* Eccrine sweat gland development and sweat secretion. *Exp Dermatol* **24** (9) 644-60 (2015)
182. Chen, L. *et al.* The murine excisional wound model: contraction revisited. *Wound Repair Regen.* **23** 874-877 (2015)
183. Muzumdar, S. *et al.* Nrf2-mediated expansion of pilosebaceous cells accelerates cutaneous wound healing. *The American Journal of Pathology* **189** (3) 568-579 (2019)
184. auf dem Keller, U. *et al.* Nrf transcription factors in keratinocytes are essential for skin tumour prevention but not for wound healing. *Mol Cell Biol* **26** (10) 3773-3784 (2006)
185. Noszczyk, B.H.M.D *et al.* p63 expression during normal cutaneous wound healing in humans. *Plastic and Reconstructive Surgery* **108** (5) 1242-1247 (2001)
186. Dong, B. *et al.* Functional redundancy of frizzled 3 and frizzled 6 in planar cell polarity control of mouse hair follicles. *Development* **145** (2018)
187. Maskey, D. *et al.* ATG5 is induced by DNA-damaging agents and promotes mitotic catastrophe independent of autophagy. *Nat Commun* **4**:2130 (2013)
190. Vishwakarma, M. *et al.* Mechanical interactions among followers determine the emergence of leaders in migrating epithelial cell collectives. *Nat Commun* **9** (2018)
191. Chapnick, D. A. *et al.* Leader cell positioning drives wound-directed collective migration in TGF β -stimulated epithelial sheets. *Mol Biol Cell* **25** (10) 1586-1593
192. Gov, N. S, Collective cell migration patterns: Follow the leader *Proc Natl Acad Sci USA* **104** (41) 15970-15971
193. Davey, C. F, Moens, C. B. Planar cell polarity in moving cells: think globally, act locally. *Development* **144** 187-200
194. D’Arcy, M. S, Cell death: a review of the major forms of apoptosis, necrosis and autophagy. *Cell Biology International* **43** (6) 582-592
195. Herranz, N, Gil, J. Mechanisms and functions of cellular senescence. *The journal of Clinical Investigation* (2018)
196. Caldon, C.E, Musgrove, E A. Distinct and redundant functions of cyclin E1 and cyclin E2 in development and cancer *Cell Division* **5** (2) (2010)

197. Pellegata, N. S. *et al.* DNA damage and p53-mediated cell cycle arrest: A re-evaluation *Proc Natl Acad Sci USA* **93** (26) 15209-15214 (1996)
198. Pourreyron, C. *et al.* Wnt5a is strongly expressed at the leading edge in non-melanoma skin cancer, forming active gradients, while canonical Wnt signalling is repressed. *PLOS ONE* (2012)
199. Hinz, B. The role of myofibroblasts in wound healing. *Current Research in Translational Medicine* **64** (4) 171-177 (2016)
200. Yang, Y., Mlodzik, M. Wnt-Frizzled/Planar Cell Polarity Signalling: Cellular Orientation by Facing the Wind (Wnt). *Annu Rev Cell Dev Biol* **31** 623-646 (2013)
201. Chapman, S. *et al.* The effect of Rho kinase inhibition on long-term keratinocyte proliferation is rapid and conditional. *Stem Cell Res Ther* **5** (2) 60 (2014)
202. Liang, C. *et al.* *In vitro* scratch assay: a convenient and inexpensive method for analysis of cell migration *in vitro*. *Nature Protocols* **2** 329-333 (2007)
203. Han, G., Ceilley, R. Chronic Wound Healing: A Review of Current Management and Treatments. *Advances in therapy* **34** (3) 599-610 (2017)
204. Singh, N. *et al.* Preventing foot ulcers in patients with diabetes, *Journal of the American Medical Association*, **293** (2) 217–228 (2005)
205. LoGerfo, F.W., Coffman J.D., Vascular and microvascular disease of the foot in diabetes. Implications for foot care. *New England Journal of Medicine*, **311** (25) 1615–1619 (1984)
206. Spravchikov, N. *et al.* Glucose effects on skin keratinocytes: implications for diabetes skin complications. *Diabetes*, **50** (7) 1627–1635 (2001)
207. Tsourdi, E. *et al.* Current Aspects in the Pathophysiology and Treatment of Chronic Wounds in Diabetes Mellitus. *BioMed Research International*, **2013** (2013)
208. Larsen, B *et al.* On the pathogenesis of bedsores. *Scand J Plast Reconstr Surg*, **13** 2347-50 (1979)
209. Krouskop, T.A, A syntheses of the factors that contribute to pressure sore formation. *Medical Hypotheses*, **11** 255-67 (1983)
210. Reichel, S.M., Shearing force as a factor in decubitus ulcer in paraplegics. *JAMA*, **166** 762-3 (1958)
211. Greenhalgh, D.G., Management of the skin and soft tissue in the geriatric surgical patient. *Surg Clin North Am*, **95** (1) 104-14 (2015)
212. Signer, R.A., Morrison, S.J., Mechanisms that regulate stem cell aging and life span, *Cell Stem Cell*, **12** 152-165 (2013)
213. Marcos-Garces, V. *et al.* Age-related dermal collagen changes during development, maturation and ageing – a morphometric and comparative study. *J Anat*, **225** (1) 98-108 (2014)

214. Phillip, J.M. *et al*, The Mechanobiology of Aging, *Annu Rev Biomed Eng*, **17** 113-141 (2015)
215. Brun, C. *et al*, Phenotypic and functional changes in dermal primary fibroblasts isolated from intrinsically aged human skin, *Exp Dermatology*, **25** (2) 113-119 (2016)
216. Mendelson, D.N., Schwartz, W.B., The Effects of Aging and Population Growth on Health Care Costs, *Health Affairs*, **12** (1) (1993)
217. Filius, P.M.G., Gyssens, I.C., Impact of increasing antimicrobial resistance on wound management, *AM J Clin Dermatol*, **3** (1) 1-7 (2002)
218. Schwartz, M. *et al*, Comparison of a new fibrin sealant with standard topical hemostatic agents, *Arch Surgery*, **139** (11) 1148-1154 (2004)
219. Spotnitz, W.D., Fibrin sealant: the only approved hemostat, sealant and adhesive- a laboratory and clinical perspective, *Surgery*, **1** 1-29 (2014)
220. Chiara, O. *et al*, A systematic review on the use of topical hemostats in trauma and emergency surgery, *BMC Surgery*, **18** (68) (2018)
221. Ragusa, R. *et al*, Use of gelatin powder added to rifamycin versus bone wax in sternal wound hemostasis after cardiac surgery, *Interact Cardiovasc Thorac Surg*, **6** 52-55 (2007)
222. Wagenhauser, M.U. *et al*, Oxidised (non)-regenerated cellulose affects fundamental cellular processes of wound healing, *Scientific Reports*, **6** 32238 (2016)
223. Zhou, J. *et al*, Bacteria-responsive intelligent wound dressing: Simultaneous *In Situ* detection and inhibition of bacterial infection for accelerated wound healing, *Biomaterials*, **161** 11-23 (2018)
224. Farber, P.L. *et al*, Electricity and colloidal stability: How charge distribution in the tissue can affect wound healing, *Med. Hypotheses*, **83** 199-204 (2014)
225. Ud-Din, S. and Bayat, A., Electrical Stimulation and Cutaneous Wound Healing: A review of Clinical Evidence, *Healthcare*, **2** 445-467 (2014)
226. Sun, Y.S., Electrical Stimulation for Wound Healing: Simulation on the Effect of Electrode Configurations, *BioMed. Res. Int.*, (2017)
227. Zhao, M., Electrical fields in wound healing – An overriding signal that directs cell migration, *Semin. Cell Dev. Bio*, **20** 674-682 (2009)
228. Hampton, S. and Collins, F., Treating a pressure ulcer with bio-electric stimulation therapy. *Br. J. Nurs*, **15** 14-18 (2006)
229. Ouseph, M.M. *et al*, Autophagy is induced upon platelet activation and is essential for hemostasis and thrombosis, *Blood*, **126** 1224-1233 (2015)
230. Theilgaard-Monch, K. *et al*, The transcriptional program of terminal granulocytic differentiation, *Blood*, **105** (4) 1785-1796 (2005)

231. Riffelmacher, T. *et al*, Autophagy-Dependent Generation of Free Fatty Acids Is Critical for Normal Neutrophil Differentiation, *Immunity*, **47** (3) 466-680 (2017)
232. Rozman, S. *et al*, The generation of neutrophils in the bone marrow is controlled by autophagy, *Cell Death Differ*, **22** (3) 445-456 (2015)
233. Gay, D. *et al*, Fgf9 from dermal $\gamma\delta$ T cells induces hair follicle neogenesis after wounding, *Nature Medicine*, **19** 916-923 (2013)
234. Wong, C.O. *et al*, Lysosomal Degradation Is Required for Sustained Phagocytosis of Bacteria by Macrophages, *Cell Host Microbe*, **21** (6) 719-730 (2017)
235. Martinez, J. *et al*, Molecular characterisation of LC3-associated phagocytosis reveals distinct roles for Rubicon, NOX2 and autophagy proteins, *Nat Cell Biol*, **17** 893-906 (2015)
236. Ullah, I. *et al*, The interrelationship between phagocytosis, autophagy and formation of neutrophil extracellular traps following infection of human neutrophils by *Streptococcus pneumonia*, *Innate Immun*, **23** (5) 413-423 (2017)
237. Rinchai, D. *et al*, Macroautophagy is essential for killing of intracellular *Burkholderia pseudomallei* in human neutrophils, *Autophagy*, **11** (5) 748-755 (2015)
238. Guo, Y. *et al*, AGEs Induced Autophagy Impairs Cutaneous Wound Healing via Stimulating Macrophage Polarisation to M1 in Diabetes, *Scientific Reports*, (2016)
239. Koh, T.J. and Di Pietro, L.A., Inflammation and wound healing: the role of the macrophage, *Expert review in molecular medicine*, **13** (23) (2011)
240. Sruthi, C.R. and Raghu, K.G., Advanced glycation end products and their adverse effects: The role of autophagy, *Journal of Biochemical and Molecular Toxicology*, **35** (1) (2021)
241. Qiang, L. *et al*, Keratinocyte autophagy enables the activation of keratinocytes and fibroblasts and facilitates wound healing, *Autophagy*, (2020)
242. Low, Q.E *et al*, Wound healing in MIP-1 α (-/-) and MCP-1 (-/-) mice, *Am J Pathol*, **159** 457-463 (2001)
243. Nakamura, K. *et al*, Keratinocyte-derived monocyte chemoattractant protein 1 (MCP-1): analysis in a transgenic model demonstrates MCP-1 can recruit dendritic and Langerhans cells to skin, *J Invest Dermatol*, **105** 635-642 (1995)

“Your hardest times often lead to the greatest moments of your life.

Keep going.

Tough situations build strong people in the end.”

Roy T. Bennett